TOXICOLOGY: INTERACTION OF BRAIN ASTROCYTES WITH ZINC OXIDE NANOPARTICLES (ZnO NPs) AND RELATED INFLAMMATORY, IMMUNO AND NEUROTOXICOLOGICAL RESPONSE USING RAT MODEL

A THESIS PRESENTED BY

SRUTHI S.

TO

THE SREE CHITRA TIRUNAL INSTITUTE FOR MEDICAL SCIENCES AND TECHNOLOGY, TRIVANDRUM
Thiruvananthapuram

IN PARTIAL FULFILLMENT OF THE REQUIREMENTS
FOR THE AWARD OF
DOCTOR OF PHILOSOPHY

2018

CERTIFICATE

I, **Sruthi S**, hereby certify that I had personally carried out the work depicted in the thesis entitled "***Toxicology: Interaction of brain astrocytes with Zinc oxide nanoparticles (ZnO NPs) and related inflammatory, immuno and neurotoxicological response using rat model***". No part of the thesis contains any matter previously published or written by another person, nor any material that has been submitted for the award of any other degree or diploma of any University or Institute of higher learning, prior to this date except where due acknowledgment has been made in the text.

Place: Thiruvananthapuram

Date:

Signature:

Name: Sruthi S.

Reg. No: 2013/PhD/11

Dr. P V Mohanan

Toxicology Division

This is to certify that ***Ms. Sruthi S.*** in the Toxicology Division of this institute has fulfilled the requirements prescribed for the Ph.D. degree of the Sree Chitra Tirunal Institute for Medical Sciences and Technology, Trivandrum. The thesis entitled "***Toxicology: Interaction of brain astrocytes with Zinc oxide nanoparticles (ZnO NPs) and related inflammatory, immuno and neurotoxicological response using rat model***" was carried out under my direct supervision. No part of the thesis was submitted for the award of any degree or diploma prior to this date.

*Clearance was obtained from the Institute Animal Ethics Committee (IAEC) for carrying out the study. IAEC approval No: SCT/IAEC-131/DECEMBER/2014/86

Signature:

Date :

ACKNOWLEDGEMENT

I express my gratitude to our Director Prof. Asha Kishore and Dr. H.K. Varma, Head, Biomedical Technology Wing, Sree Chitra Tirunal Institute for Medical Sciences and Technology for providing necessary support and facilities for completing my Ph.D. work.

I sincerely thank our former Directors Prof. K. Radhakrishnan, Prof.Jagan Mohan Tharakan and former Heads of Biomedical Technology Wing Dr. G.S. Bhuvaneshwar, Dr. C.P. Sharma, Shri. O.S. Neelakantan Nair, former Dean Prof. Suresh Nair, Present Dean Dr.Kalliyanakrishnan V., Registrar Dr. George A.V., Deputy Registrar Dr. Santhosh Kumar and former Deputy Registrar Dr.Sundar Jayasingh S. for their academic assistance.

I would like to acknowledge the University Grants Commission (UGC, New Delhi) for the Junior Research Fellowship and Senior Research Fellowship (Award letter No:2121130542 date:1/07/2012).

I would like to thank my Doctoral Advising Committee members, Dr. H.K. Varma, Dr.Rekha M.R. and Dr.Kamalesh K. Gulia in their efforts in reviewing and evaluating my research work.

I am grateful to Indo-French Centre for the Promotion of Advanced Research for providing an opportunity to carry out 6-month project in University of Bourgogne, France with Raman-Charpak fellowship. I sincerely acknowledge Dr. Nadine Millot and Dr. Gerard Lizard for their valuable guidance and encouragement during my tenure at University of Bourgogne, France.

I express my gratitude to all Departments and Divisions Head, especially Dr.Prabha D. Nair (former Associate Dean and HoD, DAB), Dr. T.V. Kumary (Associate Dean) Dr. H.K. Varma, Dr. A. Maya Nandkumar, Dr. Uma Shankar P.R, Dr.Lisy K. Krishnan, Dr.Rekha M.R., Dr.Hari krishnan V.S., Dr. Manoj Komath and Dr. Annie John for providing their support in completing my work.

I would also like to thank Dr.Rémi Chassagnon, Dr. Nicolas Geoffroy, Dr. Olivier Heintz, Dr.Frédéric Herbst, Dr. Julien Boudon and Mr. Alexix Loiseau for their technical support at University of Bourgogne, France

I gratefully acknowledge the assistance provided by Dr. Suresh Babu S., Mr. Renjith Kartha, Mr. Pradeep Kumar S.S., Ms. Keerthi S., Mr. Willi Paul and Mr. Prem Mohan M.

Special thanks to the staff and students of Toxicology Division who have made my time here in the lab a memorable one. I am grateful for the friendship and unyielding support offered by Dr.Remya N.S., Dr.Syama S., Dr.Reshma S Cherian., Ms. Reshma V.G., Ms. Sukanya V.S., Mr. Shaji S., Mr. Harikumar G., Mrs. Amrutha Kumari M.S. and Mrs. Sreedevi J. I also thank former lab members Dr.Sheeja Liza Easo, Dr.Gayathri Easwer, Ms. Lekshmy M.S. and Ms. Anju Mohan for their technical support.

I thank Dr. P.V. Mohanan, Ph.D. Supervisor for his advices and support in completing my Ph.D. work.

I would like to acknowledge with gratitude my family and friends who stood by me through all the ups and downs. Words cannot express how grateful I am to my mother and father for all of the sacrifices they've made on my behalf. Your prayer for me was what sustained me thus far. I thank my mother-in law and father-in-law for their never ending love and support. I also thank my brother for prompting me to think rational. I would also like to thank Ms. Neena, Ms. Arathi and Ms. Vibha for their friendship and support. I thank my little nephews and niece for inspiring me to stay positive. Last but not the least thank my beloved, warm hearted husband Dr. Anil K. Chorpath for tolerating me and motivating me to strive towards my goal.

Sruthi S.

TABLE OF CONTENTS

LIST OF FIGURES

LIST OF TABLES

ABBREVIATIONS

µg	Microgram
µl-	Microliter
µM	Micromolar
AB/AM	Antibiotic/ Antimycotic
Ac-LDL	Acetylated Low Density Lipoprotein
ADME	Adsorption, Distribution, Metabolism, Excretion
ALP	Alkaline phosphatase
ALT	Alanine transaminase
AO	Acridine orange
AST	Aspartate transaminase
BBB	Blood Brain Barrier
BCA	Bicinchoninic acid assay
BET	Brunauer, Emmett and Teller
BP solution	Blocking and Permeabilisation solution
BSA	Bovine serum albumin
^{o}C	Celsius
cm	Centimetre
CNS	Central nervous system
CPCSEA	Committee for the Purpose of Control and Supervision of Experiments on Animals

CPM	Counts per minutes
Cyt.D	cytochalasin D
DAPI	4',6-diamidino-2-phenylindole
DCFH-DA	Dichloro-dihydro-fluorescein diacetate
dH_2O	Deionised water
DHE	Dihydroethidium
DHR123	Dihydrorhodamine 123
Dil	1,1\'-dioctadecyl –3,3,3\',3\'-tetramethyl-indocarbocyanine perchlorate
DiOC6(3)	3,3'-Dihexyloxacarbocyanine Iodide
DLS	Dynamic light scattering
DMEM F12	Dulbecco's Modified Eagle Medium/Nutrient Mixture F12
DMSO	Dimethyl Sulphoxide
DNA	Deoxyribonucleic acid
DTPA	Diethylene triamine penta acetic acid
EDTA	Ethylene diamine tetra acetic acid
EtBr	Ethidium bromide
EU	Endotoxin unit
eV	Electron volt
FACS	Fluorescence Activated Cell Sorting
FBS	Foetal Bovine Serum
FSC	Forward scatter

g	Gram
GFAP	Glial Fibrillary Acid Protein
GGT	Gamma glutamyl transferase
GPx	Glutathione Peroxidise
GR	Glutathione reductase
GSH	Reduced glutathione
GSSG	Oxidized glutathione
h	Hour
H & E	Haematoxylin and Eosin
HBSS	Hanks Balanced Salt Solution
HCT	Haematocrit
HGB	Haemoglobin
HR-TEM	High Resolution TEM
i.p.	Intraperitoneal
i.v.	Intravenous
IAEC	Institutional Animal Ethics Committee
ICP-AES	Inductively Coupled Plasma Atomic Emission Spectroscopy
IL	Interleukin
JC1	5,5′,6,6′-tetrachloro-1,1′,3,3′-tetraethylbenzimidazolylcarbocyanineiodide
kg	Kilogram

kV	Kilovolt
LC_{50}	Lethal concentration 50%
LME	L-leucine methyl ester
LMP	Lysosomal membrane permeabilisation
LPO	Lipid peroxidation
LPS	Lipopolysaccharides
M	Molar
MAPK	Mitogen Activated Protein Kinase
MCHC	Mean corpuscular hemoglobin concentration
MDA	Malonedialdehyde
mg	Milligram
min	Minutes
ml	Millilitre
mm	Millimetre
mM	Millimolar
MMP	Mitochondrial membrane potential
MRI	Magnetic Resonance imaging
MTT	3-(4,5-Dimethylthiazol-2-yl)-2,5-Diphenyltetrazolium Bromide
NADPH	Nicotinamide Adenine Dinucleotide Phosphate (Reduced)
NF-κB	Nuclear Factor –κB
NGS	Nerve guidance channel

nm	Nanometre
NO	Nitric Oxide
NOAEL	No Observed Adverse Effect Level
NRU	Neutral red uptake
P	Postnatal day
PAGE	Polyacrylamide gel electrophoresis
PARP	Poly ADP ribose polymerase
PBS	Phosphate Buffered Saline
PDI	Polydispersity index
PI	Propidium Iodide
PLT	Platelet
PS	Phosphatidylserine
RBC	Red blood cell
Rh-phalloidin	Rhodamine phalloidin
RIPA buffer	Radio immunoprecipitation assay buffer
RNA	Ribonucleic acid
RNS	Reactive nitrogen species
ROS	Reactive Oxygen Species
rpm	Revolutions per minutes
RPMI	Roswell Park Memorial Institute medium
s	Second
SD	Standard Deviation

SDS	Sodium Dodecyl Sulphate
SEM	Scanning electron microscopy
SOD	Superoxide dismutase
SSA	Specific surface area
SSC	Sideward scatter
TEM	Transmission electron microscopy
TEMED	Tetramethyl ethylenediamine
TGA	Thermogravimetric analysis
TiONts	Titanate nanotubes
TLR	Toll like receptor
USP	United states pharmacopeia
V	Volt
v/v	Volume/Volume
w/v	Weight/Volume
WBC	White blood cells
XPS	X-ray photoelectron spectroscopy
XRD	X-Ray Diffraction
ZnO NP	Zinc oxide nanoparticle
ZnO R	Zinc nanoparticles rod
ZnO SP	Zinc nanoparticles spearhead

SYNOPSIS

Title: ***Toxicology: Interaction of brain astrocytes with Zinc oxide nanoparticles (ZnO NPs) and related inflammatory, immuno and neurotoxicological response using rat model***

Nanotechnology is a relatively newer and rapidly growing branch of science that has applications in almost all the industrial sectors. The attractive future of nanotechnology is not only in their ability to miniaturize complex devices, but also in their unconventional characteristics arising from the small size. Nanoparticles differ from their parental material in physical, mechanical as well as chemical properties due to quantum confinement and large surface area to volume ratio. Zinc oxide nanoparticles (ZnO NPs) are one of the most largely produced and used nanoparticles worldwide. They are commonly used in sunscreen, diapers, shampoos and food packaging. As the nanotechnology sector advances, newer applications have been proposed for ZnO NPs, which include drug delivery, phototherapy, biosensors, neural prosthesis and animal husbandry. Exposure risk of ZnO NPs increases with the increased industrial production and commercial use. Safety and toxicity of nanoparticles is a major concern and goal of nanotoxicology is to ensure safer applications of nanoparticles as well as to predict the unwanted outcomes.

It has been reported that ZnO NPs is highly toxic to liver, kidney, heart and lungs. The toxicity is mainly attributed to high dissociation and reactive oxygen species (ROS) generation. The neurotoxic potential of ZnO NPs is a less explored area and the existing literature mainly concentrates on the neurons and neuronal progenitor cells

(NPCs), as they are the primary cells in signal transduction. Neurons are unable to perform many metabolic functions independently however, glial cells ensure the normal functioning of the brain. They are the major class of brain cells that deals with homeostatic and metabolic functions and include astrocytes and microglia. Astrocytes are the principal cells involved in the brain metal homeostasis and neuronal nourishment. Astrocytes are an integral part of blood brain barrier (BBB) and provide an ample environment for neuronal functioning. Microglia on the other hand, are the chief scavenger cells of the brain. Oxidative burst in microglia often leads to leakage of free radicals in the extracellular space, damaging other cells in the vicinity. Both glial cell activation and dysfunction are linked with neurodegenerative diseases like Alzheimer's and Parkinsonism.

Glial cells are the first cells to encounter any foreign substance reaching the brain. The interaction of glial cells with nanoparticles is not explored much among the scientific community. Hence an effort was made to study the interaction of brain astrocytes with Zinc oxide nanoparticles. Based on the available literature the present study hypothesised that interaction of ZnO NPs with astrocytes can lead to inflammatory, immuno and neurotoxicological response in rat. Three objectives were formulated to test the hypothesis. The detailed objectives are given below;

- **Objective I**: Synthesis and characterization of ZnO NPs.
- **Objective II**: Nano-bio interactions *in vitro* using glial cells
    - Phase 1: Interaction of ZnO NPs with BV2 and C6 glial cells.
    - Phase 2: Interaction of ZnO NPs with rat primary astrocytes

- **Objective III**: *In vivo* acute toxicity studies using Wistar rats. Target organ toxicity, immunotoxicity, toxicokinetics, bio-distribution, histopathology and elemental analysis.

The thesis comprises of six chapters. The background and relevance of the study is given in the **first** introductory **chapter**. This chapter has briefed on nanotechnology, nanoparticles and major mechanisms of metal oxide nanotoxicity. It gives an idea about the physicochemical properties contributing to nanotoxicity. An introduction of neurotoxic potential of metal oxide nanoparticles and major glial types (astrocytes and microglia) are outlined in this chapter. The significance of ZnO NPs and its toxic potential are also mentioned here.

Second chapter emphasize on the review of literature. This chapter explained the existing literature on the application, synthesis strategies and toxicity of ZnO NPs. Published results on the neurotoxic potential of ZnO NPs are briefly discussed here. Importance of glial cells in brain functioning and brain pathologies is also discussed in this chapter.

Third chapter details the materials and methodologies adapted to fulfil the objectives. This chapter is divided into three major sections corresponding to three objectives. The first objective describes the synthesis and characterization of ZnO NPs. The wet precipitation synthesis of ZnO NPs using two sets of experimental condition is explained. Physicochemical characterization of ZnO NPs was carried out using transmission electron microscopy (TEM), scanning electron microscopy (SEM), dynamic light scattering (DLS), zeta potential measurement, thermogravimetric analysis

(TGA), Brunauer-Emmett-Teller (BET) analysis, X-ray diffraction (XRD) and X-ray photoelectron spectroscopy (XPS). Endotoxin content and protein corona formation were determined as a part of biological characterization.

The second objective includes, cell-nano interactions by *in vitro* methods, and is further divided into two phases. The first phase explains *in vitro* studies using microglial and macroglial cell lines, BV2 and C6 respectively. The cells were exposed to different concentrations of ZnO NPs for 3, 6 and 24 h. The cytotoxicity of BV2 cells were analysed using MTT and trypan blue exclusion assays. Particle uptake by the cells and morphological changes were studied using flow cytometry and phase contrast microscopy respectively. Generation of ROS in the presence of ZnO NPs was studied using fluorescence probe DHE and DHR123. Griess reagent assay was used to estimate nitrile radical. Mitochondrial membrane potential (MMP) and lysosomal stability was studied using $DIOC_6$ (3) and acridine orange (AO) respectively. The extend of cell membrane damage and cell cycle pattern changes were studied using propidium iodide (PI) staining. Mechanism of cell death was assessed by Poly ADP Ribose Polymerase (PARP) cleavage and DNA ladder assay.

The cytotoxicity was also estimated at 3, 6 and 24 h by MTT and neutral red uptake (NRU) assays in C6 cell line. Cell phenotype was assessed by Giemsa staining as well as rhodamine phalloidin staining. ROS generation was studied fluorometrically using DCFH-DA. MMP changes in presence of ZnO NPs were assessed by JC1 probe. Flow cytometry analysis of annexin V/PI staining was used to study cell death.

Second phase of this section describes the isolation and characterization of primary astrocytes and its cytotoxicity in presence of ZnO NPs. The cells were isolated from 0-2 day old rat pups and characterized subsequently. Dose response and lethal concentration 50 (LC_{50}) was calculated from the MTT and NRU assays. Total cell count was determined from the Trypan blue exclusion method. Particle uptake was assessed by flow cytometry and the cellular phenotype was studied by Giemsa and actin stains. Changes in membrane permeability were evaluated using PI counterstained with calcein AM. The MMP changes and lysosomal stability were determined using JC1 and AO respectively. DCFH-DA and Griess reagent was used for the estimation of free radicals. Annexin V/PI and caspase activity detection kit were used to study apoptosis. Cytotoxicity imparted by zinc salt ($ZnCl_2$) and bulk formulations of ZnO was compared with ZnO NPs to study the role of ZnO NPs dissolution and size on cytotoxicity. MTT, NRU, trypan blue, Caspase activation and Clonogenic assay assays were used for the comparative study.

The third objective of this study explains the bio- nano interaction of ZnO NPs using the Wistar rat. The rats were divided into two groups and exposed to a single dose of (10mg/ml) of ZnO NPs both via intraperitoneal (i.p.) and intravenous (i.v.) administration. Body weight and behavioural patterns of the animals was documented regularly. Three animals from each group were sacrificed on 3^{rd}, 14^{th} and 21^{st} day of exposure. Urine and blood samples were collected prior to sacrifice. The gross pathology, histopathology and antioxidant estimations were carried out. Blood samples were subjected to haematology and biochemistry analysis. The brain, spleen, liver,

kidney, urine and faecal samples were subjected to inductively coupled plasma (ICP) analysis to study the biodistribution and kinetics of the ZnO NPs. Immunological response was analysed by splenocytes proliferation assay. Brain volume was measured to determine the oedema and BBB integrity.

The fourth and fifth chapter details the results and discussion respectively. Both of these chapters are divided into three sections each. The first section describes the characterization of ZnO NPs of two different morphologies. The particles ZnO R and ZnO SP were named after the morphologies they exhibit. ZnO R exhibits rod shaped morphology with a size average of 40 nm, whereas ZnO SP exhibits spearhead shaped morphology with an average size of 20 nm. The High resolution TEM (HR-TEM) images of both ZnO R and ZnO SP did not indicate any crystal defects. BET analysis showed a specific surface area of 37±0.61 and 49±0.31m^2/g for ZnO R and ZnO SP respectively. TGA analysis of ZnO R revealed a 4% weight loss between 200°C -300°C. Similarly, ZnO SP exhibited a 3% weight loss between 100°C -450°C. These weight losses corresponded with surface adsorbed water and atmospheric molecules. XRD analysis showed crystal phase purity of ZnO R and ZnO SP with an average crystal size of 45 and 20 nm respectively. XPS analysis showed traces of impurities for ZnO R whereas ZnO SP was devoid of any impurities. Endotoxin content in the samples was less than 0.05EU/ml. ZnO SP was selected as a material of interest (here after named as ZnO NPs) for the present study because it exhibited a better purity and dispersity. ZnO NPs exhibited protein corona formation which was influenced by the nature of biological media and time of exposure.

The second section corresponds to the ZnO NPs interaction *in vitro*, which is further divided into two phases. The first phases describe the toxicity of ZnO NPs on BV2 and C6 cell lines. Particle uptake in both cells was proved by flow cytometry analysis. BV2 cells showed a time and dose dependent cytotoxicity in response to ZnO NPs. Cell density was severely affected in treated samples at 6h. Morphological analysis showed vacuolization and disintegration of cells at 24h of exposure. Estimation of superoxide radical, H_2O_2 and reactive nitrogen species indicated ZnO NPs mediated sudden oxidative burst in BV2 cells. A dose and time dependent increase in lysosomal membrane permeabilisation (LMP) was also observed. MMP measurement showed an initial hyperpolarisation at 6h, which declined by 24h of incubation. Membrane permeability was severely affected in BV2 cells exposed to ZnO NPs. No changes in cell cycle patterns or presence of apoptotic marker population (sub G1) were observed in ZnO NPs exposed cells. The lack of cleaved PARP and DNA ladder formation further confirmed the absence of apoptotic mode of cell death in BV2 cells.

MTT and NRU assays with C6 cells exhibited a time and dose dependent toxicity. Both 40 and 80 µg/ml treatment groups showed changes in cellular phenotype at 6h and 24h. Mitochondrial clumping and dose dependent loss of MMP was evident in all the treated samples. A time and dose dependent change in ROS generation was observed and was influenced by high incidence of catalase activity in glial cells. The dose dependent increase in annexin positive cells, nuclear condensation and cytoplasmic blebbing indicate ZnO NPs induced apoptosis.

The second phase of the second section explains the cytotoxicity on primary astrocytes. The cells isolated from 0-2day old rat pups were identified as astrocytes by staining with GFAP. The primary astrocytes exhibited time and dose dependent toxicity in response to ZnO NPs and the LC_{50} was around 60µg/ml. Nuclear and cytoplasmic modifications were seen in presence of high concentrations (40 and 80 µg/ml) of ZnO NPs. ZnO NPs exposure resulted in the disintegration of stress fibres and changes in focal adhesion points, which indicated cytoskeletal rearrangement. A dose and time dependent decrease in cell number was observed in treated groups. The cells showed MMP loss and LMP at 6h of treatment. Mitochondrial clumping was evident in all treated groups. No nitrile radical formation was detected in the presence of ZnO NPs, however a dose dependent increase in ROS production was evident. ZnO NPs induced caspase mediated apoptosis in astrocytes as revealed by annexin positive cells and caspase 3/7 activation assay. The clonogenic assay showed loss of cell survival capacity in ZnO NPs treated groups. The ZnO NPs and $ZnCl_2$ exhibited higher toxicity compared to the bulk counterparts. It was found that the nanoparticles elicited toxicity both by ROS generation and particle dissolution, whereas the bulk counterparts induced toxicity by the release of Zn^{2+} ions.

The third section explains the results of *in vivo* bio-nano interaction study. The animals (rats) injected with ZnO NPs did not show any neurotoxicity. No loss of body weight was observed in treated animals except 14^{th} day i.v. injected ones. Haematological parameters were normal in treated animals. Elevated serum SGPT and SGOT levels indicated loss of cellular integrity which was further confirmed by the

atrophic lesions in the histology of liver. Liver antioxidant levels were also elevated on the 14th day of observation. Zinc content showed a slight increase on 3rd day which reverted to normal state by 14th day. Both iron (Fe) and copper (Cu) content of liver was altered in treated groups. Normal histology and splenocytes proliferation rate indicated absence of toxicity in spleen. Comparable levels of serum creatinine and urea in both control and test group indicated normal kidney function which was further supported by urine histopathology analysis. No marked difference in zinc content was observed in the kidney. The initial reduction in iron and copper contents were reverted to normal state by the 14th day in i.v. administered animals. Brain volume and histology did not show any evidence of toxicity. Brain antioxidants were comparable in both control and treatment group except for glutathione reductase (GR). Elemental analysis of brain showed similar amount of zinc in both control and treated group whereas, altered iron content was observed in i.v. injected animals.

The sixth and final **chapter** is summary and conclusion of the study. Nano formulations of ZnO NPs with different morphologies were synthesized successfully. The physicochemical characterization ensured highly pure, endotoxin free form of nanoparticles for the bio-nano interaction studies. *In vitro* studies showed time and dose dependent toxicity on glial cells. Plasma membrane integrity, cytoskeletal structure, lysosomal stability and mitochondrial activity were severely affected in astrocytes exposed to ZnO NPs. The microglial cells were more sensitive to ZnO NPs than astrocytes. The mode of cell death was different in cell systems when exposed to ZnO NPs. The microglia underwent caspase independent necrotic mode of cell death, whereas

astrocytes manifested caspase dependent apoptosis. Both particle dissolution and free radical formation contributed to the *in vitro* toxicity. Extend of cytotoxicity was influenced by the physicochemical characteristics of nanoparticles. A single administration of ZnO NPs (10mg/ml) did not induce neurotoxicity in rats but enhanced hepatic toxicity. No toxicity was observed in the spleen and kidney. The administration of ZnO NPs leads to altered metal homeostasis. The present study concludes that ZnO NPs at relatively small concentrations are capable of inducing toxicity. Hence, appropriate safety measures may be recommended while handling the ZnO NPs to prevent unforeseen outcomes

CHAPTER 1: INTRODUCTION

1 INTRODUCTION

Nanoscience is the study of structures, atoms, molecules and materials whose size is 1 to 100 nm on the nanometre scale and nanotechnology deals with manipulating materials at an atomic scale. Nobel laureate **Richard Feynman** laid foundation to nanotechnology with his famous lecture "There's Plenty of Room at the Bottom" in an American Physical Society meeting at the California Institute of Technology (CalTech) on December 29, 1959.Prof. Feynman addressed the scientific community to 'think small' even long before the term nanotechnology was coined. The field of nanotechnology began to expand to newer dimensions, with the advancement of electron microscopy techniques. Nanotechnology has emerged as a hot topic of research in science by the end of 20th century. The promise of nanotechnology is the development of novel products with unique characteristics and its applications are growing rapidly in every field of science and technology. With the advancement of nanotechnology, novel and innovative nanoparticles are being formulated and launched in the market for various industrial and biomedical applications (Bao *et al.* 2013). Nanoparticle based products such as electronic devices, optical devices, sensors, clothes, sunscreens, food and medicines are already a part of our daily life. According to nanotechnology Consumer Product Inventory (CPI) there was around 54 manufacture identified nanotechnology products in 2006 which has grown to more than 1600 products by 2015 (Vance *et al.* 2015).

1.1 NANOPARTICLES

Nanoparticles are the materials having a size less than 100nm, at least in one dimension (Auffan *et al.* 2009) and it differs from the parent material in physical, chemical and mechanical properties. At nanoscale (1-100nm) quantum effect rule the property and behaviour of the particle. This implies that the optical, electrical, magnetic and chemical properties of nanoparticles change as a function of size. The quantum properties give tunability to the nanoparticles and hence the aforementioned properties may be manipulated by changing the size of the particles. Gold nanoparticle is a typical example of size dependent properties of nanoparticles. The colour of the gold nanoparticles in suspension changes as the size varies with in the 1-100nm scale (Wolfbeis 2015). Nanoparticles possesses high surface reactivity compared to their parent particles because of their high surface area to volume ratio.

Nanoparticles can be natural or anthropogenic in origin. The naturally occurring nanoparticles includes volcanic ashes, sand, dust particles, oceanic spray and biological matters like viruses and prions. Anthropogenic nanoparticles comprises of engineered nanoparticles, diesel exhaust particles, welding and combustion fumes (Buzea *et al.* 2007). Nanoparticles are broadly classified into inorganic and organic nanoparticles. Organic nanoparticles include polymer based nanoparticles, liposome, protein based nanoparticles, dendrimers and hydrogels. Inorganic nanoparticles constitute one of the most widely used and studied nanoparticles. These include metals, metal oxides, semiconductor nanoparticles, some minerals and silica.

1.2 NANOTOXICOLOGY

The concept of toxicology begins with the classical Paracelsus theory, where exist a linear relationship between the dose and toxicity. Nanotoxicology is a relatively new branch of toxicology which deals with toxicity of nanoparticles. This branch of toxicology emerged long after the commercialization of many nanotechnologies derived products. The nanoparticles do not show a linear relationship between dose and toxicity and as result it is impossible to design nanotoxicological studies using classical toxicology methods. Consequently, one of the major challenges encountered in nanotoxicology is the lack of internationally validated and harmonized guidelines/protocols.

The risk of nanoparticles exposure increase with the its wider application. Exposure occurs both at occupational as well as consumer level. Occupational exposure to nanoparticles happens through, dermal penetration, ingestion and inhalation of the fine particles at work place. Consumer level exposure is possible when a person accidentally ingests or inhales the nanoparticles containing products. More over the leachates from nanoparticle based products may cause environmental toxicity (Nohynek *et al.* 2008). The intentional exposure includes all biomedical interventions involving nanoparticles such as use of nanoparticles as diagnostics, imaging and treatment modalities (Choi and Wang 2011).

Nanoparticles mediated toxicity is mainly due to the induction of reactive oxygen species(ROS). The ROS generated further induces inflammatory responses, genotoxicity, fibrosis, mitochondrial damage, membrane damage, as well as lysosomal

destabilization (Manke *et al*. 2013). Apart from these outcomes, nanoparticles may induce direct mechanical injury to the cells and organisms. For example graphene induces toxicity by mechanical damage of the cell membrane (Manke *et al*. 2013).

1.3 BACKGROUND OF THE STUDY

Metal oxide nanoparticles are separate class of nanomaterials that are produced at the industrial scale. Major metal oxide nanoparticles include zinc, titanium, iron and silver oxide nanoparticles. One reason for their popularity is the ability to form particles of varying shapes and sizes according to the synthesizing conditions. Metal Oxide nanoparticles exhibit unique properties owing to its small size and high edge surface sites. The smaller size leads to change in surface properties, chemical reactivity, crystalline parameters, stability, electrical properties and other physico-chemical characteristics (Fernández-García and Rodriguez 2011).

Metal oxide nanoparticles are widely used in industrial as well as health care applications (Mueller and Nowack 2008). There are several products containing metal oxide nanoparticles such as iron nanoparticles based MRI contrast agents and cosmetics containing zinc and titanium oxides. Many of the nanoparticles are investigated for tumour therapy, drug deliver, gene delivery and bio-sensing applications. Exposure risk of nanoparticles increases with its increasing use and applications. Humans get exposed to nanoparticles from the ambient air, consumer goods, manufacturing process and by intentional administration in the form of drugs and diagnostic modalities. The same physico-chemical properties which give them enormous bio application potential also give rise to their toxicity.

1.3.1 MECHANISM OF NANOPARTICLE TOXICITY

Nanoparticle toxicity, consider the interaction of nanoparticles with biological system as a function of its physico-chemical properties. Metal oxide nanoparticles constitute the lion share of all nanoparticle based products. Nanoparticles may interact with the biological system in unpredictable ways due to its small size, high surface area to volume ratio and quantum confinement. For instance, gold is an inert material whereas gold nanoparticles are highly reactive (Panyala *et al*. 2009). Being smaller in size these nanoparticles can travel throughout the body and access otherwise highly protected sites like cell nucleus, blood brain barrier and placenta(Kessler 2011). The nanoparticles entry to the cell is mainly by endocytosis. Lin *et al.,* reported that nanoparticles can directly enter the cells bypassing endocytosis. They interact with lipid membrane to induce structural defects in the membrane. Moreover, large surface area of nanoparticles results in exposure of more reactive sites at the surface of nanoparticles which in turn leads to the high surface reactivity.

The nanoparticles upon interacting with biological system induce ROS generation and oxidative stress mediated damage. These include damage in proteins, DNA and lipid membrane as well as inflammation. Cells possess inherent antioxidant mechanisms to normalize the ROS generated during normal metabolisms. In presence of nanoparticles, the ROS generation may go beyond the capacity of cellular antioxidant machinery. Nanoparticles act as pro-oxidants molecules by generating ROS and have ability to inhibit antioxidant molecules. The following are the different mechanism of ROS production.

1. Direct interaction of nanoparticles with acidic compartments like lysosomes, results in toxic ions release and subsequent ROS production by chemical reaction.
2. Nanoparticles interfere with mitochondrial electron transport chain and oxidative phosphorylation resulting in ROS generation.
3. Nanoparticles interact with redox active enzymes like NADPH oxidase leading to oxidative stress.
4. Nanoparticles may interact with cellular receptors triggering the downstream signalling pathways like NF κB activation.

Other possible outcomes of nanoparticles interaction include particle dissolution to release toxic ions which can also affect the normal functioning of the biological system (Soenen *et al.* 2011). The nanoparticle dissolution inside cellular compartments disrupts the metal homeostasis and the ions released may interfere with enzyme activities. Perinuclear localization of nanoparticles hinders the functioning of transcription and translation process of the cells. Many mRNA stabilizing enzymes have metal responsive domains which get activated in presence of metal ions and thereby disturbing the transcriptome. The nanoparticles like gold alter gene expression profile of cells by directly interacting with DNA as well as by induction of oxidative stress. Moreover, nanoparticles adsorb proteins on its surface forming protein corona. The adsorbed proteins may undergo conformational changes that are no longer recognized as native by the immune system leading to immune reactions. The mechanism of nanoparticle toxicity is summarized in the **Figure.1.1.**

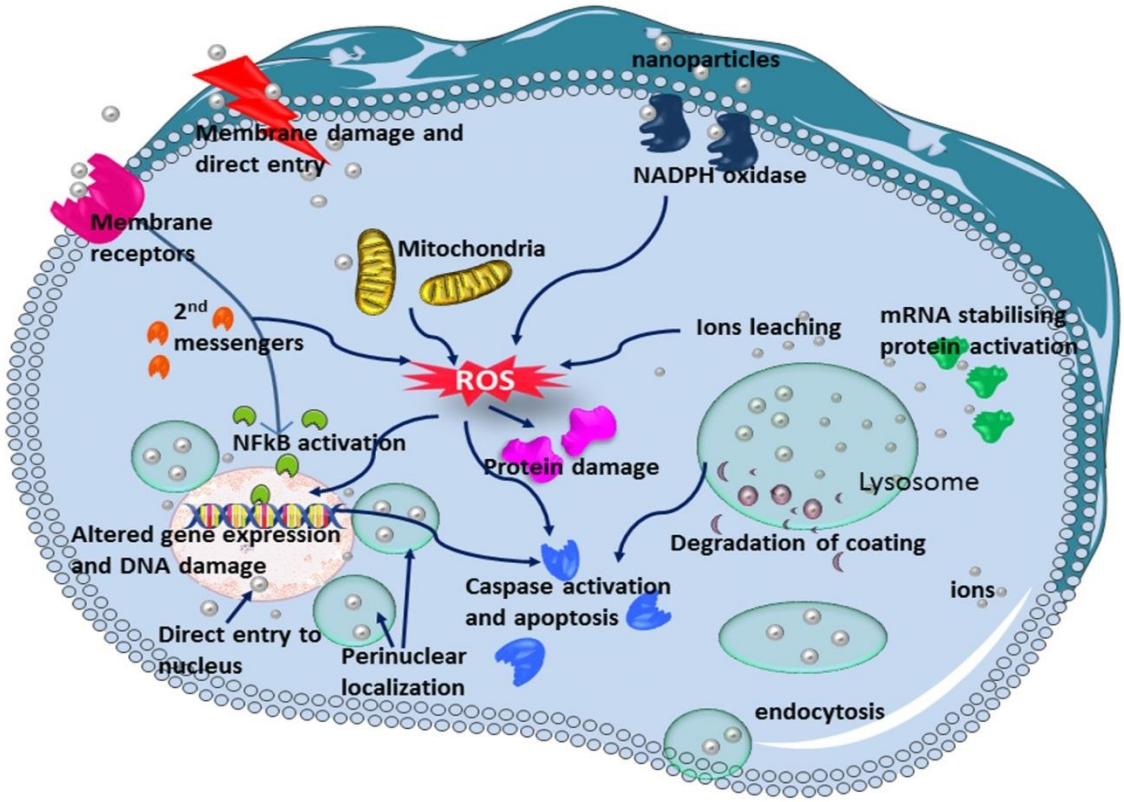

Figure 1:1: Mechanisms of nanoparticle toxicity

1.3.2 FACTORS INFLUENCING NANOPARTICLE TOXICITY

The physico-chemical characteristics of nanoparticles such as size, shape, crystallinity, surface chemistry, stability, aggregation and agglomeration statuses influence its interaction with the biological system. Hence it is very essential to use completely characterized nanoparticles for the study. The size and surface composition of nanoparticles influence their adsorption, distribution, metabolism and excretion and toxicity (ADME &T) inside the body. The means and extend of internalization of nanoparticles is influenced by the particle size. Smaller particles are taken up more efficiently when compared to larger particles. Increased particle uptake may lead to a

dose dependent alteration in membrane permeability and mitochondrial activity besides DNA damage and apoptosis. Shapes of the particles are another factor that influences the toxicological interaction. Studies suggest that the spherical particles are internalized more effectively by the cells than the rod and sheet shaped particles (Zhu *et al.* 2012). However, rod and fibre shaped particles elicit more toxicity because of the large surface area possessed by them to interact with the cellular moieties(Hsiao and Huang 2011). Nanoparticle toxicity is also affected by the pH of the dispersed medium. Metal oxide nanoparticles show high dissolution at acidic pH. For instance, CuO nanoparticles show high toxicity at acidic pH than alkaline pH due to particle dissolution(Chang *et al.* 2012). The crystallinity of the nanoparticles is a factor controlling ROS generation. TiO_2 nanoparticles of different crystalline phases were found to induce ROS at different rates with amorphous phase generating highest ROS and rutile samples the lowest (Jiang *et al.* 2008). Surface coating and surface charge of the nanoparticles also influence the particle uptake and toxicity. Coated ZnO nanoparticles show less toxicity in human hepatic stellate cells compared to bare ZnO NPs (Osmond-McLeod *et al.* 2014). Cellular uptake pathways of nanoparticles are charge independent. However cells exhibit better affinity for cationic nanoparticles and are taken up at a higher extend (Fröhlich 2012). The particle aggregation and agglomeration are yet another factors contributing to toxicity of the nanoparticles. The nanoparticle aggregation is an undesired trait with regard to biomedical application, as the larger aggregates or agglomerates reduces the bioavailability and retention of the nanoparticles in the biological system (Zhu *et al.* 2012). However, from toxicological perspective, particle aggregation leads to less

toxicity and efficient clearance by the biological system. Different metal oxide nanoparticles in same cell system may follow identical uptake pathway yet elicit varied biological response, depending on the properties of the particles(Xia *et al.* 2008). Various physicochemical factors contributing to the toxic bio-interaction are depicted in **Figure 1.2**.

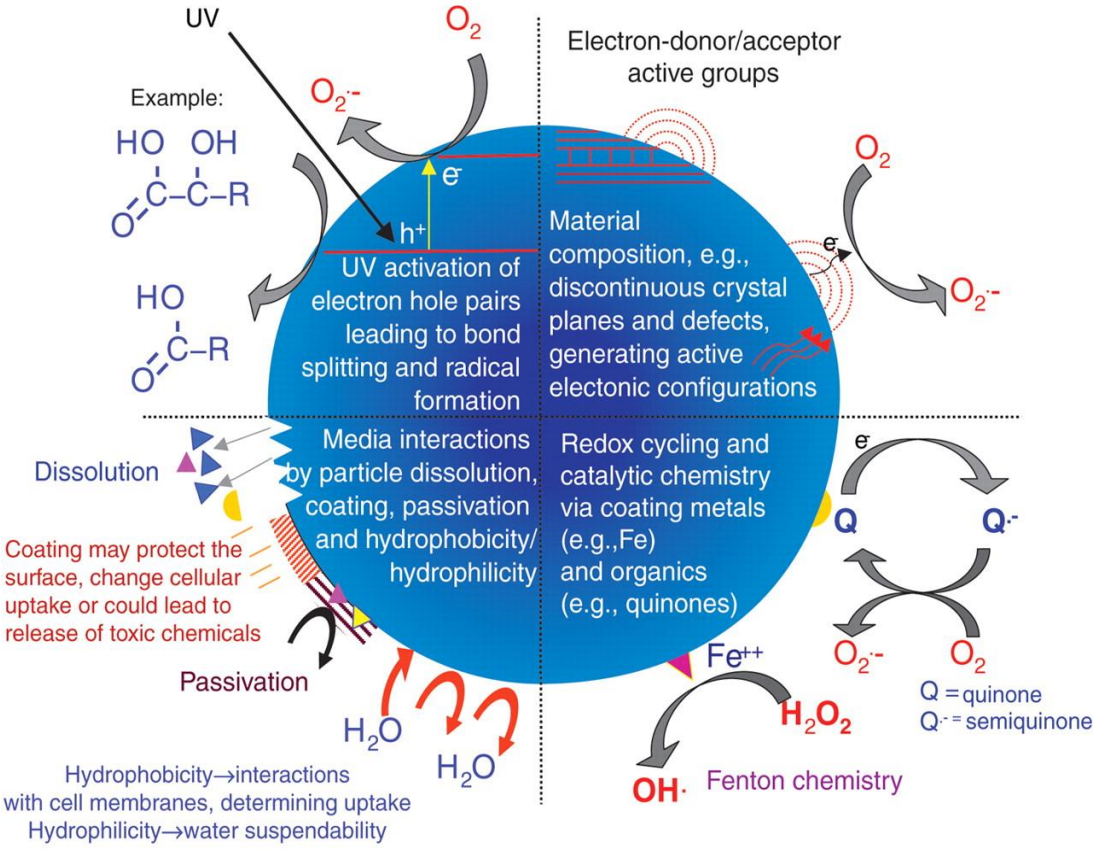

Figure 1:2: Factors contributing to nanoparticle toxicity. Adapted from (Nel *et al.* 2006)

There are different routes of nanoparticle entry to the body such as oral, dermal, inhalation and parenteral routes. Apart from the conventional routes, nanoparticles may

also enter the system via hair follicles and olfactory neuronal pathways (Oberdörster *et al*. 2009). Out of all the portals of entry, the respiratory route is considered as the major route of entry in accidental exposure nanoparticles. There are number of nanotechnology based consumer goods that have found places in our daily life like wrinkle free cloths and body sprays containing silver and zinc nanoparticles (Kessler 2011). This fact should be read along with the findings that the nanoparticles reaching the body via inhalation can translocate to other organs like heart, liver, kidney, and brain via systemic circulation (Geiser and Kreyling 2010). Hence the biological interactions of nanoparticles have to be thoroughly scrutinized before its extensive application to ensure its biosafety.

1.3.3 NEUROTOXICITY OF NANOPARTICLES

Even though the nanotoxicology has made much progress in elucidating the mechanism of toxicity under various exposure scenarios, not much is known about its neurotoxic potential. The inhalation of ultra-fine particles in the ambient air has been linked to neurodegenerative diseases (Oberdörster *et al*. 2004). Recent research shows that the nanoparticles reach brain via systemic circulation and the olfactory neuronal pathways (Kozlovskaya *et al*. 2014). Brain is a highly protected entity due to the critical function it performs in the body. The entry of molecules to brain is tightly regulated by the presence of special barrier called blood brain barrier (BBB). The BBB has tight junctions and low level of paracellular transport. Only particles less than 8nm cross the BBB via free diffusion. Because of the smaller size, nanoparticles may translocate across BBB via systemic circulation and interfere with the normal functioning of the

brain. In a study conducted by Takeda *et al*., nanoparticles were found to translocate from mother to foetus and induced cranial nerve dysfunction in the offspring (Takeda *et al*. 2009). Some nanoparticles are reported to induce transient opening of the BBB (Lockman *et al*. 2008) which results in the entry of larger particles into the brain. Evidences are also accumulating on the olfactory neuronal pathway of nanoparticle translocation(Oberdörster *et al*. 2004). **Figure 1.3** shows potential pathways of nanoparticle mediated neurotoxicity. Nevertheless, major share of existing data comes from *in vitro* studies, which concentrate mostly on the neuronal cells. Studies on other cells types of the brain like glia and oligodendrocytes are still lagging behind. Toxicological interactions of nanoparticles with these cells have to be evaluated as they protect and provide ambient conditions for the proper functioning of neurons.

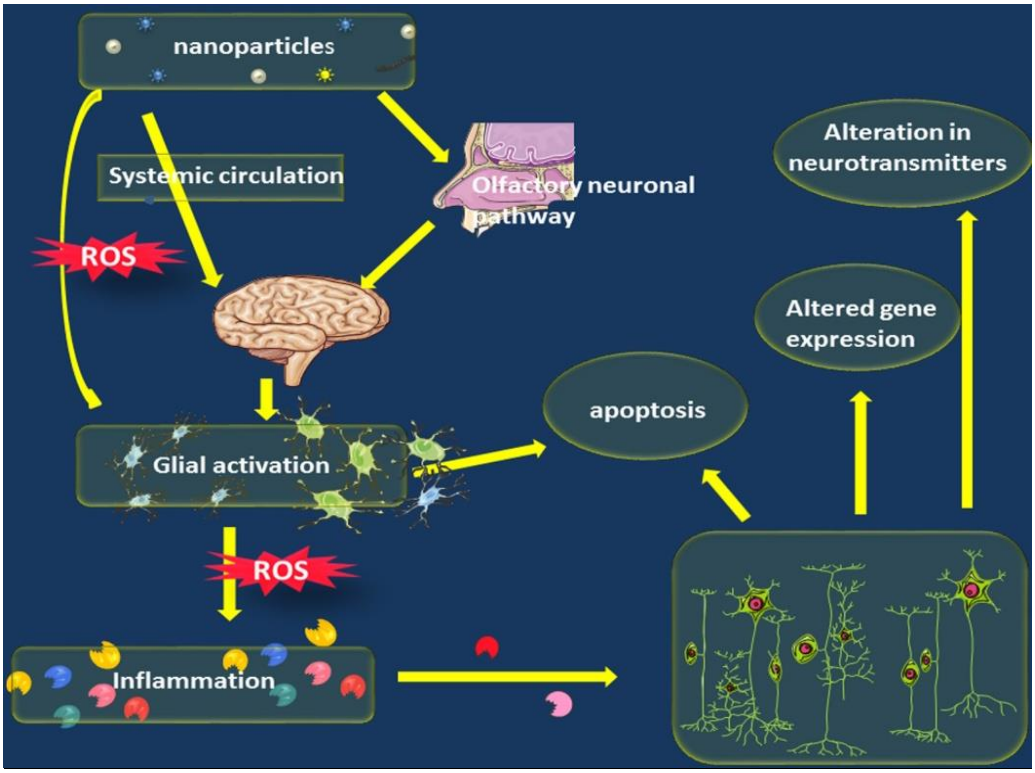

Figure 1:3: Mechanism of nanoparticle neurotoxicity

1.3.3.1 Glial cells

Glia as the name reveals were earlier thought as mere binding cells of the brain which holds the nerve cells together. Later it was understood that these cells perform important roles in brain without which brain stops functioning. There are three different kinds of glial cells in central nervous system (CNS) which are astrocytes, microglia and oligodendrocytes. These cells coordinate in conjunction with neurons to provide normal brain functions. **Figure 1.4** shows cells of the brain and their association with each other.

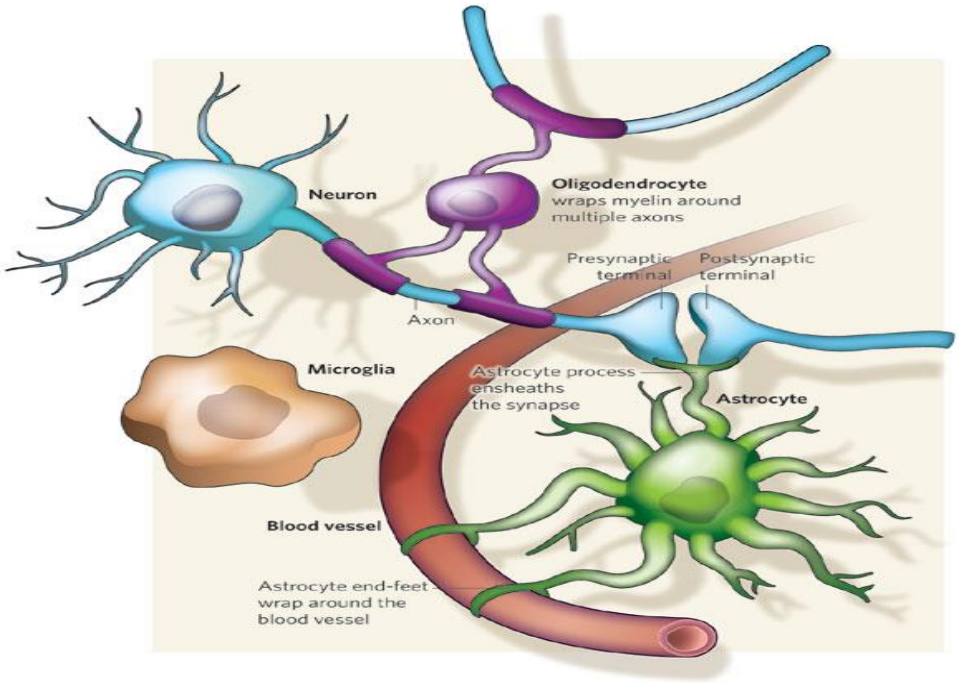

Figure 1:4: Brain cell interaction. Adapted from (Allen and Barres 2009)

1.3.3.1.1 Astrocytes

Astrocytes (also known as macroglia) are the house keepers of the brain. The increase in number, size and complexity of astrocytes across higher forms of animals

indicates its importance in brain functions. These star shaped cells are involved in metal homeostasis of the brain. The brain contains high concentration of metal ions like iron and zinc when compared to rest of the body. These ions are required for nerve signalling, are integral part of many metabolic processes, act as cofactors of enzymes in biosynthetic pathways and in cell cycle regulation. Astrocytes regulate the storage and release of these ions by synthesising metallothioneins and ferritins that bind to the free ions (Zatta *et al*. 2009). Apart from mineral homeostasis, astrocytes play diverse housekeeping functions such as metabolic compartmentation and nurturing of neurons. Astrocytes regulate synaptogenesis, synaptic pruning, maturation and maintenance of synaptic connections. It also regulates blood flow in the brain via Ca^{2+} flux. Astrocytic metabolism of neurotransmitters like GABA helps in terminating nerve signals. CNS injuries and neurodegenerative conditions are linked to dysregulation of metal homeostasis and astrocytes activation called reactive astrogliosis (Sofroniew 2009).

1.3.3.1.2 Microglia

Microglia are the primary immune cells of the brain and constitute about 10-15% of the total cells in brain. Microglia share many properties with tissue macrophages. During brain pathologies these glial cells undergo activation and produce ROS (Liu and Hong 2003). The response of microglial cells to environmental toxins may bring much complicated outcomes in the brain. Microglial cells possess, pattern recognition receptors on their surface. These receptors can transduce the foreign toxic signals to ROS production. Apart from producing ROS, microglial cells possess chemo-secretory functions, which lead to release of chemokines and associated inflammatory response in

the brain. On the brighter side, these cells remove cellular debris and pathogens from the brain and help to keep brain clean. The exact role of these cells are debated, with evidence put forth towards the protective functions as well as pathological role (Kigerl *et al.* 2014).

1.3.3.2 Glial cells and nanoparticles

Exposure to environmental toxin is linked with neurodegenerative diseases. Glial cells maintain the ambient conditions required for the proper functioning of the neurons. For the same reason, glial cells are the first to encounter any external insults targeting brain. In a post-mortem study on glioma patients treated with thermotherapy, the nanoparticles and their aggregates were mostly sequestered in microglia with a minor uptake by astrocytes. No particles could be detected in neurones (van landeghem 2009). Such external stimuli result in glial cell activation and subsequent release of inflammatory cytokines and ROS generation. This in turn leads to secondary toxicity in response to the external stimuli. The role of aluminium, zinc and copper ions' accumulation on neurodegenerative conditions like Alzheimer's disease are reported elsewhere (Zatta *et al.* 2009). Glial cell activation is a hallmark of neurotoxicity and nano-glial cell interaction studies are of extreme importance as the nanoparticles cross BBB and release toxic ions.

1.4 MOTIVATION OF THE STUDY

Risk factors of nanoparticles include their exceptional ability to breach biological barriers like BBB and placenta, besides their unpredictable behaviour in biological system. It has been reported that nanoparticles localises in brain to induce oxidative

stress and protein aggregation/fibrillation (Zaman *et al.* 2014).Both oxidative stress and fibrillation has been linked to neurodegenerative pathologies. Increased incidence of neurodegenerative diseases worldwide, emphasize on the relevance of addressing nanoparticles mediated neurotoxicity.

ZnO NPs are one of the industrially produced nanoparticles and contain covalently bonded zinc and oxygen arranged in a wurtzite crystal structure. ZnO NPs are wide band gap semiconductor (energy gap 3.37eV at room temperature) used for UV absorption, photo catalysis, sensor manufacturing and photo-electronic devices. Moreover, many biomedical applications like drug delivery, phototherapy and bio-sensing have been envisaged for ZnO NPs (Wang 2004). Different applications of ZnO NPs have been summarised in **Figure 1.5**.

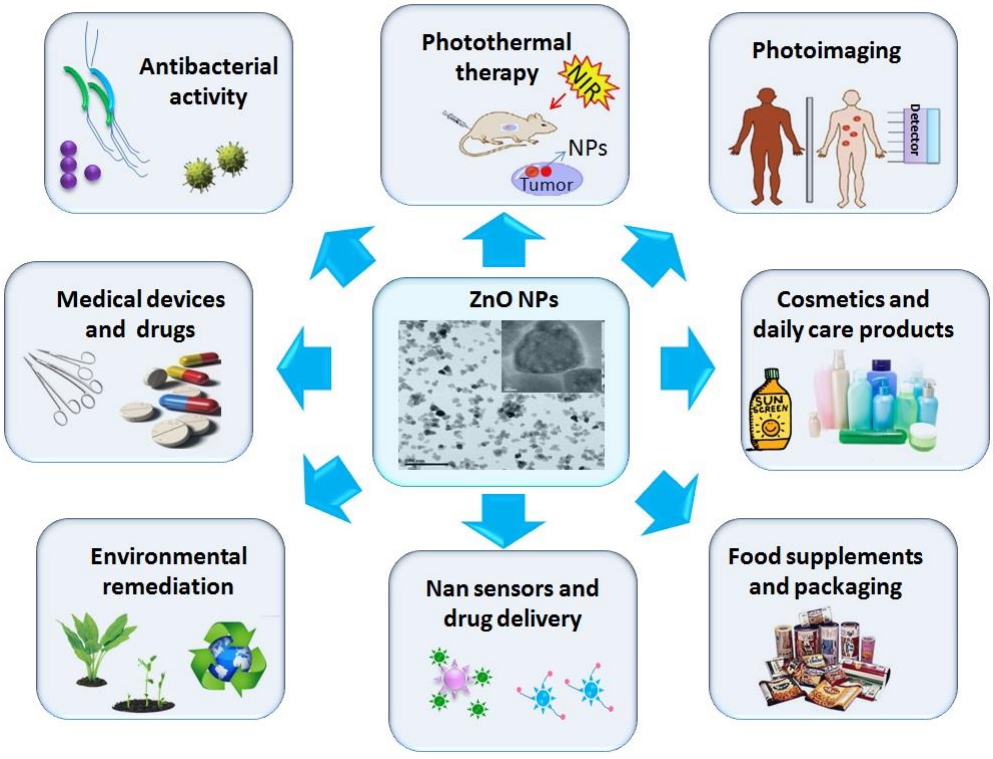

Figure 1:5: Applications of ZnO NPs

Human exposure to ZnO NPs increased because of its wide application in cosmetics and daily care products. The Food and Drug Administration (FDA) do not require manufactures to analyse the nanoscale ingredients for safety, if the bulk material is already proven safe (Duvall, 2012). However existing research data clearly suggests that the nanoparticles have physical, chemical and biological properties entirely different from the bulk counterpart. It was reported that ZnO NPs is highly reactive and induce ROS mediated single stranded DNA breaks at a relatively low concentration of 10µg/ml (Chang *et al.* 2012). It is assumed that the low concentrations ZnO NPs in the existing products are safe however, there is no evidence to confirm that this concentration is safe in the long run. The greatest risk is for people working in nanoparticles manufacturing units, where exposure is too high. Another vulnerable group is foetus and children whose cells divide at a much faster rate and making them more susceptible to ROS mediated DNA damages.

Being a nanoparticle of extreme demand, the toxicity studies on the ZnO NPs have received much attention. The toxicological interaction of ZnO NPs has been elucidated by researchers all over the world. Most of them attribute the toxicity to particle dissolution and ability to induce ROS. However, a very few studies have been devoted to neurotoxic potential of ZnO NPs. It has been reported that exposure of ZnO NPs induce cytotoxicity in neuronal progenitor cells and neurons (Deng *et al.* 2009). The ZnO NPs interact with neurons affecting the voltage gated channel and synaptic plasticity. Kao *et al.*, has reported the *in vivo* olfactory neuronal pathways of ZnO NPs entry in the brain and associated inflammation response (Kao *et al.* 2012).

Most of the studies concentrate on the neurons/ associated brain pathologies. Studies on the bio-nano interactions of glial cells with ZnO NPs are not much explored. Neurodegenerative conditions to external toxicants mediated glial cell activation and disruption of mineral homeostasis have received much attention recently (Robert *et al.* 2015). The finding of Amara *et al.*, (2015) stated that ZnO NPs reaching the brain, disrupt the copper and iron balance (Amara *et al.* 2015). Based on the above findings it was decided to study direct interaction of ZnO NPs with glial cells, which are of extreme importance in assessing the neurotoxic potential.

1.5 OBJECTIVES

Zinc oxide nanoparticles are present in large number of consumer products. The safety/toxicity of this nanoparticle is not fully studied at the moment. The ZnO NPs mediated toxicity has been demonstrated in many cell lines however, neurotoxic potential of this nanoparticle is not much known. Available data shows that the ZnO NPs is toxic to neurons and have genotoxic potentials even at sub lethal concentrations. The interaction of glial cells with nanoparticles is not much explored among the scientific community. Glial cells are involved in the zinc homeostasis and are the first to encounter any foreign body reaching the brain. Hence an effort was made to study the interaction of brain astrocytes with zinc oxide nanoparticles. Based on the available literature the present study hypothesises that the interaction of astrocytes with ZnO NPs may lead to inflammatory, immuno and neurotoxicological response in rat. The present study has three objectives to achieve the hypothesis. The detailed objectives are given below;

- **Objective I**: Synthesis and characterization of ZnO NPs.
- **Objective II**: Nano-bio interactions *in vitro* using glial cells
  - Phase 1: Interaction of ZnO NPs with BV2 and C6 glial cells.
  - Phase 2: Interaction of ZnO NPs with rat primary astrocytes
- **Objective III**: *In vivo* acute toxicity studies using Wistar rats. Target organ toxicity, immunotoxicity, toxicokinetics, bio-distribution, histopathology and elemental analysis

Biological interaction of nanoparticles depends heavily on its size, morphology, crystallinity, purity and surface chemistry, thus it is important to use completely characterized nanoparticles for biological studies. The bio-interaction studies using commercially available nanoparticles often leads to inconsistent results due to unknown specifications. In the present study two different batches of ZnO NPs were synthesized and characterized for a better understanding of the bio-nano interaction. The cellular interaction of ZnO NPs was studied using both microglia as well as astrocytes (macroglia). The biological techniques were standardized using immortalized glioblastoma cells called C6. BV2 cells were used for the microglial interaction studies. BV2 cells are immortalized microglial cells which exhibit phenotype, similar to that of primary microglia. The interaction of ZnO NPs with macroglia was studied using rat primary astrocytes. The cytotoxicity of the nanoparticles was studied at different time points using different concentrations. The results were compared with that of bulk ZnO and $ZnCl_2$ to see, if the nanoformulation of ZnO behaves differently from their bulk and

ionic counterparts. Also the *in vivo* biodistribution and toxicokinetics of ZnO NPs were studied in rats after acute exposure. The study is summarized in the **Figure 1.6.**

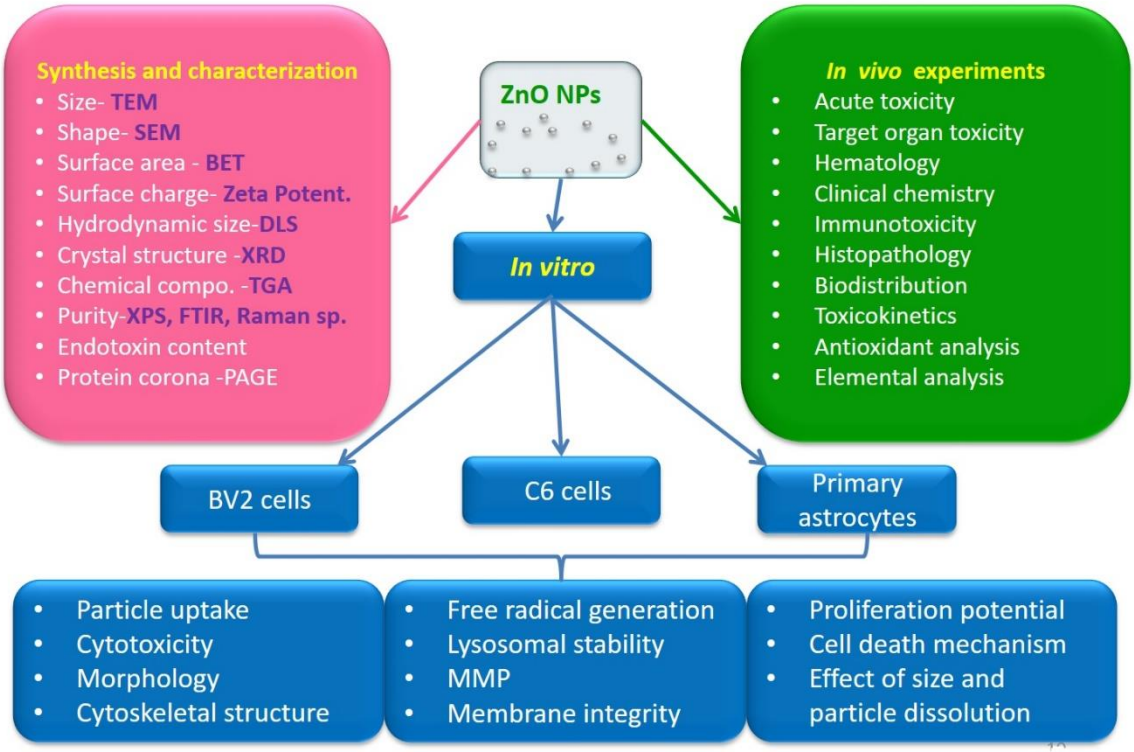

Figure 1:6: Experimental design of the thesis

1.6 THESIS OUTLINE

This thesis is divided into six chapters. The **first introductory chapter** gives an overview of the background and significance of the study. The chapter briefs about nanoparticles, factors influencing nanoparticles toxicity and mechanism of toxicity. A concise description about neurotoxic potential of nanoparticles and role of glial cells in neurotoxicity are emphasised in this chapter.

The **second chapter** is the **review of literature** available on the topic. The chapter reviews available literature on the synthesis and applications of ZnO NPs. This

chapter briefs about mechanism of nanoparticles toxicity and glial cell involvement in ZnO NPs mediated neurotoxicity.

The **third chapter** includes **materials and method** and is divided into sections. The first section deals with synthesis and characterisation of ZnO NPs. The wet precipitation synthesis of ZnO NPs using two different set of reagents and temperature was carried out and physico-chemically characterised. Preliminary cytotoxicity evaluation of the synthesised material carried out using L929 cells is also described. The second section describes the cell nano interaction studies *in vitro*. The first part of this section evaluates the *in vitro* toxicity of ZnO NPs with rat microglial and astrocytic cell line BV2 and C6 respectively. Second part of this section deals with *in vitro* nano cell interaction studies using rat primary astrocytes. The isolation and characterisation of the primary astrocytes and cytotoxicity evaluation of these cells using various assays are detailed here. The third section of this chapter represent nano bio interaction studies using rats. This section dedicates to the biodistribution studies and toxicokinetics of ZnO NPs. The two modes of exposure and related pathological changes in the internal organs are explained in this section.

The **fourth chapter** represents **results** of the study. This chapter is divided into three sections. The first section details results of synthesis and characterisation of ZnO NPs. The second section has two parts. The first part explains the outcomes of the cellular interaction studies using BV2 and C6 cell lines. The second part of this section illustrates the cell characterisation and interaction of ZnO NPs with primary astrocytes. The third section of this chapter explains the fate of ZnO NPs in the *in vivo* system. The

biochemical, immunological and histopathological changes in response to ZnO NPs and the organ distribution, quantification and retention of nanoparticles are explained in this section.

The **fifth chapter** is on **discussion of the results**. This chapter is again divided in to three sections. The first section discusses the results obtained for ZnO NPs synthesis and characterisation. The second section elaborates on the results obtained for the cell nano interaction *in vitro*. The first part suggests the mode of cell death in different cell lines and details the cellular and molecular mechanism underlying ZnO NPs interaction with BV2 cells. The second part of this section proposes the cytotoxicity mechanism of ZnO NPs with primary astrocytes. The outcomes of the ZnO NPs interaction with glial cells are explained in this section. The third section elaborates the finding on the biodistribution, toxicokinetics, immunotoxicity and histopathology.

Summary and conclusion of the work is detailed in the sixth chapter.

CHAPTER 2: REVIEW OF LITERATURE

2 REVIEW OF LITERATURE

2.1 ZnO NANOPARTICLES (ZnO NPs)

ZnO NP is a white odourless powder with a molecular weight of 81.38g/mol. It is a wide band gap semiconductor (3.37eV at room temperature) with wurtzite crystal structure (**Figure 2.1**). ZnO NPs are used for both industrial and biomedical applications owing to their unique electrical, optical, catalytic and photochemical properties. These properties are easily tuned according to the requirements, by changing the size, doping with other compounds and by adjusting the synthesizing conditions (Taratula *et al.* 2006).

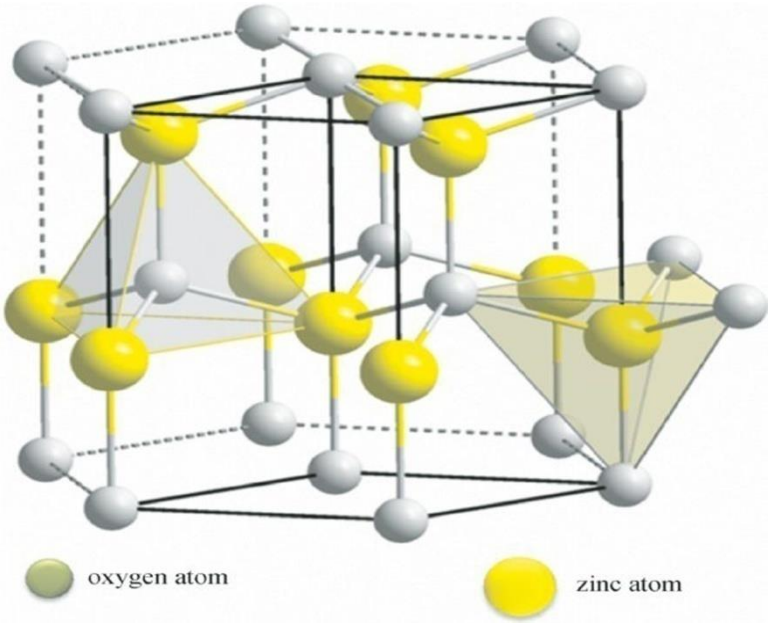

Figure2:1: Wurtzite crystal structure of ZnO NPs. Adapted from https://commons.wikimedia.org/w/index.php?title=File:Wurtzite_polyhedra.png&oldid=161320121

One of the most attractive features of the ZnO NPs is that, nanostructures with unique morphologies like nanohelix and nanorings will be synthesised easily and cost

effectively (Wang 2004). Some of the morphological structures exhibited by ZnO NPs are summarised in the **Figure 2.2.**

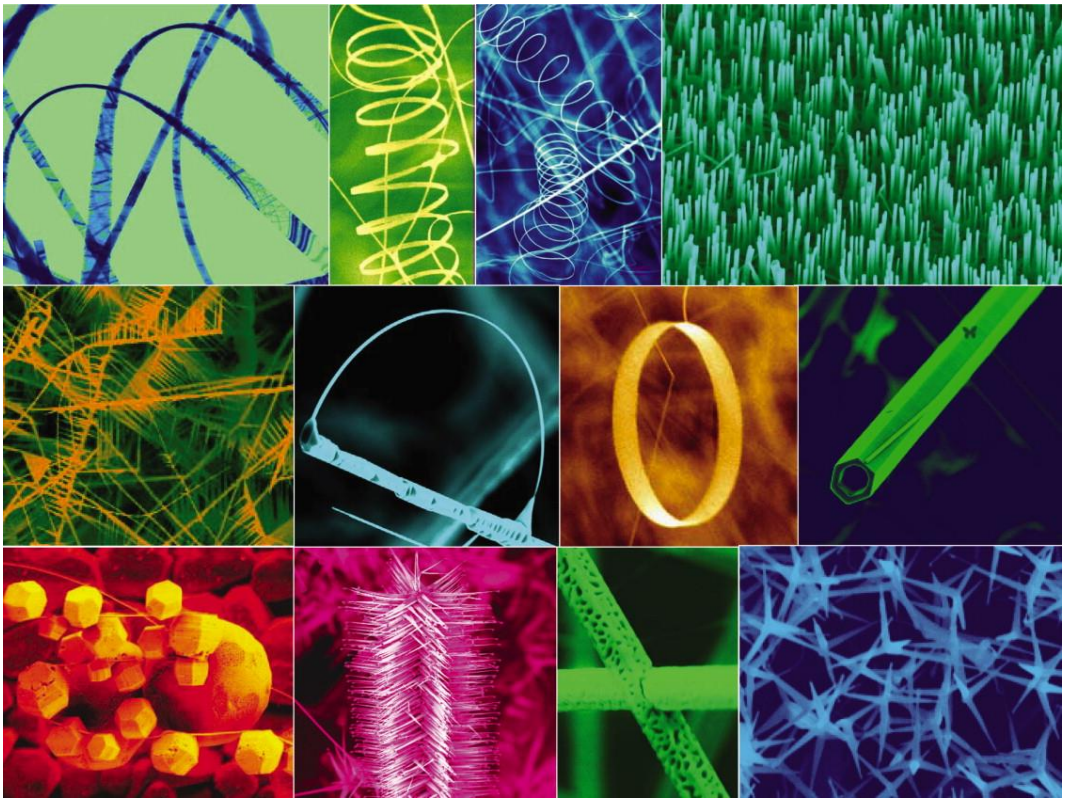

Figure 2:2 Morphologies exhibited by ZnO NPs. Adapted from (Wang 2004)

ZnO NPs have hydroxyl groups attached to its surface. At acidic pH the surface moieties get protonated to form $ZnOH_2^+$ that gives a positive charge for the particle. At alkaline pH the surface gets deprotonated to form negatively charged ZnO^-. The ZnO NPs have an isoelectric pH of ~9 (Degen and Kosec 2000), meaning the particle exhibit a net positive charge throughout the physiological pH. A number of ZnO NPs based products are available in the market. ZnO NPs have good gas sensing properties and are used for manufacturing gas sensors (Kumar *et al.* 2015). These nanoparticles are most commonly used in rubber and ceramic industry to improve the toughness and aberration

resistance. It is an important constituent of cosmetic products as a UV blocking agent. Apart from that ZnO NPs are used in food packaging, ointments and daily care products due to its antimicrobial and antifungal properties.

2.2 SYNTHESIS OF ZnO NPs

ZnO NPs may be synthesized by both physical and chemical methods. Physical method involves synthesis by spray pyrolysis, vapour deposition, laser ablation and thermal decomposition. One advantage of the physical method over chemical method is that it does not require washing, drying and calcinations to obtain pure nanoparticles. However, this method often requires costly vacuum system and experimental conditions. The quality of the nanoparticle is low compared to chemical method.

By chemical method nanoparticle with high purity and narrow size distribution can be synthesized cost effectively using optimal reaction conditions. Nanoparticle of different size with novel electrical, optical, mechanical and chemical properties are synthesised by chemical method. Different chemical methods have been described in literature for the synthesis of ZnO NPs such as:

- Sol – gel method,
- Microemulsion synthesis
- Hydrothermal/solvothermal synthesis and
- Wet precipitation.

The size, morphology and uniformity of the particles depend on the synthesizing conditions like solute concentration, temperature, pressure, reagents, method of addition

of the particle and pH. Several reports indicate that more tunable materials are obtained by chemical method synthesised (Kołodziejczak-Radzimska and Jesionowski 2014).

2.2.1 SOL GEL METHOD

This method involves formation of the ZnO NPs network through hydrolysis and polycondensation reactions of a molecular precursor in a liquid to form a colloidal suspension (Sol). The sol undergoes subsequent gelation creating ZnO NPs network in a continuous liquid phase (gel). The gel is dried to remove the liquid phase and resulting ZnO NPs is subjected to further processing. The synthesized nanoparticles are used for various optoelectronic and thin film coating applications (Li *et al*. 2005). On the other hand, this method involves the usage of organic solvents and is not environmental friendly.

2.2.2 MICROEMULSION

Microemulsions are homogeneous in macroscale and microheterogeneous in nanoscale. It is a dispersion of two immiscible liquids consisting of nano-sized domains of one or both liquids in the other, stabilized by an interfacial film of surface active molecules. This method involves mixing two microemulsions containing metal salt and a reducing agent respectively to form ZnO NPs. The exchange of reactants between micelles takes place by Brownian movement and van der Waals forces. The size and morphology of the particles are influenced by temperature, substrates and the ratio of two-phase components. Particles with any size and morphology are synthesized by this method. On the other hand the method involves the use of surfactants and organic

solvents and often require calcinations to form high quality nanoparticles (Kołodziejczak-Radzimska and Jesionowski 2014).

2.2.3 HYDROTHERMAL METHOD

This method is a simple bottom-up approach that involves use of precursor molecules dissolved in water to build nanoparticles. The process is carried out in a closed reaction vessel under controlled conditions (temperature between 100 to 300°C) that aids in the chemical reaction between the precursors. This environmental friendly method does not involve use of organic solvents and additional processing of precursor molecules. Hydrothermal, green method is used to synthesis single crystals for advanced applications.

2.2.4 WET PRECIPITATION METHOD

It is relatively easy to synthesize a variety of particles having different structure and properties with wet precipitation method in comparison with hydrothermal method. ZnO NPs are either directly precipitated from the reaction mixture or follow a metastable state of $Zn(OH)_2$ and is subsequently converted into ZnO. The following are the reaction equation; (Moezzi *et al.* 2011)

$$Zn^{2+}_{(aq)} + OH_{(aq)} \rightarrow Zn\,OH)^{+}_{(aq)}$$

$$Zn(OH)^{+}_{(aq)} + OH_{(aq)} \rightarrow Zn(OH)_{2(s)}$$

$$Zn(OH)_{2(s)} \leftrightarrow Zn(OH)_{2(aq)}$$

$$Zn(OH)_{2(aq)} + OH_{(aq)} \rightarrow Zn(OH)^{-}_{3(aq)}$$

$$Zn(OH)^{-}_{3(aq)} + OH_{(aq)} \rightarrow Zn(OH)^{2-}_{4\,(aq)}$$

$Zn(OH)_{2(aq)} \rightarrow ZnO_{(s)} + H_2O_{(l)}$

$Zn(OH)_{2\,(s)} \rightarrow ZnO_{(s)} + H_2O_{(l)}$

$Zn(OH)^{-}_{3(aq)} \rightarrow ZnO_{(s)} + H\,2O_{(l)} + OH_{(aq)}$

$Zn(OH)^{2-}_{4(aq)} \rightarrow ZnO_{(s)} + H_2O_{(l)} + 2OH^{-}_{(aq)}$

Different parameters like pH of the system, solubility, nature of reactants, temperature, reactant stoichiometry and method of combining the reactants influence the size, morphology and purity of the ZnO NPs synthesized.

2.3 BIOMEDICAL APPLICATION OF ZnO NPs.

2.3.1 ANTIBACTERIAL AGENT

ZnO NPs possess antibacterial properties due to photo-catalysis and generation of ROS. They have positive surface charge there by bind to the negatively charged bacterial membrane and enter the cells by endocytosis. Differential mechanisms has been reported for the bactericidal properties of nanoparticle, including the direct destruction of bacterial cell wall, release of Zn^{2+} ions and damage of cellular metabolism (Sirelkhatim *et al*. 2015). Antibacterial agents containing ZnO NPs are used in dental composites (Aydin Sevinç and Hanley 2010) and daily care products such as mouthwash, diapers and shampoos (Hernández-Sierra *et al*. 2008).

2.3.2 CANCER THERAPY

ZnO NPs are proposed to be an effective cancer therapeutic agent. It exhibit preferential toxicity on cancer cells compared to normal cells (Hanley *et al*. 2008). ZnO NPs, owing to its strong positive charge at physiological pH easily enter the cancer cell

as they possess large amount of negatively charged molecules on their surface. Moreover the cancer cells are highly sensitive to the ROS, resulting in an elevated toxicity and apoptosis compared to normal cells (Rasmussen *et al*. 2010).

2.3.3 BIO- IMAGING

ZnO NPs exhibit intrinsic fluorescence properties with excitonic emission at near-UV, blue and green regions. Compared to the other fluorescent probes, ZnO NPs exhibit high stability and reduced photo-bleaching (Wu *et al*. 2008). ZnO NPs with fluorescent properties are used for the imaging of cancer cells and bacteria by functionalizing with appropriate receptor molecules (Sudhagar *et al*. 2011; Wang *et al*. 2009). Functionalization aids in site specific accumulation and detection of the cells or molecules of interest.

2.3.4 DRUG DELIVERY

ZnO NPs possess large surface area that provides more sites for surface functionalization. Smaller size of ZnO NPs helps in increasing the drug retention time and reducing the drug load. ZnO NPs reported to be used for delivering carcinoembryonic antigen to the dendritic cells without losing the property of the antigen (Cho *et al*. 2011). Yuan *et al* has reported the use of chitosan coated ZnO NPs for doxorubicin delivery into cancer cells (2010). They are also used as a constituent in nanocarriers systems for drug delivery applications, where it undergoes dissolution in acid vesicles to release the drug from the carrier. For eg., ZnO NPs are proposed as nanolids in silica nanoparticle used for drug delivery (Muhammad *et al*. 2011).

2.3.5 GENE DELIVERY

Gene therapy is a promising field for the treatment of many deadly clinical conditions like cancer and neurodegeneration. The ZnO NPs are investigated as an agent for gene delivery applications. One of the major challenges in this sector is developing a proper vector that protects the DNA and its effective delivery to the site of interest (Zhang and Liu 2010). The morphology of ZnO NPs modified to form tetrapodes like phage vectors. This act as a vehicle for effectively delivering plasmid DNA into the cells (Nie *et al.* 2006).

2.3.6 BIOSENSORS

Nanoparticles possess high density of reactive sites due to high surface area. This property is exploited in sensor applications, where biological moieties (e.g. enzymes) are immobilized on the surface of nanoparticle to detect other molecules in the system (Ansari and Husain 2012). ZnO NPs are one of the widely used nanoparticles for biosensor application due to number of reason such as easiness in fabrication, polymorphic nature, optical properties and high electron mobility. Moreover ZnO NPs have a high isoelectric pH of 9.5, making it possible for protein adsorption via electrostatic interaction (Xu *et al.* 2013). ZnO NPs were successfully demonstrated to detect acetylcholinesterase (Wang *et al.* 2014), glucose (Hwa and Subramani 2014), xanthine (Devi *et al.* 2012) and urea (Ali *et al.* 2009).

2.3.7 PHARMACEUTICAL AND COSMETIC APPLICATIONS

ZnO NPs are anti-inflammatory in nature and accelerate wound healing. It is used in dermatological applications like wound dressings, ointments and used as a restorative material in dentistry. Due to better uptake and retention, ZnO NPs are reported as a zinc supplement in animal feeds (Zhao *et al*. 2014). ZnO NPs are physical UV blockers widely used in sunscreens and also blocks UV-A and UV-B radiation. Nano-formulation of ZnO is transparent in light, compared to the white colour given by the bulk ZnO. This has increased the popularity of nanobased sunscreen (Smijs and Pavel 2011)

2.3.8 NEUROBIOLOGICAL APPLICATION

The ZnO NPs nanoparticles are used for the detection of neurotransmitters inside the brain. Zhao *et al*.,(2013)demonstrated usage of (3-aminopropyl) triethoxysilane (APTES) capped luminescent ZnO NPs for the detection of dopamine. ZnO NPs based sensors are proposed for the detection of acetyl choline (Zhang *et al*. 2014) and dopamine (Fang *et al*. 2014). The nanoformulation of ZnO NPs are used as a drug to deliver zinc (Zn^{2+}) across brain for anxiety disorders and depression (Torabi *et al*. 2013). ZnO NPs are reported as a zinc supplement to interact with opioidergic system and relieve pain. The analgesic property of ZnO nanoformulation is better than the bulk formulation (Kesmati and Torabi 2014). NGS are implanted in brain to enhance the central nervous system (CNS) repair in case of injuries. ZnO NPs are suggested as a component in nerve guidance channel (NGS). Presence of ZnO NPs enhances the

regeneration by stimulating the neurons and reducing the astrocytes cell adhesion (Seil and Webster 2008).

2.4 TOXICITY OF ZnO NPs

The ZnO NP mediated toxicity is demonstrated in a number of organisms. They show preferential toxicity towards gram positive bacteria such as *S. aureus* compared to gram negative bacteria like *E. coli* and *P. aeruginosa*. The differences in susceptibility is due to the cell wall compositions of gram positive and negative bacteria (Premanathan *et al.* 2011). ZnO NPs also hinders growth of algae (Ma *et al.* 2013). In a study conducted by Brayner *et al.*,(2010) ZnO NPs inhibited photosynthetic ability of cyanobacteria. Toxicity of ZnO NPs has been reported in a large number of higher plants including radish, lettuce, rye grass, corn, wheat and cucumber. ZnO NPs affect root elongation, and seed germination resulting in biomass reduction (Ma *et al.* 2013). Similarly toxicity has been reported in lower vertebrates like aquatic crustaceans (Blinova *et al.* 2010), earthworms (Khare *et al.* 2011), *C. elegans* (Khare *et al.* 2011), soil arthropods (Manzo *et al.* 2011) etc.,. ZnO NPs exposure affect the development and egg hatching in zebra fish (Bai *et al.* 2010).

The toxicity of ZnO NPs on mammals has been demonstrated both *in vitro* and *in vivo*. Inside the cells ZnO NPs undergo dissolution in lysosomes (Cho *et al.* 2011). Particle dissolution and ROS production leads to cytotoxicity, oxidative stress, lipid peroxidation, increased intracellular Ca^{2+} ion concentration, alteration in mitochondrial membrane potential, lysosomal destabilization, inflammatory cytokine release, DNA damage and cell death (Vandebriel and De Jong 2012). As a result of inhalation

toxicity, the ZnO NPs enters lungs and other parts of the body via systemic circulation and induce hazardous effect. The acidic nature of the lung fluids aids in particle dissolution and induce inflammation (Adamcakova-Dodd *et al*. 2014). ZnO NPs do not cause skin inflammation (Monteiro-Riviere *et al*. 2011). i.v. administration of ZnO NPs leads to systemic distribution in liver, spleen, lung, heart and kidney. The nanoparticle interaction causes histopathological lesions, oxidative stress and inflammation in tissues (Sruthi and Mohanan 2016) and neurotoxicity in old mice (Tian *et al*. 2015). The toxicity of ZnO NPs has been summarized in the **Figure 2.3**.

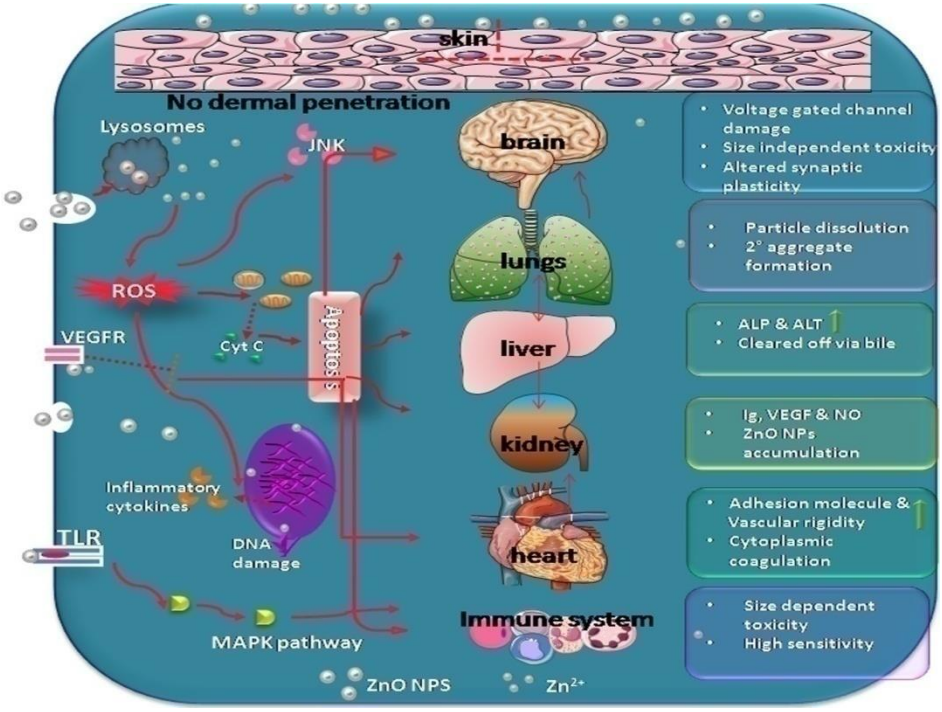

Figure 2:3: Toxicity induced by ZnO NPs

2.4.1 MECHANISM OF TOXICITY

There are several reports available on the toxicity of ZnO NPs and is mainly due to the particle dissolution and generation of ROS. Addition of antioxidants mitigated the

toxic effect of ZnO NPs (Punnoose *et al.* 2012). The iron doping increases the stability of ZnO NPs, resulting in decreased dissolution and reduced toxicity in zebra fish and rodent lungs (Xia *et al.* 2011). Dissolution of ZnO NPs in aqueous solution follows the equation (Yamabi and Imai 2002);

$$ZnO\ (s) + H_2O\ (l) \leftrightarrow Zn(OH)_2\ (s)$$

$$Zn(OH)_2 \leftrightarrow Zn(OH)^+(aq) + OH^-(aq)$$

$$Zn(OH)^+(aq) \leftrightarrow Zn^{2+}(aq) + OH^-\ (aq)$$

There are three main mechanisms of ZnO NPS induced toxicity which include the flowing;

2.4.1.1 Oxidative stress

The reactivity and ROS generation arises either from the activation of the electron hole pairs or from the crystal defects like oxygen vacancies and increased interstitial zinc (Kumar and Rao 2015). These nanoparticles directly interact with the biomolecules like lipid membrane to generate superoxide radicals. ZnO NPs and Zn^{2+} released by dissolution will interact with cellular organelles such as mitochondria and endoplasmic reticulum. The exposure of these nanoparticles results in loss of mitochondrial membrane potential and activation of MAPK pathways leading to apoptosis (Sharma *et al.* 2012). Interference of Zn^{2+} with electron transport chain further amplifies ROS production. Superoxide radicals generated by ZnO NPs are extremely powerful in destroying the bio-molecules. Superoxide radicals induce DNA damage and elevated death receptor gene expression (Yang *et al.* 2009). ROS generation disrupt the cellular equilibrium of oxidants and antioxidants leading to oxidative stress. Oxidative

stress results in increased intracellular Ca^{2+} concentration leading to mitochondrial perturbation and cell death (Xia *et al.* 2008). The toxic outcomes of ZnO NPs are detailed in **Figure 2.4**.

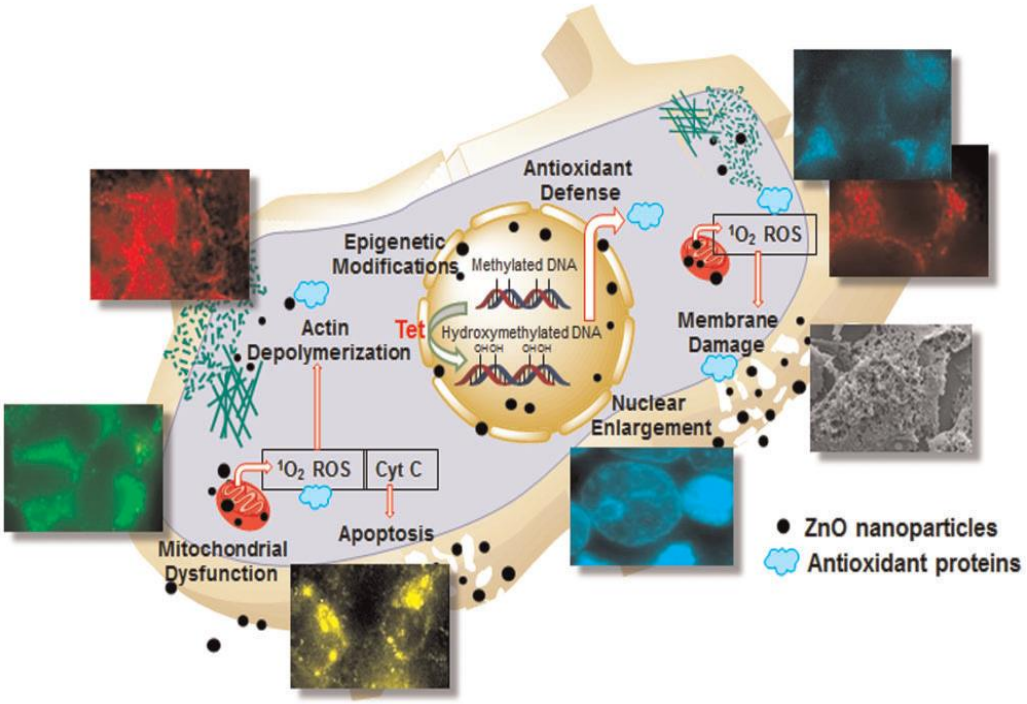

Figure 2:4: Free radical mediated toxic outcomes of ZnO NPs. Adapted from (Choudhury *et al.* 2017)

2.4.1.2 Coordination effect

ZnO NPs undergo dissolution inside the cells to release Zn^{2+}. Transition metal ions, like zinc and iron act as cofactors of many proteins and are crucial for the functioning of these enzymes. Zinc is a cofactor of nearly 300 enzymes in the body (Alam and Kelleher 2012). Zinc ions have the ability to form chelates with coordination molecules in the enzyme there by altering the catalytic function of the protein. Such interaction often results in structural and functional irregularities of the protein(Chang *et al.* 2012). For instance Zn^{2+} dislodge Mg^{2+} from the active sites and there by inactivating

the protein (Dudev and Lim 2008). Zn^{2+} interact with metal responsive domains of mRNA stabilising protein resulting in cellular mRNA disruption (Chang *et al.* 2012).

2.4.1.3 Disruption of homeostasis

The particle dissolution inside the cells leads to disruption of zinc homeostasis and ROS (Yan *et al.* 2012). Elevated zinc content subsequently lead to oxidative stress, protein folding, mitochondrial damage, lysosomal inactivation, enzyme inhibition, genotoxicity and cell death (Xia *et al.* 2008). Disruption of zinc homeostasis result in altered activities of zinc containing enzymes (Alam and Kelleher 2012).

2.4.2 PARAMETERS INFLUENCING ZnO NPS TOXICITY

2.4.2.1 Size

The toxic potential of a nanoparticle depends on its physicochemical properties. Size is a factor that determines the toxicity of ZnO NPs. As the size of the particle decrease more ZnO NPs are taken up by the cells leading to high toxicity (Bondarenko *et al.* 2013). A size dependent ROS generation and toxicity was demonstrated in a comparative study between commercially available ZnO NPs and its bulk counterpart (Zhang *et al.* 2014). however few scientific data suggest that ZnO NPs do not show a size dependent toxicity (Wiench *et al.* 2009). This is probably because, above certain concentrations the nanoparticle undergoes agglomeration and behaves like bulk particles. Size also influences the dissolution of the particle in aqueous solution with ZnO NPs undergoing more dissolution in comparison with bulk counterparts.

2.4.2.2 Morphology

Shape of the nanoparticles influences its toxicity. Nanosticks of ZnO NPs showed highest toxicity in comparison with spheres and cubes when zebra fishes were exposed to the nanoparticles (Hua *et al.* 2014). Similar result is available on lung fibroblast cells were nanorods are more toxic than the spherical forms of ZnO NPs (Hsiao and Huang 2011). high aspect ratio ZnO NPs showed high toxicity due to rapid dissolution inside acidic compartment (H. Müller *et al.* 2010).

2.4.2.3 Protein corona

Protein corona formation increases the stability of ZnO NPs and cellular uptake. The proteins adsorbed onto the surface of the nanoparticles include immunoglobulins, lipoproteins, albumin, α-1-antichymotrypsin, α-2-macroglobulin and transferrin (Deng *et al.* 2009). These proteins have important functions in the body and influence the biodistribution and cellular uptake of nanoparticles (Vandebriel and De Jong 2012). Protein corona formation induce ligand enhanced dissolution, where the adsorbed organic material and organic acid extract metal atoms from the surface of the ZnO NPs (Nel *et al.* 2009).

2.4.2.4 Surface chemistry

Surface charge and surface coating of nanoparticles influences the toxicity (Osmond-McLeod *et al.* 2014). Coating reduces ROS mediated damage in cells by masking the active sites on the surface of nanoparticles. However coated particles being more stable in suspension are actively taken up by cell organelles and induce genotoxicity by entering the nucleus (Yin *et al.* 2010). Positively charged ZnO NPs

induce more ROS than the negatively charged particle due to increased uptake of positively charged nanoparticle (Baek *et al.* 2011).

2.4.2.5 Route of exposure

Route of exposure influence toxicity exerted by nanoparticle. Biodistribution and kinetics are affected by the mode of entry of nanoparticles (Chang *et al.* 2012). For instance, nanoparticle exposed via i.v. injection do not cross blood brain barrier while oral and inhalation exposure leads to neurotoxicity. ZnO NPs do not penetrate skin and inhalation leads to lung inflammation and systemic toxicity. i.v. administration of ZnO NPs results in particle accumulation and foam cell formation in heart and blood vessels respectively (Sruthi and Mohanan 2016).

2.4.2.6 Other factors

Temperature and pH of medium influences the toxicity of ZnO NPs and low pH and high temperature favours particle dissolution. The composition of nanoparticle and impurities also control its toxicity(Chang *et al.* 2012). ZnO NPs doped with iron results in better stability and less toxicity (Xia *et al.* 2011). Trace elements and organic molecules present as impurities in the samples and in the dispersed medium are also influence the toxicity.

2.4.3 NEUROTOXICITY OF ZnO NPS

Zinc oxide nanoparticles are used in paints, cosmetics and electronic devices. Risk of ZnO NPs exposure is extremely high due to its widespread use in consumer products. However little is known about the neurotoxic potential of ZnO NPs (Yang *et*

al. 2013). Interaction of ZnO NPs has been elucidated *in vitro* but most of the literature focuses on neuronal cells. internalisation of ZnO NPs have been demonstrated in PC-12 cells where particle induced mitochondrial impairment and cell death (Kao *et al*. 2012). It also elicit dose dependent toxicity and apoptosis in neuronal stem cells (NSC) via particle dissolution (Deng *et al*. 2009),. These particles exposed to RSC96 rat Schwann cells, induced cell cycle arrest and reduction in cell viability. The toxicity was time, dose and shape dependent. The spheres exhibited maximum toxicity and induced apoptosis at 12h of exposure, whereas flower and prism shaped nanoparticle induced toxicity only on prolonged exposure (after 48h). The toxicity was attributed to ionic fraction of the zinc and not the nanosized particulate fraction (Yin *et al*. 2012). In human neuroblastoma SHSY5Y cells, ZnO NPs induced oxidative stress, genotoxicity, cell cycle alteration and apoptosis in a time and dose dependent manner. However the study failed to address the particle internalization by the cells (Valdiglesias *et al*. 2013).

Metal oxide nanoparticles reach brain either by breaching the BBB or via olfactory neuronal pathway. Translocation of ZnO NPs across brain via olfactory neuronal pathway has been shown by Kao *et al*. The particle accumulation in the olfactory bulbs of rats after 6h of exposure electron was shown in the electron micrographs of the brain (Kao *et al*. 2012). A minimal rise in brain zinc content was observed by Cho *et al*., on repeated oral administration of ZnO NPs (2013). In mice with depressive-like behaviour model, the ZnO NPs reached brain after oral and inhalation exposure, where it interfered with spatial learning and memory by altering synaptic plasticity (Xie *et al*. 2012). ZnO NPs up on i.v. administration provoke oxidative stress,

learning, memory impairment, inflammatory cytokine production and pathological lesions in brain in an age dependent manner (Tian *et al*. 2015). Repeated oral administration of ZnO NPs (600mg/kg body weight) results in oxidative stress and elevation of inflammatory cytokines in brain. Oral administration of antioxidant molecules was found to augment the toxicity of ZnO NPs (Ansar *et al*. 2016). Nevertheless, the dose administrated was too high to be correlated to a real life exposure scenario. In a sub-acute study, rats given i.p. injection of ZnO NPs manifested no indications of weight loss, behavioural changes or increased zinc content in brain. On the other hand, a statistically significant decrease in iron and calcium were observed in the brain tissue (Amara *et al*. 2015). These studies conclude that ZnO NPs exposure lead to both direct and indirect adverse outcomes in brain.

2.4.3.1 Glial cells in neurotoxicity

All the cells in the brain that do not have the ability to transmit electrical potential is broadly classified as glia (Allen and Barres 2009). Glial cells are an important class of cells in the brain that deals with homeostatic, metabolic and immune function. Astrocytes and microglia are the major glial cells of the brain. Microglia arises from the haematopoietic stem cells whereas astrocytes differentiate from the NSCs (Jessen and Mirsky 2005). Microglia are the resident immune cells of brain which scan the brain for infections and injuries. They enter the brain from circulation early in the development of the organism. Microglia aid in the synaptic remodelling by removing the neurons that undergo apoptosis during embryonic development. Apart from the phagocytic functions, microglia are reported to release trophic factors essential for

neuronal health. It has been hypothesized that the microglia sense and modulate neuronal activities via receptors. Microglia eradicate the foreign bodies by production of ROS (Colton and Gilbert 1987). Excess ROS generated in this process are either retained within the granules or released to the extracellular space. Mass activation of microglia in response to nanoparticle leads to oxidative stress and ROS mediated damage of neurons (Block and Hong 2005). When exposed to titanium oxide nanoparticles, the microglial cells exhibited sudden oxidative burst and loss of mitochondrial activity (Long *et al.* 2006). Microglial death has been linked to neurodegenerative diseases like Alzheimer's disease and Schizophrenia (Schlegelmilch *et al.* 2011). No studies have been reported on ZnO NPs interaction with microglial cells.

Astrocytes are the most abundant glial cells in the brain. They perform a verity of function in CNS ranging from axon guidance and synaptic support to control of BBB integrity and metal homeostasis (Blackburn *et al.* 2009). Astrocytes facilitate long term recovery during brain injury by surface molecule expression and release of trophic factor. Activation of astrocytes known as reactive astrogliosis is one of the major markers of stress and brain injuries. Astrogliosis is related to up regulation of an intermediate filament called glial fibrillary acidic protein (GFAP)(Chen and Swanson 2003). Nanoparticle mediated toxicity has been demonstrated on astrocytes. Repeated i.p. exposure to very low concentration (1mg/Kg) of aluminium oxide (Al_2O_3) nanoparticle induced up regulation of GFAP in rats. The effect was significant when compared to the bulk form of Al_2O_3 (Li *et al.* 2009). On the other hand TiONts induce

senescence and caspase mediated apoptosis in astrocytes (Márquez-Ramírez *et al.* 2012). Disruption of metal homeostasis and apoptosis in astrocytes has been associated with neurodegenerative diseases (Barreto *et al.* 2011). Studies on the interaction of ZnO NPs with glial cells are negligible in comparison with neurons. Preliminary studies indicate that the ZnO NPs are toxic to glioma cells (Ostrovsky *et al.* 2009). Since glial cells are involved in zinc homeostasis in brain, more studies have to be concentrated on the interaction of ZnO NPs with glial cells.

Glial cells tend to the neurons and ensure their normal functioning. Consequently any functional abnormality or physiological response of the glial cells to the injuries can magnify the neuronal damage (Streit and Xue 2009; Aschner *et al.* 2002). Moreover, glial cells play active role in barrier functions and immune functions of brain. Thus they are the first cells to encounter any nanoparticle reaching brain. Hence it is very important to study nanoparticle interaction with glial cells.

CHAPTER 3: MATERIALS AND METHODS

3 MATERIALS AND METHODS

3.1 CHEMICALS

Sodium hydroxide, zinc chloride, zinc sulphate, zinc nitrate, sodium nitrate, RPMI-1640 media, (3-(4,5-Dimethylthiazol-2-yl)-2,5-Diphenyltetrazolium Bromide)/ MTT, Griess reagent, Histopaque, sodium dodecyl sulphate (SDS), thiobarbituric acid, acrylamide, bis acrylamide, TEMED (Tetramethylethylenediamine), tris base, trypan blue, Evan's blue were purchased from Sigma (USA). Endosafe PTS kit was acquired from Charles River (USA). Anti-GFAP antibody, Anti-beta III tubulin antibody ab18207, O4 antibody, Goat Anti-Rabbit IgG H&L (Alexa Fluor 488) ab150077, Dil-Ac-LDL and Cytopainter phalloidin were obtained from Abcam (UK). DMEM F12, fetal bovine serum (FBS), antibiotic/antimycotic, glutamax, phosphate buffered saline, 0.25% trypsin were obtained from gibco®, Life technologies (USA), calcien AM, JC-1 Dye (Mitochondrial Membrane Potential Probe) and apoptotic DNA ladder kit was purchased from ThermoFisher Scientific (USA). 30% Hydrochloric acid suprepure, Coomassie brilliant blue and Folin's reagent were bought from Merck, India. Haematoxylin, eosin neutral red, propidium iodide, ethidium bromide and DAPI (4',6-diamidino-2-phenylindole) were purchased from Himedia, India. SensoLyte ® Homogeneous AMC Caspase-3/7 Assay Kit was procured from AnaSpec, USA. 3H-tritiated thymidine was obtained from American Radiolabelled Chemicals Inc. Diethylene triaminepenta acetic acid (DTPA) and pyrogallol were from Central Drug House (CDH) analytical reagents, India. Biochemistry reagents for urine and blood

analysis were purchased from Erbamannhiem (Germany). Reagents for haematological analysis were procured from Horiba (Japan).

3.2 EQUIPMENTS

Scanning Electron Microscopy (SEM): JEOL JSM-6400F (JEOL, USA). Transmission Electron Microscope (TEM): JEOL JEM-2100 LaB6 (JEOL, USA). Specific surface area by Brunauer–Emmett–Teller (BET): BELSORP-mini (MicrotracBEL, Japan). Dynamic Light Scattering (DLS) and zeta potential: Malvern Zetasizer Nano ZS (USA) supplied with DTSNano V4.2 software. Thermogravimetric analysis (TGA): TAG24 Setaram (France). X-ray Photoelectron Spectroscopy (XPS): PHI Vera saprobe 5000 (ULVAC-PHI, INC, Japan). X-Ray Diffraction (XRD) D8 Advance diffractometer (Bruker, USA) equipped with a Vantec linear detector. Inductively Coupled Plasma Atomic Emission Spectroscopy (ICP-AES), Optima 5300 DV ICP-OES spectrometer (Perkin Elmer, USA), Endotoxin content: Endosafe PTS. Fluorescent microscope (Axio Scope A1 Carl Zeiss, Germany), phase contrast microscope (Leica), Haematology analyser: Horiba Vet abc (Japan). Biochemistry analyser: Erba Mannheim XL300 (Germany). Urine analysis: Uro-dipchek 300 (Erba Mannheim, Germany). Microtome Leica RM 2125 RT, Germany. Tissues homogenizer: (Polytron P 3100 homogenizer, Switzerland). Scintillation counter (Hidex, Finland). Laminar air flow (Mark Air particulars, India). CO_2 incubator (Sanyo, Japan. Flow cytometry (FACS Aria III (BD Biosciences) and (DAKO GALAXY flow cytometer, Germany, controlled by ‘FloMax’ software (version 2.4; Partec, Münster, Germany)). UV Visible Spectrophotometer (UV 1601, Shimadzu, Japan, Lamda 25, PerkinElmer,

Singapore). Incubator shaker (New Brunswick Scientific, USA), Biophotometer (Eppendorf, Germany), Steam sterilizer (Nat Steel, India). Monochromator based multimode microplate reader (BioTeck Instruments, USA), Thermomixer (Eppendorff, Germany). Transilluminator, Bio Imaging system (Syngene, UK). Micro-plate reader (Says Expert plus, Austria). Refrigerated centrifuge (Eppendorf, USA),

3.3 ANIMAL HUSBANDARY AND WELFARE

Wistar rats and rat pups were procured from the Division of Laboratory Animal Sciences, Biomedical Technology Wing, Sree Chitra Tirunal Institute for Medical Sciences and Technology (Govt. of India), Trivandrum. Astrocytes were isolated from postnatal 0-2 day rat pups. Healthy Wistar rats weighing 200-250g were selected for *in vivo* bio-nano interaction studies.

The animals were maintained in a 12h light and dark cycle with constant temperature of 22 ± 2°C and relative humidity of 30-70%. Animals were provided with standard pellet diet and water *ad libitum*. Individual animals were identified by marking with picric acid. Additionally, each animal cage was labelled for name, experiment number, number of animal, date of commencement and end of experimental period. All the animals were acclimatized for a period of 5 days before beginning the experiments. The animals were routinely monitored for health by cage side observation. All the animals were handled humanely, without causing any pain or distress and with due care for their welfare. The care and management of the animals were carried out in compliance with the regulations of Committee for the Purpose of Control and Supervision of Experiments on Animals (CPCSEA).

3.4 ANIAML ETHICS

All the experiments were carried out after getting the approval from the Institute Animal Ethics Committee (IAEC). Animal experiments conformed to the guidelines of IAEC regulations which are approved by the CPCSEA, Govt. of India. IAEC approval No: IAEC approval No: SCT/IAEC-131/DECEMBER/2014/86.

3.5 ZnO NPs SYNTHESIS AND CHARACTERISATION

ZnO NPs of two different morphologies rod shaped and spearhead shapes were synthesised by wet chemical method by altering the experimental conditions as shown in **Figure 3.1**.

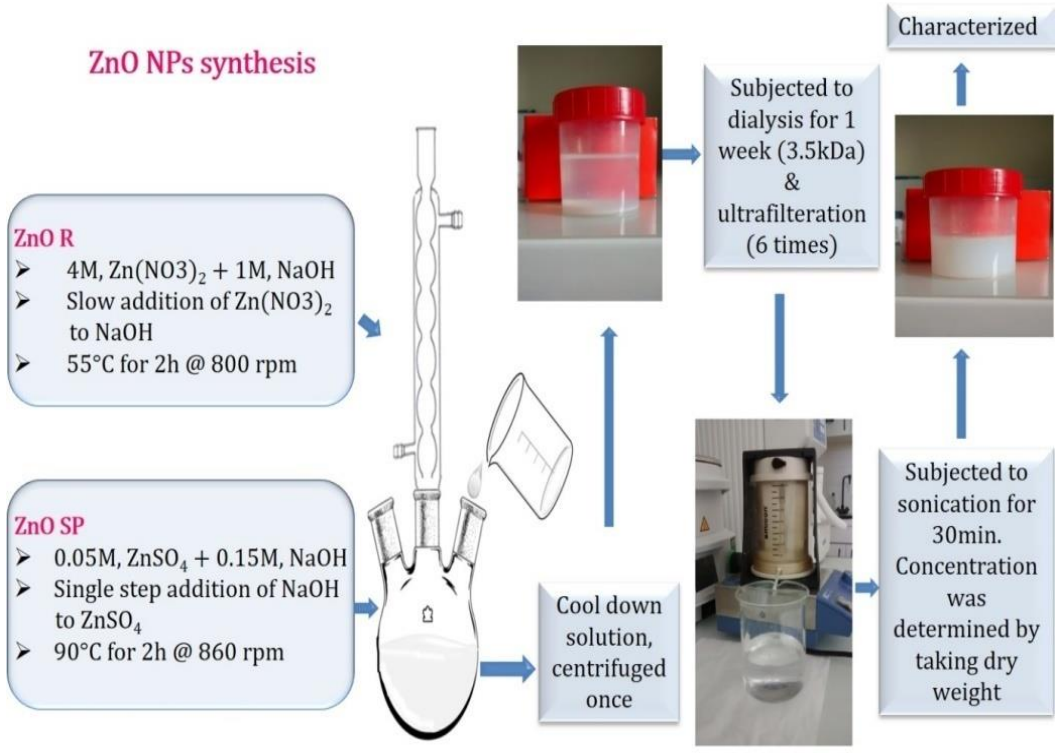

Figure 3:1: Steps of ZnO NPs synthesis

3.5.1 ZnO NPs SYNTHESIS

3.5.1.1 ZnO NPs rod shape (ZnO R)

ZnO NPs of rod shape morphology (ZnO R) was synthesised by wet chemical method using zinc nitrate ($Zn(NO_3)_2$) and NaOH as precursors (Sruthi *et al*. 2017). In brief, 100ml aqueous solutions of 12g $Zn(NO_3)_2$ and 3g sodium hydroxide (4:1 molar ratio) were prepared in distilled water. The $Zn(NO_3)_2$ solution was added drop wise to the NaOH solution heated at 55℃ under constant stirring. The solution was kept undisturbed at this condition for 2h and subsequently allowed to cool down. The pH of the solution was recorded.

3.5.1.2 ZnO NPs spearhead shape (ZnO SP)

ZnO NPs of spearhead morphology was synthesised by wet chemical method using zinc sulphite ($ZnSO_4$) as zinc salt and NaOH as reducing agent. Here, 100ml each of 0.05M (718.8mg) $ZnSO_4$ and 0.15M (300mg) NaOH (1:3 molar ratio) solution was prepared in deionised water. The $ZnSO_4$ solution was heated to 90℃. While maintaining the temperature, NaOH solution was added to the $ZnSO_4$ solution in a single step. The reaction mixture was kept under constant stirring for 2h at 860rpm. The following reaction explains the formation of zinc oxide

$$Zn^{2+}_{(aq)} + 2OH^{-}_{(aq)} \rightarrow Zn(OH) + (aq)$$

$$Zn\,(OH) + (aq) \rightarrow ZnO$$

The solution was allowed to cool down. The pH of the final solution was recorded.

3.5.1.3 Washing step

ZnO NPs synthesized by the above two methods were centrifuged at 10000rpm for 10min to remove unreacted precursors. The white precipitate was then subjected to dialysis (membrane pore size: 3.5kD) for a period of 1 week, followed by ultrafiltration (6 times). Conductivity of the ultra-filtrate was recorded and the concentration of ZnO NPs in solution was determined by taking dry weight.

3.5.2 PHYSICO-CHEMICAL CHARACTERISATION

The synthesised nanoparticles were characterised for their size, morphology, structure, colloidal stability, surface charge, purity and surface area using different techniques.

3.5.2.1 Scanning Electron Microscopy (SEM)

Morphology of the ZnO NPs were determined using SEM, JEOL JSM-6400F (JEOL, USA) operating at accelerating voltage in the range 0.5-30 kV. The samples were prepared in ethanol and sonicated for 30min before analysing. The elemental composition was analysed by EDS.

3.5.2.2 Transmission Electron Microscopy (TEM)

Size of the particle was determined using TEM; JEOL JEM-2100 LaB6 (JEOL, USA) operating at 200 kV. The images were acquired and processed by Gatan US1000 charge-coupled device (CCD) camera and Digital Micrograph software (Gatan, Inc.) respectively. Freeze dried samples (2mg/ml) were dispersed in ethanol and deposited on 300-mesh carbon film coated copper grid. The grid was allowed to dry by solvent

evaporation. The samples were observed in image mode and diffraction mode. High Resolution TEM (HRTEM) and Selected Area Electron Diffraction (SAED) analysis were carried out for the samples. Average size of the particles was calculated using Image J software.

3.5.2.3 Brunauer-Emmett-Teller (BET) analysis

Specific surface area (SSA) analysis of the samples was done by Brunauer-Emmett-Teller (BET) method using, BELSORP-mini (MicrotracBEL, Japan) with N_2 gas adsorption. Powder was out gazed at 200°C for 1.30h. The surface area was determined from the isotherm of nitrogen adsorption.

3.5.2.4 Dynamic Light Scattering (DLS)

Size of ZnO NPs in solution was measured by dynamic light scattering (DLS). Hydrodynamic diameter of the nanoparticle in water, PBS and cell culture medium was measured by Zetasizer Nano ZS (Malvern, USA) supplied by DTSNano V4.2 software. Also DLS measurements were done by dispersing different concentration of ZnO NPs in water to study the effect of concentration and particle aggregation on hydrodynamic diameter. The mean hydrodynamic diameter was calculated using auto correction function of the scattered light intensity. The dispersity of particle in solution was analysed from the Poly Dispersity Index (PDI).

3.5.2.5 Zeta potential

Surface charge of ZnO R and ZnO SP was measured from the Zeta potential. Zeta potential (ζ) was measured over different pH using a Zetasizer Nano ZS (Malvern,

USA) instrument supplied by DTS Nano V4.2 software. The ZnO NPs solution was prepared in 10^{-2} M NaCl aqueous solutions. The ζ potential was calculated from the measured value of the electrophoretic mobility, with the aid of instrument software using Henry's equation:

$$Ue = 2\varepsilon\zeta f(\kappa a) \div 3\eta$$

Where Ue is the electrophoretic mobility, ε represent dielectric constant, f(κa) is the Henry function and η is the viscosity of the dispersant.

3.5.2.6 Thermogravimetric analysis (TGA)

Water desorption and purity of ZnO R and ZnO SP were analysed by thermogravimetric analysis (TAG24 Setaram, France). 10mg of ZnO NPs was taken in platinum pans and loaded to the instrument. The temperature range was set between 25-700°C and at the rate of 7°C/min, under atmospheric air.

3.5.2.7 X-Ray Diffraction (XRD)

XRD analysis of the samples was done using D8 Advance diffractometer (Bruker, USA) equipped with a Vantec linear detector using the Kα1 and Kα2 copper radiations. The samples scanned at a 2θ angle range between 20-90°. The step size was kept constant throughout (0.025°) and the counting time was 2s/step.

3.5.2.8 X-Ray Photoelectron Spectroscopy (XPS)

The XPS analysis of the ZnO NPs was done by X-Ray Photoelectron Spectroscopy (XPS), PHI Verasaprobe 5000 (ULVAC-PHI, INC, Japan) with

aluminium Al κα1. All the binding energies were corrected for the charge shift using adventitious C1s peak at 284.8eV.

3.5.3 BIOLOGICAL CHARACTERIZATION

3.5.3.1 Endotoxin detection

Endotoxin content of ZnO NPs (ZnO SP) was assessed using Charles River Endosafe PTS kit. Endotoxin present in the sample reacts with the Limulus amebocyte lysate and form a gel clot. The gel clot formed corresponds to the amount of endotoxin present in the sample. ZnO NPs (100µg/ml) were dispersed in endotoxin free water. These particles were centrifuged at 14000rpm for 15min. The supernatant was analysed for endotoxin contamination. 25µl of the supernatant was added to the cartridge well and loaded on to the Endosafe PTS. Readings were taken and the endotoxin content is expressed in EU/ml.

3.5.3.2 Effect of cell culture media on the size of the nanoparticles

The ionic composition of the media may influence the size of ZnO NPs (ZnO SP), which was assessed by incubating the samples in two different culture media (RPMI and DMEM F12) over different time periods (5min, 30min, 60min and 24h). The hydrodynamic size of the particles was measured using DLS.

3.5.3.3 Protein corona formation

3.5.3.3.1 Preparation of sample for protein corona

Protein corona formation was determined as per the method described by Jedlovszky-Hajdu *et al*., (2012). ZnO NPs at a concentration of 0.04 and 1mg/ml was

used for protein corona identification. Different concentrations of ZnO NPs (ZnO SP; 10µg/ml, 40µg/ml and 1mg/ml) were mixed with 10% v/v (protein concentration in *in vitro* cell culture experiment) of FBS. The aliquots were incubated at 25°C for 1h. After incubation, the particle-protein corona complex was isolated by centrifuging at 10000rpm for 30 min at 4°C. The pellet containing the particle-protein complex was washed thrice in PBS at 4°C by centrifuging at 10000rpm for 30min. Pellets were resuspended in SDS gel loading buffer (50mM Tris HCl – pH 6.8, 100mM dithiothreitol, 2% w/v SDS, 0.1% bromophenol blue, 10% w/v glycerol) and stored at -20°C until further use.

3.5.3.3.2 Identification of protein corona by SDS-PAGE

The particle-corona complex in gel loading buffer was heated at 100°C for 5 min. Samples were loaded in 12% SDS-PAGE gels and run at a voltage of 8 V/cm for stacking gel and 15 V/cm for resolving gel. The SDS reagents and gel was prepared as given in **Appendices A.1**. The gel was stained with Coomassie brilliant blue (**Appendices A.2**). Images were taken in a Bio Imaging system (Syngene, UK).

3.6 BIO-NANO INTERACTIONS *IN VITRO* USING GLIAL CELLS

3.6.1 CELLULAR INTERACTION OF ZnO NPS WITH BV2 CELL LINES

Cellular interaction of ZnO NPs was studied in BV2 microglial cell line. BV2 is a rat cell line exhibiting phenotype of primary microglia. The cells exhibit a doubling time of approximately 20h. The cell viability, mitochondrial activity, free radicle production, lysosomal activity and apoptosis in presence of ZnO NPs were studied using different assays as shown in **Figure 3.2.**

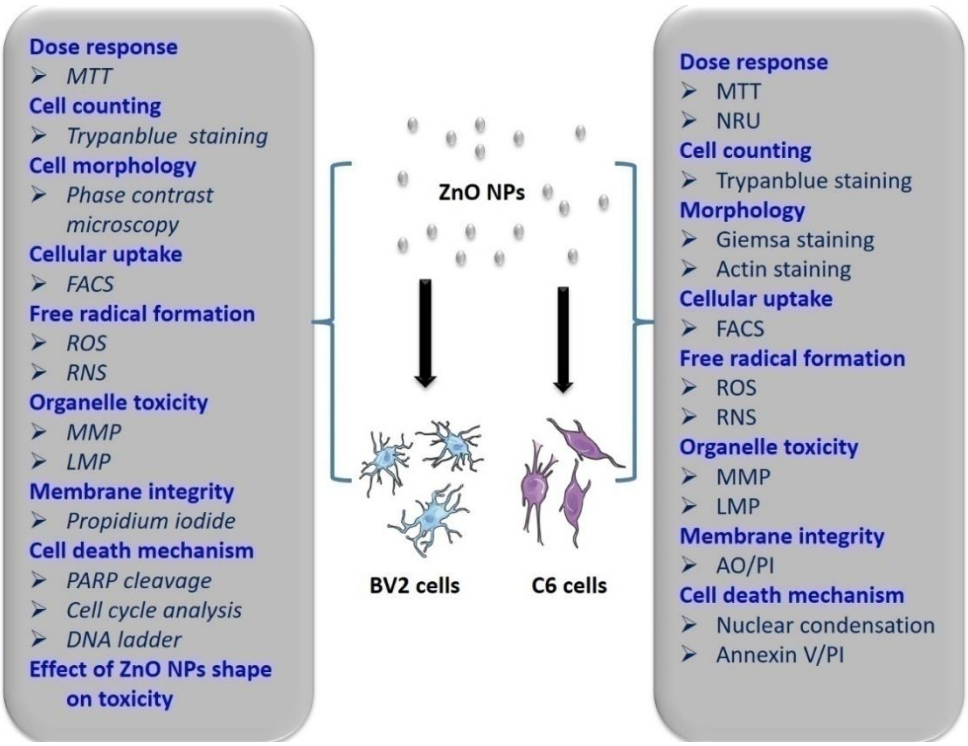

Figure 3:2: Flow chart of cellular interaction using BV2 and C6 cell lines

3.6.1.1 Cell culture and particle treatment

BV2 cells were cultured in RPMI medium supplemented with 10% heat inactivated FBS and 1% antibiotic/antimycotic (AB/AM) solution. Cells were seeded in appropriate seeding density and kept overnight in 5% CO_2 incubator at 37°C. The ZnO NPs stock solutions (4mg/ml) were sonicated for 10min before each experiment to ensure uniform distribution and exposure in the cell culture dishes. The cells were exposed to 1, 5, 10, 20, 40 and 80 µg/ml ZnO NPs for different time durations (3, 6 and 24h).

3.6.1.2 Dose response by MTT assay

Cell viability was assessed as a function of mitochondrial activity using MTT (3-(4, 5-Dimethylthiazol-2-yl)-2, 5-Diphenyltetrazolium Bromide) assay. Cells were seeded in 12 well plates at an initial seeding density of $5x10^4$ cells/well and incubated overnight at 37°C and 5% CO_2. Cells were harvested by centrifugation at 200g for 5 min, after 6 and 24h of ZnO NPs treatment. The pellets were incubated with MTT (0.05mg/ml) for 3h in the dark. The cell suspension was centrifuged at 1200rpm for 5min. The formazan crystals formed was solubilised (for 15min) using 200µl DMSO. 100µl each of this solution was transferred to 96 well plates in duplicates and absorbance was read at 540nm using Tecan Infinite® 200 PRO (Switzerland).

3.6.1.3 Interference of ZnO NPs with MTT result

Many nanomaterials may directly interact with MTT and interfere with assay result. The particle interference on MTT result was studied by incubating ZnO NPs of different concentrations (1, 5, 10, 20, 40 and 80µg/ml) with 100µl, 0.05mg/ml MTT for 3h followed by 100µl DMSO. The absorbance was measured at 540nm using plate reader Tecan Infinite® 200 PRO (Switzerland).

3.6.1.4 Cell count by Trypan blue exclusion assay

Total number of cells in the medium was assessed using trypan blue exclusion assy. Trypan blue is a vital dye which is impermeable to cells with intact membrane. In presence of trypan blue, dead cells stain blue whereas live cells remain colourless. In brief, cells were seeded in a 12 well plate at a density of $5x10^4$cells/well and incubated overnight in CO_2 incubator. The cells were exposed to ZnO NPs of different

concentration (1, 5, 10, 20, 40 and 80µg/ml) for 6 and 24h. Cells harvested by centrifugation at 1500rpm for 5min were resuspended in 200µl PBS. Cell counting was performed under phase contrast microscope (Axiovert 40 CFL, Zeiss) using Neubauer counting chamber by mixing cell suspension with equal proportion of trypan blue. Four large squares at the corner were counted and number of cells (n) per ml were calculated using formula; n = (total number of cells counted ÷ total number of squares counted) x dilution factor x 10^4.

3.6.1.5 Cellular phenotype by phase contrast microscopy

Cells were seeded in 12 well plates at an initial seeding density of $5x10^4$cells/well. The morphology after 6 and 24h of ZnO NPs exposure was evaluated under phase contrast microscope (Axiovert 40 CFL, Zeiss) fitted with camera (Axiocam ICm1, Zeiss).

3.6.1.6 Particle uptake by flow cytometry

Uptake of ZnO NPs by microglia was analysed using flow cytometry following the method of Suzuki *et al*., (2007). In flow cytometry, forward scattered (FSC) light indicates the size of the cell and side-scattered (SSC) light indicates the cell granularity. Particle uptake by the cells leads to increase in granularity and corresponding increase in SSC while the FSC of the cell remains the same. In this experiment, cells were seeded in 6 well plates at an initial density of 1×10^5 cells/well and kept overnight for incubation. Cells were then exposed to 5, 20, and 80µg/ml concentrations of ZnO NPs for 3h. Cells were harvested and centrifuged at 1200rpm. The pellet was resuspended in 500µl PBS

and analysed using flow cytometry (DAKO GALAXY flow cytometer, Germany) controlled by 'FloMax' software (version 2.4; Partec, Münster, Germany).

3.6.1.7 Free radical formation

3.6.1.7.1 Superoxide radicals by DHE staining

Superoxide anions production in presence of ZnO NPs was measured using a cell permeable molecule, Dihydroethidium (DHE; Life Technologies, St Aubin, France). DHE upon reaction with superoxide anions forms a red fluorescent product 2-hydroxyethidium, which intercalate with DNA. The cells were seeded in 12 well plates at a density of $5x10^4$ cells/well kept overnight in CO_2 incubator. The cells were exposed to 5, 20, 40 and 80µg/ml of ZnO NPs for 6 and 24h. Cells were harvested by direct pipetting and centrifuged at 1200rpm for 5min. The pellets were resuspended in 1ml PBS (1X) and transferred to cytometer tubes. 1.25µl of DHE (1.6mM) were added to each tube and incubated for 15min at 37°C and analysed by DAKO GALAXY flow cytometer (DAKO, Germany) through 590/10nm band pass filter.

3.6.1.7.2 Hydrogen peroxide by DHR123 staining

Hydrogen peroxide production in presence of ZnO NPs was estimated using the dihydrorhodamine 123 (DHR 123, Sigma-Aldrich, USA). DHR 123 is an uncharged and non-fluorescent molecule that passively diffuses across plasma membranes. Inside cytoplasm DHR123 is oxidized by hydrogen peroxide to give a green fluorescence cationic compound rhodamine 123. Here, the cells seeded at an initial density of $5x10^4$ cells/well were exposed to 5, 20, 40 and 80 µg/ml of ZnO NPs for 6 and 24h. The cells

harvested after centrifugation were resuspended in 1ml 1X PBS. 2mM DHR123 at a final concentration of 6µM were added to each tube and incubated for 15min at 37°C. Fluorescence was measured using DAKO GALAXY flow cytometer (DAKO, Germany) with 520/20 nm band pass filter.

3.6.1.7.3 Nitrile radicals by Griess reagent assay

The nitric oxide production in BV2 cells were analysed by Griess reagent (Sigma-Aldrich, USA) assay. In brief, cells were seeded at a density of $1X10^4$cells/well in a 96 well plate and incubated overnight. Cells were then exposed to 1, 5, 10, 20, 40, and 80ug/ml of ZnO NPs for 6 and 24h. 50µl of supernatant was mixed with 50µl of Griess reagent and incubated at room temperature for 10min. The absorbance was read at 540nm using a multiwell plate reader (Bio-Tek, Winooski, USA). The concentration was calculated from the sodium nitrate (0.5, 2.5, 5 and 7.5 µg/ml) standard graph.

3.6.1.8 Mitochondrial membrane potential by $DiOC_6(3)$ staining

Mitochondrial membrane potential of BV2 cells were examined using fluorescent probe 3,3'-Dihexyloxacarbocyanine Iodide ($DiOC_6(3)$) (Life Technologies, Molecular Probes). $DiOC_6(3)$ is a cell-permeant, green-fluorescent, lipophilic dye. The dye at lower concentration selectively stains active mitochondria of living cells. The cells were seeded in a 12 well plate at an initial density of $5x10^4$cells/well and incubated overnight at 5% CO_2 incubator. The cells were exposed to 1, 10, 20, 40 and 80µg/ml of ZnO NPs for 6 and 24h. Cells incubated with 4% paraformaldehyde (1ml freshly prepared in DPBS) at 37°C for 10min were used as positive control. The cells washed in PBS were incubated with 0.1µM $DIOC_6(3)$ (in PBS) for 15min at 37°C. The flow

cytometry analysis was done using the DAKO GALAXY flow cytometer (DAKO, Germany) with 520/20 nm band pass filter.

3.6.1.9 Lysosomal integrity by Acridine orange (AO)

Lysosomal destabilisation in presence of nanoparticle was analysed using acridine orange (AO). AO is a lipophilic, cationic fluorochrome capable of permeating cells and organelle membrane structure. With blue light excitation, the dye differentially stains cytoplasm and acid vesicles. The dye gets protonated inside acidic vesicles and emits orange fluorescence whereas the cytoplasm remains green in colour. The cells seeded at an initial density of $5x10^4$cells/well were exposed to ZnO NPs (5, 20, 40, and 80µg/ml) for 6 and 24h. The cells harvested by direct pipetting were washed with PBS and incubated in 1ml AO solution (2µg/ml in PBS) for 15min at 37°C. The analysis was done using DAKO GALAXY flow cytometer (DAKO, Germany) with 590/10nm band pass filter filters.

3.6.1.10 Cell membrane integrity by Propidium Iodide (PI) staining

The membrane integrity in BV2 cells was analysed by Propidium Iodide (PI) staining. The principle underlying PI staining is dye exclusion; the live cells with intact membrane exclude PI. Otherwise, PI penetrates damaged and permeable membrane of a non-viable cell. Cells seeded at an initial density of $5x10^4$cells/well were exposed to ZnO NPs (5, 20, 40, and 80µg/ml) for 6 and 24h. Harvested cells were washed and stained with PI (1µg/ml) for 15 min at 37°C. The flow cytometry analysis was done using DAKO GALAXY flow cytometer (DAKO, Germany) with 630nm long pass filter.

3.6.1.11 Cell cycle analysis by flow cytometry

The changes in cell cycle patterns were analysed by staining with PI. In brief, the cells seeded at an initial density of $5x10^4$cells/well were exposed to ZnO NPs (5, 20, 40, and 80µg/ml) for 24h. Cells harvested by direct pipetting were washed with PBS. The pellets were fixed using 1ml cold 80% ethanol (kept at -20°C) by vortexing to avoid cell aggregation and kept at -20°C for at least 2h (the cells may be kept at this condition for few days.). The cells were washed (2000rpm for 5 min) and resuspended in 300µl PBS containing 80µg/ml PI and 200µg/ml RNase. After 1h incubation at 37°C, the solution was made up to 1ml by adding 700µl PBS and analysed using flow cytometry (DAKO GALAXY, Germany) with 630nm long pass filter.

3.6.1.12 PARP cleavage assay

The cells were seeded at an initial density of $2x10^4$cells/well and incubated overnight. The cells were exposed to 10 and 80µg/ml of ZnO NPs for 24h. Untreated cells were used as control. After treatment, cells were harvested and centrifuged at 2000rpm and 4°C for 5 min. A cathepsin inhibitor z-FA-FMK (100µM) was used to analyse the role of lysosome on BV2 cell death.

3.6.1.12.1 Sample lysis

The cell pellets were transferred to fresh tubes and washed with 1ml cold PBS. The pellets were incubated with 80µl of RIPA buffer containing 1X antiprotease for 30min on ice. The cell suspension was centrifuged at 12000rpm, 4°C for 20min. Supernatant was collected in fresh tube (this solution may be stored at -20°C for weeks and thawed at room temperature) and the pellet was discarded.

3.6.1.12.2 Protein quantification

The concentration of protein solution is measured by BCA (Bicinchoninic acid assay) with 2% copper sulphate solution. 25µl of BSA at concentration between 1µg/ml to 0 (half the concentration in successive wells) were used as standards. The protein solutions were diluted at a ratio of 1:25 with water and incubated with BCA for 30min at 37°C. The reading was done at 570nm and concentration was calculated from the standard graph.

3.6.1.12.3 Loading and running gel

The protein isolated was loaded in 8% polyacrylamide gel at a concentration of 70µg/well. Electrophoresis was carried out for 2h (30min at 70V followed by 1.30h at 120V).

3.6.1.12.4 Gel to membrane transfer of protein

The polyvinylidene difluoride (PVDF) membrane was activated with methanol for 1min and rinsed with transfer buffer. Gel stack was prepared by sandwiching the gel and PVDF membrane between filter papers and sponges. The gel stack was kept in transfer buffer for 1h.

3.6.1.12.5 Antibody staining

The protein attached membrane was blocked using 5% milk solution for 1h at room temperature and washed 3 times with PBST (0.1% PBS-Tween 20) for 5min each. The membrane was transferred to solution containing primary antibody (1:1000) and incubated overnight at 4°C. Antibody for actin (1:10000) was used as a standard. The

solution was washed 5 times with PBST (5min each). The membrane was subsequently incubated with horseradish peroxidase–conjugated goat antimouse secondary antibody (in 1% milk) (Jackson Immuno Research Laboratories, West Grove, PA) for 1h at room temperature. Membrane was washed twice in PBST and covered in transparent plastic wrap. Immunoblot was acquired by autoradiography using enhanced chemiluminescence detection kit (Amersham).

3.6.1.13 DNA ladder assay

One of the hallmarks of apoptosis is the inter-nucleosomal DNA fragmentation carried out by activated nucleases. $3x10^6$ cells were cultured in T25 flasks for overnight. The cells were subsequently treated with 20, 40 and 80µg/ml of ZnO NPs for 24h. DNA ladder assay was performed as per the manufacturer's instructions using Quick Apoptotic DNA ladder detection kit. Cells were harvested and washed with PBS at the end of exposure period. The cells were lysed with 35µl of TE lysis buffer and 5µl Enzyme A was added to the solution. Cells were incubated for 10min in a water bath set at 37°C. Enzyme B solution was added and incubated at 50°C for 30 min. Ammonium acetate solution and absolute ethanol were added and DNA was allowed to precipitate at -20°C. This mixture was centrifuged at 12000 rpm for 10min and the supernatant was discarded. The pellet was resuspended in 70% cold ethanol and centrifuged. The pellet was air dried for 10min and resuspended in DNA suspension buffer (30µl). DNA was loaded on to 1.2% agarose gel containing 0.5µg/ml ethidium bromide in 1X TBE (Tris/Borate/EDTA) running buffer and run at 5 V/cm for 1-2h. DNA bands were then visualized using transilluminator (Bio Imaging system, Syngene, UK).

3.6.1.14 Comparative toxicity of ZnO R and ZnO SP using BV2 cells.

3.6.1.14.1 Morphology analysis by phase contrast microscopy

Morphology of cells exposed to ZnO R was analysed using phase contrast microscopy (Axiovert 40 CFL, Zeiss) fitted with camera (Axiocam ICm1, Zeiss) as described in section **3.6.1.5.** The morphology of cells exposed to ZnO SP was compared with morphology of cells exposed to ZnO R.

3.6.1.14.2 Membrane integrity by PI staining

Cells exposed to ZnO R for 24h were subjected to analysis using PI staining as described in section **3.6.1.10**. The results were compared with ZnO SP.

3.6.1.14.3 Cell cycle analysis by flow cytometry

Cells exposed to ZnO R for 24h were subjected to cell cycle analysis as described in the section **3.6.1.11** and the results obtained for ZnO SP was compared with that of ZnO R.

3.6.1.14.4 PARP cleavage assay:

Cells exposed to ZnO R for 24h were analysed for PARP cleavage using western blot as described in section **3.6.1.12**. Cathepsin inhibitor z-FA-FMK (100µM) was used to show the PARP cleavage in BV2 cells.

3.6.2 CELLULAR INTERACTION OF C6 ASTROGLIAL CELLS WITH ZnO NPS

3.6.2.1 Cell culture and ZnO NPs exposure

C6 cells lines, a chemically induced tumour of astrocytic origin was obtained from Biosurface Technology Division, Sree Chitra Tirunal Institute for Medical

Sciences and Technology. The cells were cultured in DMEM F12 supplemented with 10% FBS, 1% antibiotic- antimycotic solution, 1% glutamax and 1mM sodium pyruvate. 70-80% confluent cells were used for the experiments. Cells at an initial density of $1x10^4$ and $1x10^5$ were seeded in 96 well plates and 6 well plates respectively. Freshly prepared stock of ZnO NPs was used for the entire study. The concentrations ranged from 5 to 80µg/ml.

3.6.2.2 Assays for cell viability

3.6.2.2.1 MTT

Cell viability was assessed as a function of percentage mitochondrial activity using MTT (3-(4, 5-Dimethylthiazol-2-yl)-2, 5-Diphenyltetrazolium Bromide) assay. In brief, the cells were seeded in 96 well plates at a seeding density of $1X10^4$ cells/ well and allowed to attach overnight. The wells were exposed to 5, 10, 20, 40 and 80µg/ml of ZnO NPs for 3, 6 and 24h. The medium was replaced with 100µl MTT (50µg/ml in medium) and incubated for 3h in dark. Medium was discarded and the formazan crystals formed were solubilized using DMSO (100µl/well, incubated in dark for 15min). The reading was taken at 540nm using plate reader, ELx808 ultra-microplate reader (Biotech instruments, USA).

3.6.2.2.2 Neutral Red Uptake (NRU)

Lysosomal activity was estimated using NRU assay following the method of Borenfreund and Puerner (Borenfreund and Puerner 1985). Cells cultured at an initial density of 1×10^4 were incubated with 5, 10, 20, 40 and 80 µg/ml ZnO NPs for 3, 6 and

24 h at 37°C. 10µl of 1% neutral red was added to each well and incubated in dark for 3h. Consequently, the cells were washed with PBS and the dye taken up by the cells were solubilized using 100µl acid alcohol (1%, v/v, acetic acid and 50% ethanol) by keeping the cells on an incubator shaker at 60 rpm, 37°C for 30min. Absorbance was measured at 540nm using a ELx 808 multiwell plate reader (Bio-Tek, Winooski, USA).

3.6.2.3 Particle uptake (ZnO NPs) in C6 cells

ZnO NPs uptake by C6 cells were analysed using flow cytometry as described in section **3.6.1.6**. In brief, the cells seeded at an initial density of $1x10^5$ were exposed to 10 and 80µg/ml of ZnO NPs for 4h and analysed using flow cytometry (BD FACSAria™, BDBioSciences, USA).

3.6.2.4 Particle dissolution and related cytotoxicity

Cytotoxic effect of particle dissolution in the medium was assessed by MTT assay. 5, 10, 20, 40 and 80µg/ml of ZnO NPs were incubated with DMEM F12 supplemented with 10% FBS for 72h. The solution was centrifuged at 10000rpm for 10 min and the supernatant was taken. The cells seeded at an initial density of $1x10^4$cells/well were exposed to the supernatant for 24h and MTT assay was carried out as per section **3.6.2.2.1**. The results were compared with MTT data obtained from the direct exposure of ZnO NPs with C6 cells.

3.6.2.5 Cell phenotype

Phenotypic alterations including cytoplasmic morphology and cytoskeletal arrangements after ZnO NPs exposure was studied.

3.6.2.5.1 Morphology analysis by Giemsa staining

Cells at an initial density of 1×10^5 were seeded on cover slips placed in 6 well plates and kept overnight for attachment. Cells were exposed to 5, 10, 20, 40 and 80µg/ml of ZnO NPs for 6 and 24h. After washing with PBS, cells were fixed using 4% formaldehyde for 15 min. Fixed cells were stained with 10% Giemsa solution for 5min and washed. Slides were washed thrice in PBS and morphology was observed under compound microscope (Olympus CX31, Japan).

3.6.2.5.2 Cytoskeletal staining by Rhodamine phalloidin

Cytoskeletal arrangement was studied by rhodamine phalloidin staining. Phalloidin is a peptide toxin isolated from *Amanita phalloides*. It selectively binds to F-actin of cytoskeleton. The toxin is conjugated with fluorescent moiety rhodamine to visualize actin structure using fluorescence microscopy. The cells seeded at an initial density of $1x10^5$cells/well were exposed to 5, 10, 20, 40 and 80µg/ml ZnO NPs for 24h. The exposed cells were washed with PBS once and fixed using 3.7% formaldehyde for 10min. 0.1M glycine (in PBS) for 5min was used to quench excess aldehyde. Cells were permeabilised using 0.1% Triton-X 100 (in PBS) for 1min. The cells were incubated with rhodamine phalloidin (1:250 in PBS) for 15 min. The cells were observed under fluorescence microscope using red filter (Axio Scope.A1, Carl Zeiss, Germany) after washing with PBS.

3.6.2.6 Mitochondrial membrane potential (MMP) by JC1 staining

Mitochondrial membrane potential (MMP) was analysed by JC1 (5, 5′, 6, 6′-tetrachloro-1,1′,3,3′-tetraethylbenzimi- dazolylcarbocyanine iodide). JC1 is a lipophilic

cationic dye used to detect mitochondrial membrane potential. The dye exists as a monomer inside the cytoplasm giving green fluorescence. The dye aggregates to form polymer of red fluorescence inside energized mitochondria with high membrane potential. In brief, the cells were seeded at an initial seeding density of $1X10^6$cells/well. Culture at confluency was exposed to 5, 20 and 40 µg/ml of ZnO NPs for 24h. At the end of exposure, 1µM JC-1 was added to each well and incubated for 20min at room temperature. The cells after washing was observed under fluorescence microscope (Axio Scope.A1, Carl Zeiss, Germany) using green and red filter and photographs were taken.

3.6.2.7 Detection of reactive oxygen species(ROS) by DCFH-DA

Reactive oxygen species generation in presence of ZnO NPs was analysed by probe, 2′7′-dichlorofluorescein diacetate (DCFH-DA). Cell membranes are freely permeable to esterified forms of H_2DCF. Once inside the cells, DCFH-DA undergo deacetylation by intracellular esterase to become 2′,7′-dichlorofluorescin (DCFH). DCFH trapped inside cells are oxidised by the ROS to form a fluorescent molecule 2′,7′-dichlorofluorescein (DCF). In brief, the cells at an initial density of $1x10^4$/wells were allowed to attach overnight. Cells were exposed to 5, 10, 20, 40 and 80µg/ml ZnO NPs for 6 and 24h. Medium was replaced with PBS containing 1µM DCFH-DA and incubated in dark for 45 min at 37°C. Cells were washed with PBS and the fluorescence was read using fluorescence plate reader (Plate ChameleonTM V, Hidex, Finland) at an excitation and emission wavelength of 495nm and 529nm respectively.

3.6.2.8 Influence of catalase activity on generation of ROS

Astroglial cells exhibit high catalase activity. Influence of catalase activity on ZnO NPs induced ROS was assessed using a catalase inhibitor sodium azide (NaN_3). Cells seeded at initial density of $1x10^4$ were allowed to attach overnight. The cells were pre-incubated with 0.1µM NaN_3 for 1h. Medium was replaced with fresh medium containing 5, 10, 20, 40 and 80µg/ml ZnO NPs. ROS production was estimated in presence of DCFH-DA as described in section **3.6.2.7**. The results were compared with that of cells exposed to ZnO NPs in the absence of catalase inhibitor.

3.6.2.9 Nuclear condensation by DAPI staining

The chromosomes condensation is an indicator of apoptosis. Nanoparticles mediated nuclear condensation was analysed using DAPI. Cells were incubated with 5, 10, 20, 40 and 80µg/ml ZnO NPs for 24h. The medium was removed and washed with PBS. The cells were fixed using 4% formaldehyde and stained with DAPI (1µg/ml) for 5 min. Cells were stained with 5µg/ml acridine orange to demarcate the cell boundary. After washing with PBS, cells were observed under fluorescent microscope using blue and green filter (Axio Scope.A1, Carl Zeiss, Germany).

3.6.2.10 Apoptosis by Annexin V/ PI staining

Cellular apoptosis in presence of ZnO NPs was analysed using Annexin/PI kit (Alexa Fluor® 488 Annexin V/Dead Cell Apoptosis Kit, ThermoFisher scientific, USA). Phosphatidyl serine (PS) is a molecule located at the inner surface of the plasma membrane. During apoptosis, the PS gets exposed to external cellular environment. Annexin V is a cell impermeable 35-36kDa protein that has affinity for PS. PI on the

other hand is only permeable to cells with ruptured membrane. The present experiment was carried out as per the manufacturer's instruction with slight modification. The cells were exposed to 5, 10, 20, 40 and 80µg/ml of ZnO NPs for 24h. The cells harvested by trypsinization was centrifuged at 1700rpm and washed with cold PBS. Medium was removed and the cells were stained with 5µl of annexin V for 10min. 1µl of 100µg/ml PI constituted in 1X annexin binding buffer (ABB) was added to each tube and incubated for 5min. The samples were kept on ice and immediately analysed using FACS at fluorescence emission of 530nm and 575nm for annexinV and PI respectively. Gating was done using four controls: cells alone, cells with annexin V, cells with PI and finally cells with annexin V and PI. The cells subjected to FACS were later observed under microscope (Axio Scope.A1, Carl Zeiss, Germany) to confirm the annexin V/ PI staining.

3.6.3 CELLULAR INTERACTION OF ZnO NPS WITH PRIMARY ASTROCYTES

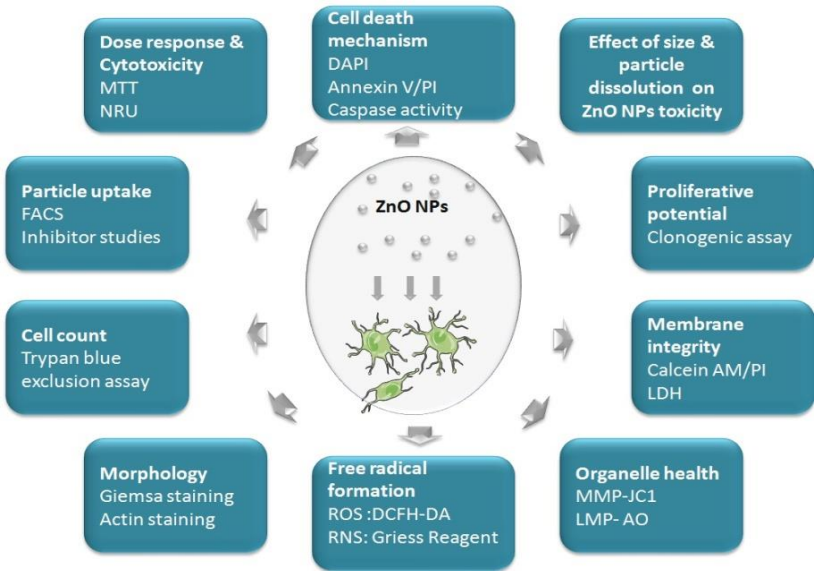

Figure 3:3: Flow chart of assays carried out to study interaction of ZnO NPs with astrocytes.

3.6.3.1 Isolation of Astrocytes

Primary astrocytes were isolated from post-natal 0-2 day old rat pups according to protocol described by Weinstein DE (2001) with slight modification. As shown in **Figure 3.4**, the pups were decapitated using scalpel blades. The head was transferred to 70% alcohol. Downstream isolation procedures were carried out by placing on ice, in sterile hood. Whole brain was isolated intact and the meningeal layer was carefully stripped off in cold HBSS (Hanks Balanced Salt Solution) with the aid of forceps. The tissues were subjected to mechanical mincing using a scalpel blade and followed by enzymatic digestion using 0.25% trypsin at 37°C for 10min. Equal volume of DMEM F12 supplemented with 10% FBS was used to deactivate the trypsin. 0.02% deoxyribonuclease was added to the solution and cell suspension was triturated using fire polished pasture pipettes. The single cell suspension was transferred to a fresh tube by passing through a 70µm nylon mesh. The cells were centrifuged at 1700rpm for 5min and resuspended in complete medium containing DMEM F12 (Dulbecco's Modified Eagle's Medium F12) supplemented with 10% heat-inactivated FBS (fetal bovine serum), 1% penicillin/streptomycin and 1% glutamax. The cell suspension was pelleted and re-suspended in fresh complete medium. The suspension was filtered through a 100-µm nylon membrane and plated into T75 culture flasks. The culture was kept undisturbed for 7 days in a 5% CO_2 incubator at 37°C.

3.6.3.2 Primary astrocytes purification

Loosely adherent microglia and oligodendrocyte were eliminated by chemical and mechanical means. The cells on attaining complete confluency were treated with

50µM L-leucine methyl ester (LME) for 1h. The LME is a lysosomotropic agent which selectively kills microglia. After treatment, the medium was discarded and the flask was rinsed using HBSS. The cells were harvested by trypsinisation and sub-cultured at 1:2 dilutions. The first passage on reaching confluency were covered using a cling film to stop gaseous exchange with environmental air and kept on an incubator shaker at 37°C and 260rpm for 24h. This shaking process dislodges the loosely adherent microglia and oligodendrocytes in the culture (Foo *et al*. 2011). After discarding the medium, the cells were washed using sterile HBSS and sub-cultured at 1:2 dilutions.

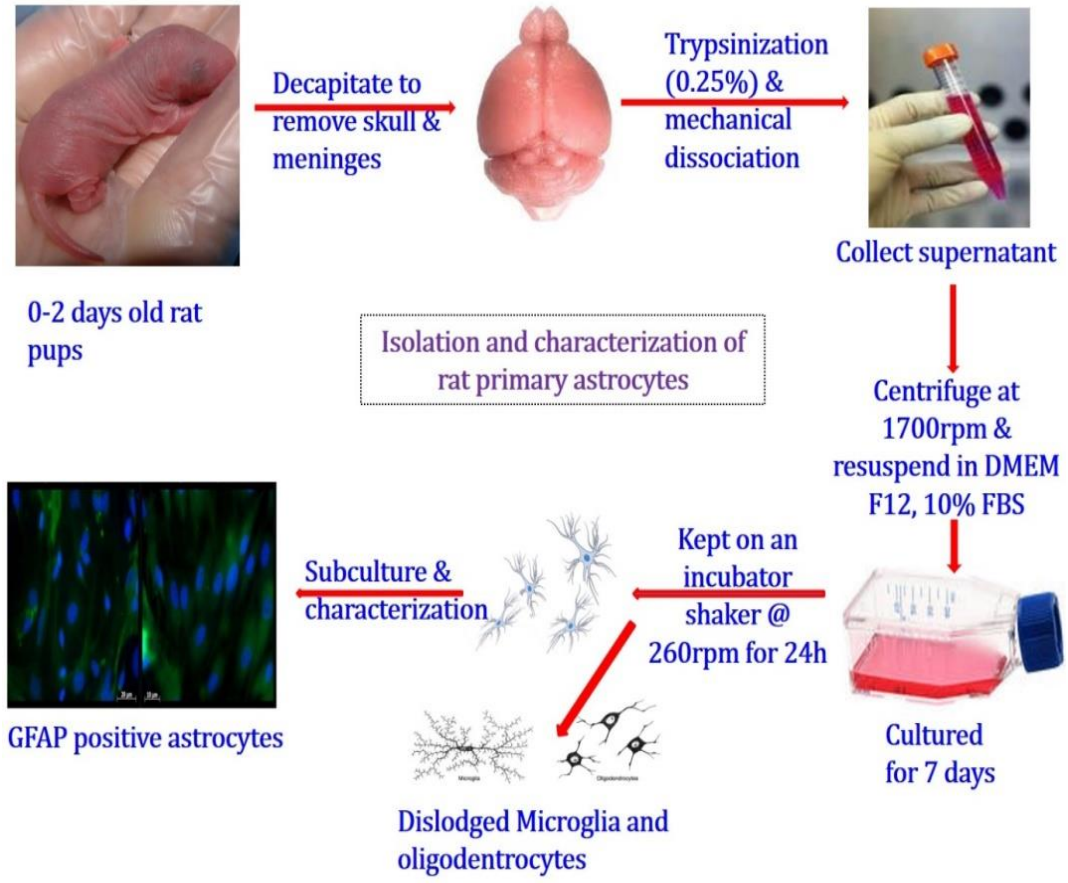

Figure 3:4: Isolation and purification of astrocytes

3.6.3.3 Characterization of primary astrocytes

Astrocytes marker Glial Fibrillary Acid Protein (GFAP) was used to characterise primary astrocytes. β3 tubulin was used to identify the neurons. The cells at 4^{th} passage were seeded on a coverslip at an initial density of $1X10^5$ cells. The cells were allowed to attach overnight. Before removing the complete medium, cells were incubated with 4% formaldehyde (in water) for 4min to minimize the cell damage during fixation. Medium was discarded and cells were washed with sterile HBSS (3 times in 3min gap). Cells were later fixed using 1.2% formaldehyde for 15min. The excess aldehyde was quenched by adding 0.1M glycine (in PBS) for 5min. Cells were treated with BP (Blocking and Permeabilisation) solution for 30min at room temperature to permeabilise the cells and block the unwanted sites. The BP solution was prepared by adding 200µl of Triton X 100 and 500µl of 5% FBS and was made up to 10ml in 1X PBS. After removing the BP solution, primary antibody (1:500 dilutions in PBS) was added to the wells and incubated overnight (not less than 16h) at 4°C. The cells were washed thrice with PBS (in 3min gap) and incubated with secondary antibody (1:500 dilutions in PBS) in dark for 2h at room temperature. Nucleus of the cells was demarcated using 1µl of DAPI (1mg/ml) for 5min. The cells were washed thrice with 1X PBS and observed under microscope using blue and green filter. To analyse the proportion of neuronal population, cells were seeded separately and stained for the neuronal marker β3 tubulin following the same procedure described above. Cell surface marker O4 antibodies were used as oligodendrocytes marker. The staining procedure was same as that described above except for the permeabilisation step. The antibody was diluted in PBS containing

5% FBS. The acetylated low density lipoproteins conjugated with fluorescent probe 'Dil' (Dil-Ac-LDL) were used to identify contaminating microglia and endothelial cells. These cells internalise the Dil-Ac-LDL by scavenger receptor and metabolises the Dil-Ac-LDL resulting in intracellular accumulation of 'Dil'. The cells were incubated with 10µg/ml of Dil-Ac-LDL for 4h at 37°C and 5% CO_2. 1µg/ml of DAPI for 5min was used to demarcate the nucleus in all experiment. The cells were washed using PBS and observed under microscope (Axio Scope.A1, Carl Zeiss, Germany).

3.6.3.4 Cell culture and Nanoparticle treatment

Cells were maintained in T25 flask containing complete medium (DMEM F12 with 10% heat-inactivated FBS (fetal bovine serum), 1% penicillin/streptomycin and 1% glutamax). The medium was changed in every 3 days. The culture from 4^{th} to 8^{th} passage with 70-80% confluency was used for the experiments. For all the *in vitro* experiments, the following seeding densities were used, unless otherwise stated. An initial seeding density of $1x10^4$cells/well and $5x10^4$cells/well were used in 96 well plates and 4 well plates respectively. An initial seeding density of $1x10^5$cells/well was used in 6 well plates and 35mm dishes. The cells were allowed to attach overnight before nanoparticle treatment.

Freshly prepared ZnO NPs stock was used for the experiments. The stock solution was diluted to a range of working stock for the experiments (1, 5, 10, 20, 40 and 80µg/ml).

3.6.3.5 Cell viability and dose response

3.6.3.5.1 MTT assay

The dose response in primary astrocytes was studied using MTT assay as per section **3.6.2.2.1**. Cells seeded at an initial density of $1x10^4$/well were exposed to 1, 5, 10, 20, 30, 40, 60, 80 and 100µg/ml of ZnO NPs for 6 and 24h.

3.6.3.5.2 NRU assay

Cells seeded at an initial density of $1x10^4$/well were exposed to 1, 5, 10, 20, 30, 40, 60, 80 and 100µg/ml of ZnO NPs for 6 and 24h. The NRU assay was carried out as described in section **3.6.2.2.2.**

3.6.3.6 Cellular uptake by flow cytometry

Cellular uptake of ZnO NPs was analysed using flow cytometry as per section **3.6.1.6.** Cells resuspended in 500µl PBS were analysed using flow cytometry (BD FACSAria™, BD BioSciences, USA) for SSC/FSC ratio.

3.6.3.7 Particle uptake in presence of inhibitor

The endocytic pathway of ZnO NPs was analysed by exposing cells with Cytochalasin D (Cyt. D). Cyt. D is a cell permeable mycotoxin that inhibits actin polymerization. It is a nonspecific inhibitor of endocytic pathway. Here, the cells seeded at an initial density of $1x10^4$ were allowed to attach overnight. The cells were pre-incubated with 5µM Cyt. D for 4h. Cells were subsequently exposed to different concentrations of ZnO NPs (5, 10, 20, 40, 80 µg/ml) for 24h and NRU assay was carried out as described in section **3.6.2.2.2.**

3.6.3.8 Cell morphology analysis by Giemsa staining

Cells seeded at an initial density of $1x10^5$/well were exposed to 20, 40 and 80µg/ml of ZnO NPs for 6 and 24h. Giemsa staining was carried out as described in section **3.6.2.5.1.**

3.6.3.9 Cytoskeletal analysis by rhodamine phalloidin staining

Cells seeded at an initial density of $1x10^5$/well were exposed to 20, 40 and 80µg/ml ZnO NPs for 6 and 24h. Actin staining was done using rhodamine phalloidin as described in section **3.6.2.5.2.**

3.6.3.10 Detection of reactive oxygen species (ROS) by DCFH-DA

Reactive oxygen species generation in presence of ZnO NPs was analysed by flow cytometry using DCFH-DA. In brief, the cells seeded at an initial density of $1x10^5$/well were incubated with ZnO NPs (5, 10, 20, 40 and 80µg/ml) for 6h. The cells were trypsinized and washed with PBS. The cell samples were incubated with 1µM DCFH-DA for 45min at 37°C. After washing with PBS, the cells were resuspended in 200µl cold PBS and measured immediately using BD FACSAria™, (BD BioSciences, USA) at an excitation and emission wavelength of 495nm and 529nm respectively. Gating was done with respect to positive control (freshly prepared 0.1mM H_2O_2).

3.6.3.11 Detection of reactive nitrogen species (RNS) by Griess reagent assay

Cells seeded at an initial density of $1x10^4$/well were exposed to 1, 5, 10, 20, 40 and 80µg/ml ZnO NPs for 6 and 24h. The RNS production in astrocytes was analysed by

Griess reagent assay as described in section **3.6.1.7.3.** LPS (1µg/ml) treated samples were used as positive control.

3.6.3.12 Lysosomal integrity by acridine orange

Cells were stained with AO for assessing the lysosomal integrity in astrocytes. Cells at an initial density of 5×10^4/well were seeded in 4 well plates and allowed to attach overnight at 37°C. The cells were exposed to ZnO NPs of concentration 20, 40 and 80µg/ml for 6h. At the end of treatment, the cells were incubated with acridine orange (2µg/ml in citrate phosphate buffer) for 15min at 37°C. Cells were washed with PBS and observed under fluorescence microscope using green and red filter (Axio Scope.A1, Carl Zeiss, Germany).

3.6.3.13 Mitochondrial membrane potential by JC1 staining

Astrocytes were seeded at an initial density of $1x10^5$/well and exposed to ZnO NPs (5, 20, 40 and 80µg/ml) for 6 and 24h. MMP was measured using JC1 as described in section **3.6.2.6**

3.6.3.14 Apoptosis by Annexin V/PI staining

Apoptosis in primary astrocytes exposed to ZnO NPs was analysed using flow cytometry, BD FACSAria™ (BD BioSciences, USA). The cells were seeded at an initial density of $1x10^5$/well were exposed to 5, 10, 20, 40 and 80µg/ml of ZnO NPs for 24h. Rest of the experimental procedures were same as described in section **3.6.2.10.**

3.6.3.15 Caspase 3/7 activation assay

Caspase 3 and 7 are two executioner caspases that act downstream of caspase dependent apoptosis signal cascade. Caspase 3/7 activation in response to ZnO NPs exposure was assessed by the Ana spec SensoLyte® Homogeneous AMC caspase 3/7 assay kit as per manufacturer's instructions. Astrocytes seeded at initial density of $1x10^4$/well in 96 well plates were exposed to different concentration of ZnO NPs (5, 10, 20, 40 and 80 μg/ml). Caspase 3/7 substrate was added subsequently to the plates and incubated for 60min on a plate shaker. Reading was taken at an excitation/emission wavelength of 354/442nm respectively using fluorescent plate reader (Tecan Infinite M200, Switzerland). The caspase activity was calculated by normalising against total protein.

3.6.3.15.1 Protein estimation: Lowry's method

Cell lysis was carried out as described in section **3.6.1.12.1.** Total protein in the lysate was estimated by Lowry's method (Lowry *et al.* 1951). This method has sensitivity between 0.01-1mg/ml and is based on the reaction between copper ions produced by the oxidation of peptide bonds with Folin-Ciocalteu reagent. The experimental procedure is carried out as described in **Table 3.1**. Reading was taken at 660nm using Lambda 25, UV/Vis spectrophotometer, Perkin Elmer, USA. The protein concentration is calculated from the bovine serum albumin (BSA) standard graph.

Reagent	Blank	Test
Distilled water	1ml	0.9ml
Tissue homogenate	-	0.1ml
Solution C	5ml	5ml
Incubate at room temperature for 10min.		
Folin's reagent	0.5ml	0.5ml
Incubate at dark for 30min		

Table 3.1: Protein estimation by Lowry's method

3.6.3.16 Cell membrane integrity by Calcein AM-PI staining

Membrane damage was assessed by double staining with calcein AM and propidium iodide (PI). Calcein AM is a best indicator of cell viability due to its good cell retention capabilities and its insensitivity to small fluctuations in the physiological pH range. This probe is also ideal for analysing cell adhesion, chemotaxis and multidrug resistance. Calcein upon hydrolysis by cellular enzyme is converted into a polyanionic fluorescein derivative that has about six negative charges and two positive charges at pH 7. PI (propidium iodide) on the other hand, penetrates the cells with compromised membrane integrity. The cells seeded at an initial density of $1x10^5$/well were treated with 20, 40 and 80µg/ml ZnO NPs for 6 and 24h. Medium was discarded and the cells were washed with PBS. Calcein AM was added to the wells and incubated at 37°C for 40min. The cells were then treated with PI for 5min. The cells were washed with PBS and observed under fluorescent microscope, Axio Scope.A1 (Carl Zeiss, Germany) using green and red filter.

3.6.3.17 Nuclear condensation by DAPI staining

The chromosomes condensation is an indicator of apoptosis. ZnO NPs mediated nuclear condensation in astrocytes was analysed using DAPI staining. Astrocytes seeded at an initial density of $1x10^5$/well were incubated with 20, 40 and 80µg/ml ZnO NPs for 6 and 24h. The medium was discarded and cells were washed with PBS. The cells were fixed using 4% formaldehyde and stained with DAPI (1µg/ml) for 5min. After washing with PBS, cells were observed under fluorescent microscope, Axio Scope.A1 (Carl Zeiss, Germany) using blue filter.

3.6.3.18 Effect of particle size and dissolution on astrocytes

Effect of ZnO size and dissolution on cytotoxicity was studied by comparing ZnO NPs with ZnO bulk formulation (0.7 to 1.5µm) and $ZnCl_2$ (Bulk particles possess large size than individual nanoparticles. $ZnCl_2$ is a salt of zinc which readily dissociates in water to form zinc ion).

3.6.3.18.1 Cytotoxicity by MTT

ZnO NPs, ZnO bulk and $ZnCl_2$ (1, 5, 10, 20, 40 and 80µg/ml) were exposed to cells seeded at initial density of $1x10^4$cells/ well. Cell viability was measured after 6 and 24h of exposure by MTT assay as described in section **3.6.2.2.1.**

3.6.3.18.2 Cell count by trypan blue exclusion assay

Total cell count as a function of toxicity was carried out using trypan blue exclusion assay. The cells were seeded at an initial density of $1X10^6$cells/well were exposed to ZnO NPs, $ZnCl_2$ and ZnO bulk particle at 1, 5, 10, 20, 40 and 80µg/ml for

24h. The cells were harvested by trypsinisation and centrifuged at 1700rpm. Trypan blue exclusion assay was carried out as per section **3.6.1.4.**

3.6.3.18.3 Detection of ROS by DCFH-DA assay

ROS generated in presence of ZnO NPs, ZnO bulk and $ZnCl_2$ were detected using DCFHDA probe. Astrocytes seeded at an initial density of $1x10^4$/well were allowed to attach overnight and exposed to particles for 6 and 24h. ROS measurement was done as per section **3.6.2.7.**

3.6.3.18.4 Evaluation of proliferative capacity and survival rate by Clonogenic assay

The clonogenic assay was carried out to determine the effect of ZnO NPs, ZnO bulk and $ZnCl_2$ on growth and survival of the cells. Single cell suspensions of astrocytes were seeded in 6 well plates at a density of $2X10^4$cells/well. Astrocytes immediately after seeding were exposed to 10, 20, 40 and 80 µg/ml of ZnO NPs, ZnO bulk and $ZnCl_2$ for 3h. The cells were subsequently replated at a density of 200 cells/well in 6 well plates. The dishes were left in incubator maintained at 37°C with 5% CO_2 supply until the cells in control plates formed adequately large number of clones (clones containing more than 50 cells are considered representative of viable cells).

3.6.3.18.4.1Plating efficiency (PE) and surviving Fraction (SF)

Plating efficiency (PE) is the ratio of number of colonies formed to the number of cells seeded. Different cells have different PE. The PE of astrocytes was calculated using the formula;

$$PE = (No: of\ Colonies\ formed \div No: of\ cells\ seeded) \times 100$$

Number of colonies formed after treatment, denoted in terms of PE is called SF. It is calculated from the formula;

$$SF = No: of\ Colonies\ formed\ after\ treatment \div (No: of\ Cells\ seeded \times PE)$$

3.6.3.18.5 Evaluation of apoptosis by Caspase 3/7 activation assay

Caspase 3/7 activity in response to ZnO bulk formulation and zinc salt ($ZnCl_2$) was detected using SensoLyte Homogeneous AMC Caspase - 3/7 Assay Kit as per section **3.6.3.15.** Cells were seeded at an initial density of $1x10^4$/well and duration of treatment was 24h. The results were compared with caspase activity on ZnO NPs exposure.

3.7 ACUTE TOXICITY STUDIES USING WISTAR RATS

In vivo acute bio-nano interaction studies were carried out in Wistar rats. The detailed flow chart is given in **Figure 3.5**

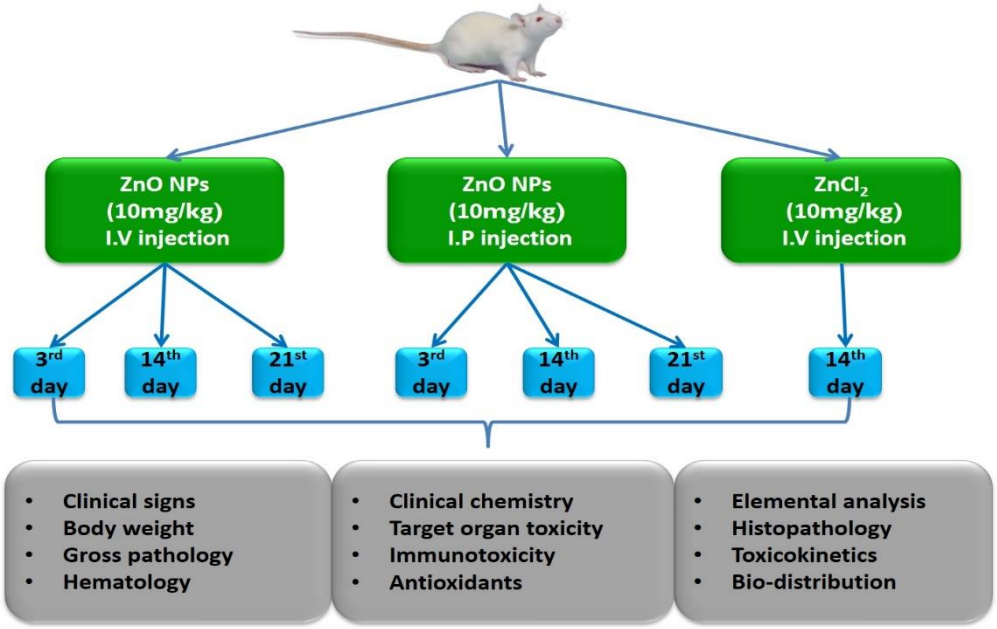

Figure 3:5: Flow chart of *in vivo* bio-nano interaction studies

3.7.1 EXPERIMENTAL DESIGN AND DOSAGE

Healthy Wistar rats weighing 200-250 grams were used for the study. Animals were randomly divided into 8 groups of three animals each, based on the time of observation and route of exposure. The details of the experimental design are given in the **Table 3.2**. The first group received no treatment and were kept as control animals. Three groups of animals received single dose (10mg/kg body weight) of ZnO NPs in saline as i.v. injections. Another three groups received single dose (10mg/kg body weight) of ZnO NPs in saline as i.p. injections. The eighth group was given $ZnCl_2$ (10mg/kg body weight) as i.v. injection. Animals were sacrificed on 3rd day, 14th day and 21st day of exposure. The $ZnCl_2$ exposed animals were sacrificed on 14th day.

Dose	**Route of exposure**	**Number of animals**		
		3rd day	**14thday**	**21st day**
Control (Saline)	Intravenous (i.v.)	3	-	-
10mg/kg ZnO NPs	Intravenous (i.v.)	3	3	3
	Intraperitoneal (i.p.)	3	3	3
10mg/kg $ZnCl_2$	Intravenous (i.v.)	-	3	-

Table 3.2: Experimental design and dosing in Wistar rats

3.7.2 CLINICAL/BEHAVIOURAL SIGNS OF NEUROTOXICITY

Home cage observations of animals were carried out regularly (twice a day till the completion of experiment) to check for clinical signs of stress and neurotoxicity. Apart from the behavioural signs related to nervous system, the animals were monitored for the unusual behaviours like spinning, staggering, hunched body poster and lethargy, lack of grooming, ruffled skin coat and reduced food and water intake.

3.7.3 BODY WEIGHT OF ANIMALS

Body weights of all the animals were recorded regularly throughout the experimental period.

3.7.4 EUTHANIZATION AND SAMPLES COLLECTION

Urine and faecal matter of the animals were collected at the last day of each observation period. Blood samples were collected from the optical sinus of each animal into non-vacuum blood collection tubes at the end of observation period by anesthetizing the animals. The animals were subsequently euthanized by cervical dislocation.

3.7.5 ORGAN WEIGHT

Organs including brain, liver, kidney and spleen were collected from the euthanized animals and wet weight of the organs was recorded.

3.7.6 GROSS PATHOLOGY

Euthanized animals were subjected to gross pathology examinations. Here, the animal bodies were scrutinized for any visible changes like lesions, lumps, colour changes or damages in the body surface, organs and tissue.

3.7.7 HAEMATOLOGY

The blood samples collected in heparinized blood collection tubes were subjected to haematology analysis. The haemoglobin (HGB) level, haematocrit (HCT), red blood cell (RBC), white blood cell (WBC) and platelet (PLT) count were measured using automated haematology analyser, Horiba Vet abc (Japan).

3.7.8 TARGET ORGAN TOXICITY

Organ and fluid samples collected from the animals were analysed to study ZnO NPs mediated organ toxicity. The serum biochemistry analysis was carried out to study liver and kidney functions. Brain, liver, spleen and kidney were subjected to histopathology analysis. Urine analysis and splenocytes proliferation assay was also carried out to study ZnO NPs mediated toxicity on kidney and spleen respectively. Brain and liver samples were subjected to antioxidant assay. Brain volume was measured to study the effect of ZnO NPs on BBB integrity. Blood, brain, liver, spleen, kidney, faeces and urine were subjected to Inductively Coupled Plasma Atomic Emission Spectroscopy to study biodistribution, toxicokinetics and metal homeostasis.

3.7.8.1 Serum biochemistry

The blood samples collected in plain blood collection tubes were allowed to clot. Serum was isolated by centrifuging the tubes at 3500rpm for 15min. Liver and kidney functions were assessed from the serum biochemistry. The samples were analysed for creatinine, protein, albumin, bilirubin, cholesterol, gamma glutamyl transferase (GGT), alkaline phosphatase (ALP), aspartate aminotransferase (SGOT), alanine transaminase (SGPT) using biochemical analyser, Erba Mannheim XL300 (Germany).

3.7.8.2 Urine analysis

Urine collected in sterile airtight tubes were examined for pH, specific gravity, glucose, protein, nitrite, blood, leukocytes, ketones, urobilinogen and bilirubin using urine analyser, Uro-dipchek 300 (Erba Mannheim, Germany).

3.7.8.3 Brain volume

Wet weight of the brain collected from the animals was recorded. The organs were subsequently freeze dried to measure the dry weight of the samples. The difference in the % water content was plotted as change in brain volume.

3.7.8.4 Inductively Coupled Plasma Atomic Emission Spectroscopy (ICP-AES)

Elemental analysis in tissue samples of ZnO NPs exposed rats were studied using Inductively Coupled Plasma Atomic Emission Spectroscopy (ICP-AES). ICP-AES make use of the excitation emission property of electrons. The electron upon excitation with high temperature argon plasma will get excited to a higher energy level. This electron will return to the ground state by emitting energy at a different wavelength. The fundamental characteristic of this process is that each element emits energy at specific wavelengths peculiar to its atomic character. The energy emitted by the electron depends on the electronic configuration of the atomic orbital. Each element can emit energy at different wavelengths, however, in AES a single or few wavelengths are chosen for a given element. The intensity of the energy emitted at a particular wavelength is directly proportional to the amount of element per sample analysed. Hence it is possible to estimate an element both qualitatively and quantitatively by determining the wavelength and intensity at which energy is emitted.

3.7.8.4.1 Sample processing

Blood, urine, brain, liver and kidney collected from the animals were freeze dried. 500mg of the tissues were treated with 10% HNO_3 in clean Teflon tubes. Tissue samples were serially treated with 4ml of 50% HNO_3 twice, 2ml of 100% HNO_3 twice,

followed by $HNO_3/HOCl_3$ (1:1 ratio) once in a sand bath. The acid digestion was continued until samples were completely digested and the acid was evaporated. This process ensured removal of carbonaceous matter to get heavy metals. The resulting residue was rinsed with nanopure water (resistivity -18.3MΩ.cm) into a 50ml volumetric flask and ICP-AES analysis was carried out (The solution can be stored at 4°C for later analysis).

Faecal samples for AES were processed with slight modification. The samples were serially digested in a sand bath with 50% HNO_3 twice, followed by 100% HNO_3 thrice and single step digestion in $HNO_3/HOCl_3$ (1:1 ratio). After the acid digestion, the samples were mixed with 2ml HF and 1.5g H_3BO_3 and melted until evaporation. The resulting residues in tubes were rinsed with nanopure water into a 50ml volumetric flask and stored at 4°C for further analysis by ICP-AES.

3.7.8.4.2 Element detection

The elemental analysis in digested samples was analysed by Inductively Coupled Plasma Atomic Emission Spectroscopy (ICP-AES), Optima 5300 DV ICP-OES spectrometer (Perkin Elmer, USA). Zinc content in the brain is estimated as a measure of ZnO NPs. The zinc is detected at the wavelength of 213.9nm. Copper and iron content in brain were measured along with zinc content to study the influence of ZnO NPs on metal homeostasis. Iron and copper were detected at wavelengths of 238.204 nm and 324.75nm respectively. The results were compared with control samples to assess the particle distribution and kinetics.

3.7.8.5 Histopathology

Histopathological analysis was carried out in brain, liver, spleen and kidney collected from each treatment groups. The tissue samples for histopathology were washed in saline and collected in 10% neutral buffered formaldehyde immediately after euthanization to prevent tissue degradation.

3.7.8.5.1 Tissue processing

Tissue samples were cut into small pieces in order to fit into tissue cassettes. The samples were processed to remove the water from the tissue and gradually infiltrated with paraffin to make thin sectioning possible. The details of the experiment are given in the **Table 3.3**.

Solutions	Duration
Isopropanol I	1h
Isopropanol II	1h
Xylene I	45min
Xylene II	45min
Xylene III	45min
Paraffin wax I	1.15h
Paraffin wax II	1.15h

Table 3.3: Sample processing for histopathology

3.7.8.5.2 Embedding

Processed tissues were picked out of cassettes. They were put into moulds and carefully filled with molten paraffin. It was made sure that the tissues are aligned

properly in the paraffin blocks. The blocks were allowed to cool down before taking them for sectioning.

3.7.8.5.3 Sectioning and slide preparation

The sectioning of the embedded tissue was done using microtome fitted with disposable metal knifes. The sectioning was done by keeping the paraffin blocks cool to avoid cracks in the paraffin sections. The distance between the block and the knife was adjusted in such a way to ensure tissue sections of 5µM thickness. Cut out sections of tissues were floated on a warm water bath to remove wrinkles. The sections were picked upon clean glass microscopic slides pre-coated with Meyer's egg albumin. The slides were pre-treated in solution containing 17.5g NaOH (in 70ml de-ionized water) and 96% ethanol (105ml) for 2h and rinsed in de-ionized water prior to using for histopathology.

3.7.8.5.4 Haematoxylin and Eosin (H&E) staining of slides

H & E staining is the standard protocol used for the morphological examination of tissue sections. The sections were stained as described in the **Table 3.4**. Regressive haematoxylin staining was used in the current study, where a part of the dye is removed by acid alcohol solution to be counterstained by Eosin. On completion of the staining procedure, slides were mounted using DPX to make the samples scratch proof and to provide better optical clarity for slides under microscope.

Steps	Duration
Xylene I	10min
Xylene II	10min
Absolute alcohol	5min
70% alcohol	5min
Distilled water	5min
Harris haematoxylin	8min
Distilled water	Rinse
Acid alcohol	1-2dip
Distilled water	Rinse
Scott's tap water	5min
Distilled water	Rinse
1% Eosin	5min
Distilled water	1dip
70% alcohol	2min
Absolute alcohol	5min
Xylene I	10min
Xylene II	10min

Table 3.4: Procedure for Haematoxylin and Eosin (H&E) staining of tissue sections

3.7.8.6 Antioxidant assay

Antioxidant levels in the brain and liver were estimated after 3rd, 14th and 21st day of exposure.

3.7.8.6.1 Sample preparation

Brain and liver were collected from the animals on 3rd, 14th and 21st day of particle exposure. The organs were washed in saline and transferred to a container kept on ice. 10% tissue homogenate was prepared in 0.1M phosphate buffer of pH 7.4 by

keeping the samples on ice. The tissue was homogenised at 900rpm using tissue homogeniser, Polytron P 3100. The supernatant of the homogenate was collected after centrifuging at 3500rpm for 10min at 4°C. The supernatant was kept on ice for further use.

3.7.8.6.2 Total protein estimation

Total protein in the homogenate was estimated by Lowry's method. This method has sensitivity between 0.01-1mg/ml and is based on the reaction between copper ions produced by the oxidation of peptide bonds with Folin-Ciocalteu reagent. The experimental procedure is as described in the **Table 3.1**. Solution C described in the table was prepared by mixing 50ml solution of sodium carbonate (1g in 50ml distilled water) and 1ml solution of sodium potassium tartarate (10mg) and 5mg copper sulphate. Reading was taken at 660nm using Lambda 25, UV/Vis spectrophotometer, Perkin Elmer, USA. The protein concentration is calculated from the bovine serum albumin (BSA) standard graph.

3.7.8.6.3 Lipid peroxidation

Lipid peroxidation was assessed following the protocol of Ohkawa *et al*., (1979). The experimental procedure is as described in the **Table 3.5**. This method estimates the malonedialdehyde (MDA), an end product of lipid peroxidation. The pink coloured adduct formed from the reaction between thiobarbituric acid and MDA is measured spectrophotometrically (Lambda 25, UV/Vis spectrophotometer, Perkin Elmer, USA) at 532nm as a measure of lipid peroxidation.

Regent	Blank	Test
0.8% TBA	1.5ml	1.5ml
8.1% SDS	0.2ml	0.2ml
20% acetic acid	1.5ml	1.5ml
Tissue homogenate	-	0.2ml
Distilled water	1.0ml	0.8ml
Incubate in water bath at 90° C for 1h		
Distilled water	1ml	1ml
Centrifuge at 3500rpm for 10min		

Table 3.5: Procedure for LPO assay

3.7.8.6.4 Reduced Glutathione (GSH)

GSH level was detected following the method reported by Moron *et al*., (1979). The experimental details are described in the **Table 3.6**. It involves spectrophotometric detection of yellow coloured product formed from the reaction between GSH and DTNB [5, 5'-dithiobis-(2-nitrobenzoic acid)]. The reading was taken at 412nm using Lambda 25, UV/Vis spectrophotometer, Perkin Elmer, USA.

Reagent	Blank	Sample
0.2M phosphate buffer (pH-8)	4ml	4ml
Tissue homogenate	-	0.5ml
2mM DTNB	0.5ml	0.5ml
Distilled water	0.5ml	-

Table 3.6: Procedure for determination of GSH concentration

3.7.8.6.5 Glutathione peroxidase (GPx)

GPx is an enzyme family that catalyse the conversion of hydrogen peroxides to water by the reaction: $2GSH + H_2O_2 \rightarrow GS\text{-}SG + 2H_2O$. GP_X activity was measured as

described by Rotruck *et al*., (1973). Reading was taken at 412nm using spectrophotometer (Lambda 25, UV/Vis spectrophotometer, Perkin Elmer, USA). The steps involved in the experimental procedure are given in the **Table 3.7**.

Reagent	Blank	Test
0.1M phosphate buffer (pH -7)	-	0.4ml
Sodium azide	-	0.1ml
EDTA	-	0.1ml
Tissue homogenate	-	0.1ml
Hydrogen peroxide	-	0.1ml
Distilled water	1ml	1ml
4mM GSH	-	0.2ml
Incubate at 37°C for 0, 90 and 180s for each group of test		
10% TCA	-	0.5ml
Centrifuge at 3500rpm for 5min at 4°C. Collect the supernatant.		
Supernatant	-	1ml
0.3M phosphate solution	4ml	4ml
0.6mM DTNB	0.5ml	0.5ml

Table 3.7: Procedure for GPx activity estimation

3.7.8.6.6 Glutathione reductase (GR)

The conversion of GSSG back to GSH is carried out by GR in the presence of NADPH. The protocol described by Mize and Langdon (1962) is given in **Table 3.8**. The reading was taken at 0, 1, 2 and 3min at a wave length of 340nm (Lambda 25, UV/Vis spectrophotometer, Perkin Elmer, USA).

3.7.8.6.7 Superoxide dismutase (SOD)

SOD converts superoxide radicals to water molecules. The assay was followed as given in **Table 3.9** below (Marklund and Marklund 1974). SOD activity was measured

soon after the addition of pyrogallol at 0, 1, 2 and 3min at 420nm using Lambda 25, UV/Vis spectrophotometer, Perkin Elmer, USA.

Reagents	Blank	Test
0.1M phosphate buffer (pH-7.6)	2.1ml	2ml
0.5mM EDTA	0.5ml	0.5ml
20mM oxidized glutathione	0.15ml	0.15ml
Incubate at 37°C for 10min		
2mM NADPH	0.15ml	0.15ml
Tissue homogenate	-	0.1ml

Table 3.8: Procedure for GR activity estimation

Reagent	Blank	Standard	Test
0.1M Tris buffer (pH -8.2)	3.1ml	2.6ml	2.5ml
1mM EDTA	0.1ml	0.1ml	0.1ml
1mM DTPA	0.5ml	0.5ml	0.5ml
Tissue homogenate	-	-	0.1ml
Pyrogallol	-	0.5ml	0.5ml

Table 3.9: Procedure for SOD activity estimation

3.7.8.7 Splenocytes proliferation assay

The splenocytes of animals isolated after each observation period were used to assess its proliferating capacity. Spleen was transferred to cold PBS containing AB/AM immediately after isolation. Under sterile condition, the spleen was placed on a metallic cell strainer kept over 10mm petridish. Spleen was mashed by gently teasing it over the metallic cell strainer. The single cell suspension was layered carefully over histopaque and centrifuged at 1500rpm for 40min. The resulting buffy coat containing cells were isolated and washed three times with PBS. The cells were cultured at an initial density of $2x10^5$cells/well in RPMI medium supplemented with 10% FBS. After 48h, 0.5µCi of

tritiated thymidine was added to each well and incubated for 24h. Cells were fixed using 5% trichloroacetic acid and lysed with SDS/NaOH lysis buffer. The radioactivity was measured adding scintillation fluid, using scintillation counter (Hidex, Finland). The values were expressed as mean ± SD of counts per minute (CPM).

3.7.8.8 Immunotoxicity

ZnO NPs mediated immunotoxicity was assessed from lymphocyte proliferation assay and NO release assay.

3.7.8.8.1 Lymphocytes proliferation assay

ZnO NPs mediated immunotoxicity was assessed by lymphocyte proliferation assay. The principle involves re-stimulation of splenocytes with antigen *in vitro* and measurement of associated proliferative capacity. Proliferative response will occur only if the animal has been previously immunised to the antigen. The lymphocytes were isolated from spleen as described in section. Isolated lymphocytes were seeded at a density of $2x10^5$cells/well and kept in an incubator overnight. 1µg/ml of ZnO NPs was added to each well and incubated at 37°C for 24h. After 24h, 0.5µCi of tritiated thymidine was added to each well and incubated for 24h. Cells were fixed using 5% trichloroacetic acid and lysed with SDS/NaOH lysis buffer. The radioactivity was measured adding scintillation fluid, using scintillation counter (Hidex, Finland). The values were expressed as mean ± SD of counts per minute (CPM).

3.7.8.8.2 NO release: Griess reagent assay

The splenocytes were isolated as described in section **3.7.8.7.** The cells at an initial density of $2x10^5$cells/well and kept overnight in 5% CO_2 incubator at 37°C. The splenocytes were subjected to Griess reagent assay as described in section **3.6.1.7.3**.

3.8 STATISTICAL ANALYSIS

All the experiments were done in triplicates and values expressed as mean ± SD. Statistical comparison between the control and experimental values were done using students' t-test. In result, analysis $p<0.05$ was considered significant.

CHAPTER 4: RESULTS

4 RESULTS

4.1 SYNTHESIS AND CHARACTERISATION OF ZINC OXIDE NANOPARTICLES (ZnO NPs).

4.1.1 ZnO NPs SYNTHESIS

There are two procedures used to synthesis ZnO NPs. The yield of ZnO R and ZnO SP are 73% and 91% respectively. The synthesised ZnO NPs is white in colour and is sparingly soluble in water. This solution was subjected to dialysis for one-week and ultracentrifugation was carried out at the end of one week. The conductivity and pH of final ultra-filtrate (**Table 4.1**) was measured and were similar to that of ultrapure deionised water, suggesting the complete removal of unreacted residues. The particle in the suspension was sonicated and remained stable up to 24h.

Sample	Conductivity (µS/m)	pH
ZnO R	3.21	7.1
ZnO SP	2.17	7
dH_2O	2.5	7

Table 4.1: Conductivity and pH measurement of ZnO NPs

4.1.2 PHYSICO-CHEMICAL CHARACTERISATION

The physico-chemical characterisations of the synthesised ZnO NPs were carried out using different techniques is detailed below.

4.1.2.1 Scanning Electron Microscopy (SEM)

The morphology of the samples was identified by SEM analysis **(Figure 4.1)**. The rod shaped morphology of ZnO R and spearhead morphology of ZnO SP were

confirmed using SEM. Both particles exhibited uniform morphology. Secondary particles formed from the aggregation were also not observed in the same morphology.

4.1.2.2 Transmission Electron Microscopy (TEM)

Size of ZnO NPs were analysed by TEM. ZnO R displayed broad size distribution with an average size of 43nm. ZnO SP exhibited a narrow size distribution with an average size of 22nm. Diffraction peaks depicted the monocrystalline nature of the ZnO NPs. The high resolution TEM (HR-TEM) images of the samples showed no signs of crystal defects. The results of the TEM analysis are shown in **Figure 4.2.**

4.1.2.3 Brunauer–Emmett–Teller (BET) analysis

The surface area and surface reactivity increases with decrease in size of nanoparticle. The specific surface area (SSA) of nanoparticles was analysed by Brunauer- Emmett -Teller (BET) method. SSA of ZnO NPs is described in **Table 4.2.** The surface area of ZnO SP was higher when compared to ZnO R. These results substantiate the findings of TEM analysis.

Sample	Specific surface area (m^2/g)
ZnO R	37.07± 0.61
ZnO SP	49.61± 0.13

Table 4.2: Specific surface area of ZnO NPs. ZnO R: ZnO NPs rod shape, ZnO SP: ZnO NPs spearhead shape. Data represents mean±SD of three independent experiments.

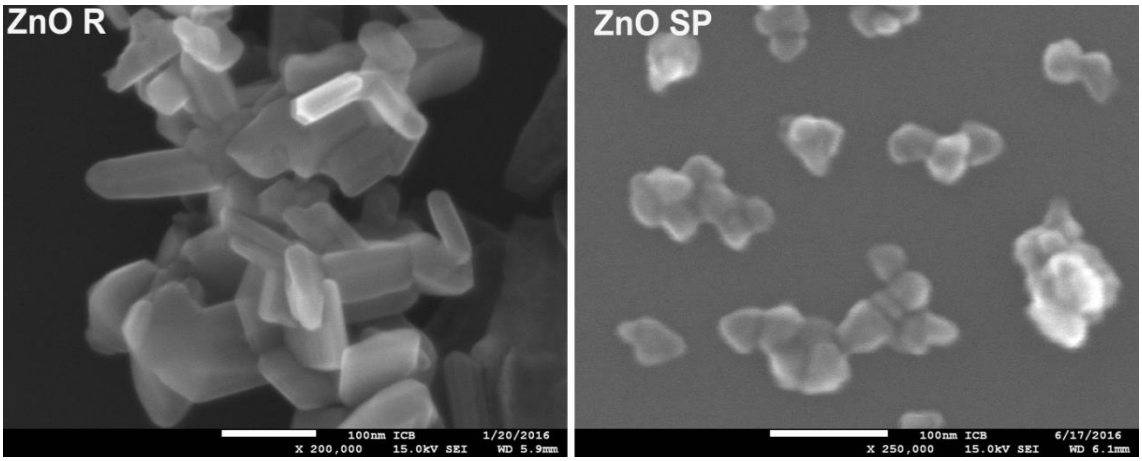

Figure 4:1: Morphology of ZnO NPs using SEM analysis: ZnO R: ZnO NPs rod shape, ZnO SP: ZnO NPs spearhead shape.

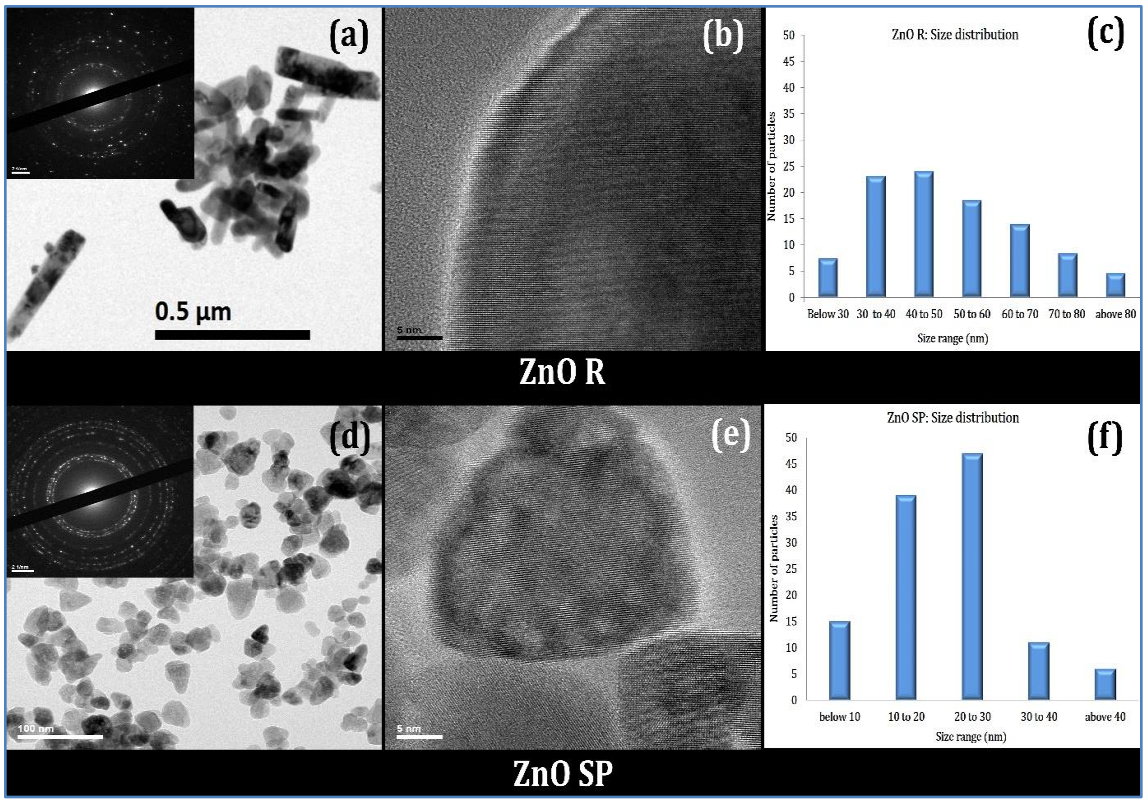

Figure 4:2: TEM analysis of ZnO NPs. **(a)**TEM image of ZnO NPs rod shape; inset shows diffraction pattern of ZnO rod shape. Magnification 50k **(b)** HR-TEM image of ZnO rod (ZnO R). Magnification 500k**(c)**Size distribution of ZnO R **(d)**TEM image of ZnO NPs spearhead (ZnO SP); inset shows diffraction pattern of ZnO spearhead. Magnification 50k **(e)**HR-TEM image of ZnO spearheads shape. Magnification 500k.**(f)** Size distribution of ZnO SP.

4.1.2.4 Dynamic Light Scattering (DLS)

Influence of media on colloidal stability was studied using DLS. The hydrodynamic diameter (Z average dm) and polydispersity index (PDI) of ZnO R and ZnO SP in water, cell culture medium (DMEM F12), and physiological saline are given in the **Table 4.3.**

Sample	Parameters	Dispersant		
		Water	**Saline**	**DMEM F12**
ZnO R	Z average dm (nm)	350.0 ± 7.31	1000 ± 18.3	805.1 ± 9.65
	PDI	0.418 ± 0.02	0.866 ± 0.44	0.508 ± 0.03
ZnO SP	Z average dm (nm)	111.0 ± 2.06	603.0 ± 14.2	436.2 ± 3.11
	PDI	0.113 ± 0.01	0.347 ± 0.04	0.420 ± 0.02

Table 4.3: Effect of dispersant on hydrodynamic diameter and polydispersity index (PDI) of ZnO NPs using DLS. Data represents mean±SD of three independent experiments.

Concentration of particles increases when the nanoparticles undergo agglomeration. To study the effect of nanoparticle concentration on particle size, hydrodynamic diameter was determined at three different concentrations (20, 40, 80 μg/ml) using DLS. The results are given in the **Table 4.4.** ZnO R exhibited concentration dependent increase in size. The PDI did not show much variation and was around 0.4. The size ZnO SP was similar in all three concentrations suggesting absence of agglomeration. The PDI of ZnO SP was around 0.1, revealing monodisperse nature of the solution.

Batch	Concentration	Z average dm (nm)	PDI
ZnO R	20 µg/ml	336.2 ± 6.78	0.422 ± 0.06
	40 µg/ml	377.7 ± 8.49	0.429 ± 0.03
	80 µg/ml	472.6 ± 10.7	0.495 ± 0.03
ZnO SP	20 µg/ml	111.2 ± 2.24	0.116 ± 0.01
	40 µg/ml	111.1 ± 0.67	0.122 ± 0.01
	80 µg/ml	111.7 ± 2.54	0.110 ± 0.03

Table 4.4: Hydrodynamic diameter and polydispersity index (PDI) of concentration of ZnO NPs using DLS. Data represents mean±SD of three independent experiments.

4.1.2.5 Zeta potential

The surface charge of ZnO R and ZnO SP was measured by zeta potential. The zeta potential was measured over a range of pH, 2 to 11. Zeta potential of both samples varied from 30 to -25 in 2 to 11 pH range. It was observed that ZnO R and ZnO SP exhibited a positive charge at physiological pH. Similarly, isoelectric pH of ZnO R and ZnO SP was 9.3 and 9.2 respectively (**Figure 4.3)**.

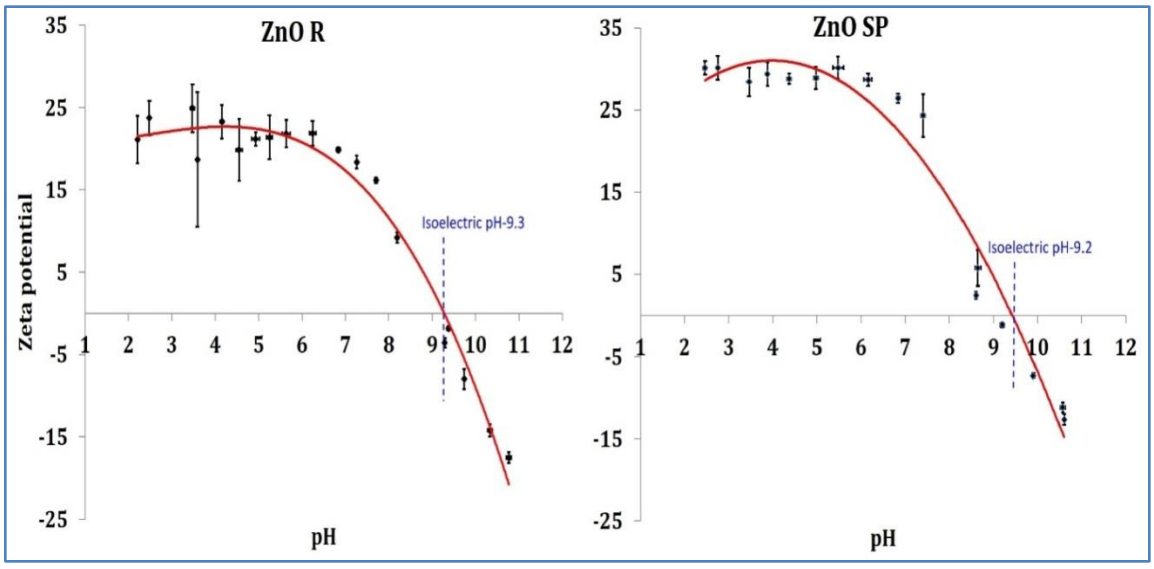

Figure 4:3: Zeta potential of ZnO rod (ZnO R) and ZnO Spearhead (ZnO SP).

4.1.2.6 Thermogravimetric analysis (TGA)

TGA is a technique which analyse the components based on the degradation temperature. 4% weight reduction was observed in ZnO R at 250°C corresponding to the adsorbed water moieties on the nanoparticle surface. ZnO SP showed a 3% weight loss between 180°C and 450°C, mainly because of the surface adsorbed water molecules and atmospheric carbonates. TGA curves of ZnO R and ZnO SP are shown in **Figure 4.4.**

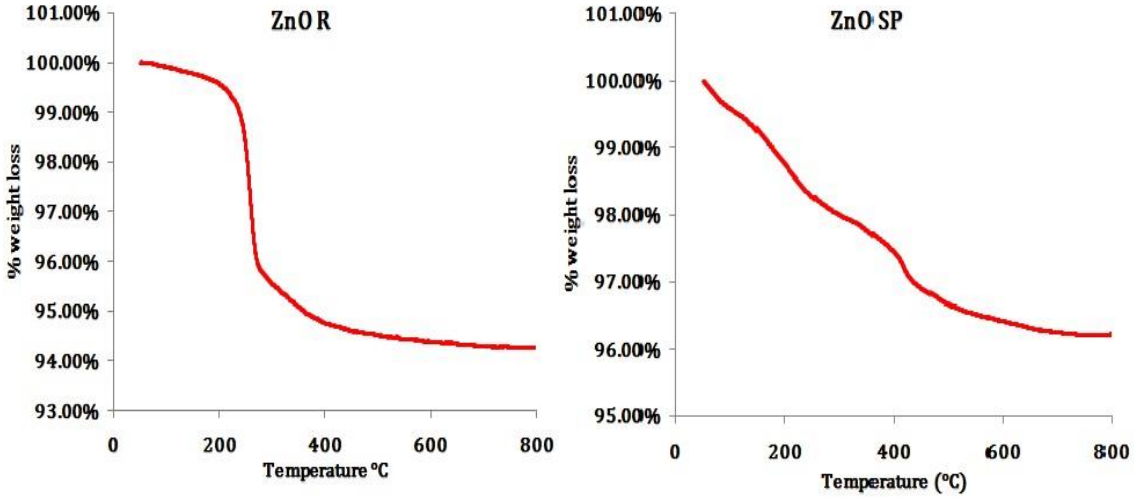

Figure 4:4: TGA of ZnO NPs rod (ZnO R), ZnO NPs spearhead (ZnO SP)

4.1.2.7 X-Ray Diffraction (XRD):

Wurtzite crystal structure of ZnO R and ZnO SP was confirmed by crystallographic patterns measurements by XRD. All the crystals of ZnO NPs belong to space group P63mc. Nanosized nature of the ZnO R and ZnO SP were confirmed by definite line broadening of diffraction peaks (**Figure 4.5)**.

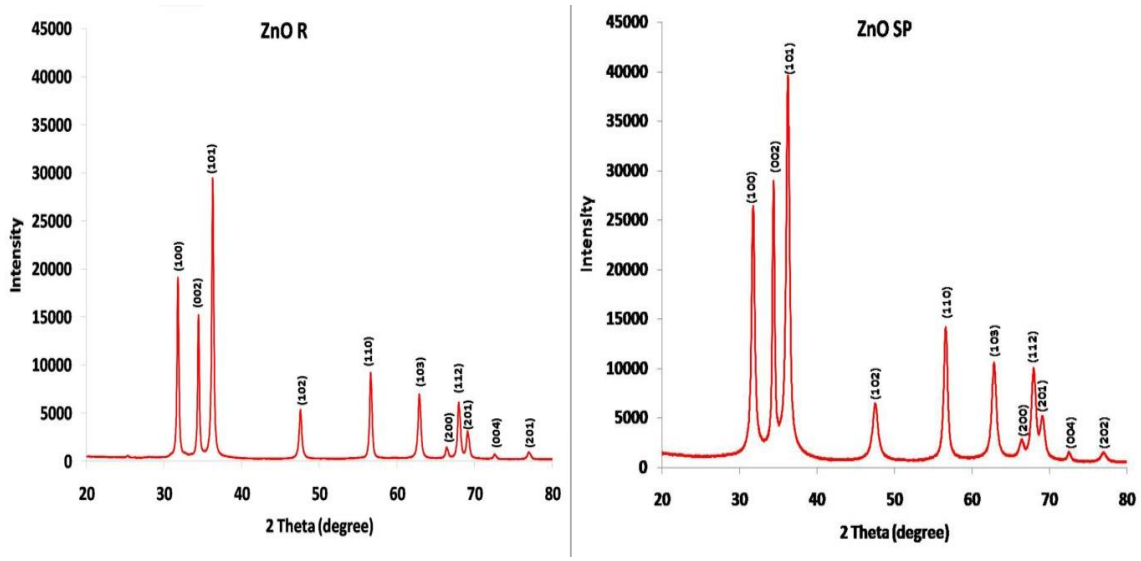

Figure 4:5: XRD analysis: ZnO NPs rod (ZnO R), ZnO NPs spearhead (ZnO SP)

The crystal size of the particles was calculated from Debye-Scherrer's equation and was around 45nm for ZnO R. ZnO R showed traces of impurities and strain calculated was 0.204.

Parameters	ZnO R	ZnO SP
Lattice constants: a (Å)	3.2502	3.2518
c (Å)	5.2081	5.2125
c/a	1.6024	1.6029
Crystal size(nm)	45	20
Strain	0.204	0

Table 4.5: Lattice parameters, crystal size and strain of ZnO NPs using XRD. ZnO NPs rod (ZnO R), ZnO NPs spearhead (ZnO SP).

The crystal size of ZnO SP was 20nm and was comparable to the value obtained in TEM analysis. The XRD pattern revealed no traces of impurities. The strain size calculated for ZnO SP was zero. The c/a ratio calculated for both samples were near to

ideal value of hexagonal cell which is 1.63. The lattice parameters of both samples are given in the **Table 4.5**.

4.1.2.8 X-ray photoelectron spectroscopy (XPS)

The XPS analysis was carried out to analyse the purity of the samples. The binding energies were corrected using the adventitious peak at 284.8eV of graphitic carbon. Peaks of oxygen and zinc spectra were fitted using binding energies of different components present (**Figure 4.6**). The lower binding energy of 529.3eV corresponds to oxides, whereas the higher binding energies of 530.7eV and 532.5eV correspond to hydroxides and carbonates of ZnO R. The Zn_2P_3 spectra showed binding energy of 1021.9eV corresponding to Zn-O.

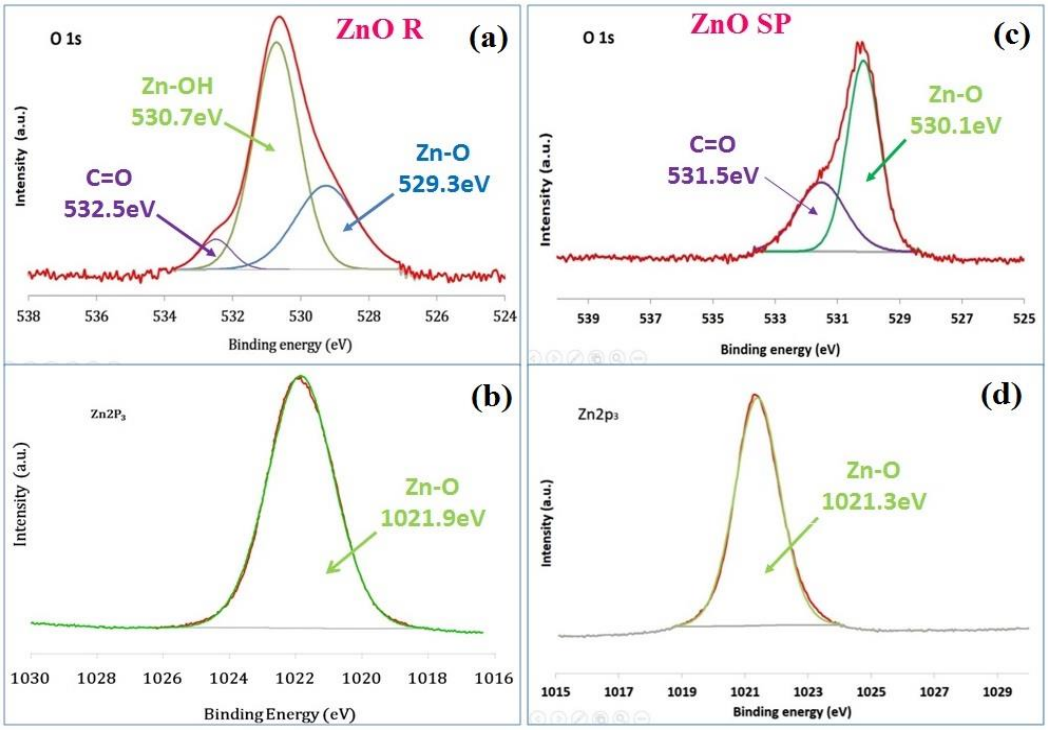

Figure 4:6: XPS analysis of ZnO NPs. **(a)** O1s spectra of ZnO R, **(b)** Zn_2P3 spectra of ZnO R, **(c)** O1s spectra of ZnO SP, **(d)** Zn_2P3 spectra of ZnO SP. ZnO NPs rod (ZnO R), ZnO NPs spearhead (ZnO SP).

O1s spectra of ZnO SP indicated two components with binding energies of 530.1eV and 531.5eV corresponding to oxides and surface adsorbed carbonates respectively. The binding energy of 1021.3eV corresponding to Zn-O were shown in Zn_2P_3 spectra of ZnO SP.

4.1.3 BIOLOGICAL CHARACTERISATION

4.1.3.1 Endotoxin detection

Toxicity data may be altered by the endotoxin contamination. The synthesised nanoparticles were subjected to determine the endotoxin contamination by PTS method. The results of the assay indicated that the endotoxin level was ≤ 0.05 EU/ml in both ZnO R and ZnO SP which is well below the USP (United States Pharmacopeia) recommended level.

4.1.3.2 Effect of cell culture media on the size of the nanoparticle

The composition of media and time of incubation may have an effect on the size and stability of the nanoparticles. ZnO NPs were incubated with two different culture media, RPMI and DMEM F12. The size of ZnO NPs incubated at different time periods and culture media is indicated in the **Table 4.6.** It was found that size of the particle fluctuated over different time period in Roswell Park Memorial Institute medium(RPMI), however the size was more or less similar in Dulbecco's Modified Eagle Medium/Nutrient Mixture F-12 (DMEM F12).

Sample	Time of exposure	Z average (nm)	PDI
RPMI	5 min.	441.58 ± 3.44	0.51 ± 00
DMEM F12		380.25 ± 3.44	0.47 ± 00
RPMI	30min.	633.72 ± 13.1	0.31 ± 0.05
DMEM F12		379.11± 5.72	0.45 ± 0.01
RPMI	60min.	620.04 ± 7.44	0.29 ± 0.03
DMEM F12		378.35 ± 6.37	0.44 ± 0.02
RPMI	24h	609.18 ± 2.26	0.28 ± 0.01
DMEM F12		372.25 ± 2.31	0.38 ± 0.04

Table 4.6: Effect of cell culture medium on the size of nanoparticles: Polydispersity index (PDI) of ZnO NPs by DLS. Data represents mean±SD of three independent experiments.

4.1.3.3 Protein corona formation

The protein corona formation influences the property of the nanoparticle. The ZnO NPs incubated with FBS for 1hwere analysed for protein corona formation. Corona formation was evident in ZnO NPs exposed to FBS. The amount of protein adsorbed on the surface depended on the concentration of protein. Two major bands were observed in SDS-PAGE gel which corresponds to albumin (66kDa) and immunoglobulins (16kDa). Similar band patterns were observed in FBS. However, ZnO NPs pre-exposed to PBS for 2h had band pattern different from that of particles directly exposed to FBS. It was observed that 16kDa protein band was not present in this case (**Figure 4.7**).

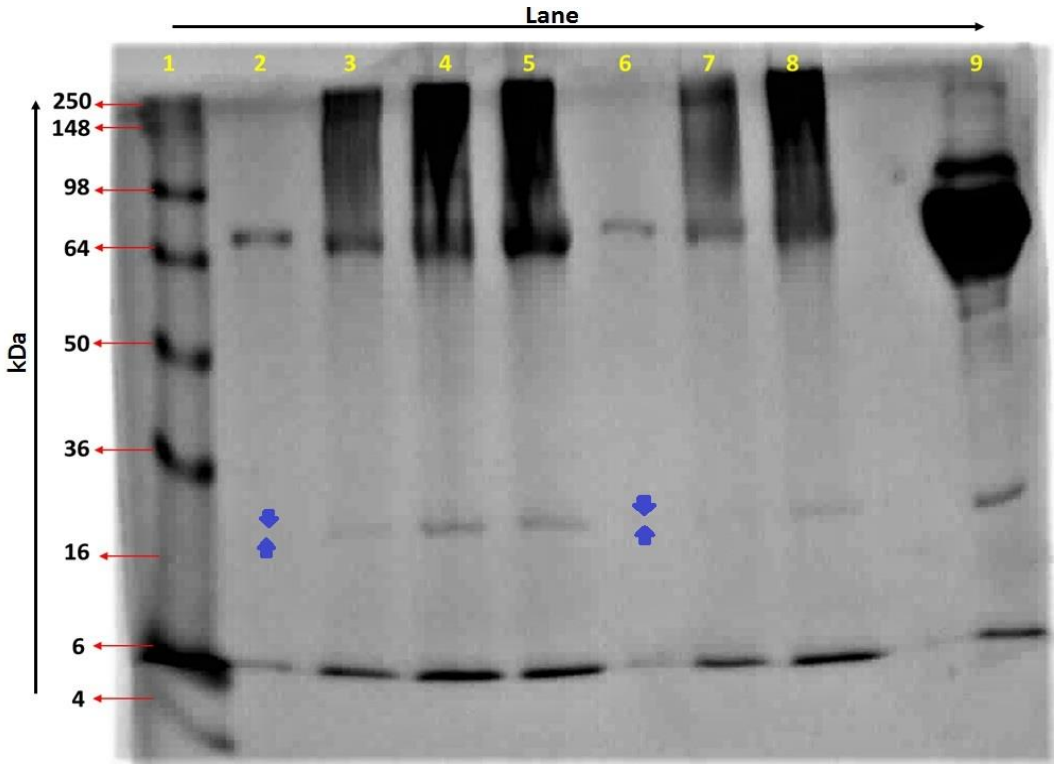

Figure 4:7: Protein corona formation in ZnO NPs. Lane1: marker, lane2 and lane 6:40µg/ml ZnO NPs in PBS with 10% FBS, lane 3 and lane7:40µg/ml ZnO NPs in water with 10%FBS, lane4:80µg/ml ZnO NPs in water with 10%FBS, lane5 and lane 8:1mg/ml ZnO NPs in water with 10%FBS, lane 9:10%FBS in water. The blue solid arrows mark the region where 16kDa bands are missing.

4.2 BIO-NANO INTERACTIONS *IN VITRO* USING GLIAL CELLS

4.2.1 CELLULAR INTERACTION OF ZnO NPS WITH BV2 CELLS

4.2.1.1 Dose response by MTT assay

Figure 4.8 indicated ZnO NPs exposure mediated alteration of mitochondrial activities of BV2. A dose dependent increase in mitochondrial activity was observed in BV2 cells incubated with ZnO NPs for 6h. A statistically significant increase in mitochondrial activity was observed in cells when exposed to 20µg/ml (117.14±4.09), 40µg/ml (144.14±4.23) and 80µg/ml (164.85± 3.86) of ZnO NPs. In contrast to this a statistically significant decrease in mitochondrial activity was observed in 5µg/ml

(80.09±4.64), 10µg/ml (65.12±2.00), 20µg/ml (42.80±1.35), 40µg/ml (36.03±4.33) and 80 (26.95±5.22) µg/ml at 24h.

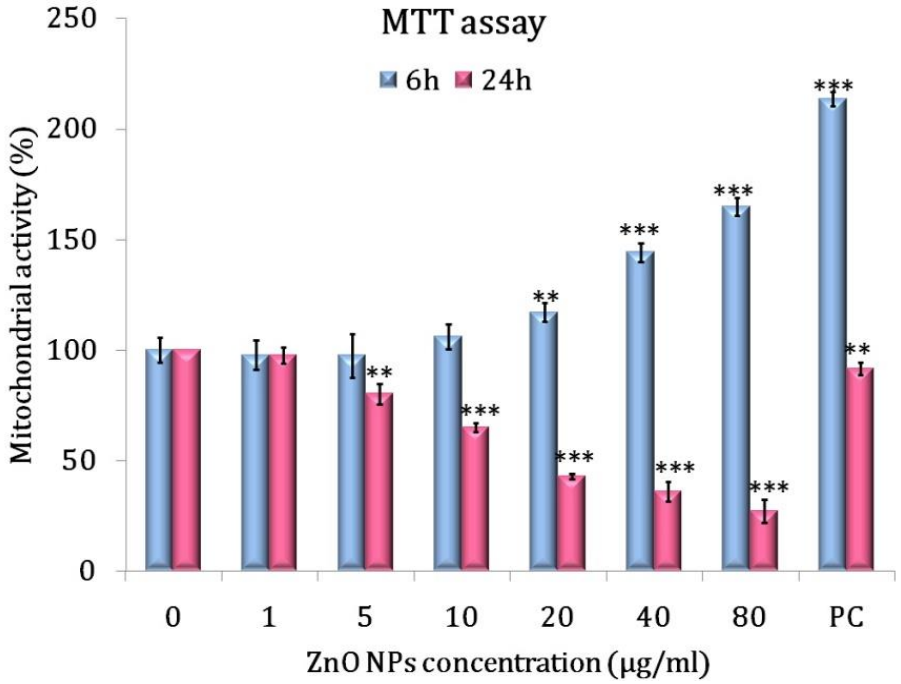

Figure 4:8: MTT assay on BV2 cells exposed to ZnO NPs for 6 and 24h. The values are expressed in percentage with respect to control. 7-Ketocholestrol treated cells were used as positive control. The data represent mean ± SD of three independent experiments. Asterisk above columns denotes statistically significant difference, compared to the control (**p< 0.01 and ***p<0.001).

4.2.1.2 Interference of ZnO NPs with MTT result

Absorbance at 540nm for varying concentrations of ZnO NPs indicates that the particles did not interfere with MTT results. **Figure 4.9** shows the similar absorbance values in both control and ZnO NPs.

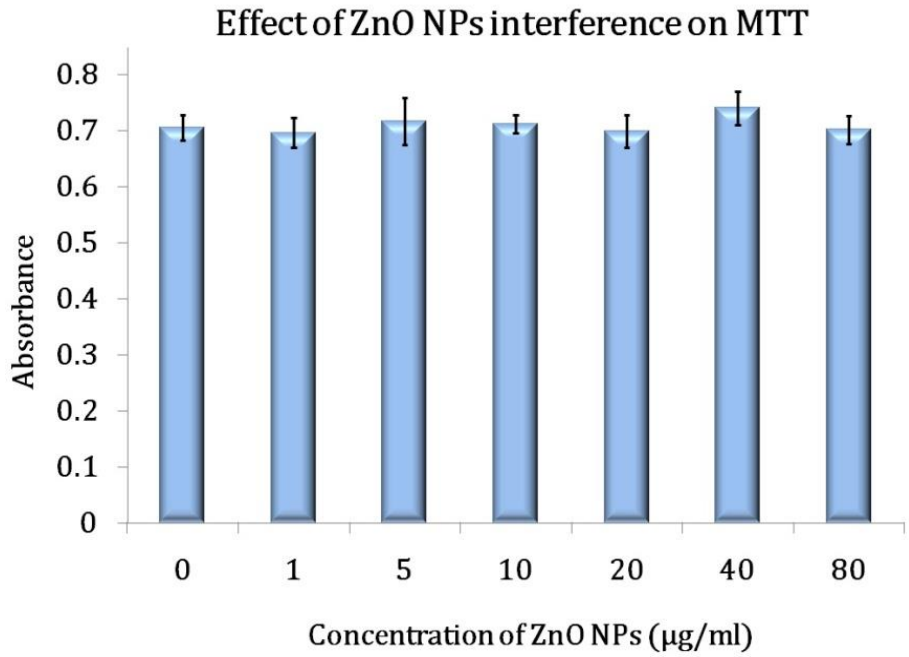

Figure 4:9: MTT assay on cell culture medium incubated with ZnO NPs for 4h. The data represent mean ± SD of three independent experiments.

4.2.1.3 Cell count by trypan blue exclusion assay

Trypan blue exclusion assay showed time and dose dependent changes in cell count **(Figure 4.10).** No statistically significant changes in total cell count were observed at 6h of ZnO NPs incubation. However, a significant increase in number of dead cells was evident for 20, 40 and 80 µg/ml ZnO NPs treated samples at 6h. A statistically significant reduction in total cell count was observed at 24h. There was a dose dependent increase in dead cells up to 20µg/ml. However, at higher concentrations (40 and 80µg/ml) the total cell count dropped markedly with a consequent decrease in both dead and living cells.

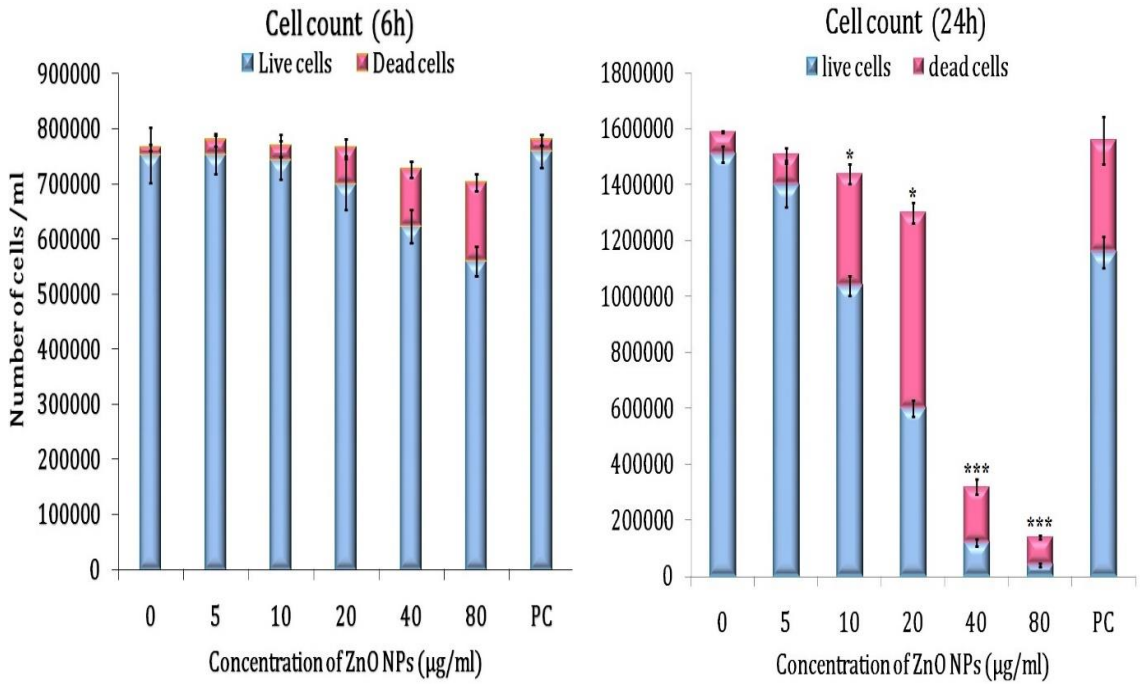

Figure 4:10:Trypan blue exclusion assay on BV2 cells exposed to ZnO NPs for 6 and 24 h. 7-Ketocholestrol treated cells were used as positive control. The data represent mean ± SD of three independent experiments. Asterisk denotes statistically significant difference in total cell count, compared to the control group (*$p<0.05$ and ***$p<0.001$).

4.2.1.4 Cellular phenotype by phase contrast microscopy:

When the cells are exposed to toxic material, it may undergo alteration in morphology. The morphology changes in presence of ZnO NPs was analysed by direct observation under phase contrast microscope. At 6h of incubation, no visible alterations in morphology was observed in treated cells except at higher concentrations; 40 and 80µg/ml ZnO NPs exposed cells exhibited disintegrated and vacuolated cells. Exposure of 40 and 80µg/ml ZnO NPs for 24h resulted in complete disintegration of the cells. Spilled out cytoplasmic contents and cell ghosts were visible in the treated cells. A very few cells remained intact at this concentration (**Figure 4.11**).

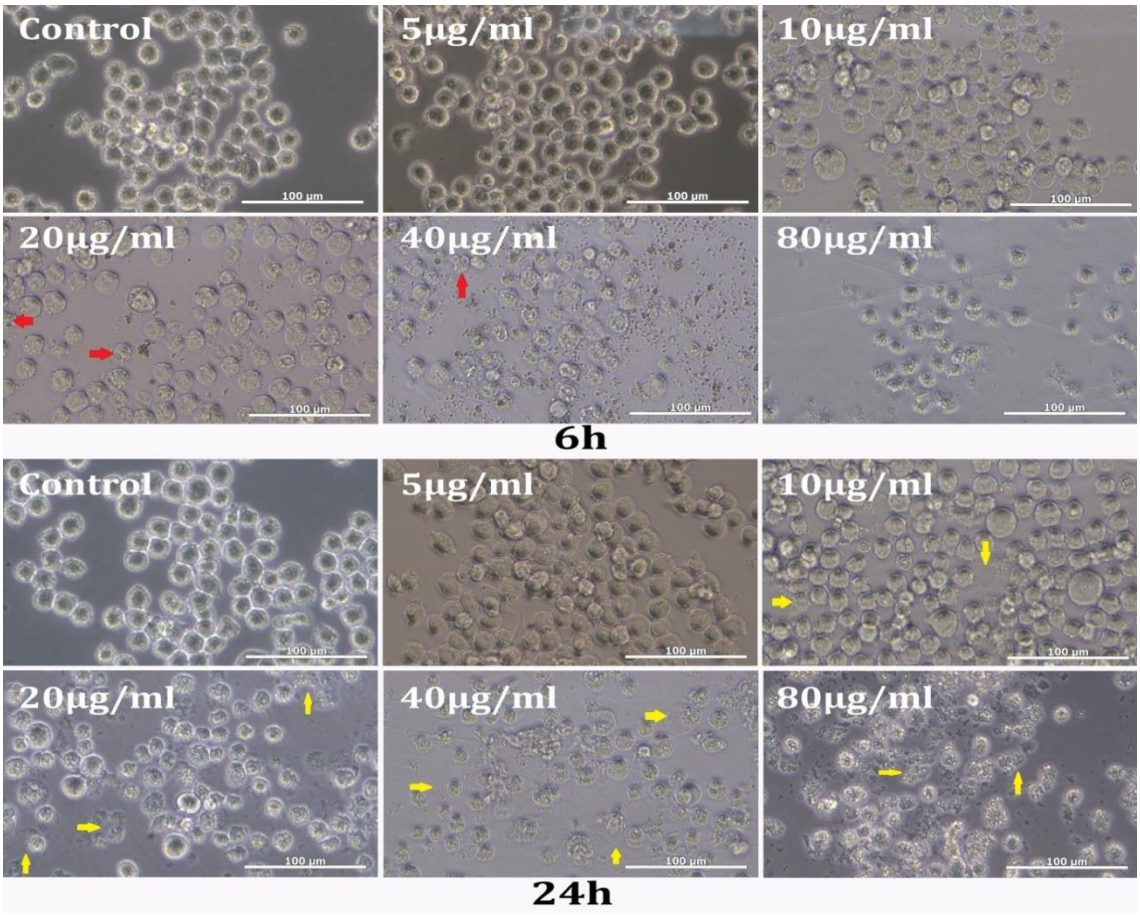

Figure 4:11:Cellular phenotype using phase contrast microscopy: BV2 cells exposed with ZnO NPs for 6 and 24h. Scale bar represents 100µm.Red arrows indicate vacuolated cells. Yellow arrows indicate cellular ghosts and spilled cytoplasmic contents. Magnification: 40X

4.2.1.5 Particle uptake by flow cytometry

Particle uptake was studied using FACS by comparing FSC/ SSC changes in the treatment and control groups. As shown in the **Figure 4.12**, a concentration dependent increase in SSC was observed without much alteration in the FSC parameter. This suggests, increased granularity in the treatment groups due to particle uptake. 80µg/ml treatment group exhibited 29.6% increase in SSC compared to in control (2.17%)and 5µg/ml (5.38%) groups.

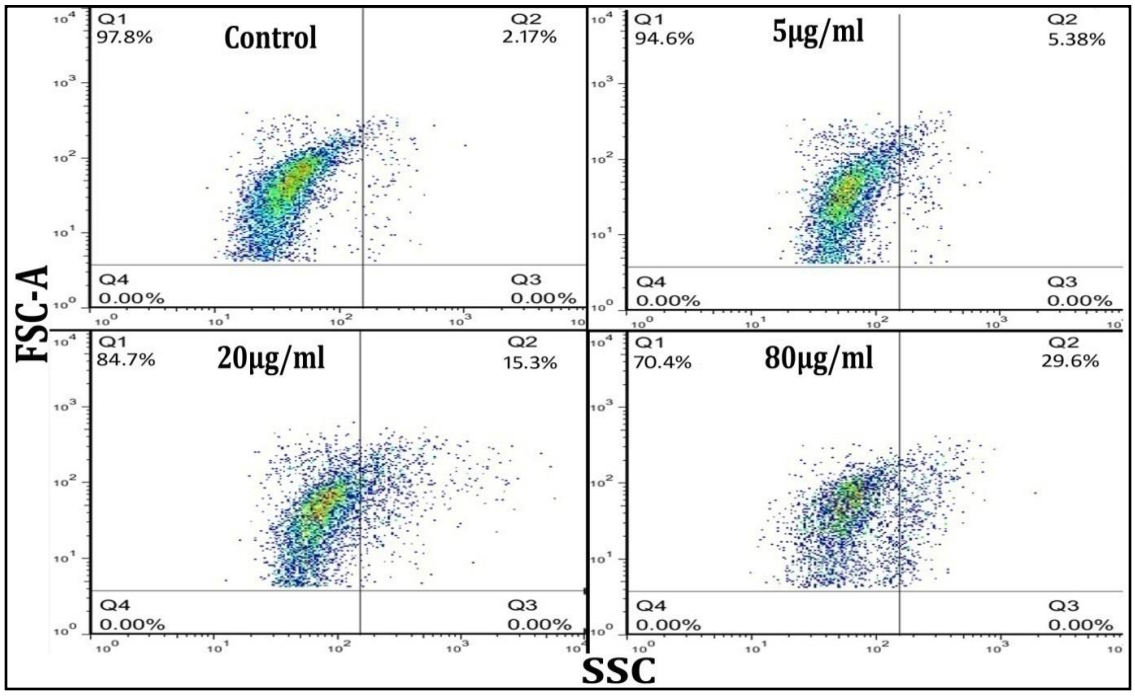

Figure 4:12: Flow cytometry analysis of ZnO NPs uptake by BV2 cells. Cellular debris was gated out to include healthy cells. n=3. SSC: Side scatter. FSC: Forward scatter.

4.2.1.6 Free radical formation:

4.2.1.6.1 Superoxide radicals by DHE staining

ZnO NPs upon interacting with cells induce superoxide anions which were detected by fluorescent probe DHE. The FACS analysis revealed a dose and time dependent increase in the DHE fluorescence as shown in **Figure 4.13**. The mean fluorescence intensity of 80µg/ml of ZnO NPs was 55.63±2.52 (at 3h), 103.08±1.18 (at 6h) and 165.39±14.24 (at 24h), whereas, the values of control were 23.39±1.05, 25.93±2.27 and 30.22±7.47for 3h, 6h and 24h respectively.

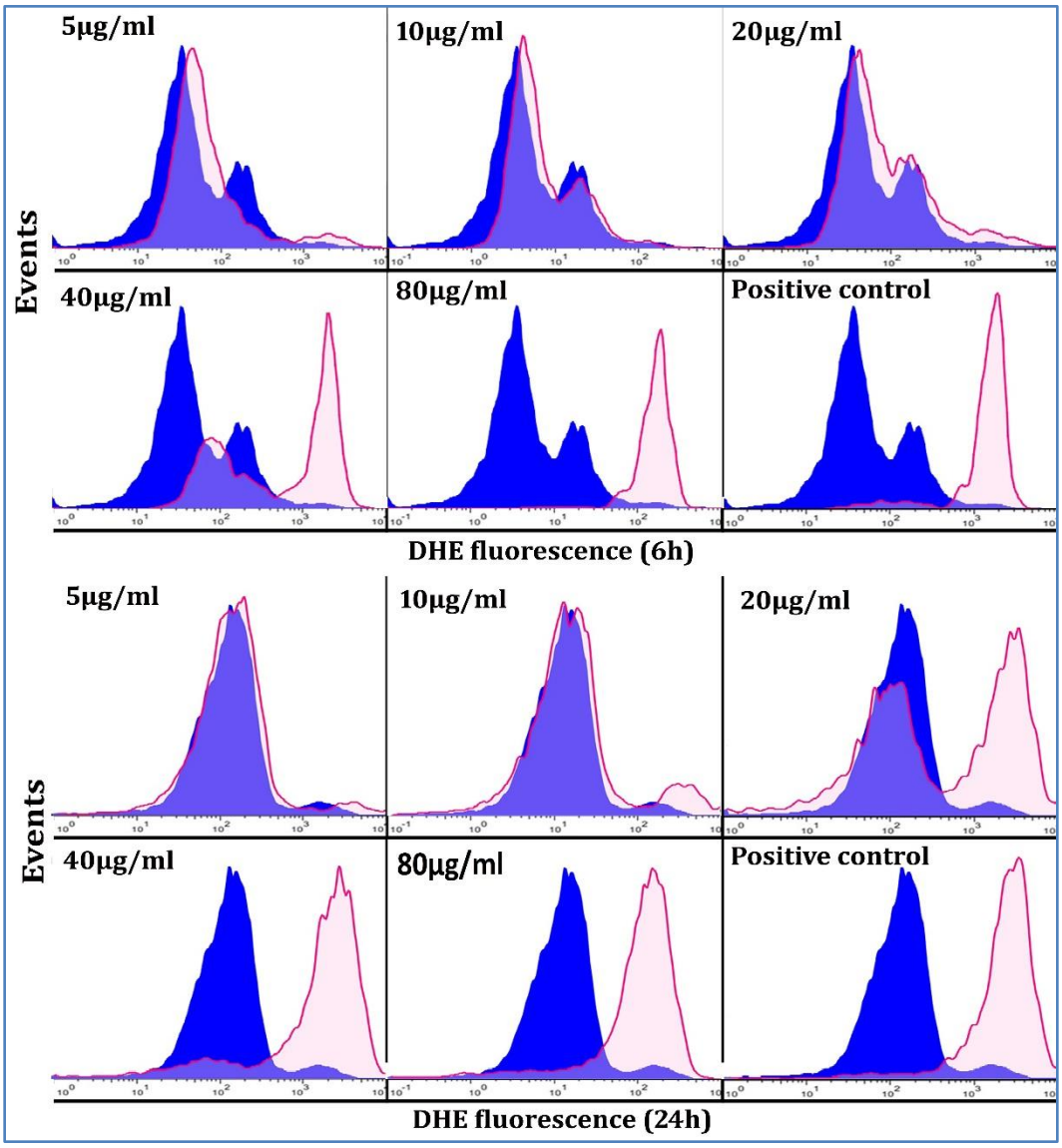

Figure 4:13: Superoxide anion production in BV2 cells exposed to ZnO NPs for 6h and 24h. Blue solid peaks denote the DHE fluorescence of untreated control and pink tinted peaks represent treatment population. 7-Ketocholestrol treated cells were used as positive control. The gated population include both dead and viable cells. n=3

4.2.1.6.2 Hydrogen peroxide (H_2O_2) by DHR 123 staining

Super oxide radicals' formed in the cells can react with water to form H_2O_2 which can readily decompose to give hydroxyl radical. The H_2O_2 level was estimated

by DHR 123 probe. Cells exhibited no significant alteration in H_2O_2 level at 6h of incubation except at 40 and 80µg/ml. The cells showed a dose dependent increase in the fluorescence at 24h with 80µg/ml treated sample displaying highest intensity **(Figure 4.14)**.

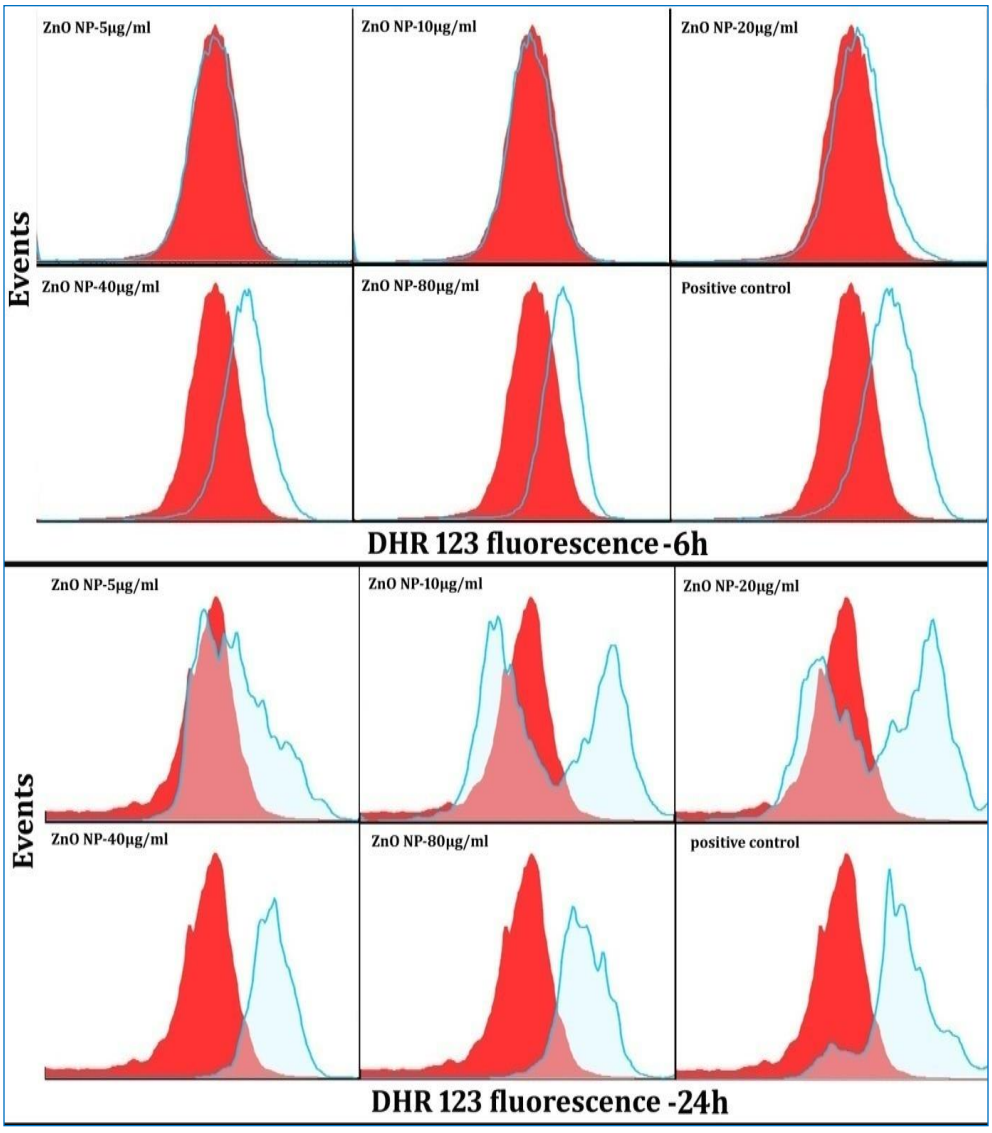

Figure 4:14: Hydrogen peroxide production in cells exposed to ZnO NPs for 6h and 24h. Red solid peaks denote DHR 123 fluorescence of untreated control and blue tinted peaks represent treatment populations. 7-Ketocholestrol treated cells were used as positive control. The gated population include both dead and viable cells. n=3.

4.2.1.6.3 Nitrile radical by Griess reagent assay

Upon activation, the microglial cells (BV2) may produce nitrile radical. The production of nitrile radical was estimated using Griess reagent after 6h and 24h of exposure to particle **(Figure 4.15).** The microglial cells displayed a dose dependent increase in nitrile radical at 6h of exposure. At 24h, there was no statistically significant increase in production of nitrile radical.

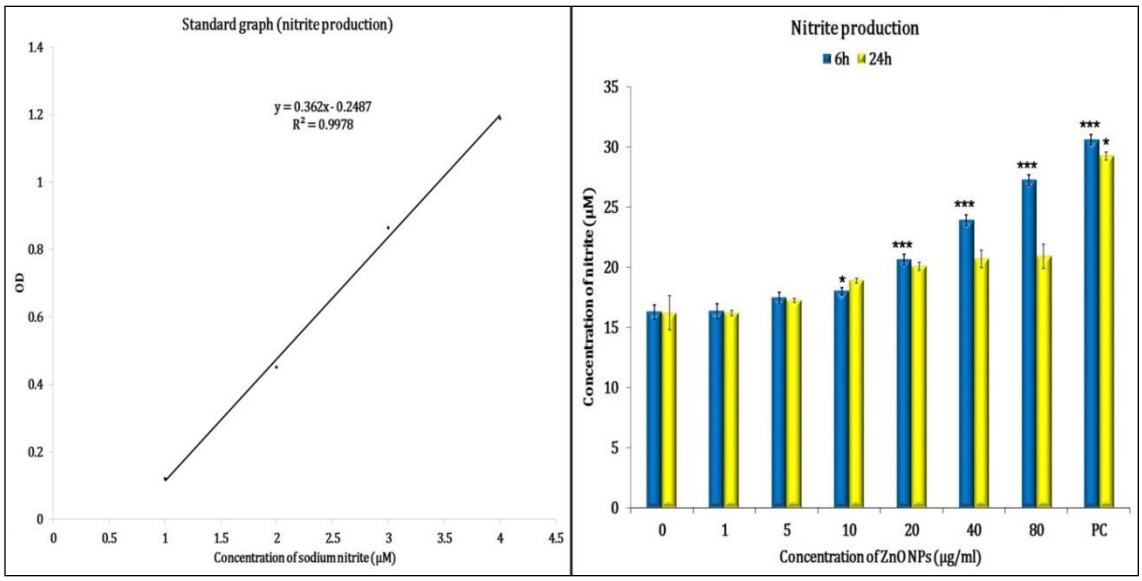

Figure 4:15: Griess reagent assay showing nitrite production in BV2 cells exposed to ZnO NPs at 6 and 24h. 1µg/ml LPS (lipopolysaccharides) treated samples were used as positive control. The data represent mean ± SD of three independent experiments. Asterisk denotes statistically significant difference, compared to the control group (*p<0.05 and ***p<0.001).

4.2.1.7 Mitochondrial membrane potential by $DiOC_6(3)$ staining

Mitochondrial membrane potential was analysed using the fluorescent probe $DiOC_6(3)$. As shown in **Figure 4.16**. It was noted that, cells manifested mitochondrial hyperpolarisation in a dose dependent manner at 6h of incubation. The cells did not show any reduction in mitochondrial membrane potential even at 24h. The membrane potential at 24h was comparable with the control.

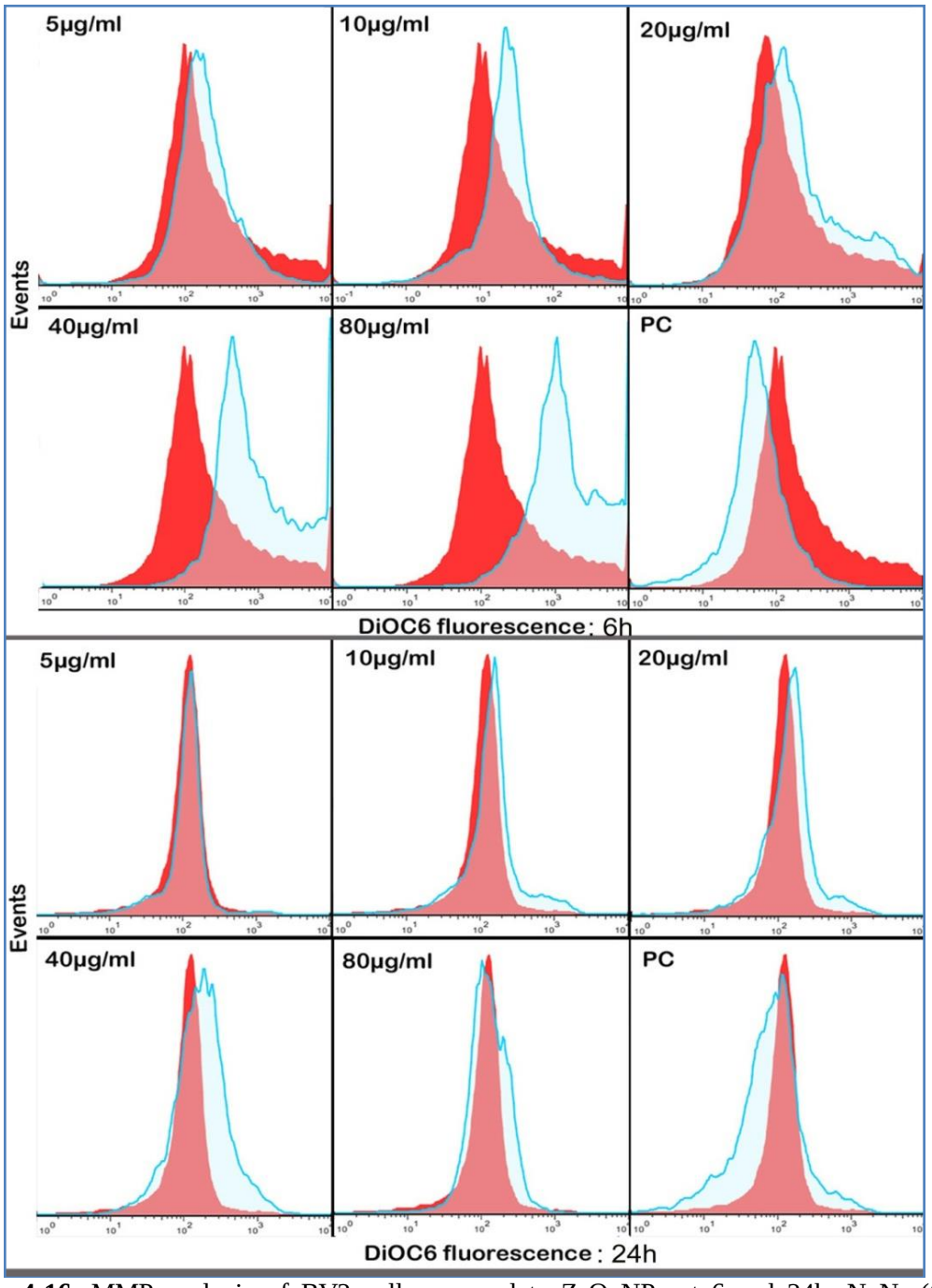

Figure 4:16: MMP analysis of BV2 cells exposed to ZnO NPs at 6 and 24h. NaN_3 (1mM) treated cells were used as positive control. Grey solid peaks represent DiOC6 intensity of untreated control while grey tinted peaks represent treatment groups. The gated population include both dead and viable cells. n=3.

4.2.1.8 Lysosomal integrity by acridine orange (AO)

Lysosomal integrity was studied using AO. The AO fluorescence analysed by FACS, revealed a time and dose dependent alteration of lysosomal activity (**Figure 4.17)**. At 6h of incubation, 40 and 80 µg/ml ZnO NPs treated group exhibited a subpopulation with reduced fluorescence. There was a reduction in fluorescence observed at 24h in all treated groups.

4.2.1.9 Cell membrane integrity by Propidium Iodide (PI) staining

Cell membrane integrity was analysed by flow cytometry using PI staining. The FACS results indicated a dose dependent increase in plasma membrane permeability **(Figure 4.18)**. High number of PI positive cells (65%) was observed in 80 µg/ml treatment groups which was comparable with the positive control (H_2O_2 treated group).

4.2.1.10 Cell cycle analysis by flow cytometry

The ZnO NPs exposed BV2 cells were stained with PI and was analysed by FACS. A slight dose dependent increase in subG1 population was observed in the treatment group with respect to control. The cells treated with 40 and 80 µg/ml had a subG1 population of 5% and 9% respectively. No sub G1 population was observed for the control group. Other cell cycle phases like G0-G1, S and G2-M were comparable in both treatment and control groups. On the other hand, cells treated with 7-Ketocholesterol showed a marked reduction of cells in S phase (9%) with respect to control group (26%). The cell cycle patterns are indicated in **Figure 4.19.**

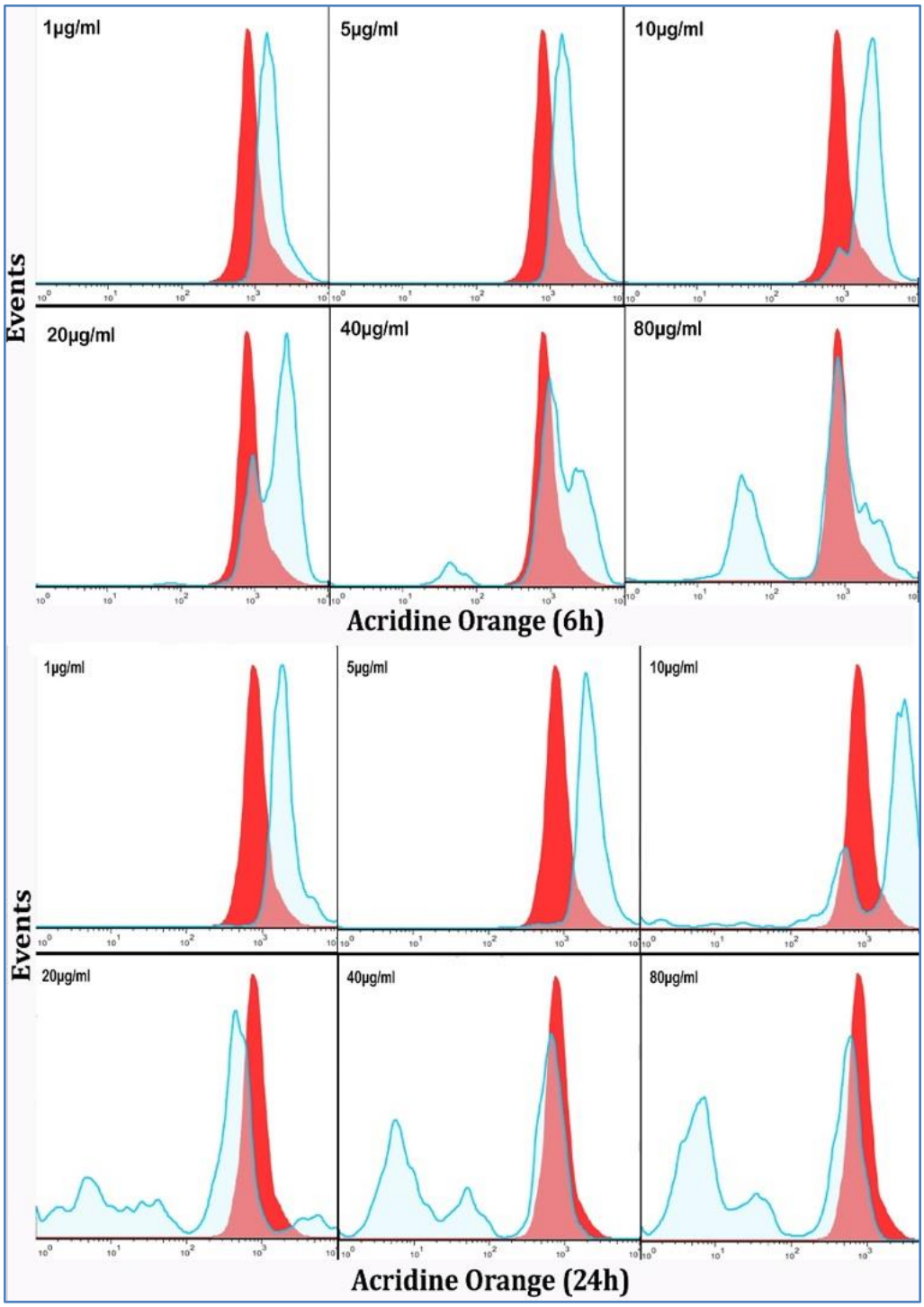

Figure 4:17: Lysosomal stability in BV2 cells exposed to ZnO NPs at 6 and 24h. The red solid peaks denote AO intensity in control population while blue tinted peaks represent treatment groups. The gated population include both viable and dead cells. n=3

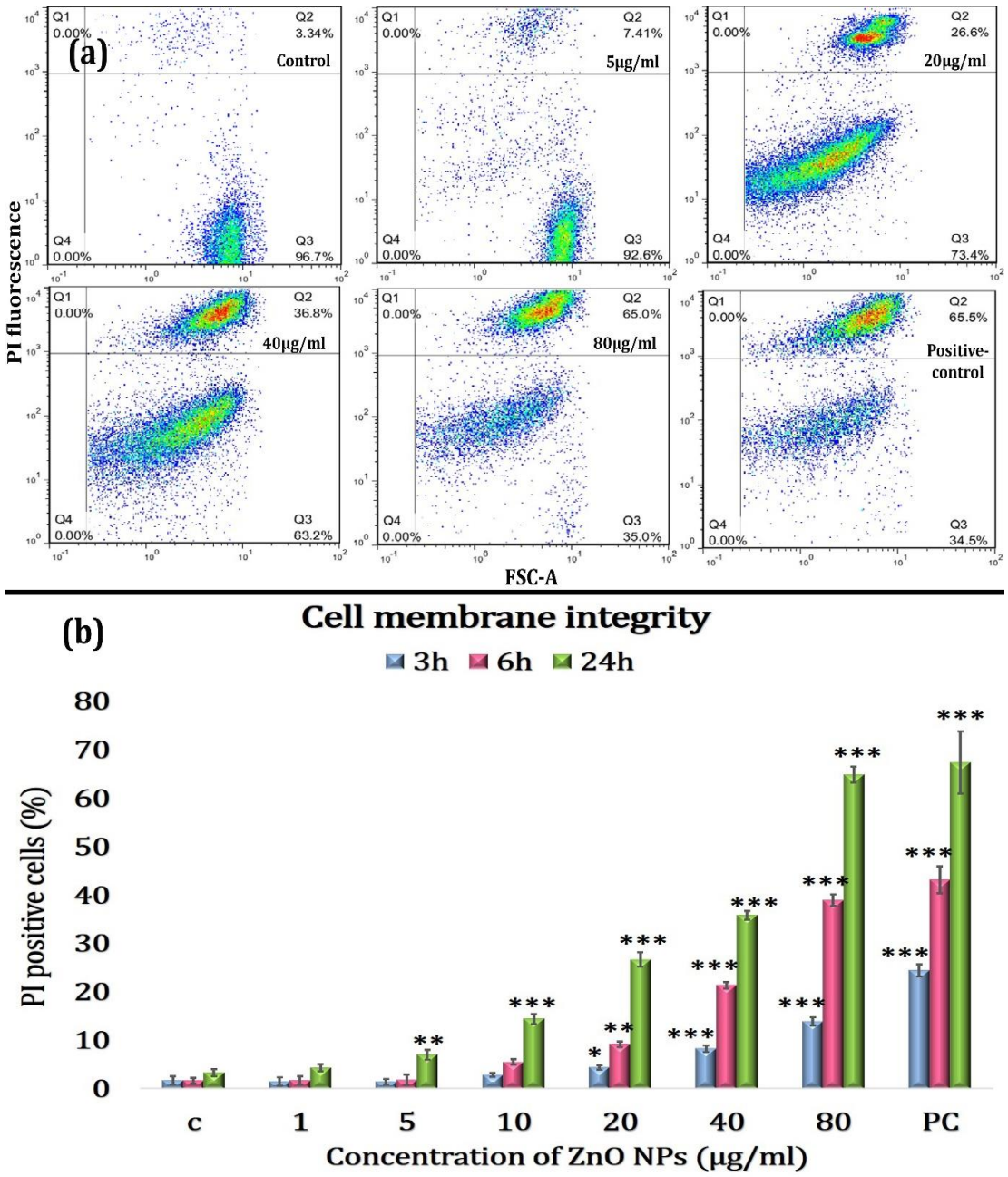

Figure 4:18: Cell membrane integrity: **(a)** BV2 cells exposed to ZnO NPs for 24 h. 7-Ketocholestrol treated cells were used as positive control. The gating was done with respect to PI fluorescence of positive control and gated population includes both live and dead cells. **(b)** Graph showing percentage of PI positive cells at 3, 6 and 24h.

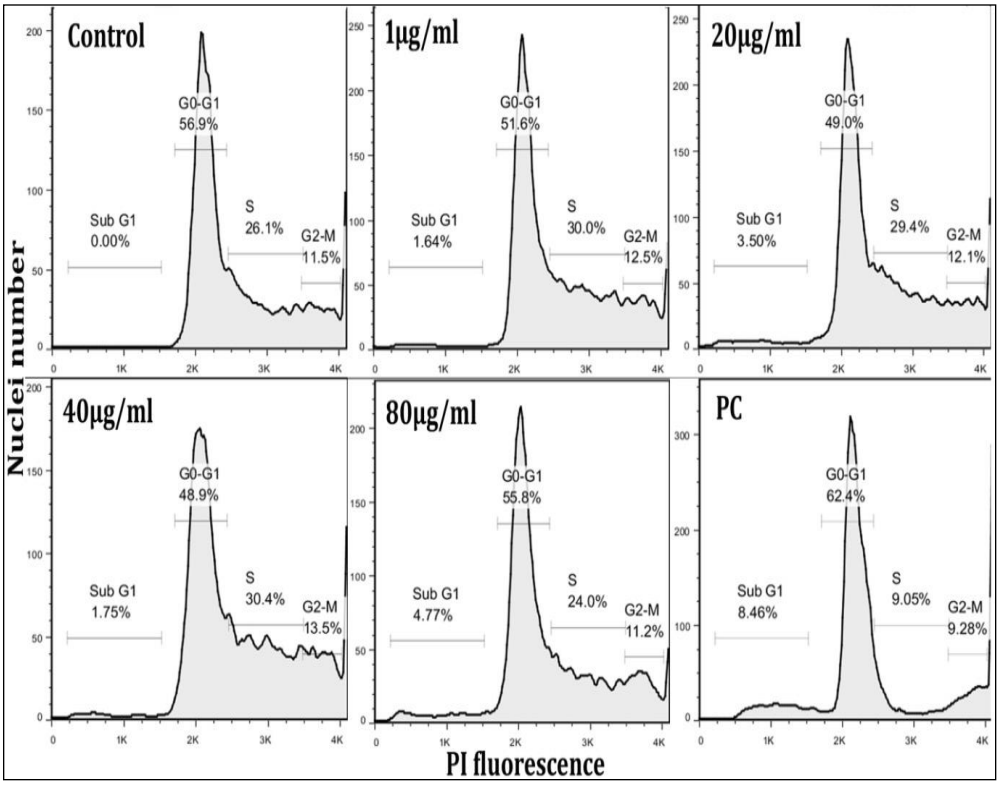

Figure 4:19: Cell cycle analysis of BV2 cells exposed to ZnO NPS at 24 h. The data is represented in PI fluorescence intensity. 7-Ketocholestrol treated cells were used as positive control. All the cellular debris has been gated out to represent the data. n=3

4.2.1.11 PARP cleavage assay

Western blotting did not indicate any sign of cleaved PARP in presence of ZnO NPs **(Figure 4.20**). ZnO NPs treatment (10 and 80µg/ml) did not induce PARP cleavage in BV2 cells. However, in presence of the cathepsin inhibitor z-FA-FMK, cells exhibited PARP cleavage both in control as well as treatment group.

4.2.1.12 DNA ladder assay

DNA ladder formation was not evident in any of the treated group. Both control and treatment samples exhibited a thick band of unfragmented DNA of more than 10,000bp size with no ladder or smear patterns (**Figure 4.21)**.

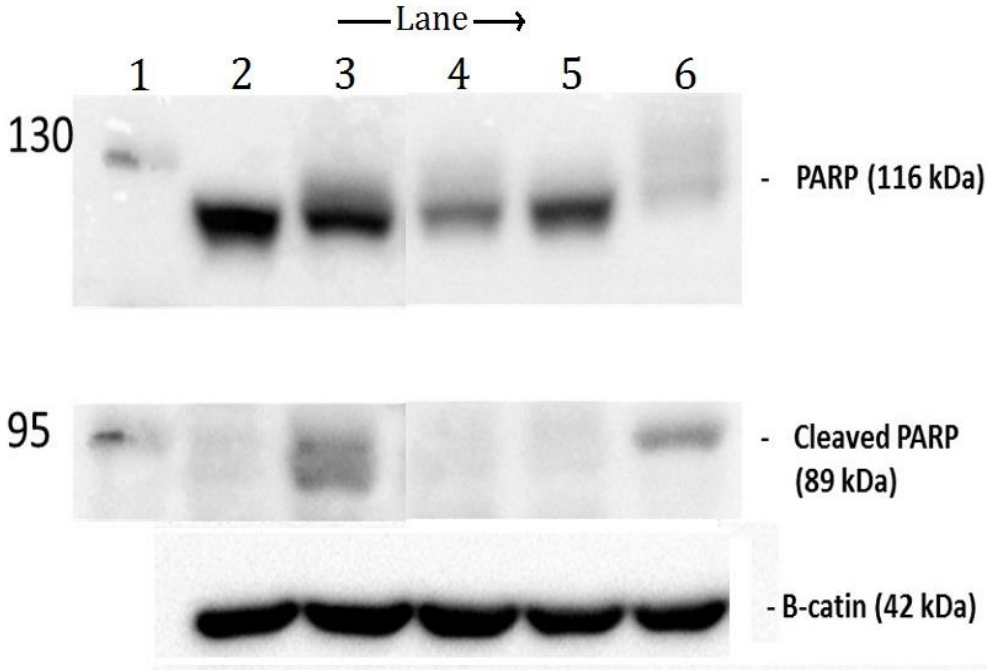

Figure 4:20: Western blot for PARP cleavage; lane 1: protein marker, lane 2: control, lane 3: control pre-treated with z-FA-FMK (25µM), lane 4: 10 µg/ml ZnO NPs, lane 5: 80 µg/ml ZnO NPs, lane 6: z-FA-FMK pre- treated cells exposed to 10 µg/ml ZnO NPs.

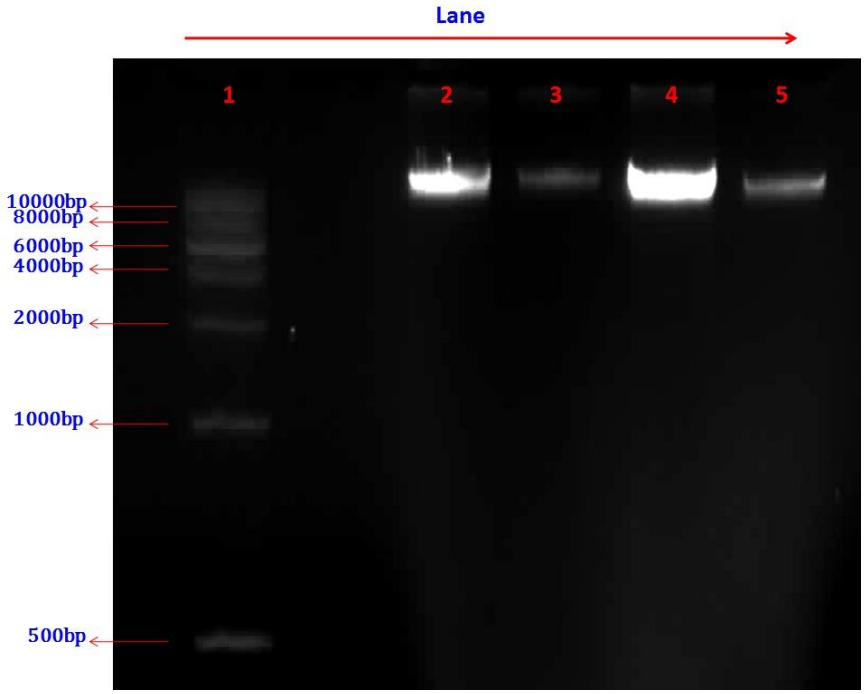

Figure 4:21: DNA ladder assay. Lane 1: Marker DNA, lane 2: Control, Lane 3: 80 µg/ml ZnO NPs, Lane 4: 20µg/ml ZnO NPs, Lane 5: 40µg/ml ZnO NPs. Base pairs (bp) of DNA markers are indicated at the left side of figure.

4.2.1.13 Comparative toxicity of ZnO R and ZnO SP using BV2 cells.

Comparative toxicity of ZnO R and ZnO SP was carried out by morphology, membrane integrity, cell cycle patterns and cell death mechanism.

4.2.1.13.1 Morphology analysis by phase contrast microscopy

Morphology of BV2 cells was slightly changed when exposed to ZnO R whereas ZnO SP induced significant changes in morphology. The size of cells was reduced in 80µg/ml ZnO R treated cells yet the cells remained intact. In contrast the cell morphology was significantly altered in ZnO SP treated cells. Moreover, disintegrated cytoplasmic contents were also observed at high concentrations (**Figure 4.22)**.

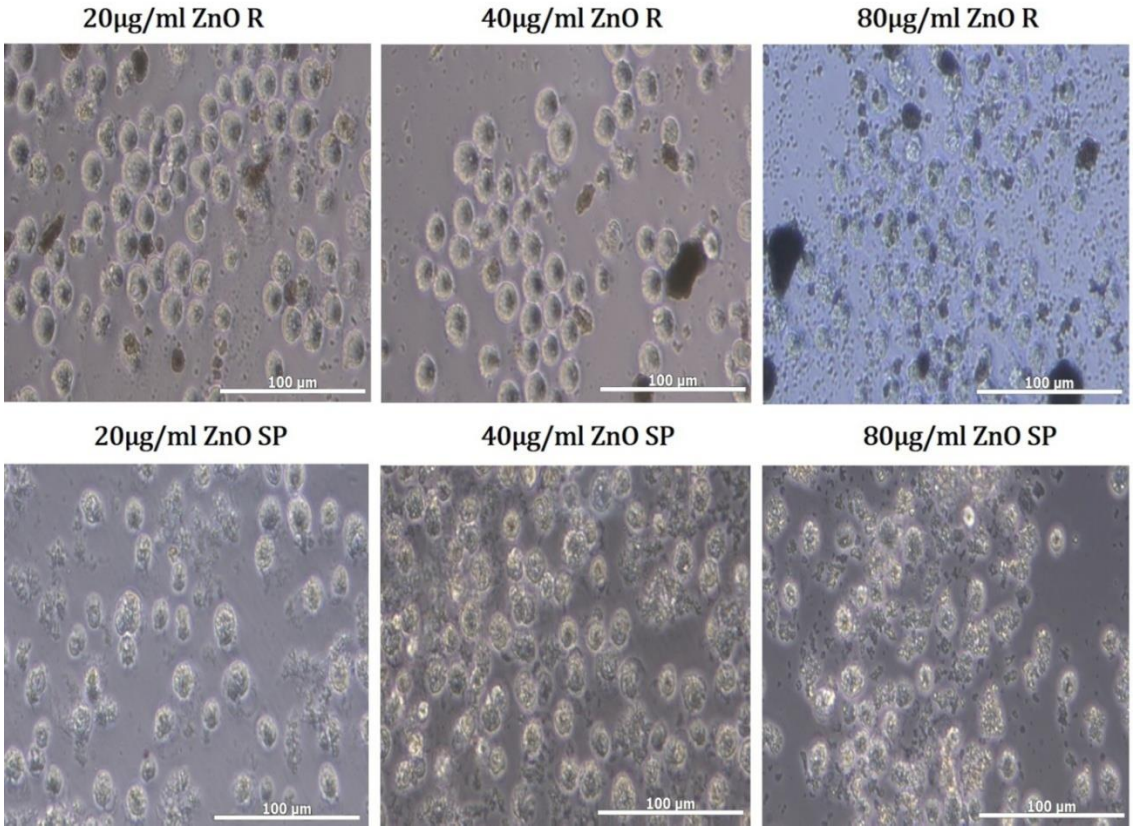

Figure 4:22:Comparative morphology of BV2 cells treated with ZnO R and ZnO SP. The treatment conditions are indicated above each micrograph. n=3. Magnifications 40X.

4.2.1.13.2 Membrane integrity by PI staining

ZnO SP treated cells exhibited statistically significant increase in PI positive cells at a concentration as low as 5µg/ml, whereas ZnO R exhibited toxicity only at 20µg/ml and above. It was found that, ZnO R was less toxic than ZnO SP (**Figure 4.23)**.

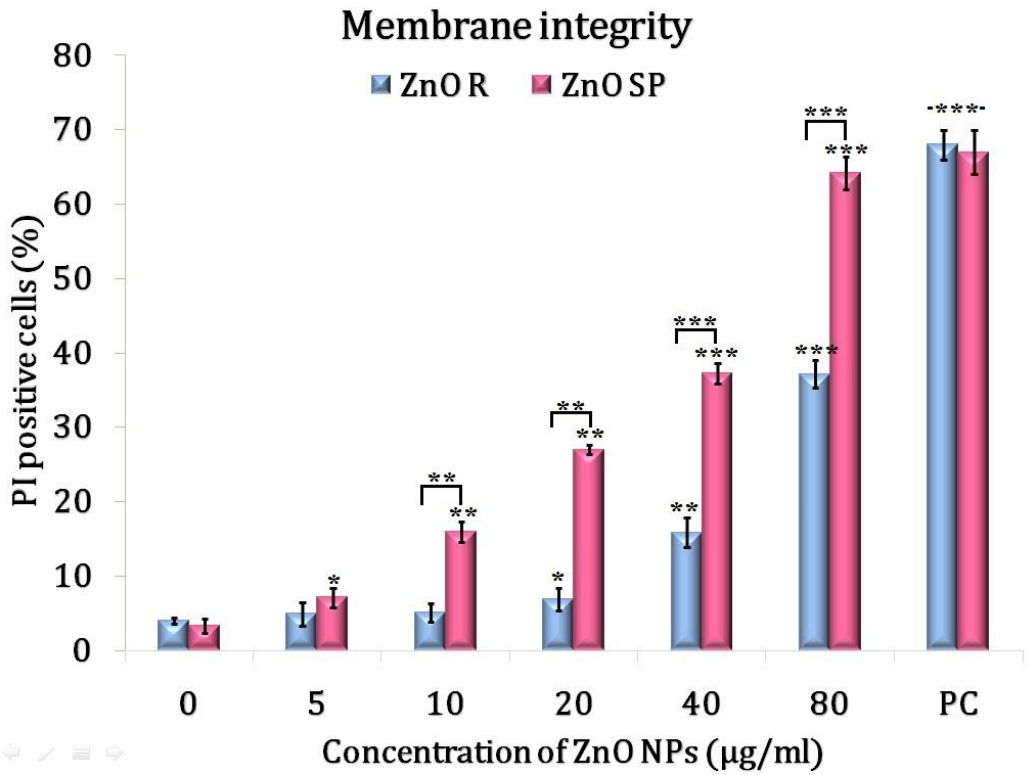

Figure 4:23:Membrane integrity by flow cytometry using BV2 cells. Cells were exposed to ZnO NPs of two different morphologies for 24h. 7-Ketocholestrol treated cells were used as positive control. The gating was done with respect to PI fluorescence of positive control. The data represent mean ± SD of three independent experiments. Asterisk denotes statistically significant difference (*p<0.05, **p< 0.01 and ***p<0.001).

4.2.1.13.3 Cell cycle analysis by flow cytometry

Cell cycle pattern did not reveal any marked difference between ZnO R and ZnO SP **(Figure 4.24).** No increase in subG1 population was evident in treated group with respect to control. On the other hand, positive control (PC) showed marked difference

in cell cycle pattern. Sub G1 population representing the apoptotic population was high (~9%) in PC in comparison with control (~1.5%).

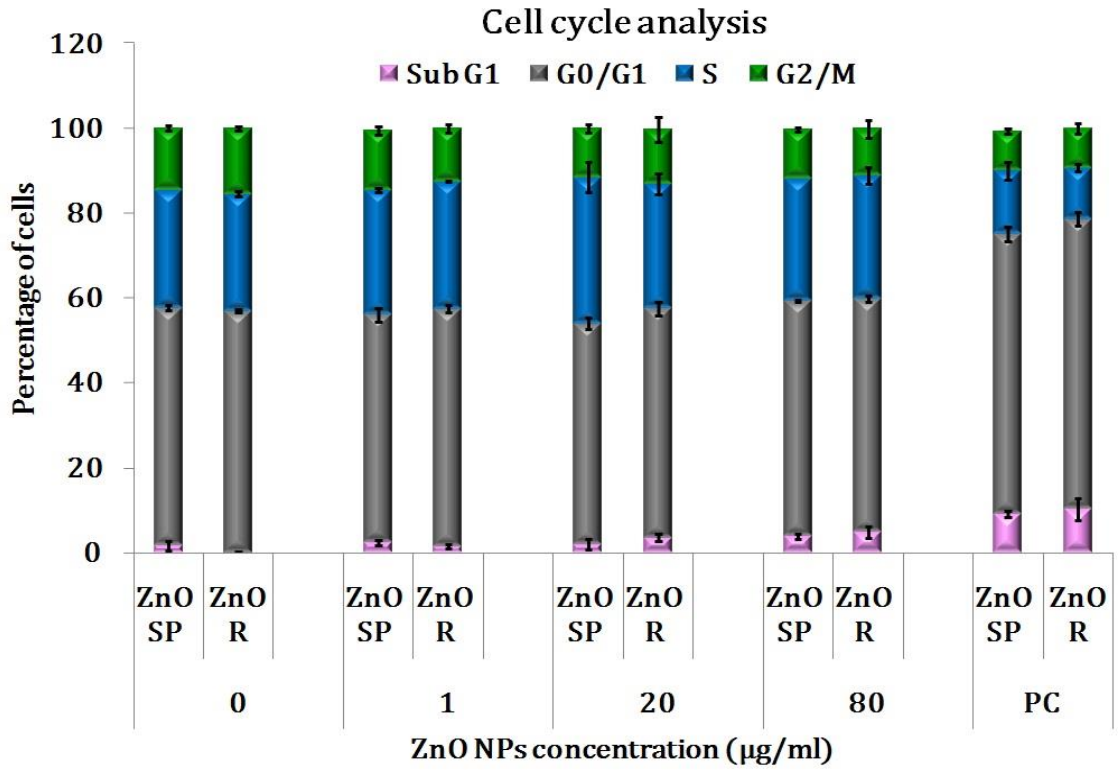

Figure 4:24: Cell cycle analysis by FACS. Percentage of cells in each phase of cell cycle is denoted. ZnO R is ZnO NPs of rod shaped morphology and ZnO SP is ZnO NPs of spear head morphology. 7-Ketocholestrol treated cells were used as positive control (PC). The data represent mean ± SD of three independent experiments.

4.2.1.13.4 PARP cleavage assay

The treatment of both ZnO SP and ZnO R did not induce any PARP cleavage in BV2 cells. On the other hand, PARP cleavage was induced by cathepsin inhibitor z-FA-FMK **(Figure 4.25).**

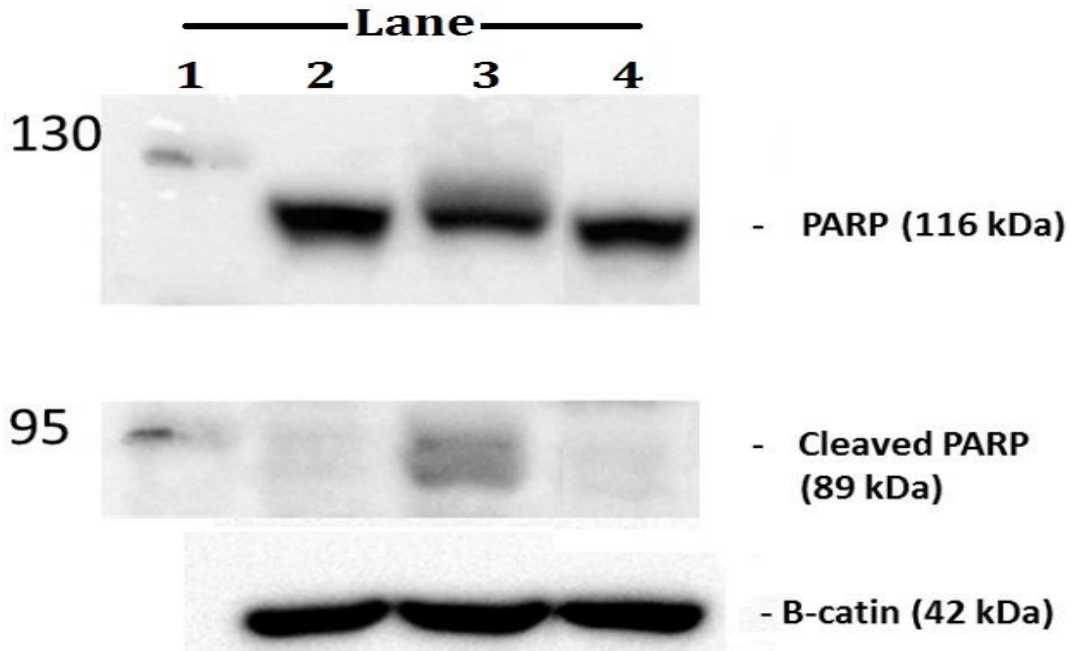

Figure 4:25: PARP cleavage assay; lane 1: marker, lane 2: control, lane 3: control pre-treated with z-FA-FMK, lane 4: Cells exposed to ZnO R (80 µg/ml). n=3.

4.2.2 CELLULAR INTERACTION OF C6 ASTROGLIAL CELLS WITH ZnO NPS

4.2.2.1 Assays for cell viability

4.2.2.1.1 MTT

A time and dose dependent cytotoxicity was observed in C6 glial cells when treated with ZnO NPs as indicated in **Figure 4.26**. Treatment of ZnO NPs exhibited a statistically significant reduction in percentage mitochondrial activity at 3h (40µg/ml: 94.44±2.25 and 80µg/ml: 85.38±1.42) 6h and 24h (5µg/ml: 94.26±0.73, 10µg/ml: 95.25± 0.42, 20 µg/ml: 75.89±2.47, 40 µg/ml: 56.69±2.82 and 80µg/ml: 29.92±6.11) of exposure.

4.2.2.1.2 Neutral red uptake (NRU)

A statistically significant reduction in cell viability was observed when C6 cells were exposed to ZnO NPs. Here cell viability was measured in terms of lysosomal activity. Cells exposed to 40µg/ml (96.31±4.71) and 80µg/ml (87.86±0.50) of ZnO NPs exhibited significant reduction in lysosomal activity after 3h of incubation. Whereas at lower concentration (up to 10µg/ml) ZnO NPs to did not induce cytotoxic response. The lysosomal activity was significantly reduced (40 µg/ml:43.30±1.82 and 80 µg/ml:35.19±0.11) at 24h of exposure **(Figure 4.27).**

4.2.2.2 Particle uptake (ZnO NPs) in C6 cells:

Particle uptake (ZnO NPs) in C6 cell was assessed by flow cytometry. **Figure 4.28,** indicated a concentration dependent increase in SSC parameters. However, there was no corresponding change in FSC parameters. This suggests that treatment of ZnO NPs increased cell granularity due to particle uptake.

4.2.2.3 Particle dissolution and related cytotoxicity

Figure 4.29 suggested no change in mitochondrial activity when C6 glial cells were exposed to supernatant of ZnO NPs. On the other hand, a statistically significant decrease in mitochondrial activity was observed inC6 cells directly exposed to ZnO NPs. The percentage mitochondrial activity observed in supernatant of 80 µg/ml ZnO NPs is95.63±1.28 whereas direct exposure of ZnO NPs is 29.92±6.11.

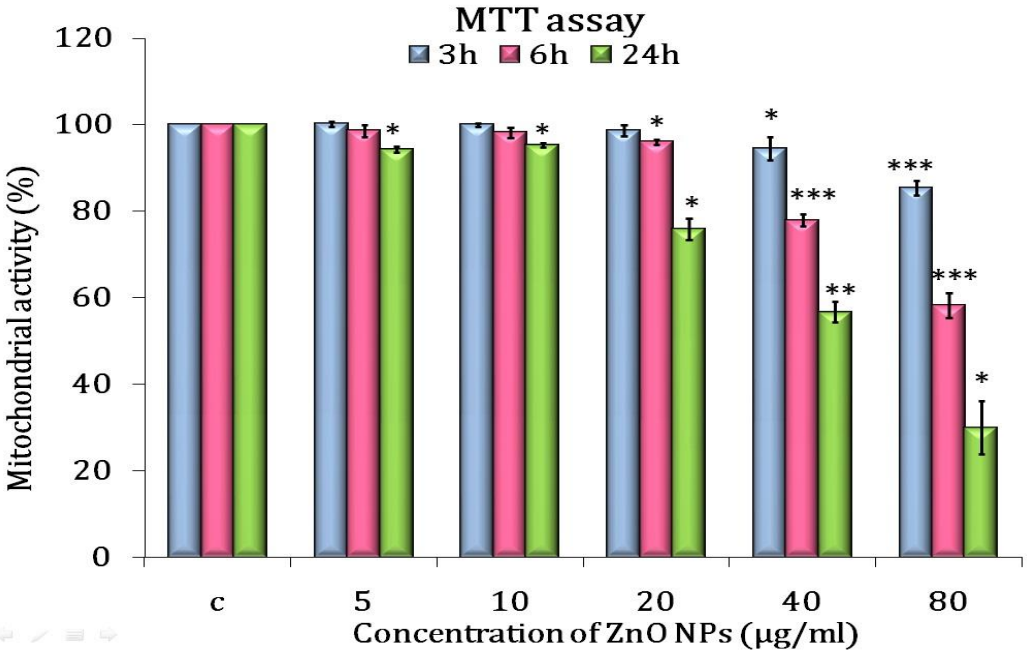

Figure 4:26: MTT assay on C6 cells exposed to ZnO NPs for 3, 6 and 24h. The values are expressed in percentage with respect to control. The data represent mean ± SD of three independent experiments. Asterisk denotes statistically significant difference (*p<0.05, **p< 0.01 and ***p<0.001).

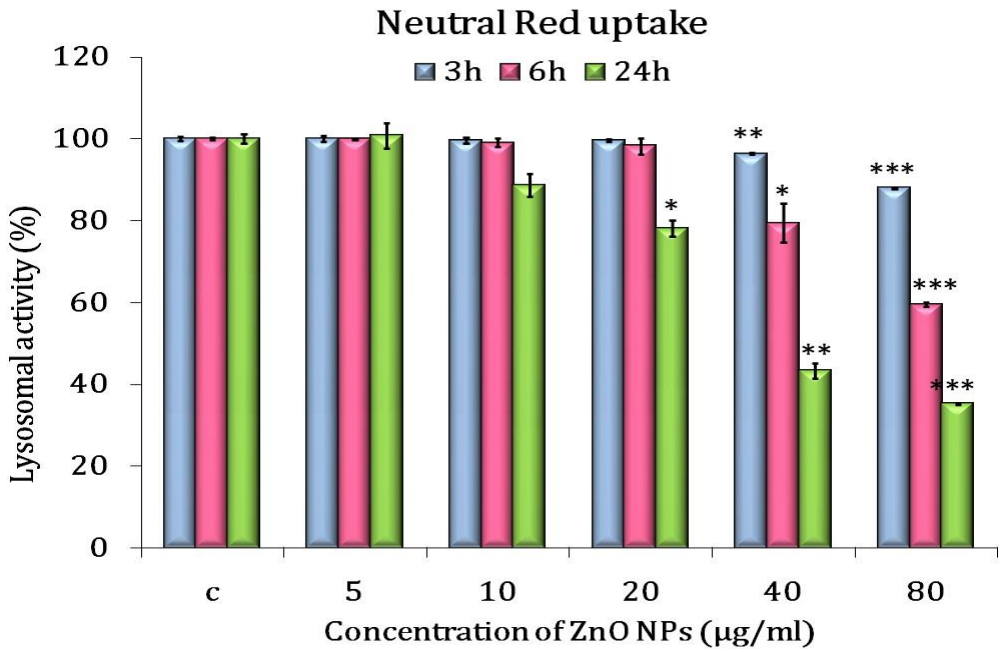

Figure 4:27: Neutral red uptake on C6 cells exposed to ZnO NPs at 3, 6 and 24h. The values are expressed in percentage with respect to control. The data represent mean ± SD of three independent experiments. Asterisk denotes statistically significant difference (*p<0.05, **p< 0.01 and ***p<0.001).

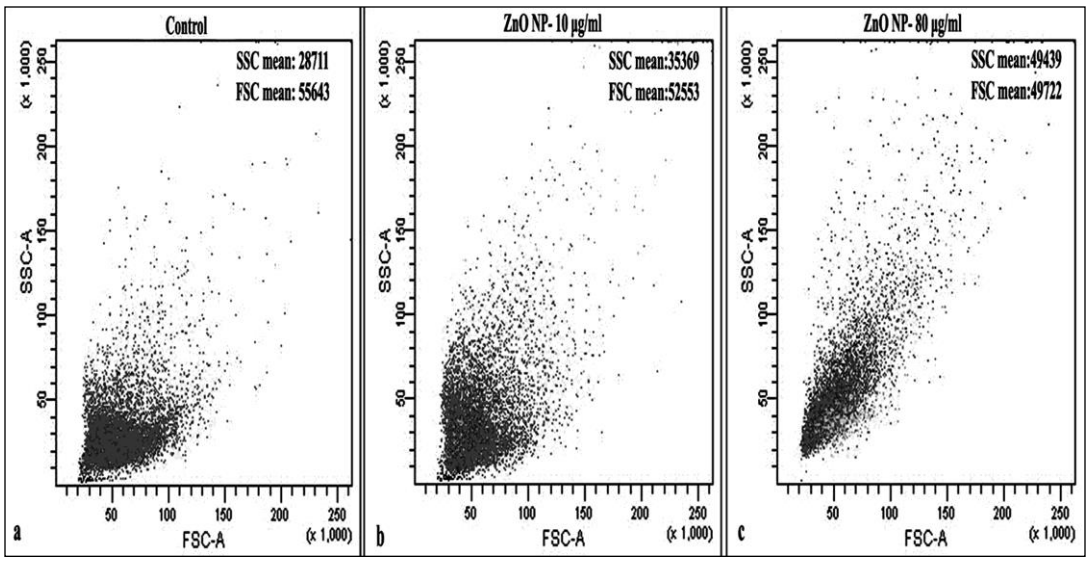

Figure 4:28:Determination of cellular uptake by flow cytometry analysis. The SSC changes indicated particle uptake by the cells. SSC: side scatter, FSC: forward scatter.

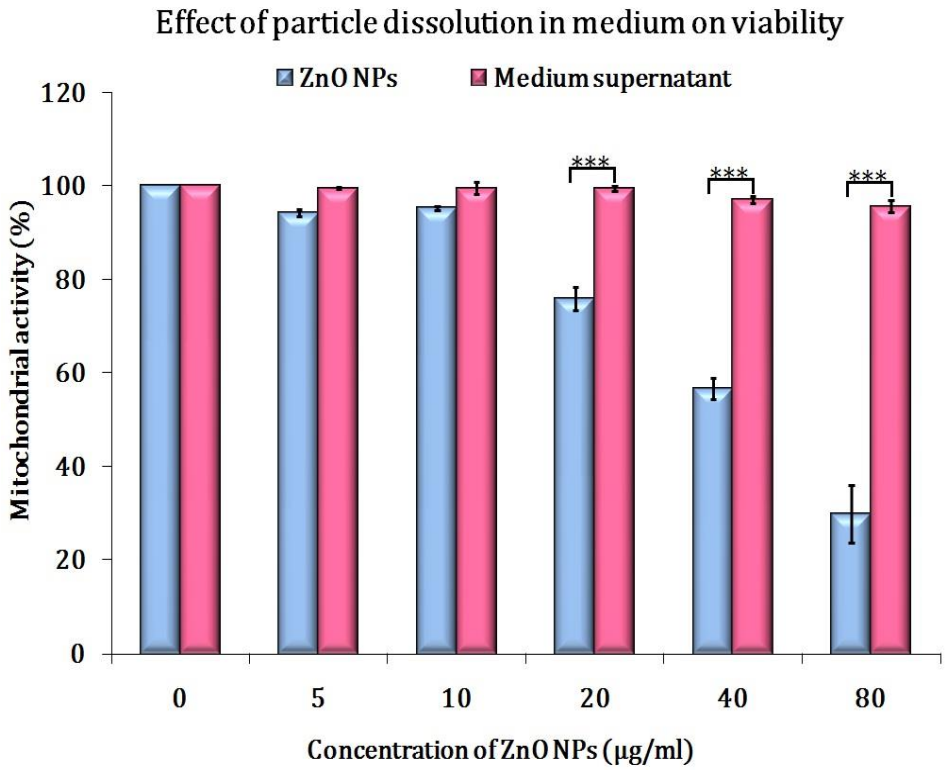

Figure 4:29: Percentage mitochondrial activity of supernatant and direct exposure. The data represent mean ± SD of three independent experiments. Asterisk denotes statistically significant difference (***p<0.001).

4.2.2.4 Cell phenotype

4.2.2.4.1 Morphology analysis by Giemsa staining

Giemsa staining revealed morphological changes in C6 cells **(Figure 4.30)**. At 6 and 24h morphological changes were not evident in cells up to 20µg/ml whereas at high concentrations of ZnO NPs cells began to form round shape even at 6h. Cell density was markedly reduced in 40 and 80µg/ml after 24h of treatment.

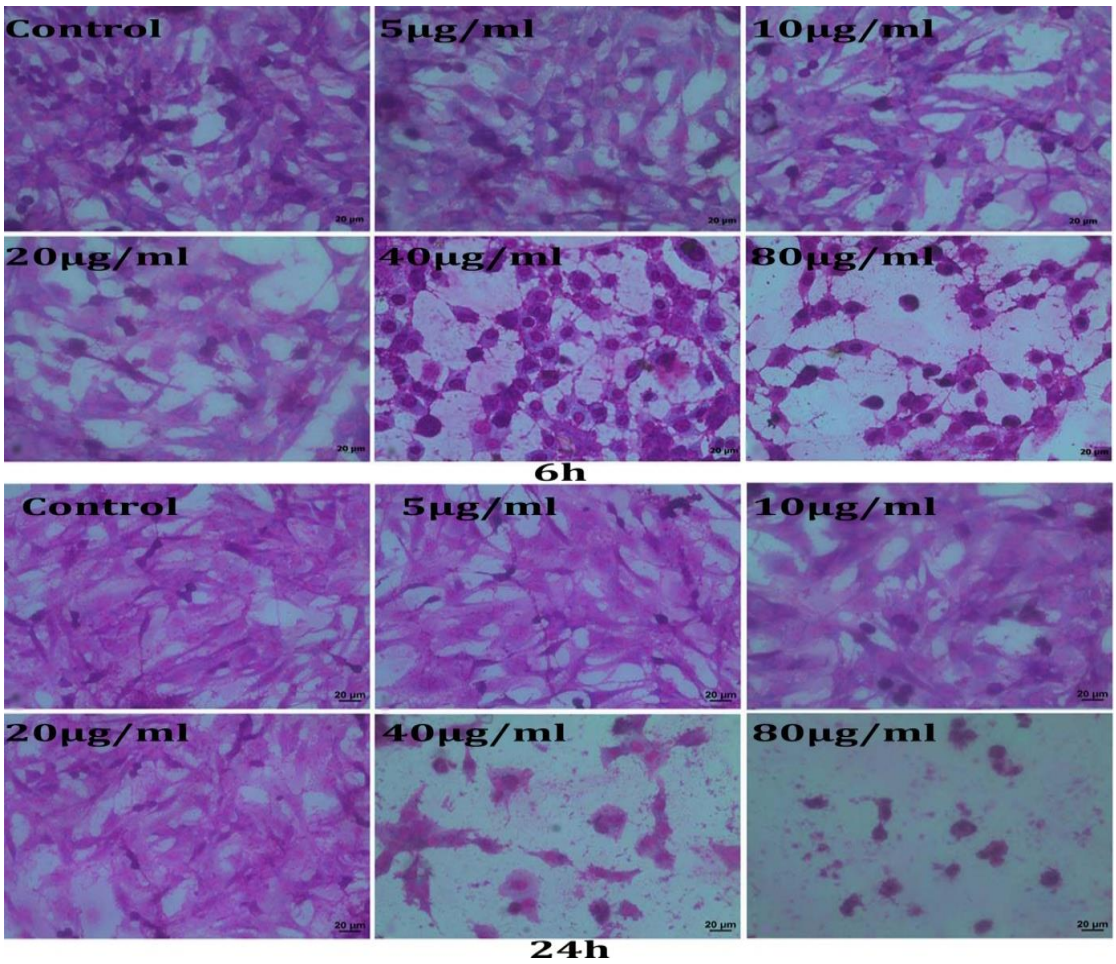

Figure 4:30: Cellular morphology analysis of C6 cells exposed to ZnO NPs for 6 and 24h using Giemsa staining. Untreated cells are used as control. The scale bar represents 20µm. magnification 40X.

4.2.2.4.2 Cytoskeletal staining by rhodamine phalloidin

No cytoskeletal rearrangement was observed in cells treated up to 20µg/ml. At higher concentrations (40 and 80µg/ml), cytoskeletal retraction and round morphology were observed in the cells **(Figure 4.31)**.

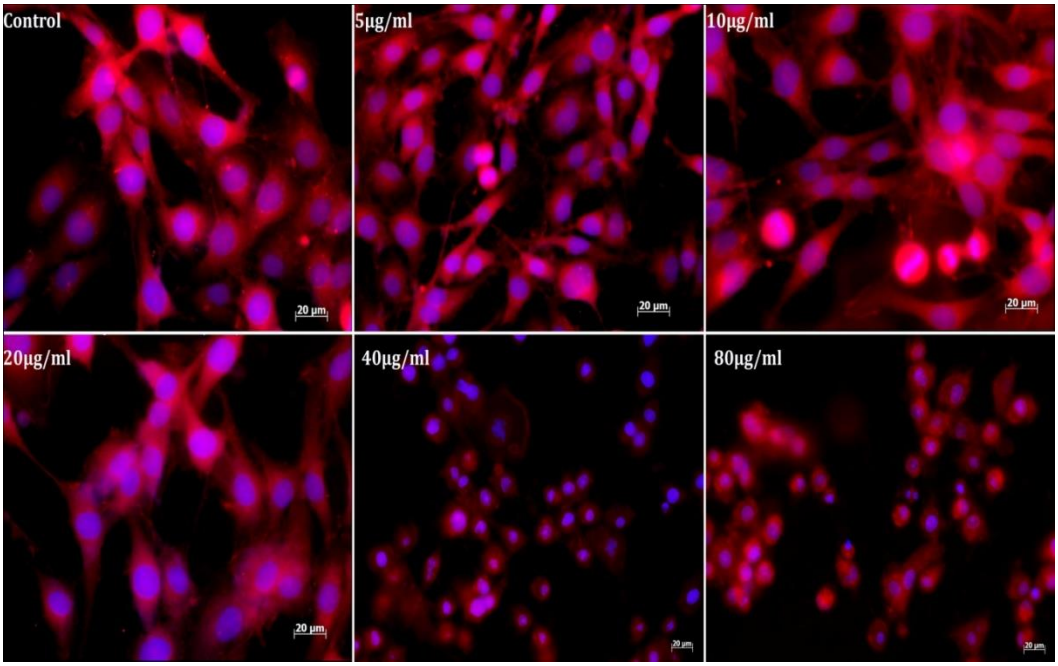

Figure 4:31: Cytoskeletal arrangement of C6 cells exposed to ZnO NPs for 6 and 24h using rhodamine phalloidin staining. Untreated cells are used as control. The scale bar represents 20µm. Magnification 40X

4.2.2.5 Mitochondrial membrane potential (MMP) by JC1 staining

The MMP was assessed by JC1 probe. **Figure 4.32** indicated loss of membrane potential in C6 cells exposed to higher concentrations of ZnO NPs. The untreated control cells exhibited highest level of the red fluorescence indicative of healthy and active mitochondria. Cells treated with 5µg/ml of ZnO NPs revealed red fluorescence comparable to that of control. Green fluorescence predominated in the cells treated with 20 and 40 µg/ml ZnO NPS suggesting loss of MMP.

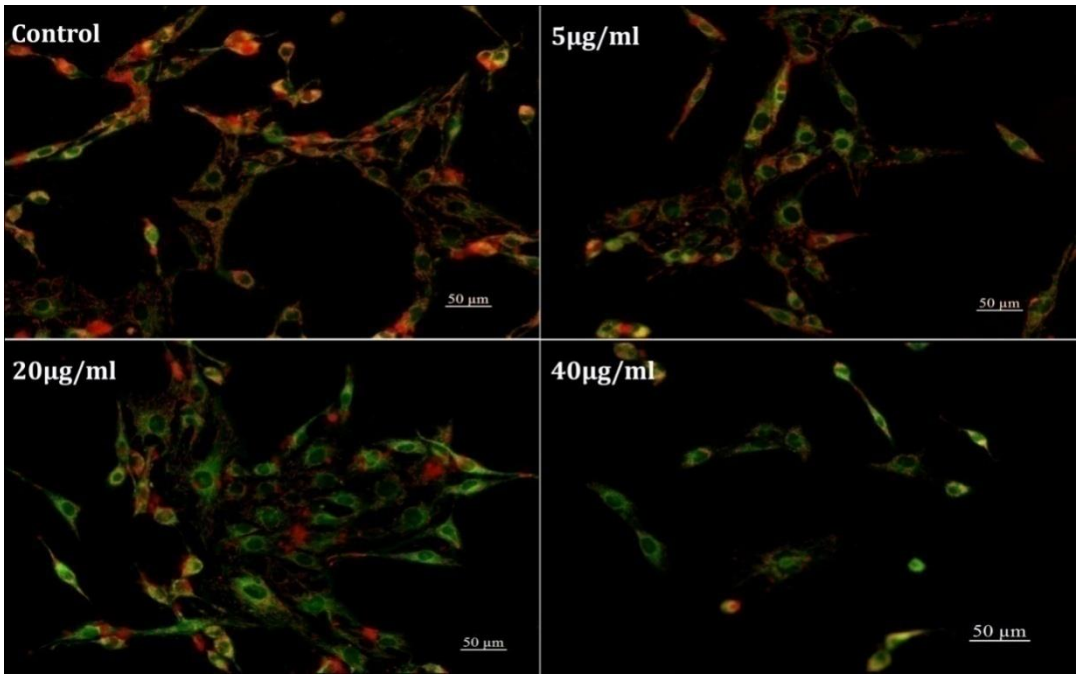

Figure 4:32: Mitochondrial membrane potential of C6 cells exposed to ZnO NPs for 6h. Untreated cells are used as control. The red signal represents J aggregates in active mitochondria and green signal represents the diffused monomers in the cytoplasm. Scale bar represents 50µm. Magnification 20X.

4.2.2.6 Detection of reactive oxygen species(ROS) by DCFH-DA

Cell treated with ZnO NPs showed a dose dependent modulation in DCF fluorescence, represented in **Figure 4.33**. The ROS generation was more pronounced at 3h of incubation (5µg/ml: 102.44±0.23 and 80µg/ml:133.79±1.98) where, cells exhibited a steady increase in DCF fluorescence. At 6h period the ZnO NPs treated cells showed high fluorescence when compared to control. None of the ZnO NPs treated group exhibited statistically significant increase in fluorescence after 24h of exposure (5µg/ml: 105.96±1.62, 20µg/ml: 113.81 ±3.64, 80µg/ml:102.78±0.97).

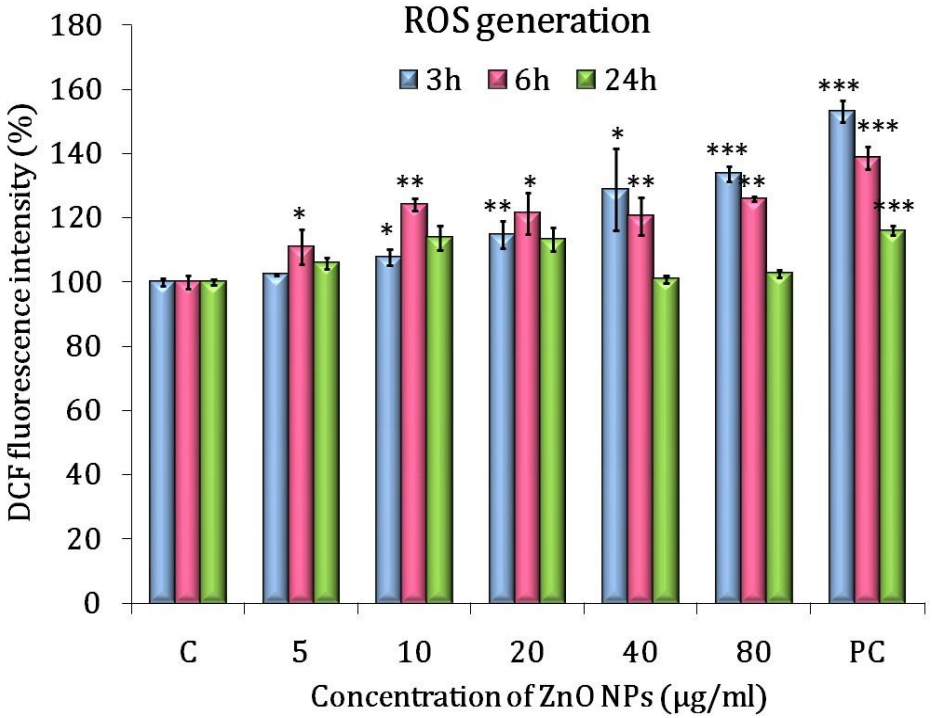

Figure 4:33: Production of ROS production in C6 cells exposed to ZnO NPs for 3, 6 and 24h using DCFH-DA. H_2O_2 treated cells are used as positive control. The values are expressed in percentage fluorescence with respect to control. The data represent mean ± SD of three independent experiments. Asterisk denotes statistically significant difference (*p<0.05, **p< 0.01 and ***p<0.001).

4.2.2.7 Influence of catalase activity on generation of ROS

Catalase is an enzyme in cells which converts hydrogen peroxides into water and oxygen. Astrocytes exhibit high catalase activity. The catalase activity may neutralise H_2O_2 generated in astrocytes. Astrocytes exhibited high ROS production compared to control cells when pre-treated with catalase inhibitor (NaN_3) **(Figure 4.34)**. A statistically significant increase in ROS was observed in cells pre-treated with catalase inhibitor and treated with ZnO NPs. ZnO NPs induced high DCF fluorescence (80µg/ml: 164.48±4.02%) in presence of NaN_3 whereas ROS generation was decreased (80µg/ml: 125.91±2.34%) in the absence of NaN3.

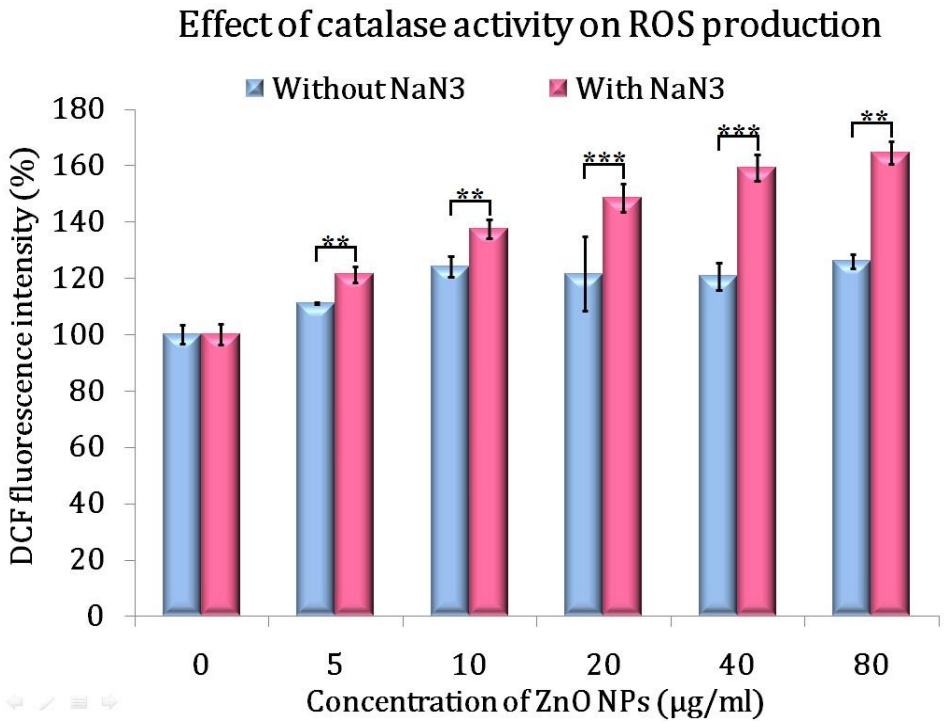

Figure 4:34: Effect of catalase activity on ROS production in C6 cells exposed to ZnO NPs for 6h. The values are expressed in percentage fluorescence with respect to control. 0.1µM NaN3 pre-treatment for 1h was used as an inhibitor of catalase. The data represent mean ± SD of three independent experiments. Asterisk denotes statistically significant difference (**p< 0.01 and ***p<0.001).

4.2.2.8 Nuclear condensation by DAPI staining

ZnO NPs exposure results in nuclear condensation of C6 cells. **Figure 4.35** shows the nuclear and chromatin condensation along with cytoplasmic shrinkage in cells treated with high concentration of ZnO NPs (40 and 80 µg/ml). The size of the nucleus shrank considerably in comparison with the control.

4.2.2.9 Apoptosis by Annexin V/ PI staining

The ZnO NPs mediated cell death were analysed by annexin V/PI staining. The annexin V positive cells indicate early apoptotic cells whereas PI positive cells represent necrotic cells. The double positive cells correspond to the late phase of apoptosis. The

cells treated with ZnO NPs showed a dose dependent increase in the number of annexin V positive cells after 24h of exposure **(Figure 4.36).** However, no significant increase in double positive cells was observed in cells stained with annexin V and PI). Figure 36**(h)** and **(i)** show microscopic evaluation of the cells (used for FACs) which revealed annexin V positive cells.

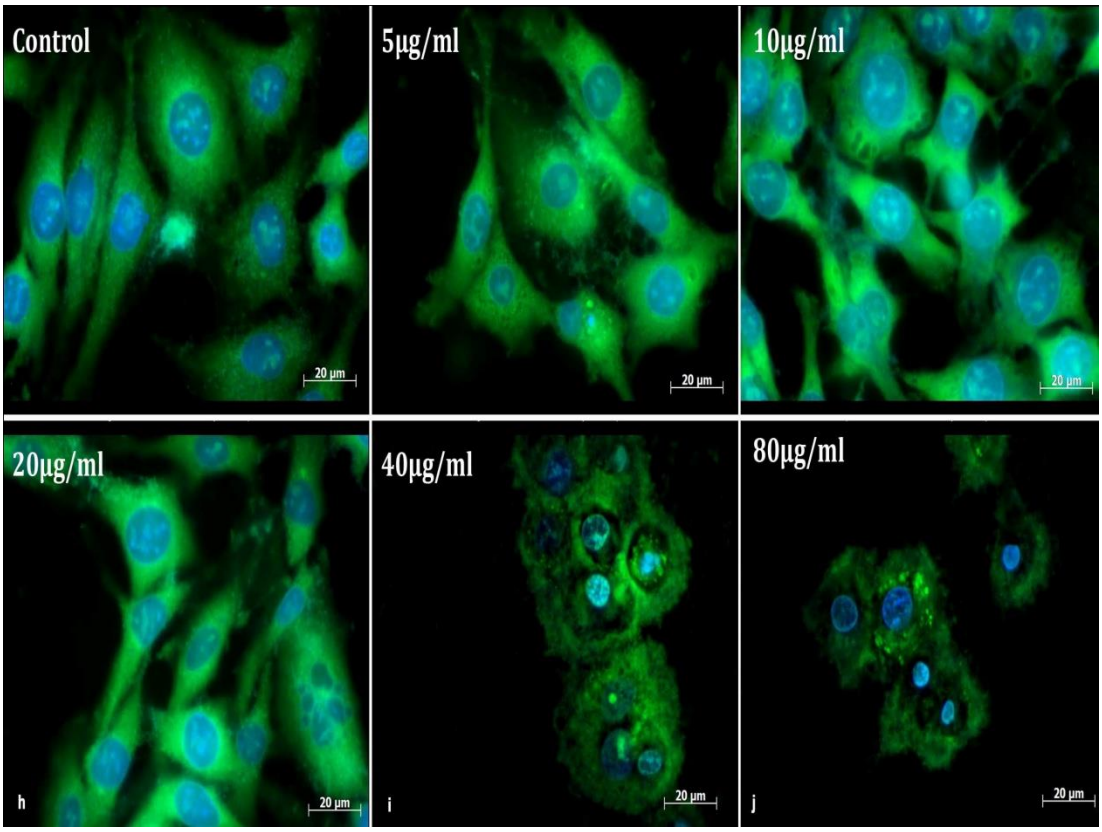

Figure 4:35: Nuclear condensation in C6 cells exposed to ZnO NPs for 24h using DAPI and AO staining. Untreated cells are used as control. Blue signals represent the nucleus while green signal represents the cytoplasm. Scale bar denotes 20µm. Magnification 40X

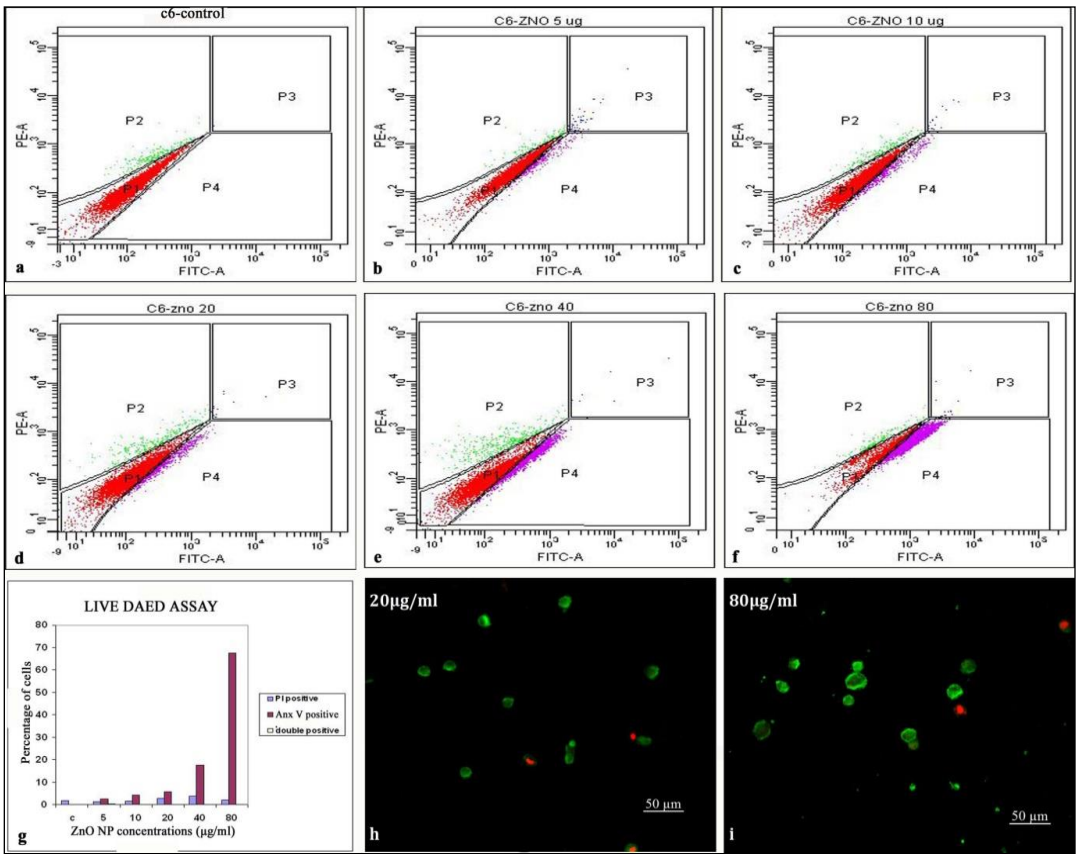

Figure 4:36: Flow cytometry analysis C6 cells exposed to ZnO NPs for 24h **(a-f)**. Quadrant P1 represent normal cells, P2 indicate PI positive necrotic cells, P4 indicate annexin V positive early apoptotic cells and P3 indicate double positive late apoptotic cells. **(g)** Cell population in each quadrant. **(h and i)** representative fluorescence micrographs of 20 and 80µg/ml treated cells. Scale bar represents 50µm. Magnification 40X

4.2.3 CELLULAR INTERACTION OF ZnO NPS WITH PRIMARY ASTROCYTES

4.2.3.1 Isolation and purification of primary astrocytes

Astrocytes isolated from the whole brain of post-natal0-2 day old rat pups were cultured in DMEM F12 medium supplemented with 10% FBS. The medium was replaced with fresh medium in every 3 days. The astrocytes exhibited a doubling time of 36h. 70-90% confluent cells were used for characterisation and bio assays.

4.2.3.2 Characterisation of primary astrocytes

The astrocytes were characterised by immunocytochemistry analysis. **Figure 4.37**shows green cells, positive for astrocytes marker GFAP. Cells were negative for neuronal marker β3 tubulin and oligodendrocyte marker O4 antibody indicating the absence of both these cell types in the culture. A few Ac-LDL positive cells (red) were present in the samples suggesting the presence of small fraction of microglia or endothelial cells in the culture.

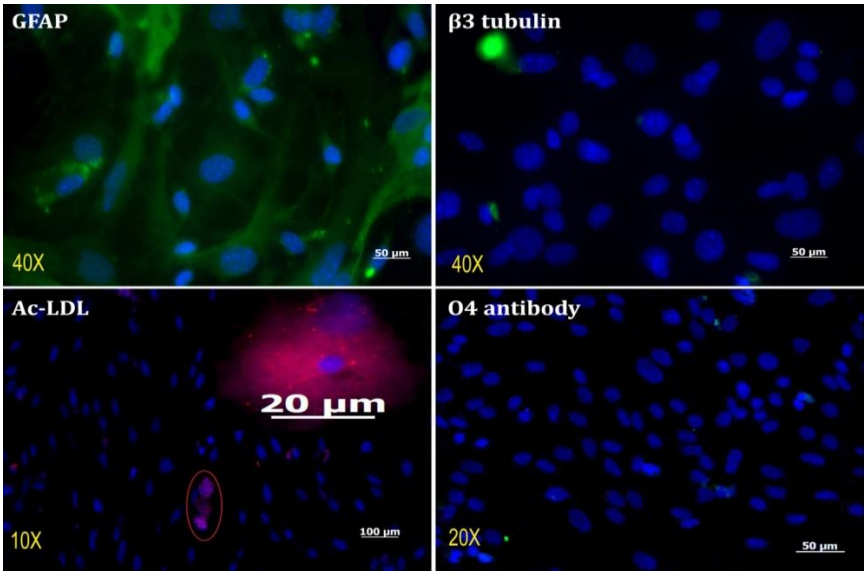

Figure 4:37: Characterisation of primary astrocytes isolated from 0-2 day old rat pups. Astrocytes specific marker GFAP, neuronal marker β3 tubulin, oligodendrocyte marker O4 antibody and Ac-LDL metabolised by microglia and endothelial cells are used. The cells in red circle are positive for Ac-LDL.

4.2.3.3 Cell viability and dose response

4.2.3.3.1 MTT assay

MTT assay was done using a range of concentrations (5-80µg/ml ZnO NPs) at 6h and 24h of exposure. Astrocytes exposed to ZnO NPs showed time and dose

dependent reduction in mitochondrial activity **(Figure 4.38)**. 20 and 100µg/ml treated cells exhibited a mitochondrial activity of 96.26 ± 5.45% and 54.45±2.28 respectively at 6h of exposure. Mitochondrial activity was further reduced to 70.90±1.78 (20µg/ml) and 27.83±0.59% (100µg/ml) at 24h.The lethal concentration (LC_{50}) was found to be 60µg/ml (49.26±1.85).

4.2.3.3.2 NRU assay

The NRU results showed a dose dependent decrease in the lysosomal activity at 6h and 24h of exposure. The drop in lysosomal activity was more pronounced at 24h of incubation **(Figure 4.39)**. On exposure of 30µg/ml ZnO NPs exposure, the percentage viability of 86.01±1.98 (6h) was reduced to 61.51±2.77 at 24h. The percentage cell viability was below 50% in 100µg/ml ZnO NPs treated cells at 6h (48.59±3.69) and 24h (27.79±5.14). The LC_{50} determined from NRU assay was 40µg/ml.

4.2.3.4 Cellular uptake by flow cytometry

A dose dependent increase in SSC/FSC ratio indicated ZnO NPs uptake by astrocytes **(Figure 4.40)**. It was observed that the SSC of cells increased in a dose dependent manner. On the other hand, FSC of all the samples remained similar. The SSC/FSC ratio of control was 0.582 whereas those of 5, 20 and 40 µg/ml treatment groups were 0.648, 0.790 and 0.954 respectively.

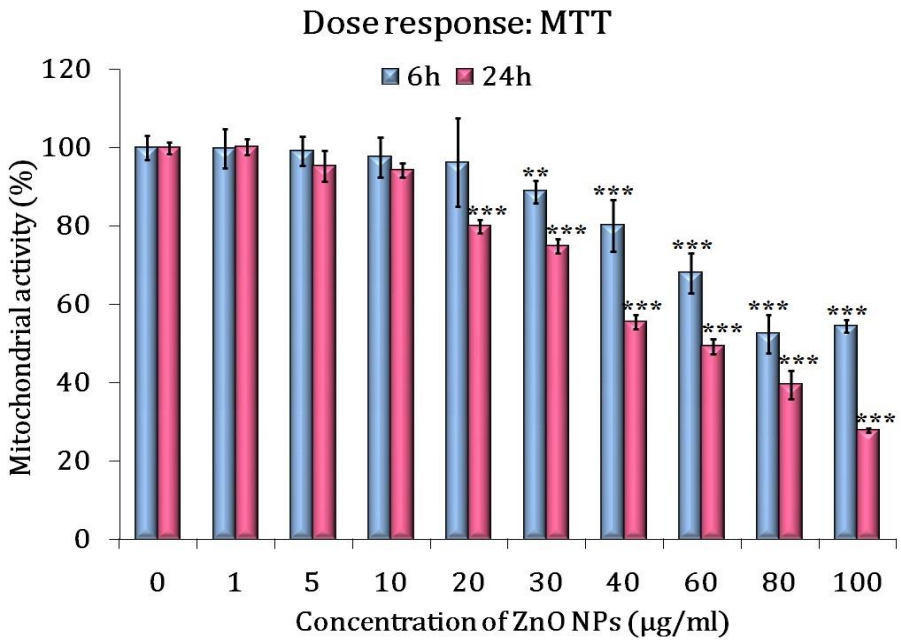

Figure 4:38: Dose response of primary astrocytes exposed to ZnO NPs for 6 and 24h. The values are expressed in percentage with respect to control. The data represent mean ± SD of three independent experiments. Asterisk denotes statistically significant difference (**p< 0.01 and ***p<0.001).

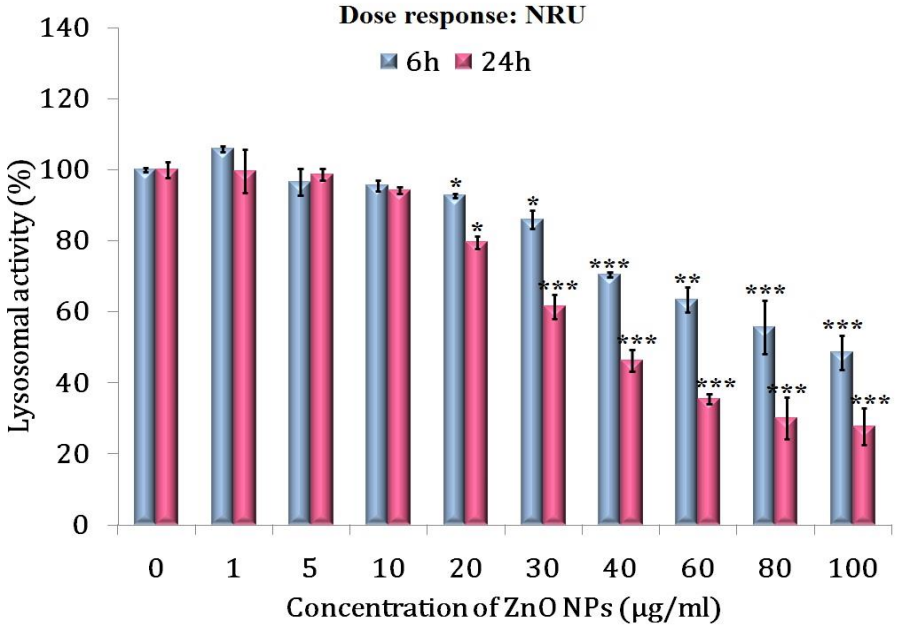

Figure 4:39: NRU assay on BV2 cells exposed to ZnO NPs for 6 and 24h. The values are expressed in percentage with respect to control. The data represent mean ± SD of three independent experiments. Asterisk denotes statistically significant difference (*p<0.05, **p< 0.01 and ***p<0.001).

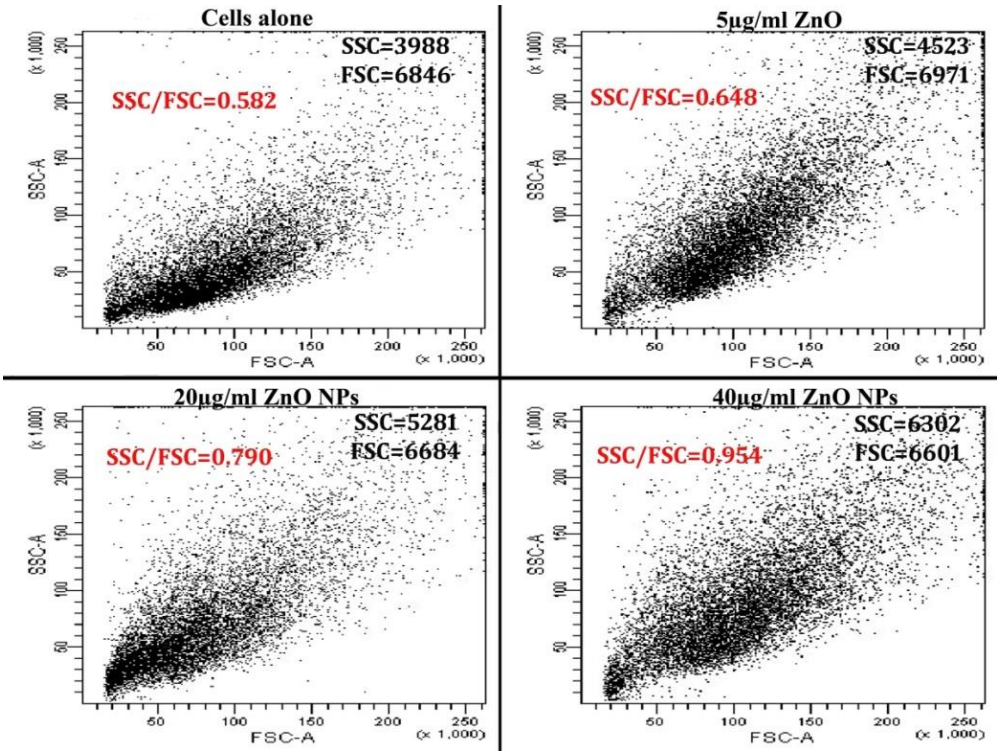

Figure 4:40: Cellular uptake by flow cytometry data indicating particle uptake. FSC and SSC parameters are indicated in the graph.

4.2.3.5 Particle uptake in presence of inhibitor

Particle uptake was confirmed by blocking the uptake using an inhibitor cytochalasin D (Cyt.D). The ZnO NPs mediated toxicity was ameliorated by Cyt.D. A statistically significant difference in viability was observed for 40 and 80 µg/ml ZnO NPs treated cells in presence of cytochalasin D **(Figure 4.41)**. It was observed that the viability of 80µg/ml treated cells was dropped to 55.82±0.52 on direct exposure, in comparison with 98.34±3.04 viability exhibited by cytochalasin D pre-treated group.

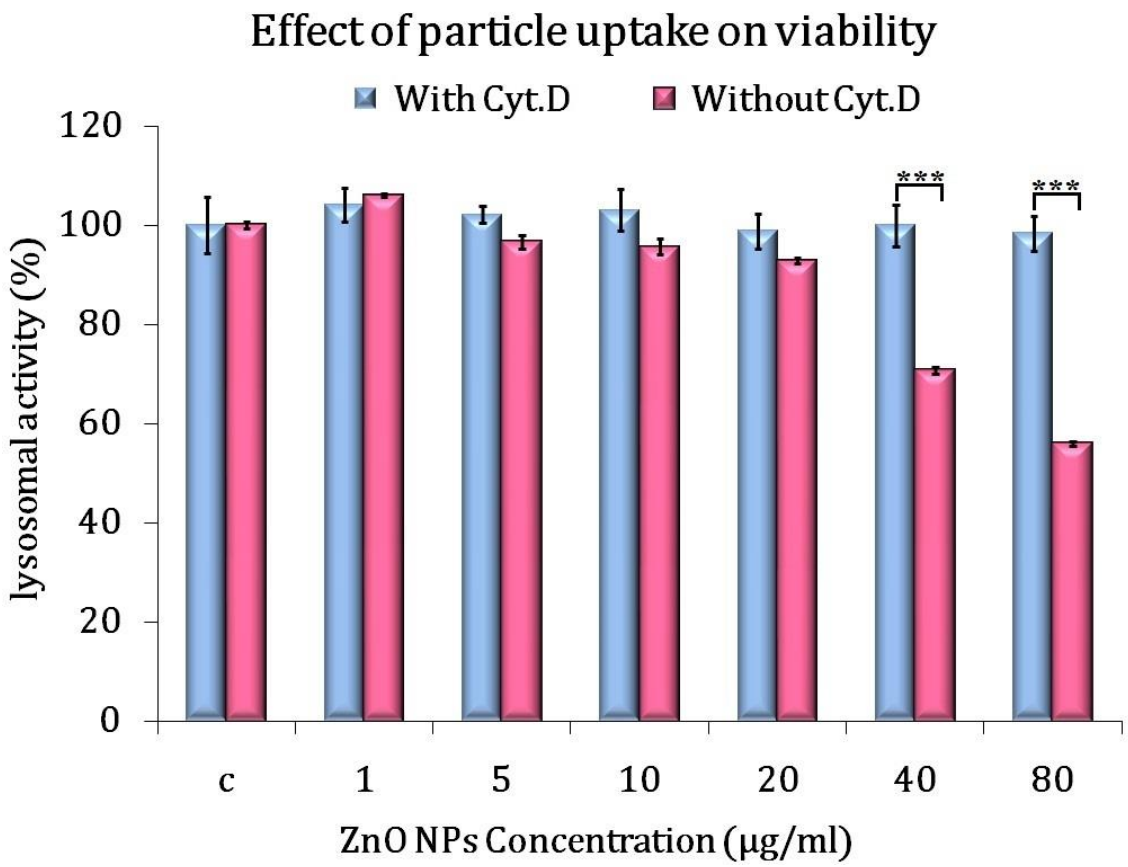

Figure 4:41: Particle uptake in presence of inhibitor cytochalasin D: effect of ZnO NPs uptake on mitochondrial activity of the primary astrocytes. The cells were exposed to ZnO NPs for 6h. 4µM cytochalasin D pre-treatment for 1h was used as inhibitor of endocytosis. The values are expressed in percentage with respect to control. The data represent mean ± SD of three independent experiments. Asterisk denotes statistically significant difference (***$p<0.001$).

4.2.3.6 Cell morphology analysis by Giemsa staining

The Giemsa staining of cells treated with ZnO NPs indicated dose and time dependent morphological alterations **(Figure 4.42)**. Shrinkage of cytoplasm was seen in 80 µg/ml treated cells at 6h, with no other changes in nuclear morphology. Cell density was severely affected in 40 and 80 µg/ml treated cells at 24h. Complete disintegration of cytoplasm morphology along with nuclear condensation was observed in both 40 and 80

µg/ml treated cells. The cellular morphology was similar to that of control when treated with 20 µg/ml ZnO NPs at 6h and 24h.

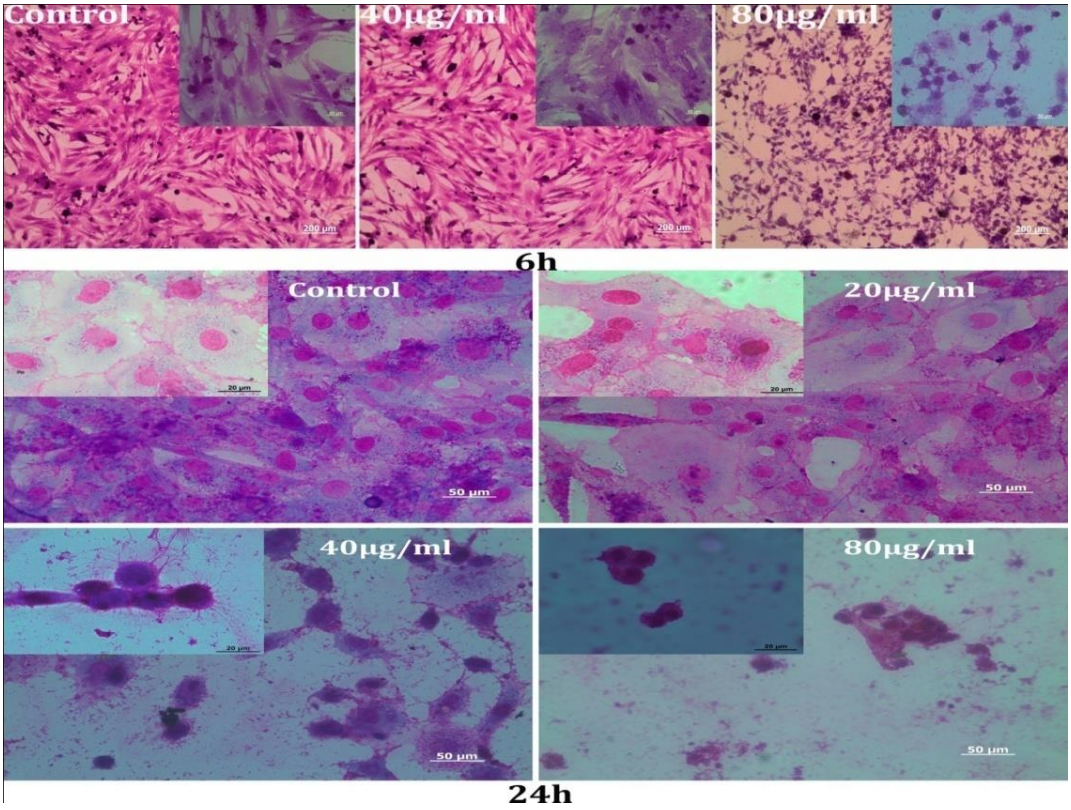

Figure 4:42: Morphology of primary astrocytes exposed to ZnO NPs for 6 and 24hby staining with Giemsa. Figure in the inset shows high magnification images of respective treatment group.6h micrograph; scale bar: 100µm, magnification 20X. 6h inset; scale bar 50µm and magnification 40X. 24h micrograph: scale bar 50µm and magnification 40X. 24h inset scale bar represents 20µm and magnification 63X.

4.2.3.7 Cytoskeletal analysis by rhodamine phalloidin staining

Structural changes in cytoskeleton were analysed using rhodamine phalloidin. ZnO NPs induced cytoskeletal alterations in the astrocytes **(Figure 4.43).** Deterioration of stress fibres along with changes in focal adhesions points were observed for 80µg/ml treatment group at 6h of incubation. All other treatment groups at 6h exhibited cytoskeletal morphology similar to that of control. At24h,40µg/ml treatment group

displayed severe alterations in cytoskeletal structure with disappearance of stress fibres and modifications in focal adhesion points. Cell density was markedly low in 80 µg/ml treatment group with complete loss of focal adhesion centres and stress fibres.

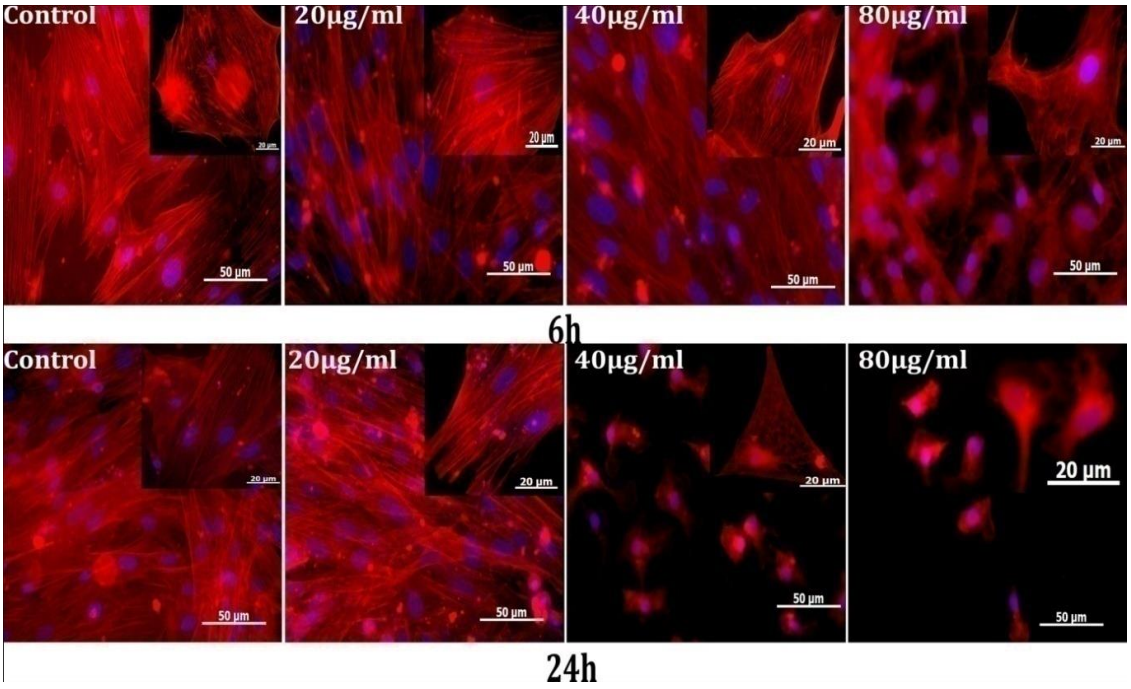

Figure 4:43: Actin staining of primary astrocytes exposed to ZnO NPs for 6 and 24h. Scale bar represents 50µm and magnification 40X. Figure in the inset shows high magnification images of respective treatment groups. The inset scale bar is 20µm and magnification 63X.

4.2.3.8 Detection of reactive oxygen species (ROS) by DCFH-DA

ROS generation in presence of ZnO NPs was estimated using the probe DCFH-DA. **Figure 4.44** indicate dose dependent increase in ROS at 6h. The lowest concentration of ZnO NPs (5µ/ml) exhibited 29% increase in ROS production whereas the 20 and 40 µg/ml treatment groups showed 38% and 49% respectively. Negative control and positive control (H_2O_2) cells exhibited a 0.4% and 98% increase respectively in ROS production.

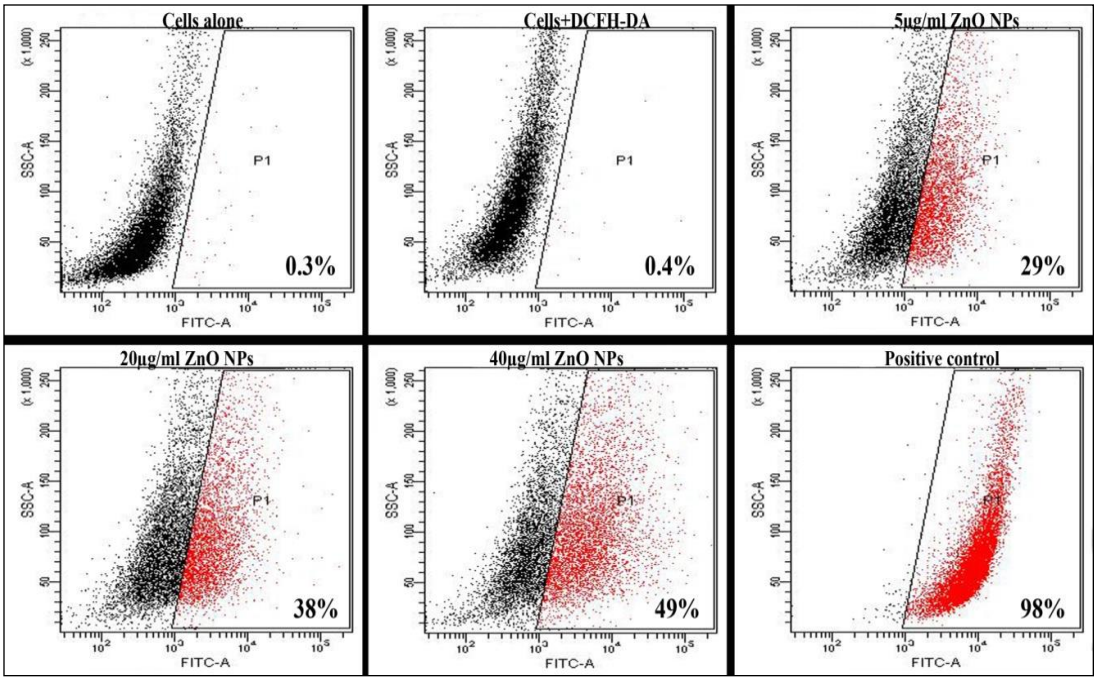

Figure 4:44: Formation of reactive oxygen species in primary astrocytes exposed to ZnO NPs for 6h. P1 quadrant represents population that are positive for DCFH-DA. H_2O_2 treated cells were used as positive control. n=3

4.2.3.9 Detection of reactive nitrogen species (RNS) by Griess reagent assay

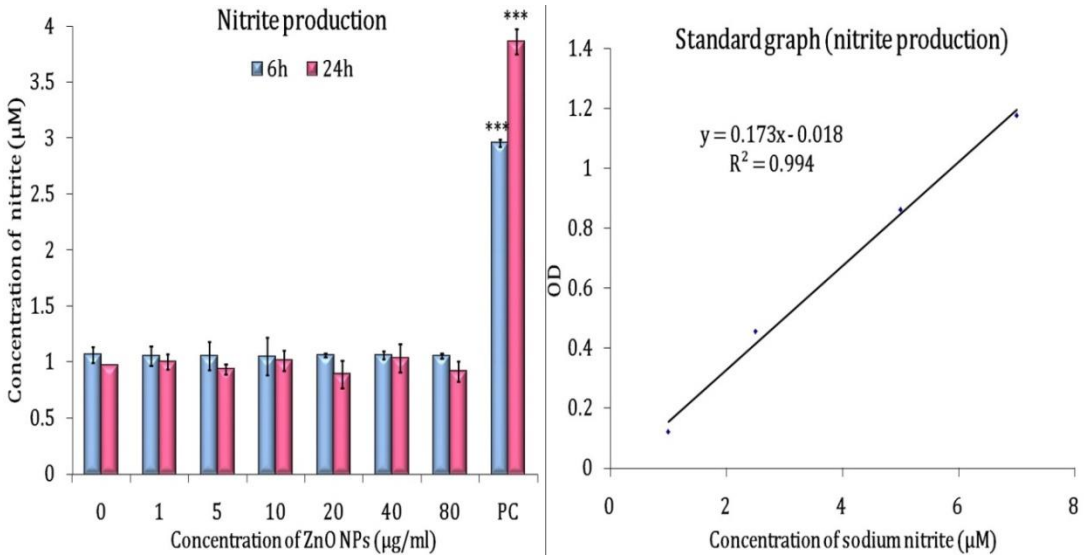

Figure 4:45: RNS production by Griess reagent assay showing nitrite production in primary astrocytes exposed to ZnO NPs for 6 and 24h. LPS treated samples were used as positive control. The data represent mean ± SD of three independent experiments. Asterisk denotes statistically significant difference (***$p<0.001$).

RNS production in presence of ZnO NPs was analysed using Griess reagent assay. The LPS treated positive control cells exhibited a statistically significant increase in RNS production with respect to cells alone. However, ZnO NPs did not induce RNS production in astrocytes. The values were similar in both negative control and treated cells **(Figure 4.45).**

4.2.3.10 Lysosomal integrity by acridine orange

Interference of lysosomal activity in presence of ZnO NPs was analysed by staining with AO. Exposure of ZnO NPs for a duration of 6h caused lysosomal destabilisation in astrocytes **(Figure 4.46).** The effect was dose dependent. Reduction in red fluorescence of AO indicated severe loss of lysosomal integrity when exposed to 80µg/ml ZnO NPs.

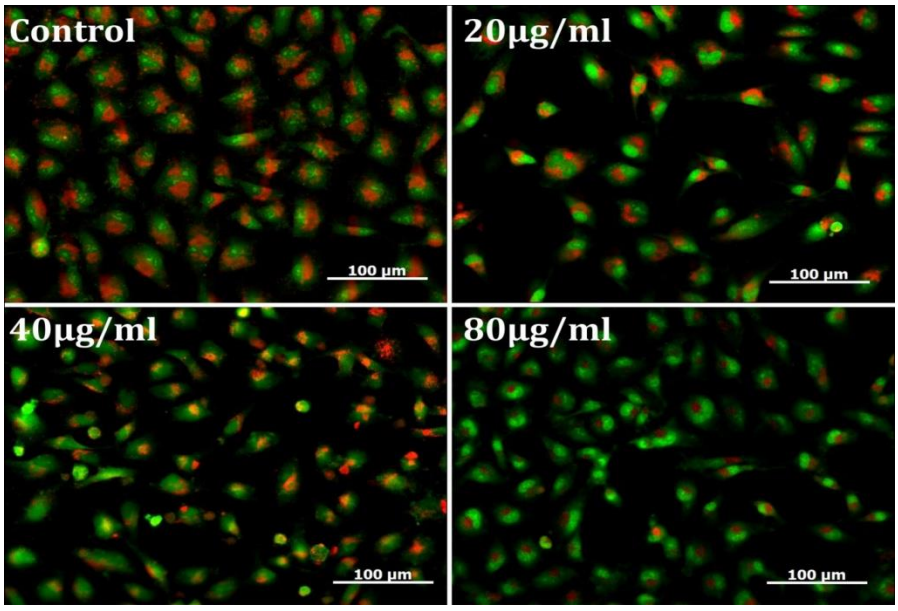

Figure 4:46: Lysosomal integrity in primary astrocytes exposed to ZnO NPs for 6h. Untreated cells were used as control. The green signal indicates the cytoplasm. Red signal shows the lysosomes. Magnification 20X

4.2.3.11 Mitochondrial membrane potential by JC1 staining

MMP was assessed microscopically from the red and green fluorescence of JC1 staining. Decline in MMP was observed in ZnO NPs treated cells in a dose and time dependent manner (**Figure 4.47)**. A very few number of cells remained in the 40 and 80µg/ml treatment group at 24h, which exhibited marked reduction MMP. Clumped mitochondria were evident in all treated cells at 6 and 24h.Whereas, active and healthy mitochondria in diffused state were observed in the control groups.

4.2.3.12 Apoptosis by Annexin V/PI staining

Annexin V/PI staining was used to study apoptosis in astrocytes. Appropriate controls were used to gate the population. There was a dose dependent increase in annexin V positive cells and annexin V/PI double positive cells **(Figure 4.48)**. Statistically significant difference was observed in 20, 40 and 80 µg/ml treated cells with respect to control (cells alone).

4.2.3.13 Caspase 3/7 activation assay:

Caspase mediated apoptosis was evaluated by Caspase 3/7 activity. Caspase 3/7 activity in response to ZnO NPs was measured fluorometrically. There was a dose dependent increase in caspase 3/7 activity when exposed to ZnO NPs. 80 µg/ml of ZnO NPs induced a statistically significant increase in caspase activity (71.94±3.83%) compared to control **(Figure 4.49).**

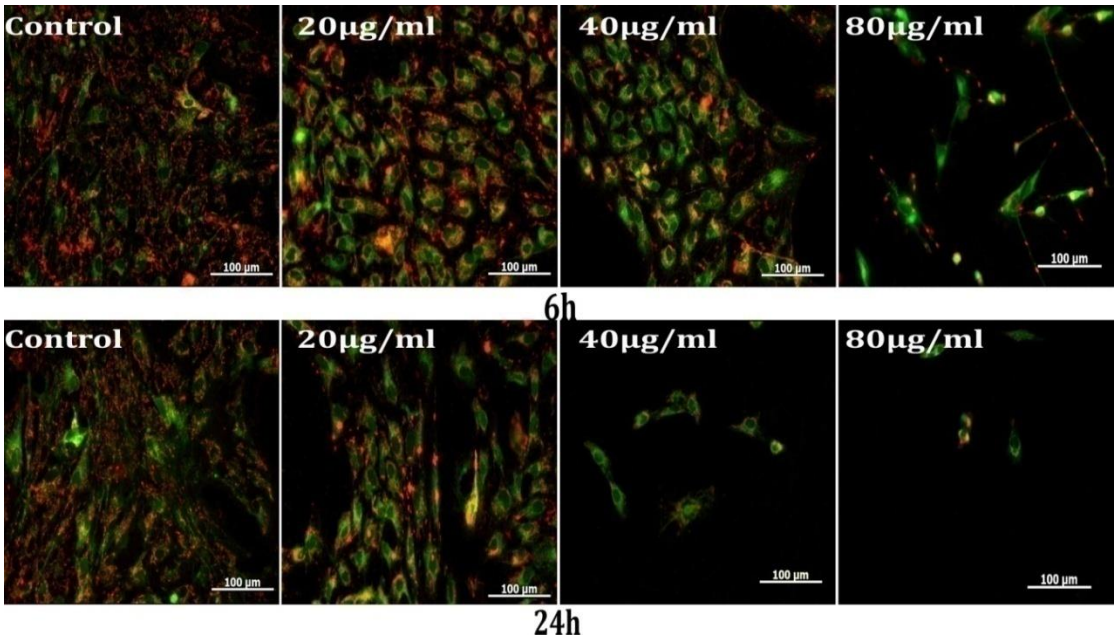

Figure 4:47: MMP analysis of primary astrocytes cells exposed to ZnO NPs for 6and 24h. Untreated cells are used as control. The red signal represents J aggregates in active mitochondria. Green signal represents the diffused monomers of JC1 in the cytoplasm. Scale bar represents 100µm. Magnification 20X.

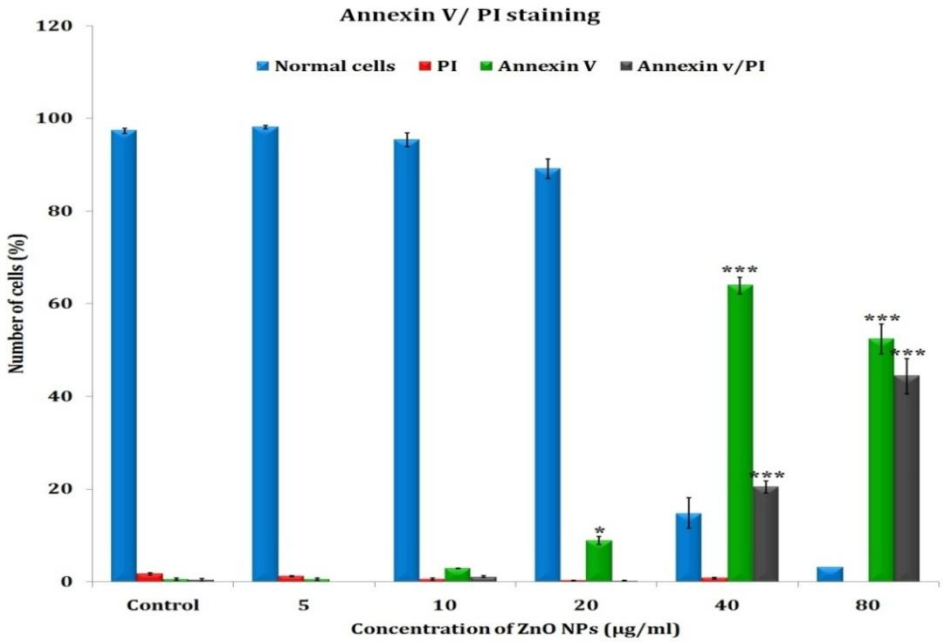

Figure 4:48: Apoptosis by annexin V/PI staining of astrocytes exposed to ZnO NPs. The data represent mean ± SD of three independent experiments. Asterisk denotes statistically significant difference group (*p<0.001 and ***p<0.001).

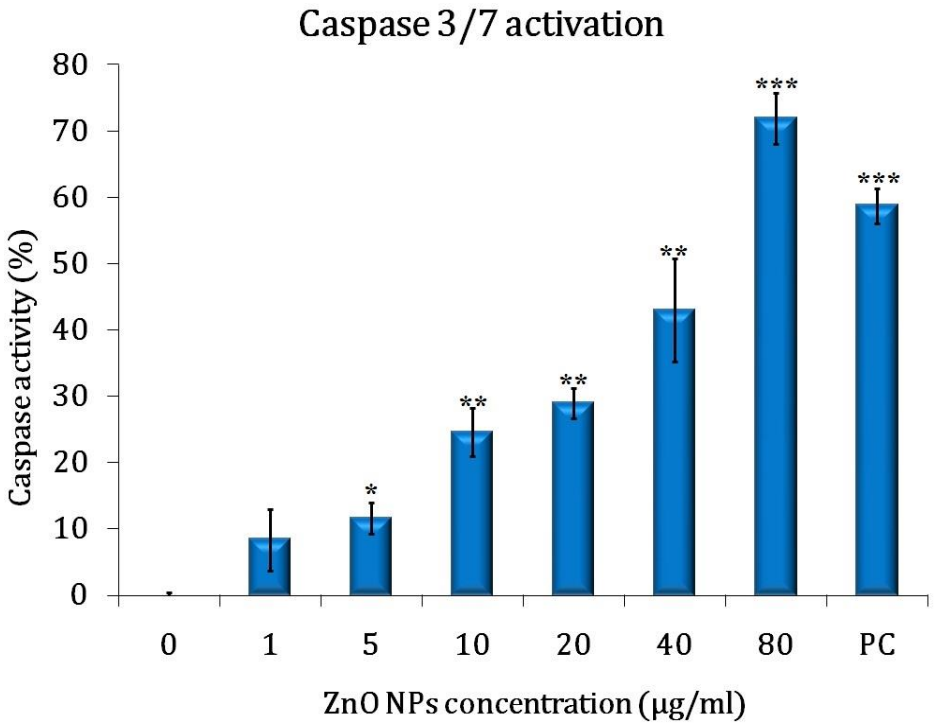

Figure 4:49: Caspase mediated apoptosis in astrocytes exposed to ZnO NPs by caspase 3/7 activation assay. Nutrient deprived cells were used as positive control (PC). The data represent mean ± SD of three independent experiments. Asterisk above columns denotes statistically significant difference, compared to the control group (*p<0.001, **p<0.001 and ***p<0.001).

4.2.3.14 Cell Membrane integrity by Calcein AM-PI staining

The event of membrane permeabilisation and cell viability was analysed using Calcein AM -PI staining. 80µg/ml of ZnO NPs exposure for 6h elicited membrane permeabilisation in astrocytes. However, the cells remained positive for Calcein at 80µg/ml concentration. Membrane integrity remained intact for all other concentration (up to 40µg/ml) at 6h of exposure. 40 and 80 µg/ml ZnO NPs exposure at 24h resulted in rigorous loss of cell number and membrane integrity. PI positive-Calcein negative cells were observed in these treatment groups suggesting complete loss of cellular

activity. Calcein positive cells with intact membrane were observed up to 20µg/ml concentrations (**Figure 4.50**).

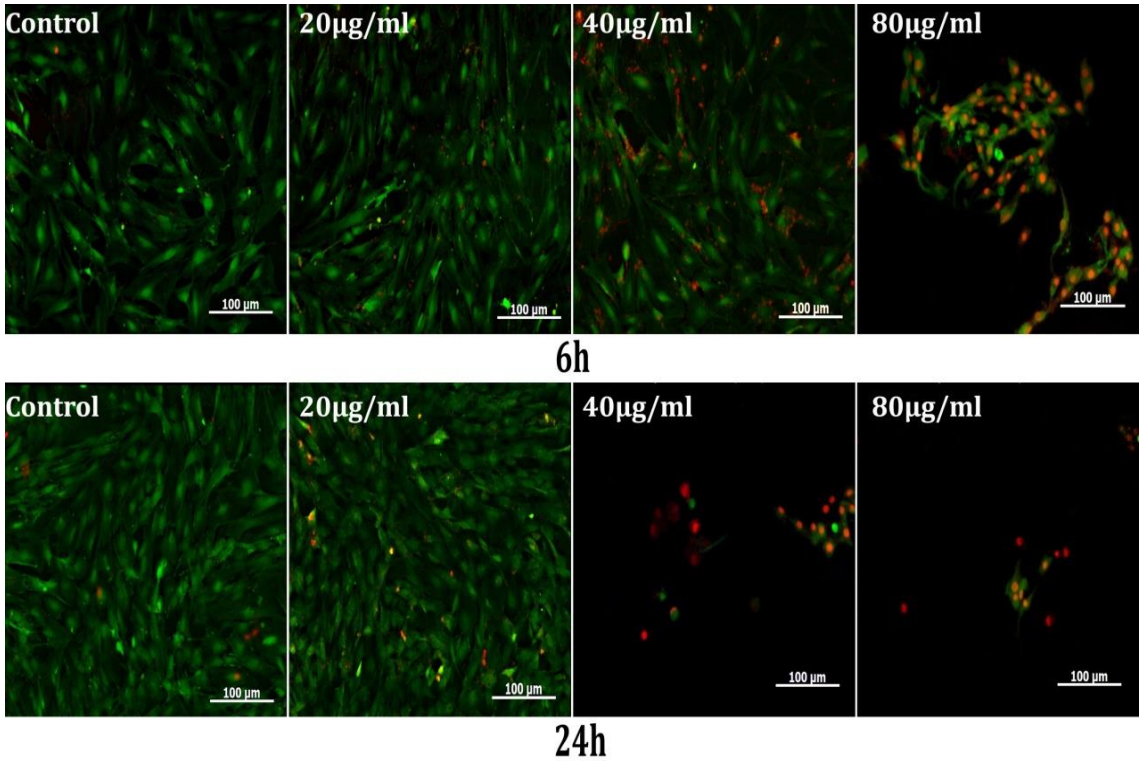

Figure 4:50: Cell membrane integrity of astrocytes treated with ZnO NPs for 6h and 4h by Calcein AM/PI staining of cells. Untreated astrocytes used as control. Green signal indicate viable and red signal indicate membrane disintegrated cells. Scale bar represents 100µm. Magnification 20X.

4.2.3.15 Nuclear condensation by DAPI staining

DAPI staining was used to study nuclear and chromatin condensation. ZnO NPs exposed cells showed nuclear condensation in a dose and time dependent manner **(Figure 4.51).** At 6h, 80µg/ml treated cells exhibited nuclear condensation. 40µg/ml treated cells also exhibited nuclear condensation at 24h.

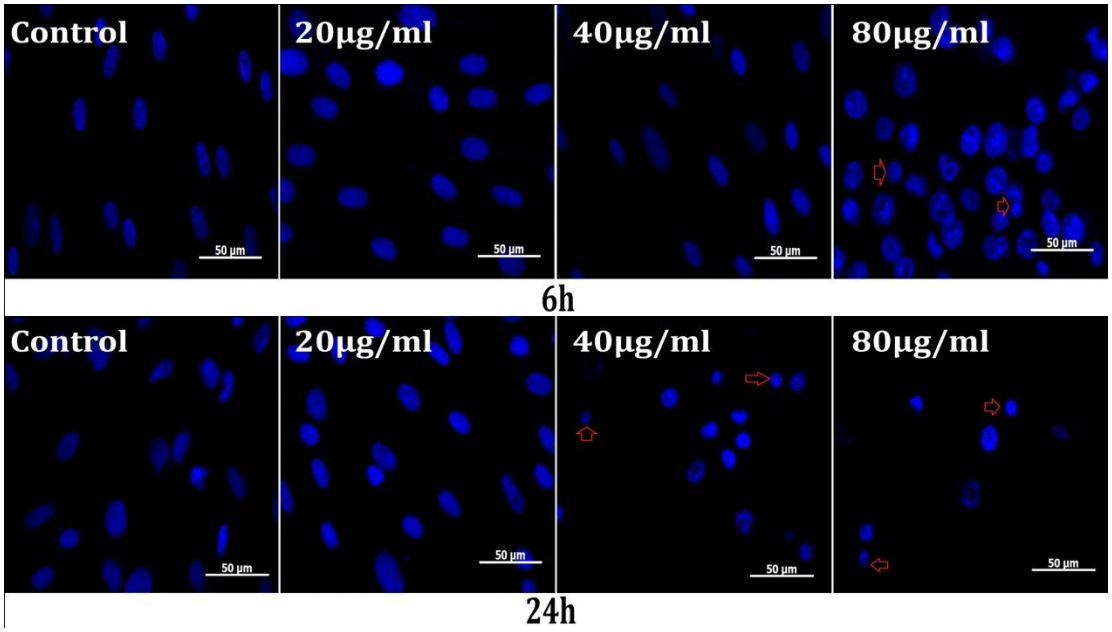

Figure 4:51: Nuclear condensation by DAPI staining in primary astrocytes exposed to ZnO NPs for 6 and 24h. Untreated cells are used as control. Scale bar represents 50µm. Magnification 40X

4.2.3.16 Effect of particle size and dissolution on astrocytes

4.2.3.16.1 Cytotoxicity by MTT

Effect of particle dissolution and size on the biological interaction of ZnO NPs was evaluated by comparing the mitochondrial activity among ZnO NPs, zinc ion ($ZnCl_2$) and bulk form of ZnO. The bulk formulation exhibited least toxicity when compared to $ZnCl_2$ and ZnO NPs. On the other hand, $ZnCl_2$ and ZnO NPs exposed cells showed a similar pattern of mitochondrial activity at 6 and 24h (**Figure 4.52).**

4.2.3.16.2 Cell count by trypan blue exclusion assay

Cell count was determined by trypan blue exclusion assay. The cell count in the culture after ZnO NPs exposure was compared with culture exposed to $ZnCl_2$ and bulk

formulation of ZnO. The nanoformulation of ZnO showed significant reduction in the total cell count at 40 and 80µg/ml. Total cell count as well as number of dead cells was higher in ZnO bulk treated cells, when compared to ZnO NPs and $ZnCl_2$ treated cells. Cell count was more or less similar in $ZnCl_2$ and ZnO NPs treated cells except at 80µg/ml **(Figure 4.53).**

4.2.3.16.3 Detection of ROS by DCFH-DA assay

The ROS generation in astrocytes exposed to ZnO NPs were compared with $ZnCl_2$ and ZnO bulk particles. ZnO NPs treated cells exhibited highest ROS production at 6h, compared to bulk formulation of ZnO **(Figure 4.54)**. The $ZnCl_2$ exposed cells responded similar to that of ZnO NPs. At 24h the ROS generation was declined in all (40 and 80 µg/ml) treated cells. This may be due to the high level of cytotoxicity and catalase activity in the treated cells.

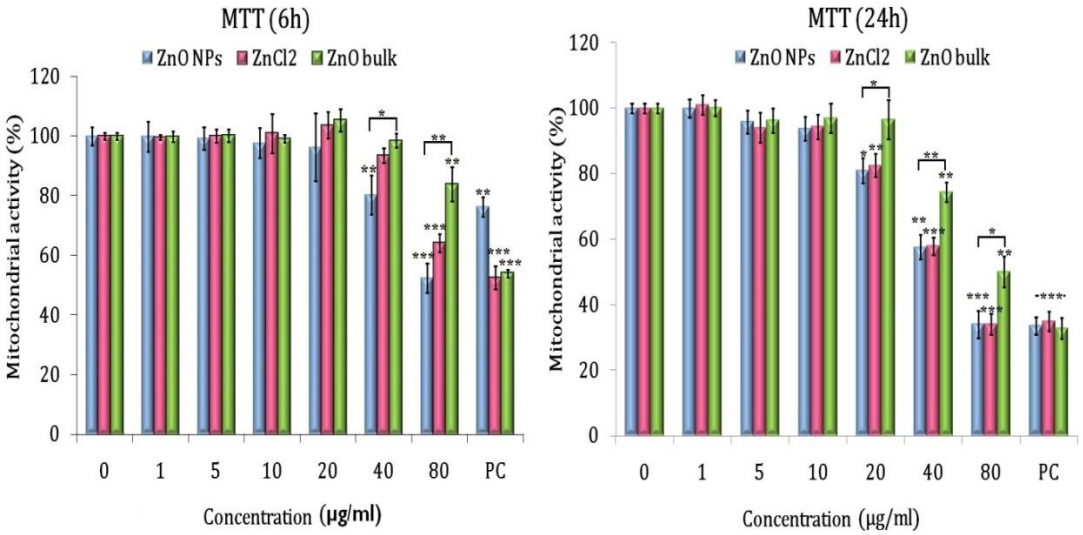

Figure 4:52: Mitochondrial activity of primary astrocytes exposed to ZnO NPs, $ZnCl_2$ and ZnO bulk particle for 6 and 24h. Phenol treated cells were used as positive control. The values are expressed in percentage with respect to control. The data represent mean ± SD of three independent experiments. Asterisk denotes statistically significant difference (*$p<0.05$, **$p< 0.01$ and ***$p<0.001$).

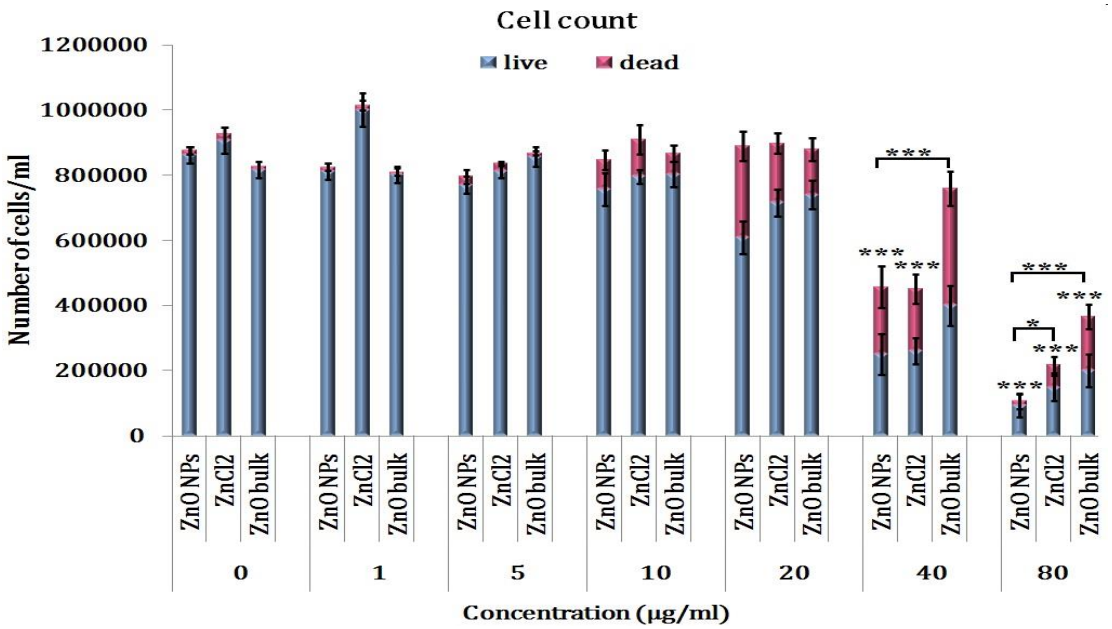

Figure 4:53: Trypan blue exclusion assay comparing the cell count in primary astrocytes exposed to ZnO NPs, $ZnCl_2$ and ZnO bulk for 24h. The data represent mean ± SD of three independent experiments. Asterisk denotes statistically significant difference in total cell count (*p<0.05, **p< 0.01 and ***p<0.001).

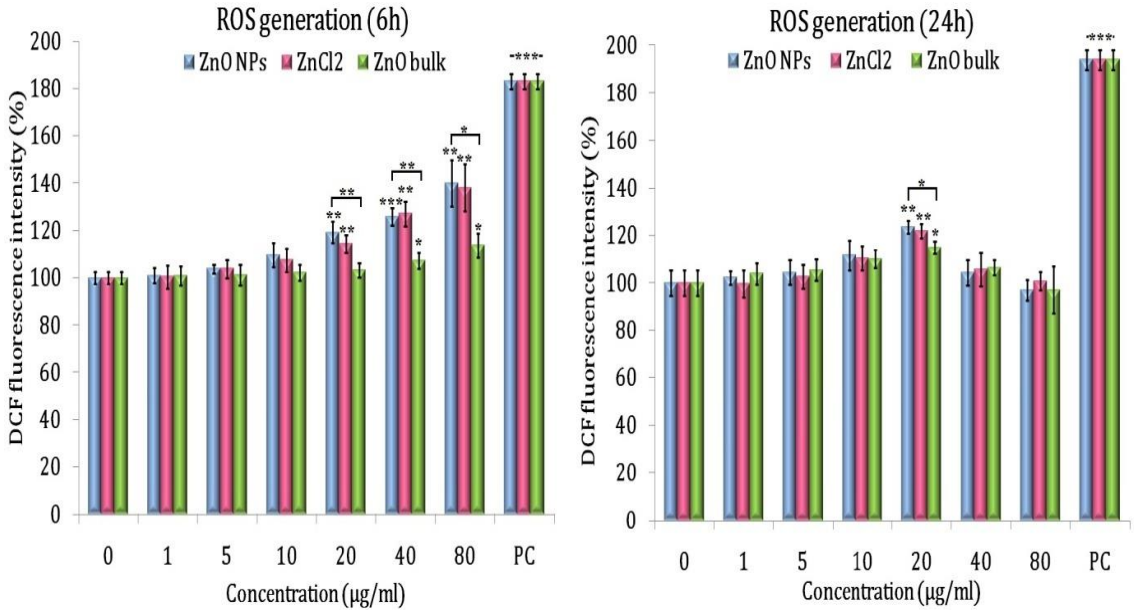

Figure 4:54: Comparison of ROS generation in primary astrocytes exposed to ZnO NPs, $ZnCl_2$ and ZnO bulk for 6 and 24h analysed by DCFH-DA. H_2O_2 treated cells were used as positive control. The values are expressed in percentage fluorescence with respect to control. The data represent mean ± SD of three independent experiments. Asterisk denotes statistically significant difference (*p<0.05, **p< 0.01 and ***p<0.001).

4.2.3.16.4 Evaluation of proliferative capacity and survival rate by Clonogenic assay

Clonogenic assay was performed to detect the cell survival and proliferation potential of the cells. The results of the clonogenic assay of ZnO NPs were compared with $ZnCl_2$ and ZnO bulk exposed cells. Cells exposed to high concentration of ZnO NPs exhibited low survival rate and proliferation potential than $ZnCl_2$ and ZnO bulk. This is due to the low number of colonies formed in ZnO NPs treated cells (**Figure 4.55**).

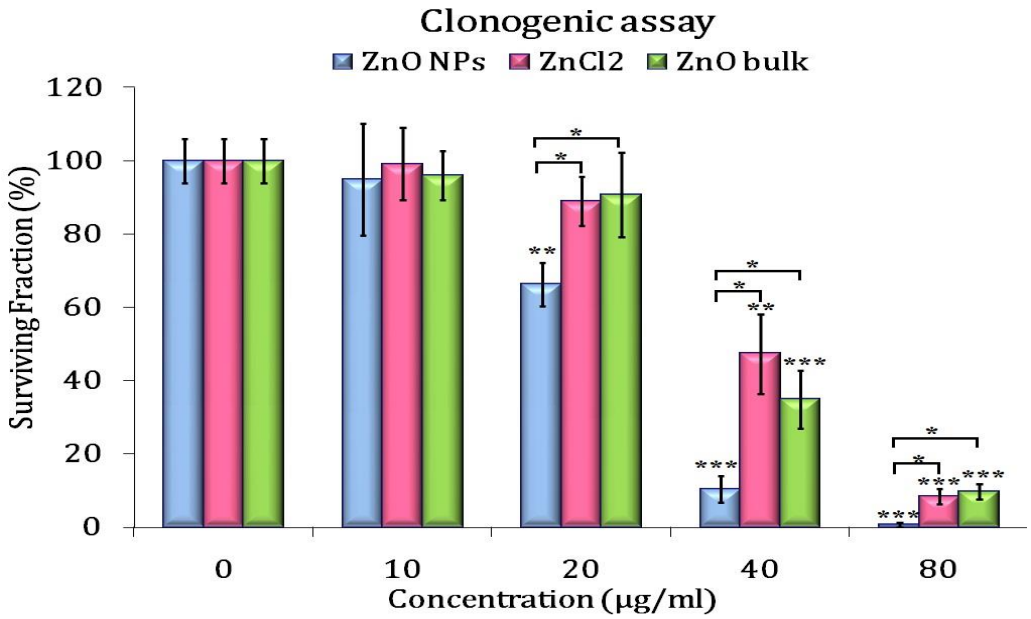

Figure 4:55: Comparison of regenerative and proliferation potential of primary astrocytes exposed to ZnO NPs, $ZnCl_2$ and ZnO bulk using clonogenic assay. The data represent mean ± SD of three independent experiments. Asterisk denotes statistically significant difference, (*$p<0.05$, **$p< 0.01$ and ***$p<0.001$).

4.2.3.16.5 Evaluation of apoptosis by Caspase 3/7 activation assay

Caspase activity was detected by Caspase 3/7 activation assay. Astrocytes exhibited a dose dependent increase in Caspase activity in ZnO NPs, $ZnCl_2$ and ZnO bulk formulation **(Figure 4.55**). The results were normalised with total protein content.

It was noted that ZnO NPs exhibited a significantly high Caspase activity when compared to $ZnCl_2$ and ZnO bulk formulation.

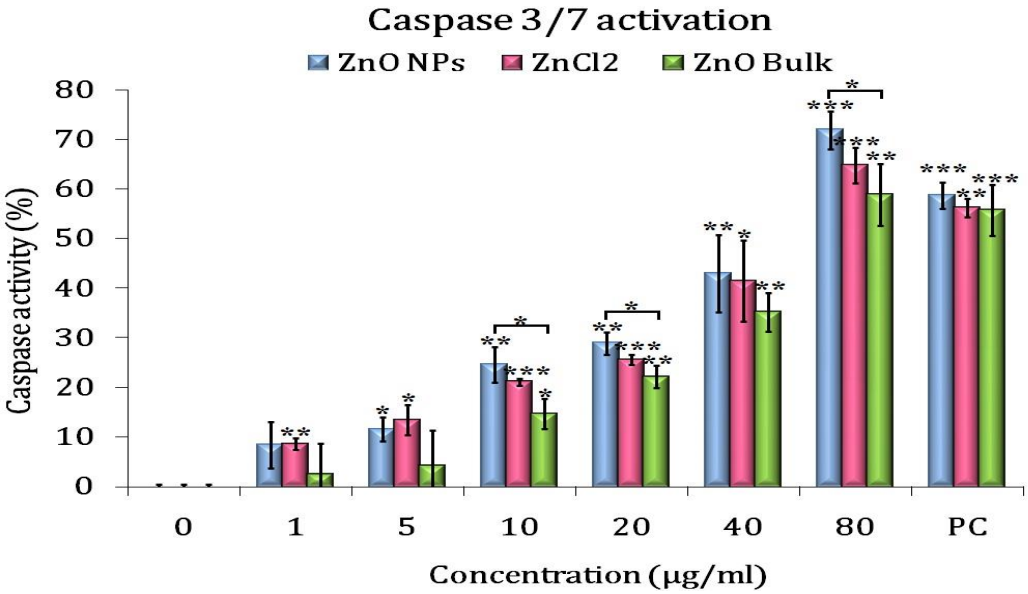

Figure 4:56: Comparison of caspase 3/7 activation in primary astrocytes exposed to ZnO NPs, $ZnCl_2$ and ZnO bulk formulation for 24h. The data represent mean ± SD of three independent experiments. Asterisk denotes statistically significant difference (*p<0.05, **p< 0.01 and ***p<0.001).

4.3 *IN VIVO* ACUTE TOXICITY STUDIES USING WISTAR RATS.

4.3.1 CLINICAL/BEHAVIOURAL SIGNS

10mg/kg of ZnO NPs were administered to Wistar rats via i.v. and i.p. injection (single exposure). Animals were monitored for 21 days for clinical and behavioural signs of stress and neurotoxicity. A set of clinical signs associated with behavioural activities, autonomous nervous system, peripheral nervous system and central nervous system activities were evaluated to study the neurotoxicological response of animals. None of the rats showed any clinical and behavioural signs of stress or neurotoxicity during the observation period **(Table 4.7**).

Neurological parameters	Clinical signs and behavioural changes	Control	ZnO NPs (i.v)	ZnO NPs (i.p)	$ZnCl_2$ (i.v)
Autonomous nervous system	Lacrimation Salivation Excretion Piloerection	Normal	Normal	Normal	Normal
Peripheral nervous system	Righting reflex Hind limb grip Strength Forelimb grip strength	Normal	Normal	Normal	Normal
Behavioural activity	Motor activity Home cage posture Rearing	Normal	Normal	Normal	Normal
Central nervous system	Clonic movements Tonic movements	Normal	Normal	Normal	Normal

Table 4.7: Clinical signs and behavioural signs of rats exposed to ZnO NPs. n=3

4.3.2 BODY WEIGHT OF THE ANIMALS

Body weights of the animals were monitored throughout the experimental periods. Body weight gain of treated animals was similar to that of control animals. However, a statistically significant reduction in weight gain was observed on 14^{th} day of i.v. administered group **(Table 4.8).**

4.3.3 ORGAN WEIGHT

Organ weights are expressed in absolute wet weight. No significant changes in organ weight were observed in animals **(Table 4.9).** The treatment group values were comparable to that of control.

Dose	Route of exposure	Observation period		
		3rdday	14thday	21st day
Control (saline)	i.v.	5.07±1.83	31.70±1.18	37.98±1.35
ZnO NPs 10mg/ml	i.v.	3.24±0.74	20.36±1.35 ***	38.35±0.44
	i.p.	7.39±1.21	31.13±2.03	38.03±1.81
ZnCl2 10mg/ml	i.v.	-	32.04 ± 1.75	-

Table4.8: Percentage body weight gain after ZnO NP. The data represent mean ± SD. n=3. Asterisk above values denotes statistically significant difference, compared to the control group (***p<0.001)

Group	Brain (g)	Liver (g)	Spleen (g)	Kidney (g)
Control	1.63 ± 0.05	12.43 ± 1.33	0.51 ±0.11	0.68 ± 0.24
ZnO NPs (i.v)	1.57 ± 0.07	10.38 ± 2.12	0.48 ±0.20	0.59 ± 0.17
ZnO NPs (i.p)	1.60 ± 0.04	11.71 ± 1.59	0.55 ±0.15	0.63 ± 0.09
$ZnCl_2$ (i.v)	1.61 ± 0.07	12.65 ± 0.93	0.53 ±0.16	0.65 ± 0.03

Table 4.9: Organ weight of animals treated with ZnO NPs. Values are represented as absolute organ weight in grams. n=3. The data represent mean ± SD of three independent experiments

4.3.4 HAEMATOLOGY AND BIOCHEMICAL PARAMETERS

Blood from the treated animals was collected at 3, 14 and 21 day of observation and subjected to biochemistry and haematological analysis (biochemical values are elaborated in the organ toxicity section). The results of the study indicated that blood cell count, blood cell volume, haemoglobin content and platelet count remained within normal range and were comparable to that of control. (**Table 4.10)**

Parameters	Control	i.v.			i.p.			$ZnCl_2$
		3rd day	14th day	21st day	3rd day	14th day	21st day	
Platelets ($10^3/mm^3$)	400.1± 86.2	527.4± 106.6	559.5± 54.3	373.9± 92.3	441.4± 47.1	600.0± 38.0	549.5± 76.7	221.4± 89.8
WBC ($10^3/mm^3$)	9.60± 1.54	15.62± 2.12	15.01± 4.24	9.70± 2.43	14.71± 3.53	14.94± 1.14	13.41± 3.45	11.06± 3.09
RBC ($10^6/mm^3$)	9.80± 1.46	7.93± 1.36	8.64± 2.92	11.06± 2.92	7.68± 1.44	8.71± 2.56	10.93± 2.17	9.33± 1.58
HGB (g/dl)	15.22± 2.23	16.88± 1.49	17.70± 2.55	17.27± 3.47	16.30± 2.49	15.26± 2.90	18.30± 1.19	18.53± 3.40
HCT (%)	46.37± 4.12	44.64± 5.72	45.46± 7.17	49.23± 3.82	46.14± 5.70	40.84± 8.13	51.28± 5.46	47.27± 5.63
MCV (μm^3)	53.16± 3.91	52.28± 6.87	53.52± 7.29	54.38± 6.10	56.66± 7.24	52.98± 5.43	55.33± 8.50	57.18± 5.78
MCH (pg)	18.08± 2.48	18.39± 3.24	21.90± 3.64	20.43± 4.35	18.45± 4.47	20.35± 1.35	19.23± 2.32	22.23± 1.37
MCHC (g/dl)	30.93± 3.35	33.53± 6.46	39.05± 6.72	36.39± 6.41	32.73± 6.37	39.31± 5.17	35.26± 4.82	39.10± 4.50

Table 4.10: Haematology parameters of Wistar rats exposed to ZnO NPs and $ZnCl_2$. WBC; white blood cells, RBC: red blood cells, HGB; haemoglobin, HCT; haematocrit, MCV; Mean corpuscular volume, MCH; Mean corpuscular haemoglobin, MCHC; mean corpuscular haemoglobin concentration. Data represents mean±SD of three independent experiments.

4.3.5 GROSS PATHOLOGY

Gross examination did not reveal any visible pathological changes in i.v. and i.p treated animals. Gross pathology of animals treated with ZnO NPs was similar to that of control (**Figure 4.57)**.

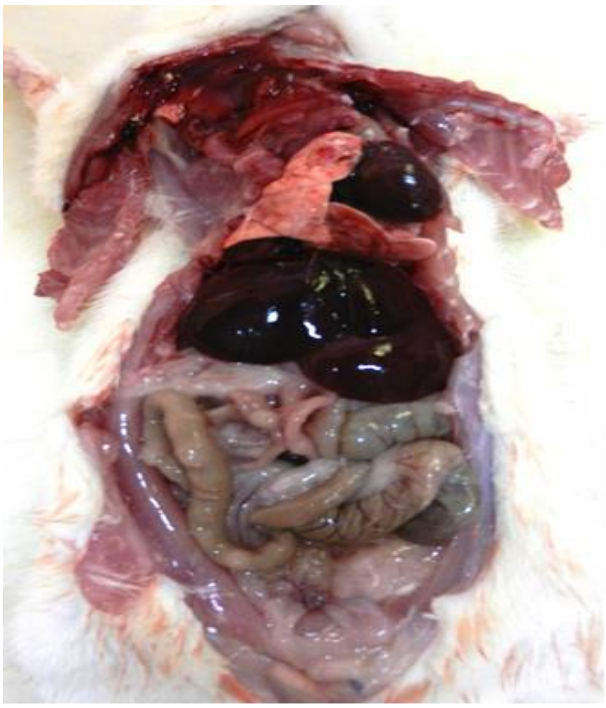

Figure 4:57: Gross pathology of animal treated with ZnO NPs

4.3.6 TARGET ORGAN TOXICITY: BRAIN

4.3.6.1 Antioxidant assays

Brain tissues were collected from ZnO NPs exposed (i.v.) animals. All the assays were carried out in 10% brain homogenate. The lipid peroxidation, GSH, GR, GPx and SOD activities were analysed for antioxidants activity (**Figure 4.58).**

4.3.6.1.1 LPO

No statistically significant alteration in malondialdehyde (MDA) production was observed in the brain of ZnO NPs (i.v.) exposed animals **(Figure 4.58, a)**. The lipid peroxidation values in treated animals were similar to that of control (control: 4.13±1.6, 3rd day: 4.47±0.7, 14th day: 4.7±1.5, 21st day: 4.6±1.3).

4.3.6.1.2 GSH:

GSH level in the brain of both control and test animals remained similar. No alteration was observed in GSH level on any of the treated animals **(Figure 4.58, b).**

4.3.6.1.3 GR activity:

A statistically significant increase in GR activity was observed in ZnO NPs exposed animals on 14th day (0.71±0.04) and 21st day (0.68±0.04) of observation **(Figure 4.58,c)**

4.3.6.1.4 GPx activity

Compared to control (0.04±0) GPx activity was not altered in ZnO NPs exposed rats on 3rd day (0.04±0), 14th day (0.05±0) and 21st day (0.04±0) of observation **(Figure 4.58, d).**

4.3.6.1.5 SOD activity

A slight increase in SOD activity was observed in the brain of ZnO NPs exposed rats (control; 8.76±0.5, 3rd day; 9.10±1.1, 14th day; 9.93±1.2 and 21st day; 8.22±0.3). However, the increase was not statistically significant (**Figure 4.58,e**).

4.3.6.2 Brain volume

The change in brain volume of rats injected with ZnO NPs (i.v. and i.p. route) is indicated in **Figure 4.59**. No statistically significant changes in brain volume was observed in ZnO NPs exposed animals compared to control (i.v- control, 78.3±3.0%, test: 78.0±6.1 %; i.p-control: 79.6±3.5 % and test: 77.2±3.6%).

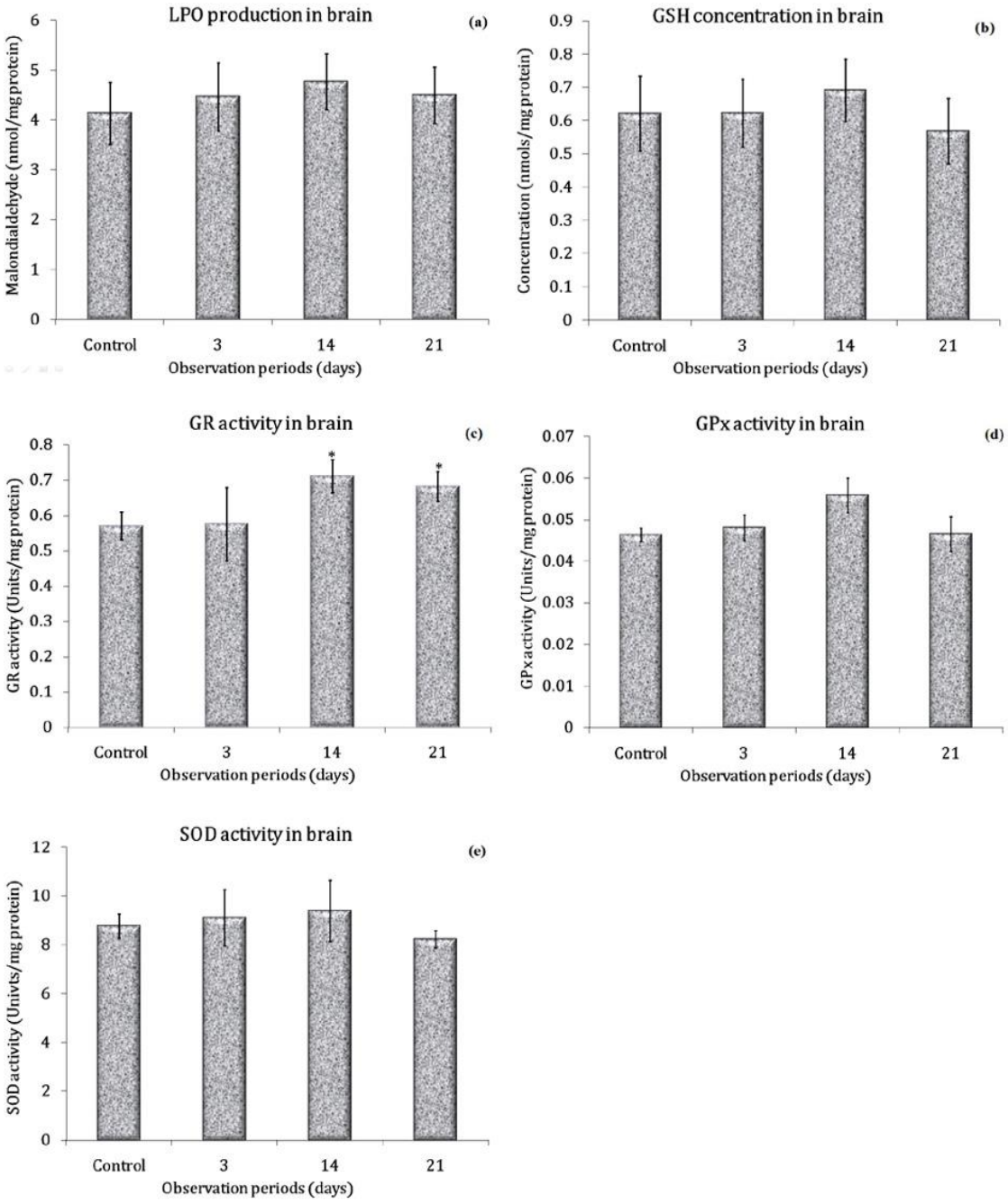

Figure 4:58: Brain antioxidants of animals exposed (i.v.) to ZnO NPs; **(a)** LPO, **(b)** GSH, **(c)** GR activity, **(d)**GPx activity, **(e)**SOD activity. n=3. The data represent mean ± SD. Asterisk denotes statistically significant difference (*$p<0.05$).

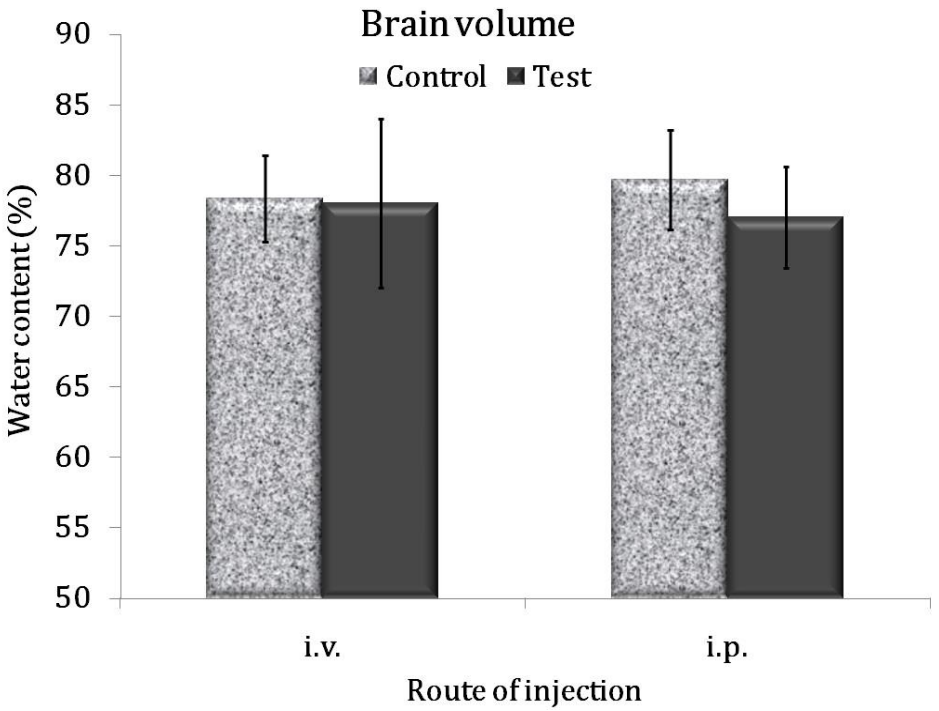

Figure 4:59: Brain volume of rats exposed to ZnO NPs (i.v. and i.p. routes). n=3. The data represent mean ± SD.

4.3.6.3 Histopathology: Brain

Figure 4.60showscerebral region of ZnO NPs (i.v. and i.p.) and $ZnCl_2$ (i.v.) exposed rats'. Histology of treated animals was comparable to that of control. No increase in microglia count was observed in treated animals.

4.3.6.4 Elemental analysis of brain

Elemental analysis of brain samples was carried out using atomic emission spectroscopy (ICP-AES). Zinc content of ZnO NPs exposed rats remained similar to that of control. However, a slight increase in iron content was observed in both i.v. and i.p. injected animals (control: 88.66±1.49, 14^{th} day i.v.: 152.13±1.8, 14^{th} day i.p.: 111.26±0.88). Copper content was similar in both control and treated animals. The

results of the elemental analysis indicated that the zinc, iron and copper content of $ZnCl_2$ exposed rats were similar to that of ZnO NPs exposed animals **(Figure 4.61)**.

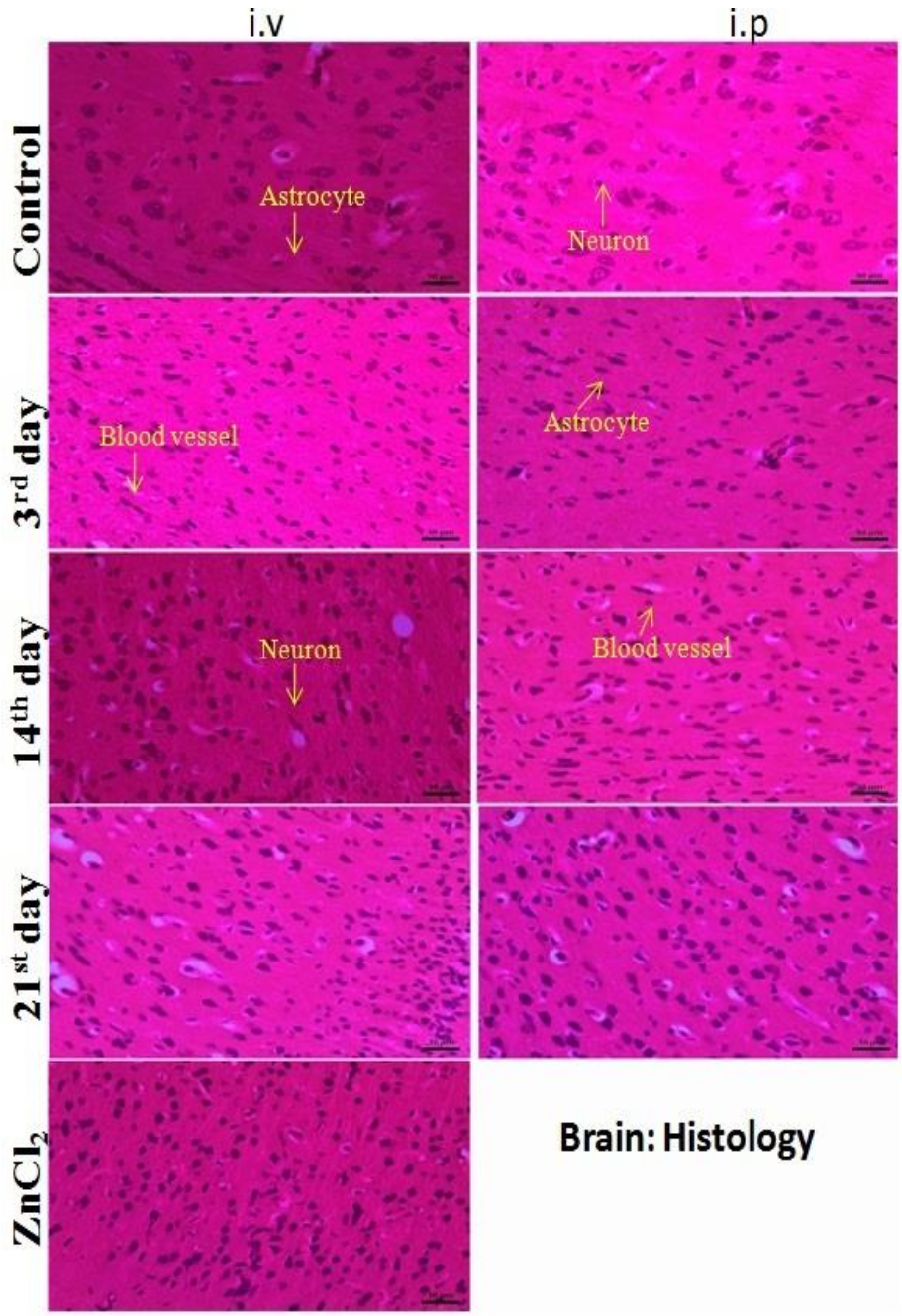

Figure 4:60: Histopathological analysis of brain of animals exposed to ZnO NPs (i.v. and i.p.) and $ZnCl_2$(14^{th} day i.v.). Magnifications 40X. Scale bar represent 30µm

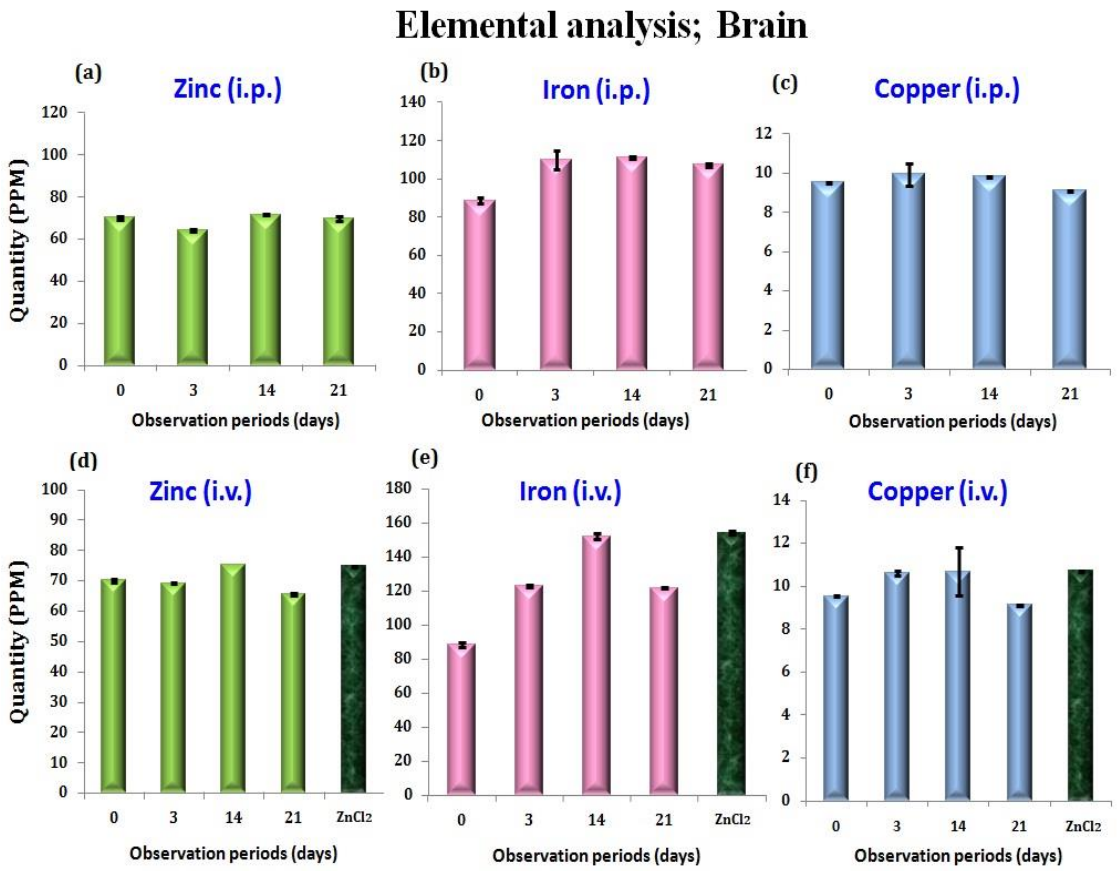

Figure 4:61: Elemental analysis in brain of animals exposed to ZnO NPs and $ZnCl_2$. N=3. The data represent mean ± SD.

4.3.7 TARGET ORGAN TOXICITY: LIVER

4.3.7.1 Liver function test

Liver function was assessed from the serum biochemistry of rats exposed to ZnO NPs and $ZnCl_2$ (i.v.). In treated animals, there was no statistically significant increase in albumin, protein, bilirubin and cholesterol when compared to control. The values are indicated in **Table 4.11**.

Group		Albumin (g/dl)	Protein (g/dl)	Bilirubin (mg/dl)	Cholesterol (mg/dl)
Control		3.88±0.45	5.50±0.31	0.04±0.01	40.07±6.60
ZnO NPs (i.v)	3rd day	3.14±0.12	5.05±1.02	0.19±0.09	40.9±11.34
	14th day	4.26±0.36	6.03±0.92	0.14±0.06	59.8±22.85
	21st day	5.25±0.74	6.08±0.88	0.09±0.08	67.7±27.58
ZnO NPs (i.p)	3rd day	4.04±0.57	5.24±0.64	0.16±0.09	52.1±17.62
	14th day	4.19±0.73	6.12±0.99	0.17±0.06	76.3±17.21
	21st day	3.34±0.51	5.09±0.87	0.14±0.07	72.4±30.01
$ZnCl_2$ (i.v)	14th day	2.10±0.99	5.10±0.66	0.14±0.05	66.5 ±28.9

Table 4.11: Liver function test in Wistar rats treated with ZnO NPs and $ZnCl_2$. n=3. The data represent mean ± SD.

4.3.7.2 Liver cellular integrity

The cellular integrity of liver was evaluated from the alanine amino transferase (ALT) and aspartate aminotransferase values (AST). The values of both ALT and AST were significantly high in the serum of ZnO NPs injected animals. ALT and AST level progressively increased in i.v injection animals whereas declined in i.p injected animals on 14th and 21st day. It was also noted that the ALT and AST levels were very high in $ZnCl_2$ treated groups when compared to control values (**Table 4.12**).

4.3.7.3 Nanoparticle mediated liver obstruction.

Liver obstruction was analysed from the serum ALP and GGT levels. The results of ALP and GGT indicated that there was no statistically significant difference between control and treated animals. The values are given in the **Table 4.13**

Group	Observation period	ALT(IU/l)	AST (IU/l)
Control		20.231±4.40	98.451±10.73
ZnO NPs (i.v)	3rd day	1201.13±88.77**	150.07±29.44
	14th day	2965.02±106.12***	258.47±19.48***
	21st day	995.34±95.93**	567.39±23.76***
ZnO NPs (i.p)	3rd day	75.13±102.69	63.48±32.03
	14th day	932.20±77.26**	54.39±27.22
	21st day	206.57±54.28*	1260.03±26.19***
$ZnCl_2$ (i.v)		3216.13± 227.15**	2007.1±33.45***

Table 4.12: Liver cellular integrity in Wistar rats exposed to ZnO NPs and $ZnCl_2$. n=3. The data represent mean ± SD. Asterisk denotes statistically significant difference (*p<0.05, **p< 0.01 and ***p<0.001).

Group	Observation period	ALP (IU/l)	GGT (IU/l)
Control		79.38±44.38	32.11±6.42
ZnO NPs (i.v)	3rd day	68.13±1.503	26.69±4.12
	14th day	75.47±10.16	30.25±1.16
	21st day	100.2±40.33	28.34±3.23
ZnO NPs (i.p)	3rd day	75.55±46.94	43.11±5.92
	14th day	84.16±55.73	24.04±5.45
	21st day	94.44 ±37.74	29.87±4.87
$ZnCl_2$ (i.v)	14th	110.2±50.16	26.64±4.33

Table 4.13:Liver obstruction studies in animals exposed to ZnO NPs and $ZnCl_2$. n=3. The data represent mean ± SD.

4.3.7.4 Antioxidant assays: Liver

Liver tissues were collected from ZnO NPs exposed (i.v.) animals. All the assays were carried out in 10% liver homogenate. The lipid peroxidation, GSH, GR, GPx and SOD activities were analysed for antioxidant assays **(Figure 4.62).**

4.3.7.4.1 LPO

LPO induction is due to oxidative damage in the lipid. Statistically significant increase in malondialdehyde (MDA) was observed in the ZnO NPs exposed animals. It was found that the LPO was maximum on 14th day post exposure thereafter the LPO started declining. The results are indicated in **Figure 4.62, a**

4.3.7.4.2 GSH

The level of GSH was altered in treated animals with respect to control. A statistically significant reduction in GSH levels was observed on 14thday and was normalised by 21st day when compared to control (**Figure 4.62, b)**.

4.3.7.4.3 GR activity

A statistically significant reduction in GR activity was observed in treated animals on 3rd, 14th and 21st day of observation **(Figure 4.62, c)**.

4.3.7.4.4 GPx activity

Figure 4.62, d shows a statistically significant reduction in GPx activity on 14thday post exposure. This increase in activity was back to normal state by 21st day of observation in treated animals.

4.3.7.4.5 SOD activity

A statistically significant reduction in SOD activity was observed in the entire treated animals when compared to control (**Figure 4.62, e)**

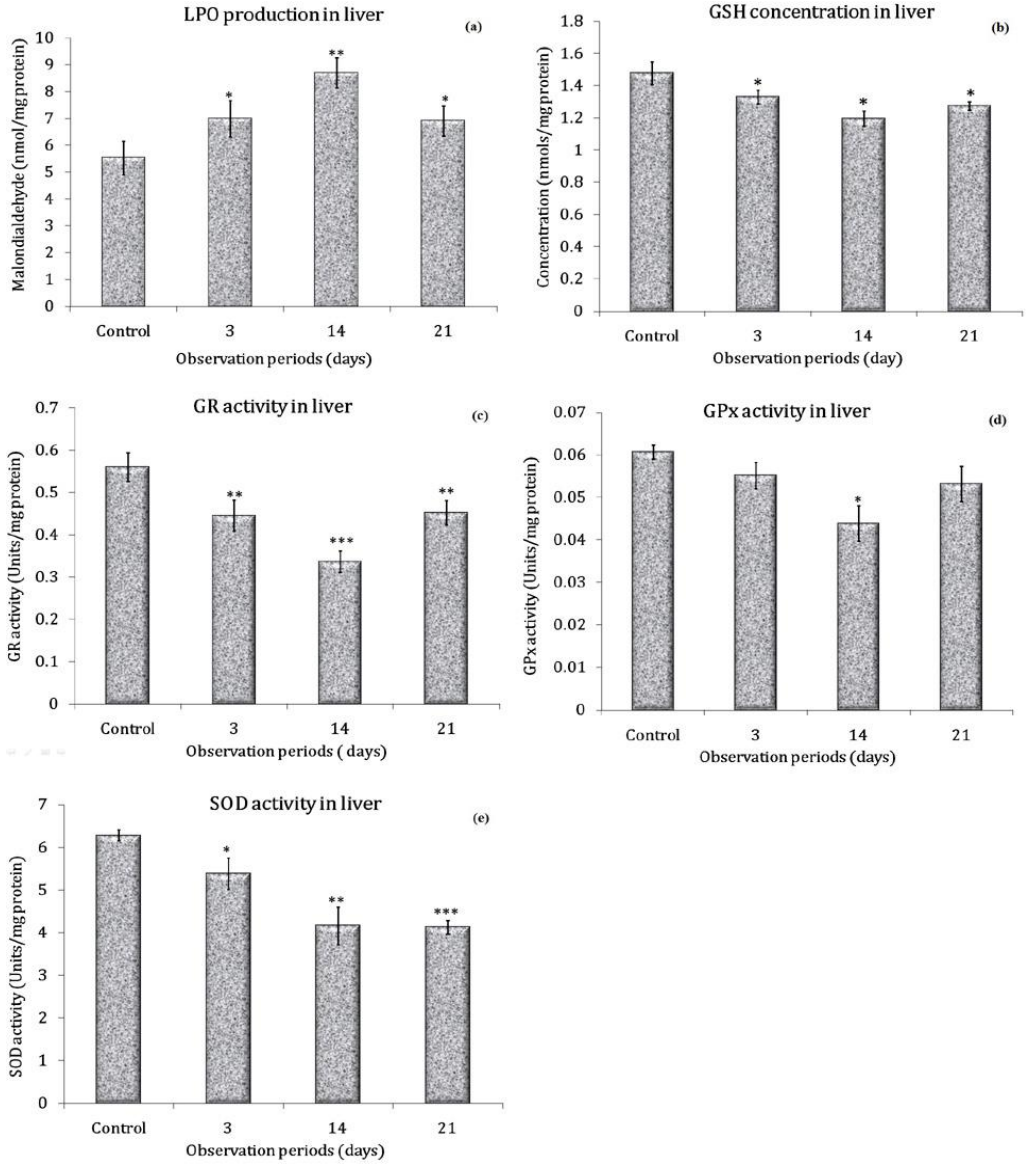

Figure 4:62: Liver antioxidants of animals exposed to ZnO NPs; **(a)** LPO, **(b)** GSH, **(c)** GR activity, **(d)** GPx activity, **(e)**SOD activity. n=3. The data represent mean ± SD. Asterisk denotes statistically significant difference (*p<0.05, **p< 0.01 and ***p<0.001).

4.3.7.5 Histopathology: Liver

Histopathological examination showed atrophic lesions in liver on 14th and 21st day of observation. Similar lesions were observed in $ZnCl_2$ treated animals **(Figure 4.63)**. No indications of mononuclear cell infiltration or increased mitotic figures were observed in the liver of treated animals.

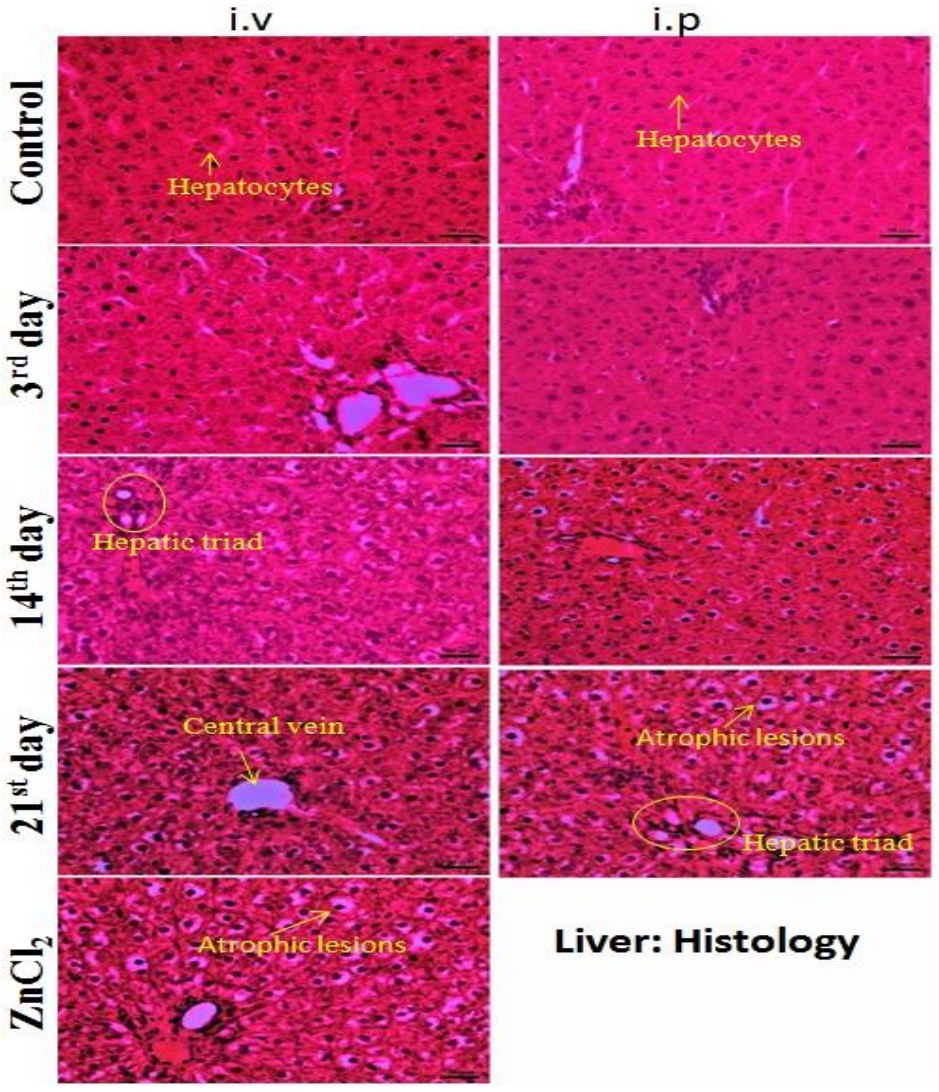

Figure 4:63: Liver histology of animals exposed to ZnO NPs and $ZnCl_2$ (14th day i.v.). Magnifications 40X. Scale bar represent 30µm.

4.3.7.6 Elemental analysis

Elemental analysis showed alteration of metal ions content in liver. Zinc content was more or less comparable to that of control in both i.v. and i.p. injected animals except on 3rd day of observation. However, ZnO NPs exposure markedly affected iron content in the liver. Iron content in ZnO NPs treated animals (3rd day i.v.: 461.65±3.22) was low compared to control animals (1203.27±12.15). A slight decrease in copper content was observed in ZnO NPs exposed animals (14th day i.v.: 11.11±0.8, 14th day i.p.: 13.32±0.18) compared to control (14.95±0.22). Elemental analysis of $ZnCl_2$ exposed animals was similar to that of ZnO NPs exposed animals **(Figure 4.64).**

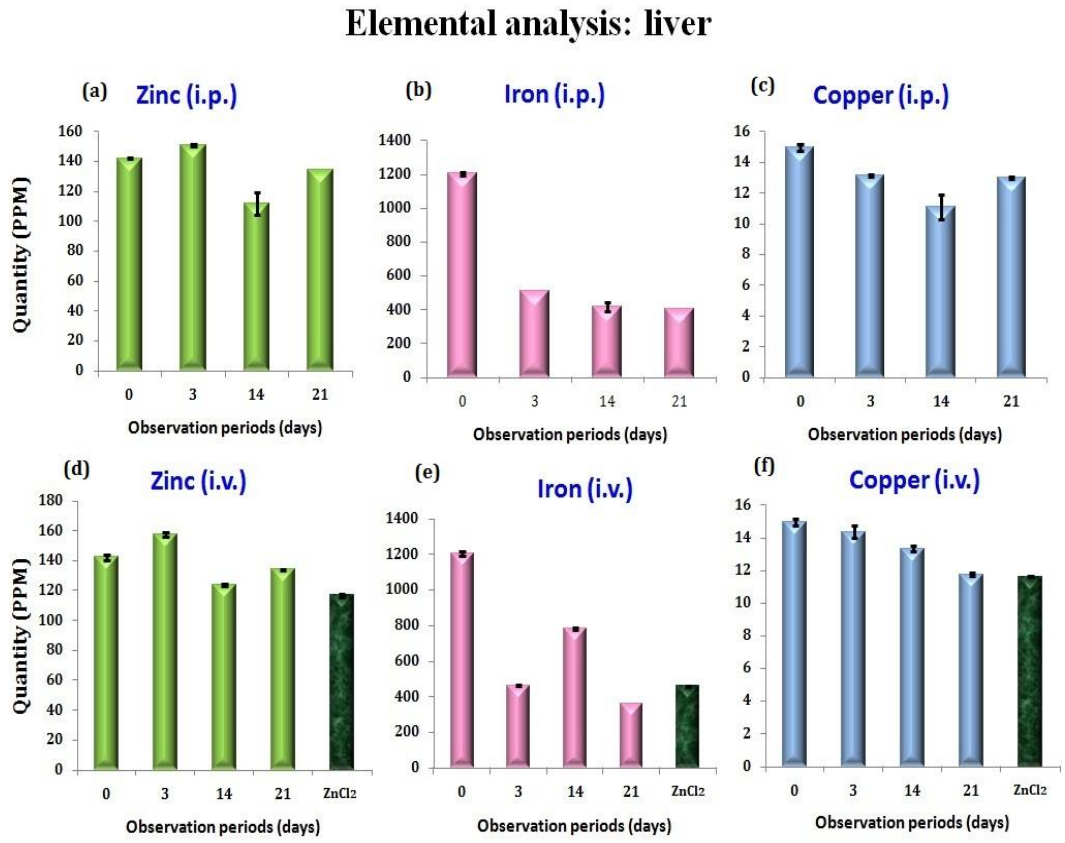

Figure 4:64: Elemental analysis of liver of animals exposed to ZnO NPs via i.p. and i.v. injection and $ZnCl_2$ (i.v.). N=3. The data represent mean ± SD.

4.3.8 TARGET ORGAN TOXICITY: KIDNEY

4.3.8.1 Kidney function test: Serum Biochemistry

Blood was collected on 3rd, 14thand 21st day post exposure of ZnO NPs and $ZnCl_2$. Serum urea and creatinine were analysed for kidney function test. Result of the study indicated that the level of serum urea and creatinine were normal in ZnO NPs and $ZnCl_2$ exposed animals when compared to control (**Table 4.14**).

Group	Observation periods	Urea (mg/dl)	Creatinine (mg/dl)
Control	0 day	18.38 ± 1.09	0.33 ±0.03
ZnO NPs (i.v)	3rd day	22.17 ± 1.43	0.31 ±0.06
	14th day	20.60 ± 1.28	0.42 ±0.04
	21st day	21.44 ± 2.46	0.38 ±0.06
ZnO NPs (i.p)	3rd day	23.03 ± 2.23	0.33 ±0.09
	14th day	20.81 ± 4.18	0.29 ±0.03
	21st day	22.65 ± 0.23	0.46 ±0.03
$ZnCl_2$ (i.v)	14th day	23.06 ± 2.13	0.31 ±0.04

Table 4.14: Kidney function study of Wistar rats exposed to ZnO NPs and $ZnCl_2$. n=3. The data represent mean ± SD.

4.3.8.2 Kidney function tests: Urine analysis:

The urine was collected on 3, 14 and 21 days after administration of ZnO NPs and $ZnCl_2$. The results of the study are summarised in **Table 4.15**. The results of the study indicated that leukocytes, nitrates, urobilinogen proteins, ketone, bilirubin and glucose were comparable in both control and treated animals. There was no treatment related reactions in the kidney.

Parameters	Control	i.v. injection			i.p injection			ZnCl 2 (I.V)
		3rd day	14th day	21st day	3rd day	14th day	21st day	
Leukocyte	-ve	-ve	-ve	-ve	-ve	-ve	-ve	-ve
Nitrite	-ve	-ve	-ve	-ve	-ve	-ve	-ve	-ve
Urobilinogen (mg/dl)	N	N	N	N	N	N	N	N
Protein-mg/dl	10	-ve	22	20	10	-ve	10	-ve
pH	6	7	6	6	7	6	6	6
Blood	-ve	-ve	-ve	-ve	-ve	-ve	-ve	-ve
Specific gravity	1.02	1.01	1.01	1.01	1.02	1.02	1.03	1.04
Ketones-mg/dl	-ve	+ve	-ve	-ve	-ve	-ve	-ve	-ve
Bilirubin	-ve	-ve	-ve	-ve	-ve	-ve	-ve	-ve
Glucose- mg/dl	-ve	Trace	-ve	-ve	-ve	-ve	-ve	-ve

Table 4.15: Urine analysis of rats treated with ZnO NPs and $ZnCl_2$. n=3. The data represent mean ± SD.

4.3.8.3 Histopathology: Kidney

No indications of lesions or mononuclear cell infiltration were observed in kidney of ZnO NPs and $ZnCl_2$ treated animals. The kidney showed normal cortex and Bowman's capsule. No fibrillation or tubular dilations were observed in the proximal and distal convoluted tubule of the deeper regions of the cortex. In all the groups' medulla, collecting tubules and collecting ducts exhibited normal histology **(Figure 4.65).**

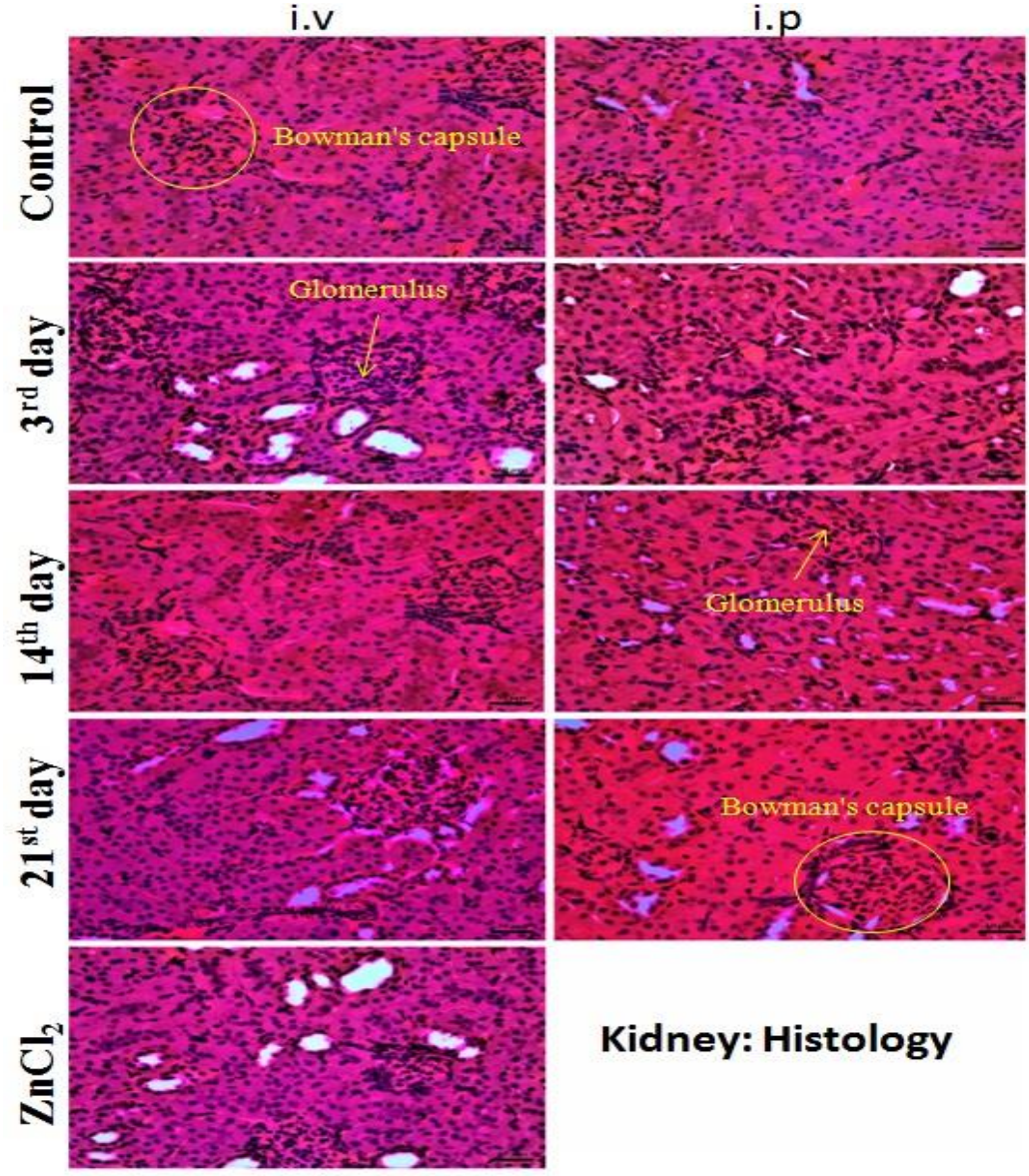

Figure 4:65: Histology of kidney of animals exposed to ZnO NPs (i.v. and i.p.) and $ZnCl_2$(14^{th} day i.v.) after 3, 14 and 21 days of observation. Magnifications 40X. Scale bar represent 30µm

4.3.8.4 Elemental analysis: Kidney

Elemental analysis by atomic emission spectroscopy revealed no significant change in zinc content in ZnO NPs and $ZnCl_2$ exposed rats throughout observation period. However i.v. and i.p. injected animals showed reduction in iron (control:

373.22±3.25, test-i.v.: 243.5±1.68, test-i.p: 267.72±4.07) and copper content (control: 60.07±0.67, test-i.v.: 35.69±0.06, test-i.p: 40.35±0.01) on 3rdday. At the end of 14th day the iron (test-i.v.: 389.22±7.01, test-i.p: 405.98±1.42) and copper (test-i.v.: 60.0±0.05, test-i.p: 64.71±0.19) content was reverted to normal level. The $ZnCl_2$ exposed animals did not show any alteration in zinc, iron and copper content **(Figure 4.66).**

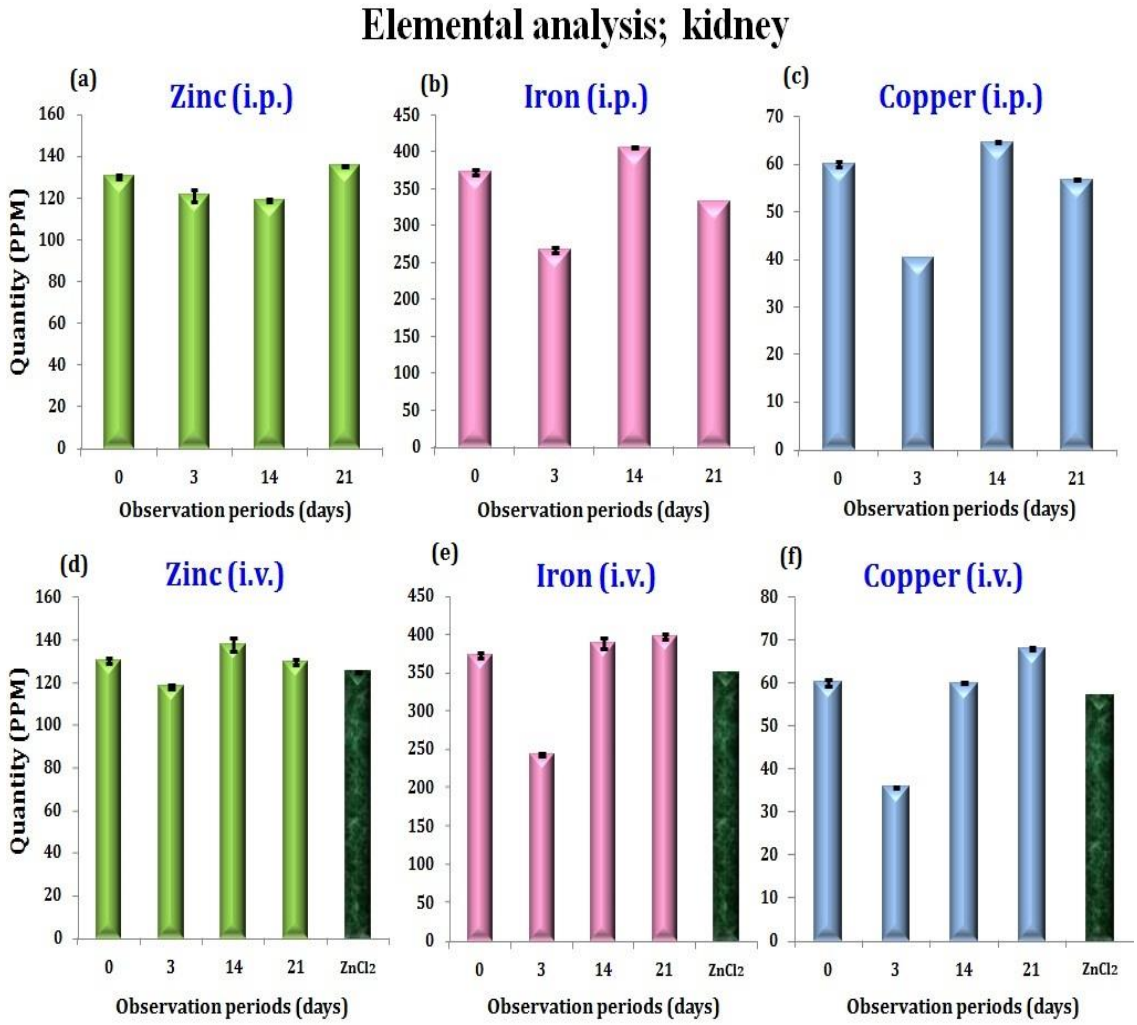

Figure 4:66: Elemental analysis of kidney of rats exposed to ZnO NPs and $ZnCl_2$. N=3. The data represent mean ± SD.

4.3.9 TARGETED ORGAN TOXICITY: SPLEEN

4.3.9.1 Splenocytes proliferation assay:

The spleen was collected from ZnO NPs exposed rats. The Splenocytes were isolated and subjected to proliferation assay using tritiated thymidine. The results of the study indicated similar proliferation rate in control and treatment groups **(Figure 4.67)**.

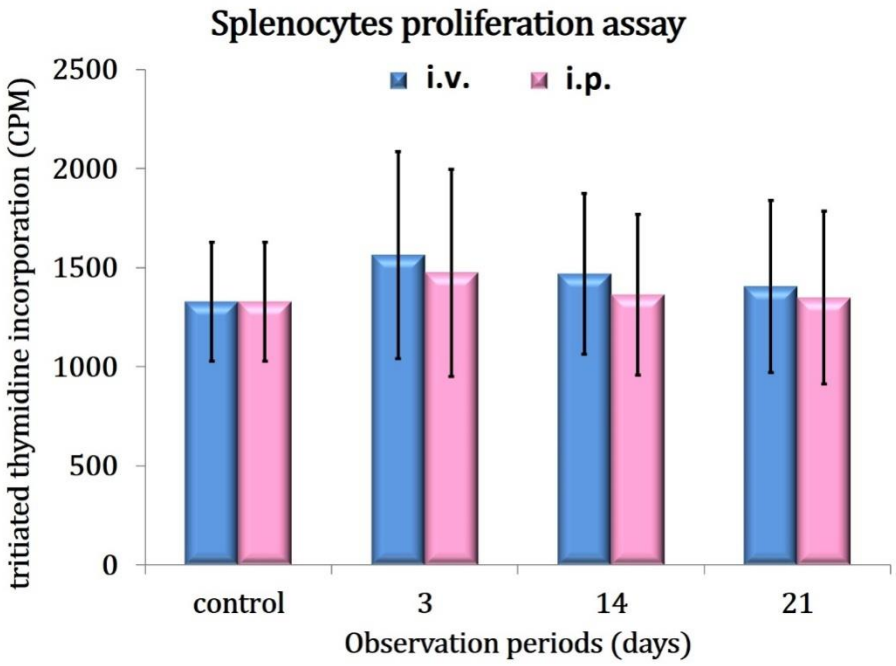

Figure 4:67: Splenocytes proliferation assay in Wistar rats exposed to ZnO NPs. N=3. Data represents mean±SD

4.3.9.2 Histopathology: Spleen

No lesions or macrophage infiltrations were observed in spleen of treated animals. Animals exhibited normal spleen architecture comprising of white pulp, red pulp and marginal zone. The overall histology of treated animals was similar to that of control. Megakaryocyte count was also normal in treated and control groups **(Figure 4.68)**.

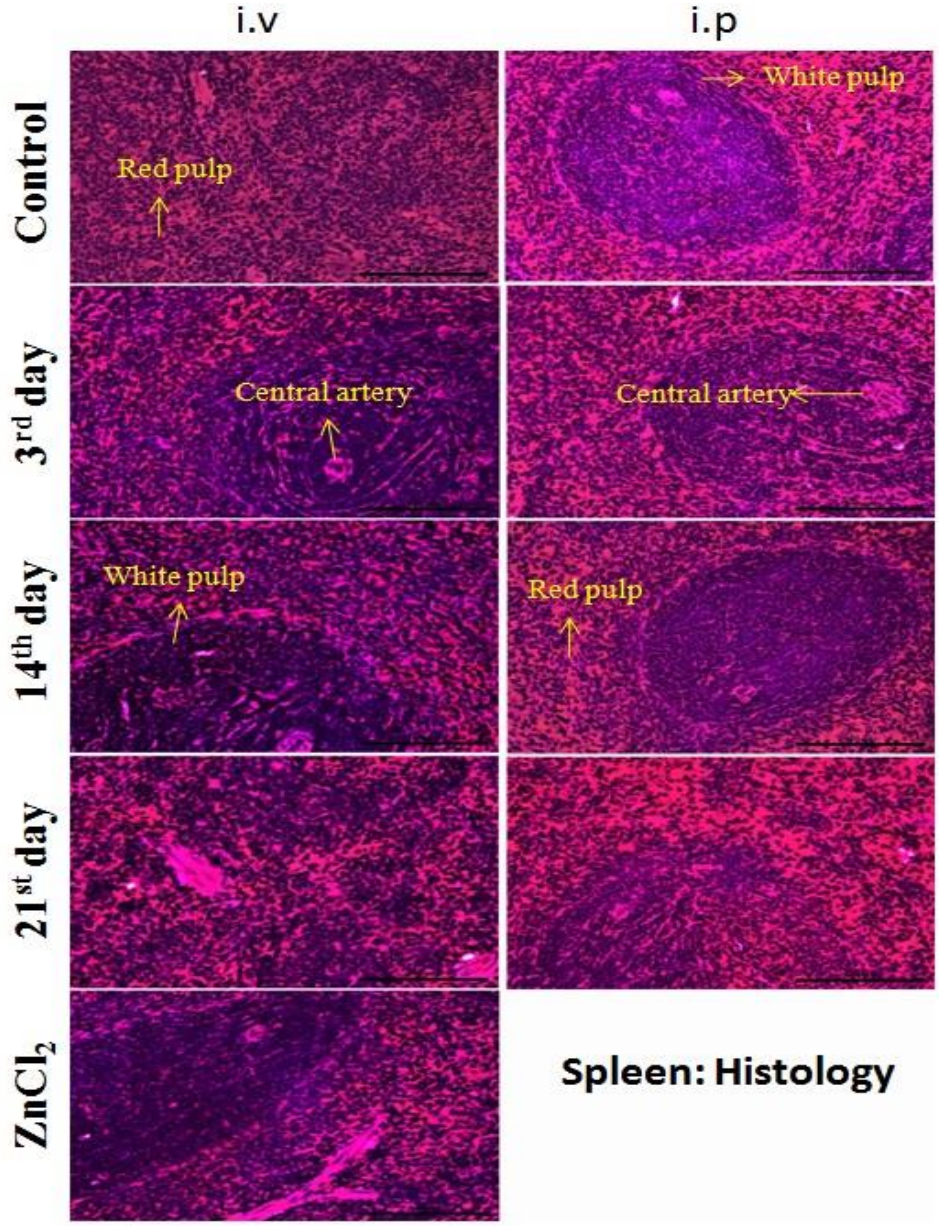

Figure 4:68: Histology of spleen of animals' exposed to ZnO NPs (i.v. and i.p.) and $ZnCl_2$(14^{th} day i.v.). Magnifications 40X. Scale bar is 30µm

4.3.9.3 Immunotoxicity by lymphocytes proliferation assay

Splenic lymphocytes were isolated from rats exposed (i.v.) to ZnO NPs. There was no alteration in lymphocytes proliferation capacity of treated and control animals

(**Figure 4.69).** The tritiated thymidine incorporation rate in control (1327.6±301.3) and observation groups (3rd day; 1563.6 ±522.6, 14th day; 1469±405.7, 21st day; 1404.6±436.0) remained similar.

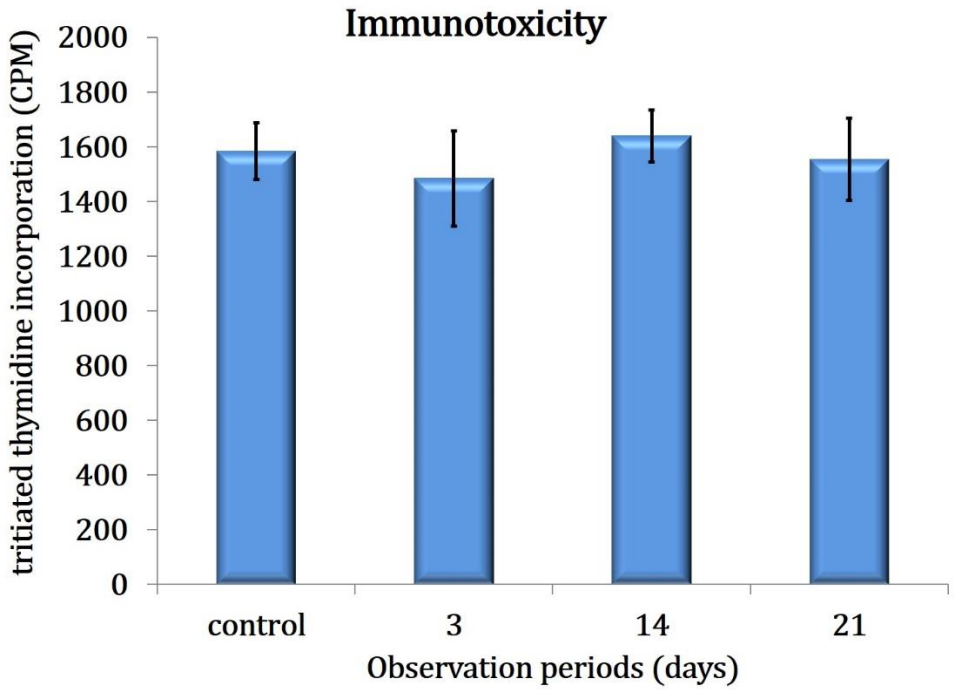

Figure 4:69: Tritiated thymidine incorporation rate in lymphocytes of animals exposed to ZnO NPs. n=3. The data represent mean ± SD.

4.3.9.4 Immunotoxicity: Nitric oxide production

Lymphocytes isolated from the spleen showed no increase in nitric oxide production (3rd day: 0.16±0.017, 14th day: 0.15±0.031 and 21st day: 0.15±0.031) with respect to control (0.16±0.0317). The cells treated with LPS showed statistically significant increase in nitric oxide production (0.24±0.038) **(Figure 4.70)**

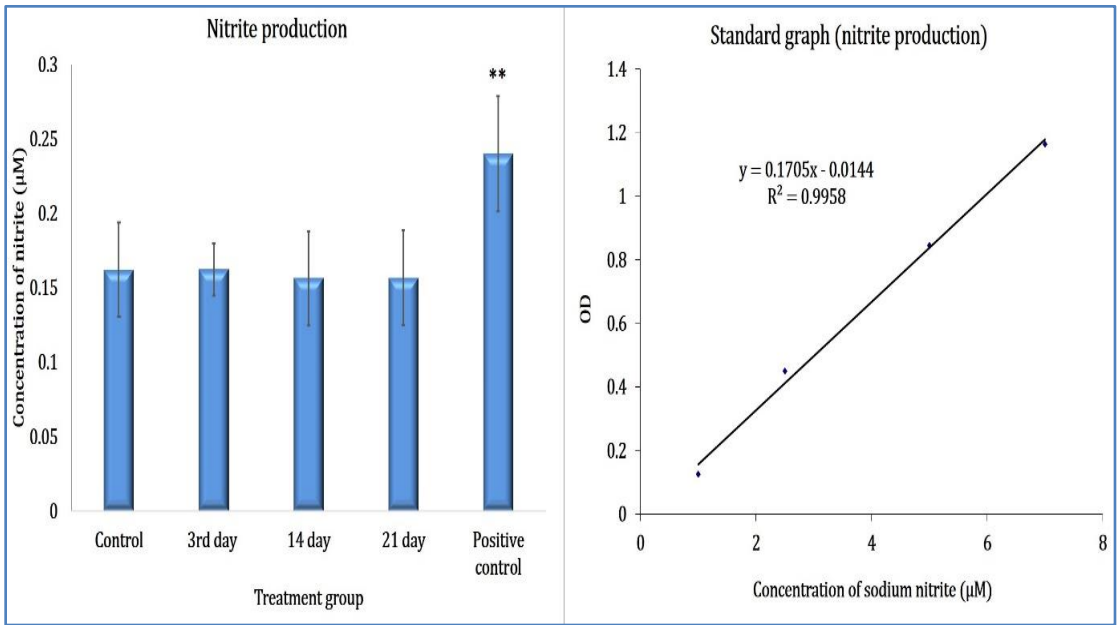

Figure 4:70 Nitric oxide production in Lymphocyte isolated from rats exposed to ZnO NPs. LPS (1µg/ml) treated samples were used as positive control. n=3. The data represent mean ± SD. Asterisk denotes statistically significant difference (**p< 0.01).

4.3.10 BIODISTRIBUTION AND TOXICOKINETICS

Toxicokinetics is the study of time course of absorption, distribution metabolism and excretion (ADME) of the toxicants. The results of the blood kinetics indicated slightly elevated zinc content on 3rd day of observation which got normalised subsequently. The results of the atomic emission spectroscopy suggest that the ZnO NPs was absorbed distributed, metabolised and excreted in 14 days' post exposure.

Liver, kidney, brain, blood, faeces and urine of ZnO NPs exposed animals were collected and subjected to ICP-AES. The results suggest that zinc content was high in liver, blood and faeces on 3rd day of observation period when compared to control. However, zinc content in urine was below the detectable limit and hence was not included here. Increased level of zinc content in the organs indicates biodistribution of

ZnO NPs. **Figure 4.71** clearly indicated ZnO NPs (zinc content) distribution in liver. High level of serum ALT and AST level along with histopathology lesions in liver of treated animals suggests ZnO NPs mediated hepatic toxicity. This finding along with high faecal zinc content observed up to 14th day suggests that ZnO NPs is metabolised mainly in liver which is ultimately excreted via faeces.

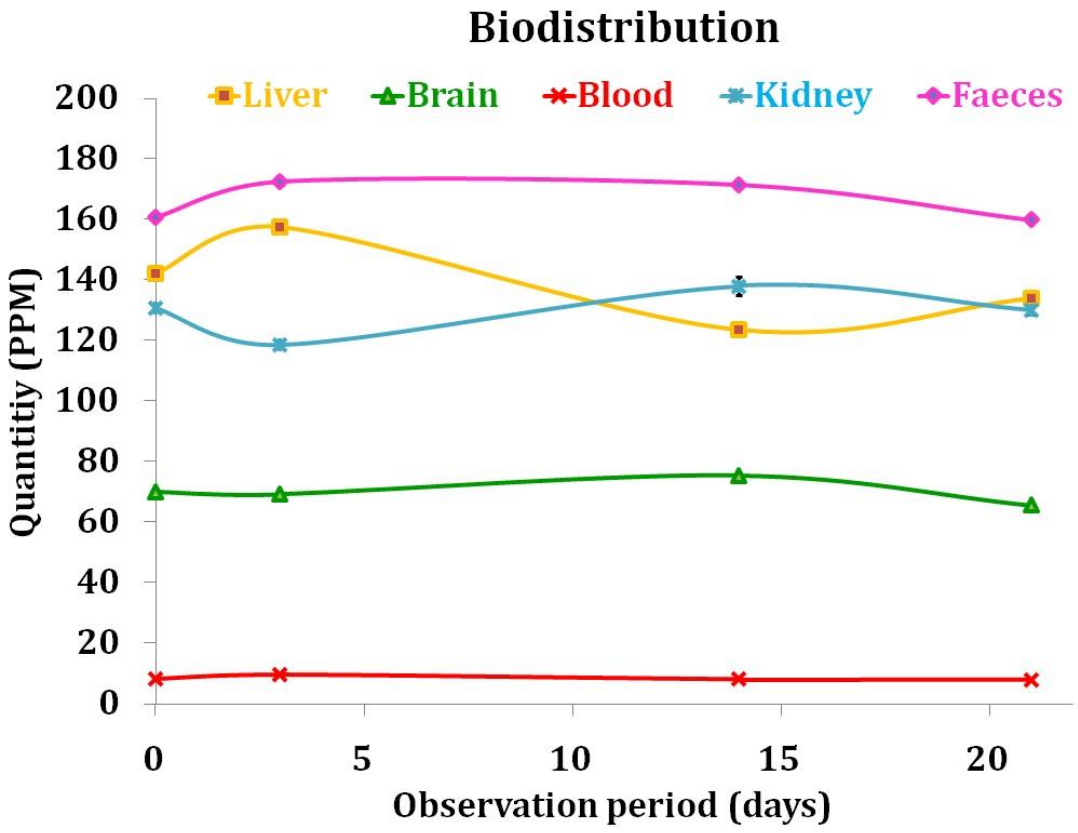

Figure 4:71: Biodistribution of ZnO NPs: The zinc content at the end of each observation period is plotted as a measure of ZnO NPs. n=3. The data represent mean ± SD.

CHAPTER 5: DISCUSSION

5 DISCUSSION

5.1 SYNTHESIS AND CHARACTERISATION OF ZnO NPs

5.1.1 PHYSIC-CHEMICAL CHARACTERISATION

One of the attractive features of ZnO NPs is that it can be synthesised easily in a variety of forms. Different morphologies of ZnO NPs can be synthesised with wet precipitation method by varying the parameters in the precipitation process. These parameters include temperature, solute concentration, method of addition of reagents and pH (Kumar *et al*. 2013). In the present study wet precipitation of zinc nitrate and zinc sulphate using NaOH yielded two different morphologies; ZnO rod (ZnO R) and ZnO spear head (ZnO SP) nanoparticles. Physico-chemical properties of nanoparticles influence its behaviour in biological system (Fernández-García and Rodriguez 2011). Because of this reason synthesised particles were subjected to detailed characterisation. Characterisation of these nanoparticles ensured ZnO NPs of known physico-chemical properties.

The synthesised ZnO NPs were characterised for its size, morphology, hydrodynamic diameter, surface area, charge, crystal structure, chemical composition and purity. As expected the rod (ZnO R) and spear head (ZnO SP) morphologies of ZnO NPs were confirmed by SEM analysis. ZnO R exhibited signs of agglomeration whereas no agglomeration was observed in ZnO SP. Size distribution is an important factor in nanoparticle characteristics. Particle with broad size distribution may not necessarily behave like nanoparticle due to aggregation and may give inconsistent results. The effect of particle ‘size’ on the toxicity can only be studied using particles of narrow size

distribution (Rice *et al*. 2013). TEM analysis gives core size of the nanoparticle, and indicated narrow size distribution of ZnO SP. When nanoparticles are dispersed in a medium, it interacts with the thin dipole layer of medium. The hydrodynamic diameter is the size of particle core along with the solvent layer. In the present study hydrodynamic size of the particle was determined by DLS measurement using different concentration of ZnO NPs. The hydrodynamic size influences the bio-interaction and particle migration in a biological system (Nel *et al*. 2009). It was noted that the hydrodynamic size of ZnO R varied with concentration while hydrodynamic size of ZnO SP remained same at all the concentrations. Small value of standard deviation observed in DLS measurements suggested narrow size distribution of the particles. The polydispersity index (PDI) lower than 0.1 is considered homogenous suspension. The PDI of ZnO SP was near to 0.1 suggesting moderately homogenous suspension. However, in DLS measurement it is not possible to draw a linearity between PDI and monodispersity and hence PDI values has to be correlated with TEM size (Gaumet *et al*. 2008). Here, the PDI values were in concordance with results of TEM and SEM analysis substantiating monodisperse nature of ZnO SP with narrow size distribution. Surface charge of the nanoparticles is a factor determining its cellular uptake and cytotoxicity. Positively charged (cationic) particles are highly cytotoxic and are more likely to induce haemolysis and platelet aggregation than neutral or anionic particles (Nel *et al*. 2009). Both ZnO R and ZnO SP exhibited a net positive charge in physiological pH. The size of the nanoparticles is inversely proportional to surface area and surface reactivity. The ZnO SP exhibited smaller size than ZnO R which explains larger surface area of ZnO

SP. The XRD pattern indicated the characteristic zincite form of ZnO R and ZnO SP. Crystal size calculated from XRD by Le Bail method (Sanches *et al.* 2015) was similar to average size obtained from TEM analysis. This suggests that the particle do not aggregates to form larger crystals. Moreover, larger particles observed in TEM analysis of ZnO R are probably mere agglomerates. A gradual weight loss in TGA analysis corresponds to surface adsorbed water and atmospheric molecules in ZnO R and ZnO SP. The XPS analysis further supported TGA data because there were no impurities detected.

Based on the physicochemical characterisation it was evident that ZnO SP showed a better dispersity and size distribution than ZnO R. Hence rest of the bio-nano interaction studies were carried out using ZnO SP alone and are designated as ZnO NPs throughout the study unless otherwise stated. A preliminary cytotoxicity study was carried out on ZnO R using BV2 cells and was compared with ZnO SP.

5.1.2 BIOLOGICAL CHARACTERIZATION

The nanoparticles owing to the high surface reactivity interact with its immediate environment leading to adsorption of biomolecules on its surface. This can either be endotoxin contamination or protein corona formation in the biological media. In either case the surface adsorbed molecules may alter the behaviours of the nanoparticles in the biological system. Endotoxin contamination often leads to false positive results or elevated toxic responses (Smulders *et al.* 2012). Estimation of endotoxin level is an important parameter in nanomaterials toxicology. It was found that the endotoxin level

in ZnO SP was less than 0.5EU/ml which is well below the USP mandated limits for biomaterials.

The presence of protein corona formation was observed in PAGE analysis. The protein corona formation may influence the uptake, accumulation, surface reactivity, degradation and clearance of the nanoparticles (Nel *et al.* 2009). Moreover, the nanoparticles may provoke conformational changes in the adsorbed proteins leading to altered bio reactivity. The corona formed on nanoparticles depends on the nature of the nanoparticle. Deng *et al* reported that different metal oxide nanoparticles with similar surface charges, exhibited different corona formation. Both compositions of the media and ionic strength of the dispersion influence the corona formation(2009). In the present study, difference in band patterns of particles incubated with PBS indicated influence of ionic corona on the protein corona formation. Moreover, differences in the hydrodynamic diameter exhibited by particles incubated in different cell culture media further support the role of ionic composition of cell culture media on the corona formation. These findings are in par with the published results. This suggest that the nano bio complex formation is influenced by ionic strength and protein composition independent of serum (Xu *et al.* 2012). The major portions of the hard corona observed in the current study were serum proteins namely albumin and immunoglobulins. It has been reported that the corona formation has a strong modulatory effect on the biotransformation of metal nanoparticles as the released ions from the nanoparticles gets trapped within the protein corona (Miclăuş *et al.* 2016).

5.2 BIO-NANO INTERACTIONS: *IN VITRO* STUDIES USING GLIAL CELLS

5.2.1 ZnO NPs INTERACTION WITH C6 CELL LINE

5.2.1.1 Cell viability and morphology changes in BV2 cells

Mitochondria are like 'canaries in a coal mine' because they are prone to early stage effects of toxic chemicals. Both MTT and trypan blue exclusion assay showed a dose and time dependent cytotoxicity in BV2 cells exposed to different concentrations of ZnO NPs. The ZnO NPs mediated toxicity has been studied in many mammalian cell lines where a reduction in cellular metabolic activity was reported (Bondarenko *et al.* 2013). Similarly, the current study indicates that ZnO NPs affect mitochondrial activity of BV2 cells in a dose dependent manner. However, unlike previous reports a dose dependent increase in MTT signals were observed in the present study at 6h of exposure. Ong *et al.,* (2014) reported that nanoparticles can directly interfere with MTT to give erroneous results. In the present study no particles interference was observed and the high MTT signals detected at 6h in the viability assays are assumed to be coming from the formazan crystal formation in the cells. This increased mitochondrial activity may be a metabolic adaptation of the cells towards stress where more energy will be needed for the maintenance and repair (Corona and Duchen 2015). Moreover, there was no corresponding increase in cell number at 6h further supporting the occurrence of transient mitochondrial hyperactivity. Morphology analysis of the cells revealed cellular disintegration leading to cytotoxicity. The cells at 6h exhibited unique morphology where cytoplasmic condensation and crenation were observed in the treated cells. There

was no membrane blebbing or size reduction however, cell ghosts (cell membrane without cytoplasm) were observed in treated wells.

5.2.1.2 Cellular uptake in BV2 cells

Cellular uptake was studied using flow cytometry. The SSC pattern change(corresponds to granularity of cells) in flow cytometry analysis is a popular technique employed for the nanoparticle uptake studies (Suzuki *et al*. 2007). The flow cytometry analysis revealed a concentration dependent increase in SSC pattern in cells treated with ZnO NPs. Cytotoxic response in cells can also lead to increased granularity and SSC. Hence here the cells were exposed to ZnO NPs for a maximum period of 4h. Short treatment period ensured enough time for endocytosis of the nanoparticles as well as minimum toxic effect. The results of the study are in concordance with published results where increased SSC patterns has been linked to cellular uptake of ZnO NPs and ROS production (Toduka *et al*. 2012).

5.2.1.3 Generation of free radical in BV2 cells

The cytotoxic potential of the nanoparticle is mainly attributed to free radicals' formation which includes ROS and RNS. Formation of free radical is associated with glial cell activation. It was reported that a mutually inclusive relationship exist between glial cell activation and free radical generation (Brown and Neher 2010). In the current study, two major biologically relevant reactive oxygen species, super oxide anions and hydrogen peroxides were estimated using DHE and DHR123 probes respectively. The results showed that the ZnO NPs are capable of generating superoxide anions and hydrogen peroxide radical in a dose and time dependent manner. However, the rise in

H_2O_2formation was slow when compared with superoxide anions. It has been reported that the ZnO NPs mediated oxidative stress is mainly by the generation of superoxide radical (He *et al*. 2016; Xia *et al*. 2008). The elevated levels of superoxide anions in the current study confirmed the above findings. The slow rise in H_2O_2 might be due to the delayed induction of SOD enzyme in the conversion of superoxide anions to H_2O_2 (Tsan and White 1992).

Zinc ions (Zn^{2+}) have the ability to directly activate nitric oxide production and microglial activation in the brain (McCord and Aizenman 2014). The RNS production assessed by Griess reagent assay showed a sharp dose dependent increase in nitric oxide production at 6h of exposure. However, the RNS generation decelerated at 24h, possibly due to decline in cell number or by stabilization of nitric oxide by endogenous mechanisms. TLR4 and MyD88-dependent secretion of neurotoxic nitric oxide and microglial activation is a condition in many brain pathologies leading to neuronal and astroglial apoptosis (Kauppinen *et al*. 2008; McCord and Aizenman 2014). Present study confirms the ZnO NPs mediated nitric oxide production in BV2 cells which may cause further complications if the same response occurs *in vivo*.

5.2.1.4 Mitochondrial membrane potential in BV2 cells

Mitochondrial membrane potential (MMP) is a key indicator of cellular health and injury. This relates to cells ability to synthesize ATP via oxidative phosphorylation. Apart from regulating energy metabolism, mitochondria play active role in apoptosis. Loss of MMP is an initial step in the activation of intrinsic apoptosis pathway (Heinicke *et al*. 2016; Vandebriel and De Jong 2012). MMP was measured using $DIOC_6$(3) for

studying the effect of ZnO NPs on mitochondria. Flow cytometry analysis indicated an increase in MMP at 6h of incubation which was declined at 24h. The increase in MMP due to mitochondrial hyperpolarisation occurs in certain cases of mitochondrial stress (Grimm *et al.* 2016). The increase in MMP act as an uncoupler in oxidative phosphorylation, subsequently leading to increased production of super oxide anion and ATP depletion. Cellular ATP level influence the decision of cells to die by apoptosis or necrosis (Roos *et al.* 2016). Initial mitochondrial hyperpolarisation and subsequent collapse has been reported in glycolytically competent immune cells in response to various toxic signals. This is suggested as a defence mechanism against apoptosis (Garedew *et al.* 2010). The BV2 cells being hemopoietic in origin could respond in similar way when exposed to ZnO NPs. The mitochondria relay on the glycolysis for ATP to maintain its hyperpolarisation, resulting in increased kreb cycle and succinate dehydrogenase activity (Dröse 2013). This may account for the initial increase in MTT signals observed in the cell viability study. Since apoptotic pathway is ATP dependent, the fast decline of ATP and resultant drop in MMP may influence the decision of cell to die by pathways other than apoptosis.

5.2.1.5 Lysosomal destabilization in BV2 cells

Nanoparticle uptake is mediated mainly by endocytosis. The endosomes ultimately fuse with the lysosomes to produce phagolysosomes where the material is degraded. ZnO NP is a material sparingly soluble in neutral pH. However, at acidic pH the material readily dissociates to zinc ions. Within the acidic compartments of lysosomes (pH- 4.5) ZnO NPs undergo dissolution to release zinc ions (Cho *et al.* 2011).

The present study investigated the effect of ZnO NPs on lysosomal membrane integrity using acridine orange (AO) staining. Flow cytometry analysis revealed a dose and time dependent lysosomal destabilization in BV2 cells. It has been reported that the ZnO NPs mediate lysosomal destabilization in macrophages (Vandebriel and De Jong 2012). The results of the current study suggested a similar response in BV2 cells. Permeabilised lysosomal membrane signal cell death either via caspase dependent or Caspase independent mechanism (Boya and Kroemer 2008). The present study focused the involvement of lysosomes on the toxicity induced by ZnO NPs.

It has been reported that protein corona formation influence the dissociation of metal oxide nanoparticles as the dissociated ions get trapped in the protein corona (Miclăuş *et al*. 2016). However, the current results concluded that the ZnO NPs readily undergo dissolution inside lysosomes despite the protein corona. The ZnO NPs along with the corona gets digested to release the zinc ions when it fuses with lysosomes.

5.2.1.6 Mechanism of cell death in BV2 cells

ZnO NPs mediated free radical formation may lead to oxidative stress and cell death. Cells exposed to nanoparticles may follow different pathways of cell death such as apoptosis, necrosis, necroptosis and paraptosis (Andón and Fadeel 2012) based on the particle interaction. To better understand the mechanism of toxicity, it is important to consider both extend and mechanism of cell death induced by nanoparticle. Extend of cell death was evaluated in propidium iodide stained cells by flow cytometry analysis. The cells exhibited a dose depended increase in PI positive cells. Early loss of

membrane integrity in ZnO NPs exposed cells points to the possibility of necrotic mode of cell death. The results were similar to the findings of Fink and Cookson 2005.

To study the mechanism of cell death, PARP cleavage assay (western blotting) was carried out. PARP cleavage by Caspase 3 is a hallmark of apoptosis. Surprisingly there was no cleaved PARP in ZnO NPs exposed cells. This clearly demonstrates that the ZnO NPs mediated cell death in BV2 cells is certainly not apoptosis and are both PARP and caspase independent. Inhibitory effect of ZnO NPs on caspase has been demonstrated in a number of studies (Huber and Hardy 2012; Velázquez-Delgado and Hardy 2012). Furthermore, no ladder formation was observed in DNA ladder assay. It is also likely that ZnO NPs directly degrade biological molecules, thereby making the detection of DNA ladder impossible. However, lack of apoptotic features like cell shrinkage and blebbing in the morphology analysis further confirms absence of apoptosis. It has been reported that mitochondria can mediate the caspase independent cell death (programmed necrosis) via release of apoptosis inducing factor (AIF) (Jaattela *et al*. 2004). This occur in two different manners, one is triggered by cathepsin B release from the lysosomes and the other one is via ROS mediated mitochondrial dysfunction (Boya and Kroemer 2008). Cells pre-incubated with Z-Fa-Fmk, an inhibitor of cathepsin did not elicit protective effect of on cells. This rule out the Cathepsin mediated cell death in BV2 cells. Hence the present study concluded that the induction of ROS by the ZnO NPs directly damages the mitochondria leading to oxidative stress and energy depletion in the cells. Subsequently the cells are forced to undergo programmed necrosis. The cell

ghosts in morphology analysis and high free radical production supports this observation.

5.2.1.7 Cell cycle analysis in BV2 cells

It has been suggested that ZnO NPs induces oxidative stress mediated DNA damage in Caco-2 cells and alter the cell cycle pattern (Setyawati *et al.* 2015). The effect of ZnO NPs on cell cycle was studied by flow cytometry analysis. No changes in the cell cycle patterns were observed in the ZnO NPs exposed BV2 cells. Cells undergoing apoptosis will reveal a sub G1 population in flow cytometry analysis. In the present study no sub G1 populations were observed in the treated cells. This further confirmed absence of apoptosis but necrosis in BV2 cells.

5.2.1.8 Comparison of cytotoxic potential of ZnO R and ZnO SP in BV2 cells

ZnO R and ZnO SP were compared for its toxicity in terms of morphology, membrane integrity, PARP cleavage and cell cycle analysis. The shape of the particles indeed influenced the toxicity. The morphology and membrane integrity changes induced by the ZnO R were significantly different from ZnO SP. No PARP cleavage or cell cycle modifications were observed in BV2 cells exposed to both particles. It has been reported that the shape, charge and size of the nanoparticle can influence nano-bio interaction. The surface charge was almost similar in both the particle however there was a significant difference in the hydrodynamic diameter. The DLS analysis indicated that ZnO R was having large size than ZnO SP. Particle agglomeration in the medium influences the cellular uptake and ROS production and may be a main reason for the low

toxicity exhibited by ZnO R. ZnO SP being small in size with no agglomeration may be taken up by the cells at a higher rate leading to high toxicity.

5.2.2 ZnO NPs INTERACTION WITH C6 CELL LINE

Astroglioma cell lineC6, a fast dividing cells were used to study the bio-interaction of ZnO NPs. Apart from mere protective and supportive role, the astrocytes are involved in many important functions of the brain. They are the principal cells involved in the maintenance of brain homeostasis and have a role in various brain pathologies.

5.2.2.1 Cell viability in C6 cell lines

MTT and NRU assays were used to investigate the effect of ZnO NPs on C6 cell line. A progressive time and dose dependent decline in mitochondrial and lysosomal activity was evident from the results. The results of study clearly indicated that ZnO NPs severely altered the cellular metabolism. Akthar *et al.*, reported the effect of ZnO NPs on various cancer cell lines. This study showed a significant reduction in cell viability in HepG2, A549 and BEAS-2B cells at 10 µg/ml and 15 µg/ml of ZnO NPs after 24h treatment (Akhtar *et al.* 2012). However, in the present study the toxic response observed from 20µg/ml suggests that C6 cells exhibit more tolerance for ZnO NPs when compared to the aforementioned cancer cell lines.

5.2.2.2 Cellular phenotyping in C6 cell lines

When adherent cells are exposed to toxic chemicals /materials/extracts of material its cytoplasmic extensions retract to form round shape. The changes in

morphology of the cells may either be due to toxicity imparted by the particles under the investigation or due to the selective disruption of cytoskeletal structure. In this study the effect of ZnO NPs on cell morphology and cytoskeletal arrangement was analysed by Giemsa and rhodamine phalloidin staining. The results of Giemsa staining revealed that the cells exposed to 40 and 80µg/ml ZnO NPs showed round morphology with low density at 6h and 24h. Even though MTT results showed a statistically significant reduction in mitochondrial activity was seen at lower concentrations, there were no morphology changes. Several nanoparticles are capable of disrupting the cytoskeletal arrangement of the cells at sub lethal concentrations leading to altered morphology and detachment of cell from the substratum (Cooper and Spitzer 2015). The results of rhodamine phalloidin staining did not reveal any cytoskeletal rearrangement at lower concentrations. Similar to Giemsa staining, retraction of cytoplasm and round morphology was observed in rhodamine phalloidin staining which is rather a direct outcome of cytotoxicity than selective cytoskeletal disruption (Sruthi and Mohanan 2015). The results are similar to the finding of Márquez-Ramírez *et al.*(2012) where there was no morphological alteration or cytoskeletal rearrangement in TiO2 (20µg/ml) exposed to C6 cells at 24h. Further the same concentration provoked cytoskeletal rearrangement at 96h. The present study concludes that the ZnO NPs induced a time and dose dependent morphological response in C6 cell line.

5.2.2.3 Production of ROS in C6 cell lines

Production of ROS is one of the major factors in nanoparticle mediated cytotoxicity. Thus, the effect of ZnO NPs on the generation of ROS at different time

periods was estimated using DCFH-DA. (Song *et al.* 2010, Huang *et al.* 2010) reported 4–8 fold increase of ROS production in Ana 1, BEAS-2B cells in presence of ZnO NPs. When compared to the above study a negligible increase (0.5 fold) in ROS production was observed in C6 cells. Moreover, a gradual decline was noted in ROS generation from 6h to 24h. The results are similar to the gradual decline of ROS and elevation of antioxidant enzymes observed at 6 and 24h when exposed to titanium dioxide nanoparticles (Huerta-García *et al.* 2014). The reduction in ROS may either be due to the exceptional antioxidant mechanism exhibited by the cells to scavenge the ROS or due to decrease in cell number. It has been reported that astrocytes possess high catalase activity (O'Malley *et al.* 1992). Catalase inhibitor sodium azide (0.1µM) was used to study the influence of catalase on the production of ROS. This exposure resulted in high ROS in sodium azide treated samples. It was noted that ZnO NPs induced a time and dose dependent generation of ROS which was attenuated to some extend by the catalase activity in the cells. The reduction in cell count observed in Giemsa staining is also directly linked to the reduction in DCF fluorescence. Hence the study concludes that both catalase activity and cell number influence the ROS detected by DCFH-DA. The reduction in ROS may be due to the synergetic effect of catalase activity and reduction in cell number.

5.2.2.4 Mechanism of cell death in C6 cell lines

Necrosis, apoptosis or combinations of both are the mechanism of nanoparticle mediated cell death. For instance gold nanoparticle reported to induce both apoptotic and necrotic cell death in the lung cancer cells (Liu *et al.* 2013). C6 cells were evaluated for

membrane integrity, chromatin condensation and outward flipping of phosphatidyl serine (PS) to resolve the ZnO NPs mediated cell death (necrosis or apoptosis). Necrosis is an energy independent process which ultimately leads to rupture of plasma membrane and spillage of contents to the microenvironment. On the other hand, apoptosis is an energy dependent phenomenon which involves complex molecular signalling cascades. It is well aware that the necrotic cells lose its membrane integrity at an early stage, whereas apoptotic cells maintain membrane integrity until late apoptosis.

The C6 cells exposed to ZnO NPs exhibited apoptotic characteristics like blebbing, reduced cell size and change in nuclear morphology (nuclear shrinkage and chromatin condensation) in presence of ZnO NPs. Flow cytometry analysis was carried out using annexin V/PI apoptotic kit to determine ZnO NPs mediated apoptosis. A dose dependent increase in percentage of annexin V positive cells were observed in C6 cells whereas no increase was observed in PI positive or double positive cells. This imply apoptotic mode of cell death in C6 cells. Externalisation of PS is an early event of apoptosis where the plasma membrane remains intact. Necrotic cells can also stain for PS concurrently with PI uptake (Fink and Cookson 2005). The results of the study concluded that ZnO NPs induced cell death in C6 is not mediated via necrosis but by apoptosis. The annexin V/PI staining indicated dose dependent increase in the number of annexin V cells. The slight increase in the percentage of PI positive cells may be due to the mechanical injury during the experimental procedure.

5.2.2.5 Mitochondrial membrane potential in C6 cells

Mitochondria play an important role in apoptosis which either act upstream or downstream of the signalling cascade (Wang and Youle 2009). The involvement of mitochondria in the apoptosis helps in better understanding the pathways of cell death. Studies have shown that mitochondria respond to cytotoxic cues either by undergoing hypopolarisation (loss of MMP) or hyperpolarisation (increase in MMP). It was also noted that certain chemicals hinder apoptosis by acting on MMP (Matarrese *et al*. 2003). In the present study the involvement of mitochondria on the cell death was analysed from the MMP using JC1 staining (Sruthi *et al*. 2017). The cells showed a dose dependent loss of MMP even at 6h of incubation, suggesting the direct involvement of mitochondria mediated apoptosis. This finding further confirms the report of Wang et al., (2014) where a loss of MMP and mitochondrial mediated apoptosis was observed in astrocytes exposed to ZnO NPs.

5.2.2.6 Effect of ZnO NPs uptake and dissolution in C6 cell line.

It is already reported that the particle dissolution accounts for the toxicity of ZnO NPs (Sasidharan *et al*. 2011). The ZnO NPs exposure leads to increased intra cellular Zn^{2+} concentration. It is disputed whether the toxicity is due to particle dissolution inside cellular compartments or in the cell culture medium. A study report on RKO cells states that the cytotoxicity induced by ZnO NPs is dependent only on the direct particle–cell interaction and not on the particle dissolution in the medium (Moos*et al*. 2010). On the other hand Buerki-Thurnherr *et al*.(2013) attributed the particle dissolution in the medium to the cytotoxicity in Jurkat cells. Particokinetics and dynamics of free diffusing

ions differ from the nanoparticles taken up by the cells. Hence it is important to understand if the toxicity is due to particle dissolution in the medium or due to the dissolution inside the cellular compartments. In the present study cytotoxicity assay carried out using supernatant of the medium incubated with ZnO NPs did not reveal significant changes in cell viability. To study whether the particles are taken up by the cells, flow cytometry analysis was carried. The increase in sideward scatter (SSC) denotes increased granularity of the cells. The ZnO NPs uptake by CHO cells has already been demonstrated using flow cytometry (Toduka *et al*. 2012). Similarly, the results of the present study indicated ZnO NPs uptake by C6 cells. Together, these results emphasise that the ZnO NPs undergo significant dissolution inside the cellular compartments and not in the free medium. It is already reported that the ZnO NPs undergo dissolution in acidic environment of lysosomes (Cho *et al*. 2011). The study confirmed that the ZnO NPs undergoes dissociation in the lysosomes to release zinc ions which results in its toxicity.

5.2.3 ZnO NPs INTERACTION WITH PRIMARY ASTROCYTES

Primary astrocytes are the major glial cells which maintain homeostasis in the brain. The isolated primary astrocytes were maintained in the laboratory conditions and used for bio-interaction studies. Primary astrocytes have their own advantages over glial cell lines. These astrocytes have phenotype similar to astrocytes in vivo. One of the challenges in using primary culture is the difficulty in getting pure culture. Endothelial cells, microglia and neurones are usually contaminated with primary astrocytes. It has been known that the mixed brain cell culture responds in different way than pure

astrocytes culture. For instance, studies show that the nitric oxide release observed in astrocytes culture is mostly coming from microglial contamination. The purity of the astrocytes used for the study was confirmed by immunostaining using markers like GFAP, B3 tubulin and O4 antibody. The culture was devoid of neurons and oligodendrocytes. Although a very small proportion of microglia or endothelial contamination were observed in the culture.

5.2.3.1 Viability and dose response in primary astrocytes

The viability and dose response in astrocytes were investigated by MTT assay and were further verified by NRU and trypan blue exclusion method. Results of the study indicated similar LC_{50} value for MTT and NRU assay. Both MTT and NRU assays revealed a time and dose dependent toxicity in cells suggesting reduced metabolic activity of the cells. The ZnO NPs mediated reduction in cell viability has been indicated in a number of mammalian cell lines by Bondarenko *et al* (2013). The results of present study are in concordance with the published results. The LC_{50} value obtained from the current study is lower (40µg/ml) than the average LC_{50} value (57.3µg/ml) of three different cell lines in presence of ZnO NPs (Ivask *et al*. 2015). This suggests that primary astrocytes are more sensitive to ZnO NPs. Treatment with a toxic component interferes with cell viability results in three different ways. The first one is the cytostatic effect where the compound being tested inhibit the proliferative capacity of the cells. The second is an anti-adhesive effect where the cells detach from its substratum to adrift in the medium. Third mechanism is cytotoxicity where the compound interacts directly

with the cells and kills them. To study the exact mechanism underlying the cytotoxicity, the viability results were compared with results of morphology analysis.

5.2.3.2 Cellular phenotyping in primary astrocytes

The cell morphology is a simple and more reliable indicator of cellular cytotoxicity. The morphological observations help in better understanding of cell viability data. Morphological changes in cells reflect the mechanism underlying the reduction in cell viability. Giemsa staining indicated a dose and time dependent morphological alterations in astrocytes. Retraction of cytoplasm, nuclear condensation, cell shrinkage and reduction in cell density were observed in cells exposed to ZnO NPs. Direct death/ deterioration of cells and decreased cell adhesion in the substratum are the two possible reasons for reduction in cell density. Actin staining was used to understand the effect of nanoparticle on cell adhesion properties. Unlike in C6 cell lines, an early dissociation of actin stress fibres and cytoskeletal rearrangement were seen in astrocytes. Stress fibres are necessary for cell to cell and cell to matrix adhesion (Pellegrin and Mellor 2007). Deterioration of stress fibres and loss of focal adhesion points observed in the study clearly indicated the adverse influence of ZnO NPs exposure on the adhesive properties of the cells. This findings are similar to previously published results (Seil and Webster 2008). The change in stress fibre orientation and loss of focal adhesion are reflected in the Giemsa staining which confirmed modification of cytoskeletal structures. Altered cytoskeletal rearrangements in primary astrocytes partially account for the low cell density and decreased viability observed in the Giemsa and MTT experiments.

5.2.3.3 Particle uptake in primary astrocytes

Flow cytometry analysis revealed dose dependent increase in SSC/FSC ratio suggestive of particle uptake in astrocytes. Cells were pre-incubated with cytochalasin D (a nonspecific endocytosis inhibitor) and subsequently exposed to ZnO NPs to confirm particle uptake. It was reported that the cytochalasin D pre-treatment inhibit the cellular uptake of ZnO NPs in macrophages (Roy *et al.* 2014). In the current study cyt. D pre-treatment protected astrocytes from ZnO NPs mediated toxicity by inhibiting the particle uptake.

5.2.3.4 Lysosomal integrity in primary astrocytes

Protective effect imparted by cytochalasin D (endocytosis inhibitor) in astrocytes confirms endocytosis mediated ZnO NPs uptake. In normal circumstances the endocytic vesicles fuse with lysosomes to form phagosomes leading to degradation of the cargo. ZnO NPs are soluble in acidic environment and results in dissociation to ionic form (Zn^{2+}). These zinc ions either via free diffusion or destruction of lysosomal membrane reach out to the cytoplasm (Cho *et al.* 2011). Astrocytes were stained with AO to study the effect of ZnO NPs on lysosomal membrane permeabilisation (LMP). A dose dependent decrease in AO red fluorescence was observed in primary astrocytes when exposed to ZnO NPs. This suggested ZnO NPs mediated LMP in astrocytes. Lysosomal disintegration leads to spillage of proteolytic enzymes in the cytoplasm leading to proteolysis of cellular components and proteins. Cells initiate/ amplify cell death programme in response to the above trauma. Extensive LMP formation may leads to necrotic cell death whereas, limited LMP trigger Caspase independent cell death with

apoptosis like morphology (Aits and Jäättelä 2013). Cho *et al.*,(2011)reported ZnO NPs mediated lysosomal destabilisation and lung injury. To the best of authors knowledge ZnO NPs mediated LMP formation in astrocytes was reported for the first time in the present study.

5.2.3.5 Generation of free radical in primary astrocytes

Free radical generation in astrocytes exposed to ZnO NPs was analysed using flow cytometry. There was a dose dependent increase in DCF fluorescence in primary astrocytes. It was reported that ZnO NPs increases ROS production in primary astrocytes (Wang *et al.* 2014) and is in agreement with the current study. Certain molecules have the capacity to induce astrocytes activation by nitric oxide production (Colombo *et al.* 2014). Zinc mediated nitric oxide production and inflammation has been linked to brain pathologies (McCord and Aizenman 2014). However, in the current study, there was no RNS production in primary astrocytes exposed to ZnO NPs, whereas the LPS treated positive control showed elevated production of RNS in astrocytes.

5.2.3.6 Mitochondrial membrane potential in primary astrocytes

Mitochondria and lysosomes play crucial role in the cellular metabolism and apoptosis. Most of the toxic responses in cells are strictly mediated by mitochondria and lysosomes. Mitochondria derive energy by oxidative phosphorylation and are the powerhouse of the cells. Mitochondrial membrane potential (MMP) relates to the capacity of mitochondrion to generate ATP. MMP is very sensitive to physiological changes in the microenvironment and loss of MMP is an early event in the Caspase mediated pathways. Altered MMP and mitochondrial damages are associated with

neurodegenerative diseases (Rainbolt *et al*. 2013). MMP measurement gives crucial information about on the health status of the cells. In the present study the effect of ZnO NPs on MMP was analysed using JC1 staining. The results revealed a time and dose dependent loss of MMP in astrocytes exposed to ZnO NPs. Mitochondria are the biggest contributor of cellular ROS owing to the its function. Mitochondrial ROS production increases in presence of ROS inducing agents, leading to oxidative stress (Perl *et al*. 2004). Apart from changes in MMP, mitochondria forms clumps during stress as an adaptive mechanism (Rainbolt *et al*. 2013). These clumps of mitochondria work together to fulfil the energy needs of the cells and failure of this ultimately lead to release of apoptotic signals from mitochondria. In the present study mitochondrial clumps were evident in all the ZnO NPs exposed cells. Marked reduction in J aggregates along with large mitochondrial clumps scattered in cytoplasmic extensions were seen in astrocytes exposed to high concentrations (40 and 80µg/ml) of ZnO NPs. The mitochondrial clumping require realignment of actin cytoskeleton (Boldogh and Pon 2006) which may account for the cytoskeletal rearrangements seen in actin staining. Together these findings reveal the role of mitochondria in ZnO NPs mediated ROS generation and toxicity.

5.2.3.7 Mechanism of cell death in primary astrocytes

It was understood from the lysosomal analysis and MMP that the ZnO NPs certainly impair the normal functioning of the astrocytes. These two organelles have the potential to activate different pathways of cell death (Jaattela *et al*. 2004; Heinicke *et al*. 2016) and a battery of assays was carried out to understand the mechanism of cell death.

PS externalisation is considered as an early event in apoptosis and there was a dose dependent increase in annexin V positive cells when treated with ZnO NPs. DAPI staining clearly indicated the presence of nuclear condensation which is a late event in apoptosis. Caspase mediated cell death was linked to loss of MMP (Lakhani *et al*. 2006). The present study indicated an early loss of MMP in treated cells and hence Caspase activity was analysed. The report indicated a dose and time dependent increase in Caspase activity in astrocytes. ZnO NPs mediated Caspase activation and apoptosis have been reported previously in a number of cell lines (Vandebriel and De Jong 2012). Apoptotic features like cytoplasmic shrinkage, retraction of pseudopodia, reduction of cellular volume (pyknosis) and membrane blebbing were observed in astrocytes apart from the above mentioned morphological and biochemical changes. The present findings are in agreement with published reports of Kromer *et al*.(2009) and also similar response was observed in C6 astroglial cell line.

In certain cases of toxic response both apoptosis and necrosis exists simultaneously. In the present study the early loss of membrane integrity without compromising cellular viability was observed at high concentration of ZnO NPs. Further, the cells with compromised membrane integrity did not indicate other necrotic features like cell swelling and cytoplasmic spillage. This finding rules out the co-existence of apoptosis and necrosis.

5.2.3.8 Effect of ZnO size and dissolution in primary astrocytes.

Toxic potential of ZnO NPs was compared with $ZnCl_2$ and ZnO bulk particles to understand the influence particle size and dissolution on cytotoxicity. $ZnCl_2$ undergoes

complete dissolution in physiological pH (~7) to release zinc ions (Zn^{2+}) thus this zinc salt was used to represent ionic counterpart of ZnO. Cell viability, cell number, ROS production and cell regeneration potential were compared among $ZnCl_2$, ZnO NPs and ZnO bulk treated astrocytes.

MTT results showed a significant difference among the ZnO NPs and ZnO bulk whereas $ZnCl_2$ behaved more or less similar to that of untreated control. ZnO bulk particle treated cells retained more cells compared to ZnO NPs and $ZnCl_2$. At high concentration (40 and 80µg/ml) the total number of cells (live and dead) were very low in $ZnCl_2$ and ZnO NPs treated samples. This finding further supports the previous assumption that high reactivity of ZnO NPs may degrade cellular components. Dead cells do not have any resistant mechanism to protect against cellular damage and are easily degraded by the ZnO NPs. ROS generation in ZnO bulk exposed cells were lower than ZnO NPs and $ZnCl_2$ treated group. Caspase activity was also high in ZnO NPs and $ZnCl_2$ exposed cells when compared to ZnO bulk. However, in clonogenic assay high number of colonies was present in the $ZnCl_2$ compared to ZnO NPs. This indicates the 'nano specific' toxicity of ZnO NPs. Short duration exposure (1h) of ZnO NPs severely interfered with regeneration and proliferative potential of astrocytes. In a similar study ZnO NPs were found to interfere with proliferative capacity and colony formation of A549 carcinoma cells and L-132 normal cells (Kim *et al.* 2010). In preliminary cytotoxicity studies, cellular response to ZnO NPs, $ZnCl_2$ and ZnO bulk may appear more or less similar. However, the findings of present concluded that the ZnO NPs exhibit nano-specific toxicity independent of its dissolution and indicated that the ZnO

NPs exposure even for a short time may have serious adverse effect on the growth and replicative abilities of the cells.

5.3 BIO-NANO INTERACTION: *IN VIVO* STUDIES USING WISTAR RATS

5.3.1 DOSE AND EXPOSURE

Adult healthy Wistar rats of body weight between 200 to 300g were used in the present study. The rats are selected because they resemble humans in physiological, biochemical and metabolic pathways. Dose is an important factor influencing toxicity. ZnO NPs lack a definite 'No Observed Adverse Effect Level' (NOAEL). The reported NOAEL after oral administration varies between 31.25 to 1000mg/kg may be due to low bio availability of different ZnO NPs formulation as reported by (Kim *et al*. 2014; Choi *et al*. 2015). Similarly it was reported that single administration of 30mg/Kg body weight of ZnO NPs induces toxicity in rats (Choi *et al*. 2015). Moreover, ZnO NPs get aggregated at higher doses and hence selected 10mg/kg body weight for the present study. The animals were exposed to ZnO NPs via intravenous (i.v.) and intraperitoneal (i.p.) injection administration to study the nanoparticles absorption, distribution and metabolism, excretion and toxicity.

5.3.2 BODY AND ORGAN WEIGHT CHANGES

The change in organ weight may be primary or secondary effect of particle exposure. Following the exposure to a compound the target organs may undergo weight loss which is a direct effect. Secondary weight changes (indirect effect) in organs may occur due to particle interference with general physiology of animals. In the present

study there was no weight changes in the organs when exposed (i.v. and i.p.) to ZnO NPs at a dose of 10mg/kg body weight. Toxicological studies point out that it is needless to express the organ weights in relative terms (organ to body weight ratio) because it increases the error rate and leads to misinterpretation of treatment effect (Hayes and Kruger 2014).

5.3.3 NEUROTOXICITY AND CLINICAL SIGNS

10mg/kg body weight of ZnO NPs was exposed to Wistar rats by single i.v and i.p administration. Following administration, the clinical signs of the animals were monitored immediately and throughout the experimental period. It was found that none of the animals showed any clinical signs such as piloerection, lacrimation, salivation, tremor, convulsions, dyspnoea, ataxia, or any other nervous system stimulations. The behaviour of the treated animals was well comparable with control animals. Zhang *et al.*, 2015 reported that orally administered graphene nanoparticles induce transient changes in locomotor activity and neuromuscular coordination. Similarly it has been stated that the neurotoxic effects are dependent on dose and physicochemical characters of nanoparticle (Mendonça *et al.* 2016). In the presently study the single i.v and i.p. administration of ZnO NPs at a dose of 10mg/kg body weight did not induce any of clinical or neurotoxicological response in rats.

5.3.4 HAEMATOLOGY

Yanagisawa *et al.*, 2009 reported that the administration of ZnO NPs altered haematological parameters as external source of zinc interfere with iron and copper

content in the blood (Yanagisawa *et al.* 2009). The results of the present study showed that ZnO NPs exposure did not affect the haematological parameters such as platelets, WBC, RBC, HGB, HCT, MCH and MCHC. In another study single administration of 30mg/kg ZnO NPs immediately induced slight alteration in the haematological parameters and reverted back by the end of 7th day (Choi *et al.* 2015). The results of the present study indicated that there were no changes in haematological parameters when exposed to 10mg/kg of ZnO NPs.

5.3.5 TARGET ORGAN TOXICITY

The distribution or accumulation of nanoparticles in the organs may lead to the organ toxicity. The major targeted organs of ZnO NPs accumulation are spleen, liver, and kidney and brain (Choi *et al.* 2015). The present study focused on the organ toxicity following single exposure of ZnO NPs at 10mg/kg for a period of 3, 14 and 21 days.

5.3.5.1 Brain

Repeated ZnO NPs exposure is shown to induce pathological lesions (Tian *et al.* 2015) in the brain. In the present study no pathological lesions observed in the brain of ZnO NPs treated animals and were comparable to control. Antioxidants were analysed to determine the extents of ZnO NPs mediated oxidative stress in brain. It was reported that oral administration of ZnO NPs results in the decline of SOD activity in the brain (Shrivastava *et al.* 2014). However, in the present study there was no change in antioxidant activity in the brain except for glutathione reductase (GR). GR maintains oxidative balance of the cells by converting the GSSG to GSH (Deponte 2013). Elevated

GR activity in the present study might be an adaptive mechanism of the brain to cope with ZnO NPs mediated free radical production. Lockman *et al.,* reported that positive charged nanoparticles alter the BBB integrity and permeability (2008). The brain volume changes in response to injuries, inflammation and disruption of BBB. However, in the present study there was no ZnO NPs mediated volume changes in treated rats indicating that ZnO NPs exposure at the given concentration does not cause mechanical damage and oedema. Apart from the direct effect, ZnO NPs may have indirect effect on the cellular mechanism. Brain possesses metal transporter proteins like DMT1 which nonselectively transport multiple divalent metals (like Zn, Cu, Fe, Mg, Co) across BBB. Elevated level of any of these metal ion may interfere with the affinity of theses transport protein leading to disruption of metal homeostasis in brain (Zheng and Monnot 2012). ZnO NPs mediated disruption of iron and copper homeostasis was reported by (Amara *et al*. 2015). In the present study, there was no alteration in zinc and copper of rat brain exposed to ZnO NPs. However, there was a slight increase in the iron content. This was in corroboration with the finding of Amara *et al*. (2015)

5.3.5.2 Liver

Liver is the main organ involved in metabolism of ZnO reaching systemic circulation. Zinc is emptied from liver along with bile salt and ultimately get excreted in faeces (Baek *et al.* 2012). ALT (SGOT) and AST (SGPT) are two enzymes located in the liver and muscles. Up on loss of cellular integrity of theses tissues, the enzymes will be released into the blood. Elevated levels of serum ALT and AST along with unaltered level of ALP indicate loss of cellular integrity in liver. This was further supported by atrophic lesions in the histopathology of liver. The present study is consistent with the finding of Yang *et al.*(2015) that ZnO NPs exposure results in elevated ALT and AST level leading to hepatic toxicity. In the present study elevated antioxidant level and lipid peroxidation were observed in rats exposed to ZnO NPs. The results were similar to the findings of Xia *et al.*(2008) and Choi *et al.*(2015). Hence the present study confirms that single exposure of 10mg/kg ZnO NPs induces altered antioxidant activity, elevated LPO, ALT and AST leading hepatic toxicity in Wistar rats.

5.3.5.3 Spleen

Spleen is an organ, structurally similar to large lymph node and has haematological and immunological functions. Spleen is considered as a target organ for ZnO NPs accumulation (Shrivastava *et al.* 2014). Splenocytes may get activated in presence of a foreign substance. ZnO NPs exposure induce splenic corpuscles enlargement and pathological lesions in rats (Sharma *et al.* 2012). In the present study no pathological lesions were observed in spleen exposed to ZnO NPs. In contrary to the present finding Cheng *et al*., reported nanoparticle mediated increase in splenocytes

proliferation (2010). The present study confirms that single exposure of ZnO NPs did not alter splenocytes proliferation or spleen histology.

5.3.5.4 Kidney

Kidney function was monitored by blood biochemical parameters. Serum urea and creatinine are two major indicators of renal function. It was reported that serum urea and creatinine levels get elevated when renal functions are affected (Wang *et al*. 2006). in the present study the serum urea and creatinine level remained normal in ZnO NPs exposed animals. It was also observed that there was no alteration in the urine parameters. A number of studies have reported histopathological changes in kidney following ZnO NPs exposure(Sruthi and Mohanan 2016). In contrary to the above finding the present study confirms that single exposure of 10mg/kg ZnO NPs do not alter serum urea, creatinine or renal histology of rats.

5.3.6 ZnO NPs ASSOCIATED IMMUNOTOXICITY

Oral administration of high concentration of ZnO NPs (750mg/kg/day) was shown to suppress innate immunity in the mice. Moreover such a high dose leads to increased nitric oxide production in splenocytes, increased inflammatory cytokine titre in serum and altered T cell surface markers (Kim *et al*. 2014). In the present study no change in splenocytes proliferation or nitric oxide production was seen suggesting that single exposure of ZnO NPs at relatively low concentration (10mg/Kg) do not induce inflammatory responses in rats. Increased WBC count is an indicator of inflammation and it is suggested that ZnO NPs exposure result in increased WBC (neutrophil) count

(Sruthi and Mohanan 2016). However, normal blood WBC count and immunoglobulin level observed in the present study confirms that single exposure of ZnO NPs fails to induce immunotoxicity in rats.

5.3.7 ADME & T

ADME & T is an abbreviation used in pharmacokinetics to denote absorption, distribution, metabolism, excretion and toxicity. ADME studies are important to understand fate of nanoparticles in biological system. Absorption refers to movement of particle from site of administration to blood stream. In the present study elevated zinc content was present in the blood on 3rd day of observation and is an evidence for absorption of ZnO NPs. Distribution refers to the transportation of particles to the targeted organs. Here the accumulation of ZnO NPs in brain, liver and kidney were analysed by ICP-MS on 3, 14 and 21 days' post exposure. A slight increase in zinc content was observed in liver but not in brain and kidney suggesting a targeted distribution. Metabolism is the process where body converts the particle from its original form to a metabolite. It is not possible to directly study the ZnO NPs metabolism because ICP-MS cannot differentiate between ZnO NPs and zinc ions. In the present study metabolism of the ZnO NPs was indirectly studied from the histopathology and biochemistry. No structural or biochemical changes were observed in brain, spleen and kidney except for the change in GR activity in brain. However, liver showed marked changes with respect to clinical chemistry and histology. This finding along with high zinc content observed in liver suggests the metabolism of ZnO NPs in the liver. Excretion refers to the removal of metabolised particles through faeces and urine. Zinc

content in urine was below detectable limits of ICP-MS whereas in faeces elevated zinc content was observed up to 14 days of observation. These results conclude that ZnO NPs metabolised in liver is discharged via faeces along with biliary drainage. Hence the present study concluded that 10mg/kg of ZnO NPs exposure leads to hepatic toxicity in rats. These findings are in agreement with the findings of Baek *et al.*,(2012).

5.3.8 BIODISTRIBUTION AND TOXICOKINETICS

Wistar rats exposed to 10mg/kg body weight of ZnO NPs via i.v. injection. Biodistribution and toxicokinetics studies were carried out 3, 14 and 21 days' post exposure using ICP-MS. From the ICP-MS results it is concluded that ZnO NPs do not get distributed in brain, spleen and kidney of the treated animals. However, liver showed elevated zinc content on 3rd day suggesting ZnO NPs distribution in the liver.

Toxicokinetics describes the way body handles toxicants as a function of time and dose. It is determined from the concentration of toxicants in blood at different time points. ADME of nanoparticle regulate its toxicokinetics. In the present study ICP-MS analysis showed elevated zinc content in blood on 3rd day of observation but not on 14th and 21stdays. This suggests that ZnO NPs is available in blood up to 3 days and are cleared from the system 3rd day post exposure.

CHAPTER 6: SUMMARY AND CONCLUSION

6 SUMMARY AND CONCLUSION

6.1 SUMMARY

ZnO NPs are semiconductor nanoparticles with numerous optoelectronic, chemical and biomedical application. This is one of the few nanoparticles produced industrially. Consumer products such as personal care products and cosmetics containing ZnO NPs are already in the market for the last several years. Nanoformulations are replacing the bulk form of ZnO used in many products because of better reactivity and optical transparency. As of now there are no regulatory guidelines available for the use of ZnO NPs in the daily care products. Conventionally the regulators are agreed to use the nanoformulations because the bulk formulations (ZnO) are considered to be nontoxic. By convention if the bulk formulation is nontoxic, its nanoforms are also approved as safe for use as in the case of ZnO. It is well known that nanoparticle exhibit unique physical, chemical and biological properties when compared to bulk particle because of its reduced surface area and quantum confinement. It is well documented that ZnO NPs are highly toxic.

The incidence of neurodegenerative disorders in the human population is increasing at an alarming rate and glial cells dysfunction is correlated with most of them. In this context, an effort was made to investigate the toxicity of ZnO NPs on glial cells. ZnO NPs of two different morphologies, ZnO R and ZnO SP were synthesised by wet precipitation method. The particles were completely characterised for physico-chemical properties, endotoxin content and protein corona formation before carrying out bio-interaction studies. Cellular interaction studies were carried out using ZnO SP and the

results were compared with ZnO R with respect to cell viability and cytotoxicity mechanism. Rat microglial cell line (BV2), rat astroglioma cell line (C6) and rat primary astrocytes isolated from the P0 old pups were used for the study. Cellular uptake, cell viability, cell number, cytoskeletal arrangement, morphology changes, ROS production, lysosomal stability, MMP, mechanism of cellular death were investigated by various cytotoxicity assays. Effect of particle dissolution and nano-specific toxicity was studied by comparing the cytotoxicity of ZnO NPs with $ZnCl_2$ and ZnO bulk particle.

In vivo acute bio-nano interactions of ZnO NPs were carried out on rats at a dose of 10mg/kg body weight via i.v and i.p injection. All the animals exposed to ZnO NPs were monitored for clinical signs of neurotoxicity, stress, and body weight changes throughout the observation period. All the animals were euthanized at the end 3, 14, and 21 days of observation period and organs were collected for further experiments. The blood samples were subjected to haematology and clinical chemistry. Brain, liver, spleen and kidney were collected for histopathology analysis. Spleen was subjected to immunotoxicity and antioxidant assay was carried out on liver and brain. Apart from these brains, liver, kidney, blood, urine and faeces were used to study biodistribution and toxicokinetics by ICP-MS.

6.2 METHODOLOGY ADAPTED FOR THE STUDY

- Synthesis of ZnO NPs with two different morphology ZnO R and ZnO SP by wet precipitation of zinc nitrate and zinc sulphate respectively using sodium hydroxide as the reducing agent

- Physico-chemical characterisation using TEM, SEM, DLS, zeta potential analysis, BET, TGA, XRD and XPS
- Endotoxin content and protein corona formation was analysed
- BV2 cells were cultured in RPMI medium with 10% FBS and cell viability (MTT), cell count (trypan blue exclusion assay), cell morphology (phase contrast microscopy), ROS production (DHR 123 and DHE), MMP ($DIOC_6(3)$), lysosomal membrane destabilisation (AO), membrane integrity (PI) and cell death mechanism (PARP cleavage assay, FACS analysis of sub G1 population) were studied
- C6 cells were cultured in DMEM F12 with 10% FBS. Cellular uptake, cell viability (MTT, NRU), Cell morphology (Giemsa staining, actin staining), ROS (DCFH-DA), MMP (JC1), cell death mechanism (Annexin V/PI kit) were analysed
- Primary astrocytes were isolated from the 0-2 day old rat pups and cultured in DMEM F12 supplemented with 10% FBS. The cells were characterised using astrocytes specific marker GFAP.
- Cellular uptake, cell viability, cell morphology changes, ROS production, lysosomal stability, MMP, membrane integrity and death mechanism were studied in primary astrocytes.
- Effect of particle dissolution and nano-specific toxicity was studied by comparing the cytotoxicity of ZnO NPs with $ZnCl_2$ and ZnO bulk.

- *In vivo* bio-nano interaction was studied by exposing Wistar rats to ZnO NPs via i.p and i.v injection. Three animals were injected with $ZnCl_2$ and saline injected samples served as control. The animals were observed for up to 21 days' post exposure.
- Animals were monitored for weight changes, clinical signs of neurotoxicity and stress throughout the observation period.
- At the end of each observation period (3,14 and 21 days) blood, urine and faecal samples were collected and animals were euthanized for organ collection
- The blood, urine, faeces and organ samples were subjected to toxicokinetics and bio distribution studies by ICP analysis. Blood samples were subjected to haematology and clinical chemistry analysis to study the systemic toxicity including liver and kidney function.
- Collected organs were subjected to histopathology analysis. Antioxidant assays were carried out on brain and liver homogenates to study the oxidative stress.
- Splenocytes proliferation assay and NO production were carried to study the immunotoxicity response.

6.3 MAJOR FINDINGS OF THE STUDY

- Single step addition of NaOH to Zinc sulphate at 90°C yielded homogenous nanoparticles (ZnO SP) of size 20nm with uniform morphology. ZnO R synthesized by drop wise addition of Zinc nitrate to NaOH at 55°C were heterogeneous in nature with an average size 45nm.
- No endotoxin contamination was observed in synthesized ZnO NPs samples.

- Protein corona formation was observed in serum exposed ZnO NPs
- ZnO NPs exposed microglia cells exhibited oxidative stress, mitochondrial hyperpolarisation and LMP leading to a Caspase independent necroptosis.
- The ZnO SP was found to be more toxic than the ZnO R.
- ZnO NPs exposed to astrocytes resulted in cytoskeletal rearrangements, mitochondrial hypopolarisation, ROS generation, and Caspase dependent apoptosis.
- ZnO NPs exhibited specific nano toxicity which was different from ZnO bulk and ionic counterparts.
- Particle dissolution inside lysosomes is the major contributing factor in ZnO NPs mediated glial toxicity.
- No clinical or behavioural signs of neurotoxicity were observed on acute exposure of ZnO NPs.
- Single exposure of 10mg/kg ZnO NPs did not alter haematological parameters.
- ZnO NPs exposure did not alter zinc content in brain. Brain histology remained normal when compared to control.
- ZnO NPs exposure resulted in up regulation of glutathione reductase in brain.
- Kidney and spleen were not affected in ZnO NPs exposed rats.
- ZnO NPs did not induce immunotoxicity in Wistar rats.
- Single exposure ZnO NPs induced LPO and altered antioxidant activity in liver.

- ZnO NPs exposure resulted in loss of cellular integrity and atrophic lesions leading to hepatotoxicity.
- ZnO NPs administration was found to interfere with metal homeostasis in brain, liver and kidney.
- Bio-distribution studies showed no marked increase in zinc content in brain, spleen and kidney.
- ADME indicated that the major route of excretion of ZnO NPs is via faecal matter. The ADME leads to altered antioxidant activity and clinical chemistry leading to disintegration of hepatic cells. This end up in toxicity.

6.4 CONCLUSION

ZnO NPs synthesized by wet precipitation method were characterized for size, shape, specific surface area, surface charge, hydrodynamic diameter, chemical structure, crystal structure and purity. The ZnO spearhead nanoparticles (ZnO SP) synthesized by single step addition of NaOH to sodium sulphate at 90°C exhibited better homogeneity and dispersity than ZnO R synthesized at 55°C. Hence ZnO SP was used for bio-nano interaction studies. The ZnO SP exhibited high cytotoxicity due to its small size and better dispersity. The cytotoxic response to ZnO NPs was cell specific. Microglia (BV2) were highly sensitive to ZnO NPs, leading to sudden oxidative burst, mitochondrial hyperpolarisation and LMP. ZnO NPs mediated necroptosis of microglial cell death was demonstrated for the first time in this study in our knowledge. Astrocytes are more tolerant to ZnO NPs than microglia. ZnO NPs exposure resulted in ROS generation and LMP in astrocytes. Unlike microglia, ZnO NPs induced mitochondrial hypopolarisation

and Caspase mediated apoptosis in astrocytes. Cytotoxicity exhibited by ZnO NPs was influence by the size, morphology and particle dissolution. Particle dissolution inside lysosomes and generation of ROS lead to ZnO NPs mediated cytotoxicity. The ZnO NPs exhibited nano-specific cytotoxicity compared to bulk counterpart and ionic ($ZnCl_2$) formulation. Cells exposed to ZnO NPs showed low survival rate and proliferative potential than ZnO bulk and $ZnCl_2$.

Single exposure of 10mg/kg body weight ZnO NPs did not elicit neurotoxicological response in Wistar rats. The treated animals exhibited no histopathological changes or glial cell alteration in brain. However elevated glutathione reductase activity and altered iron content were observed in brain. Kidney and spleen of the exposed animals indicated no signs of toxicity except for altered copper and iron contend. ZnO NPs exposure resulted in compromised cellular integrity, histopathological changes and elevated antioxidant level in liver. Moreover, altered zinc, iron and copper contents were detected in liver. The present study showed that single exposure of 10mg/kg of ZnO NPs induces hepatic toxicity in Wistar rats. Even though no change in zinc contend was observed in the brain and kidney of rats, altered metal homeostasis were seen.

The ZnO NPs exposure results in altered levels of iron and copper without altering the zinc content. This indicate that toxic potential of ZnO NPs may not be directly correlated with the amount of zinc contend in the organs. Based on the results, the present study concluded that ZnO NPs induced alteration in clinical parameters, liver antioxidant activity and histology of liver leading to toxicity. The present study

emphasises that ZnO NPs at relatively small concentrations are capable of inducing toxicity. Hence, appropriate safety measures may be recommended while handling the ZnO NPs to prevent unforeseen outcomes.

REFERENCES

Adamcakova-Dodd A, Stebounova LV, Kim JS, Vorrink SU, Ault AP, T O'Shaughnessy P, Grassian VH and Thorne PS (2014) Toxicity assessment of zinc oxide nanoparticles using sub-acute and sub-chronic murine inhalation models. *Particle and fibre toxicology* 11: 1.

Aits S and Jäättelä M (2013) Lysosomal cell death at a glance. *Journal of Cell Science* 126: 1905-1912.

Akhtar MJ, Ahamed M, Kumar S, Khan MM, Ahmad J and Alrokayan SA (2012) Zinc oxide nanoparticles selectively induce apoptosis in human cancer cells through reactive oxygen species. *Int J Nanomedicine* 7: 845-857.

Alam S and Kelleher SL (2012) Cellular mechanisms of zinc dysregulation: a perspective on zinc homeostasis as an etiological factor in the development and progression of breast cancer. *Nutrients* 4: 875-903.

Ali A, Ansari AA, Kaushik A, Solanki PR, Barik A, Pandey M and Malhotra B (2009) Nanostructured zinc oxide film for urea sensor. *Materials Letters* 63: 2473-2475.

Allen NJ and Barres BA (2009) Neuroscience: glia—more than just brain glue. *Nature* 457: 675-677.

Amara S, Slama IB, Omri K, Ghoul JE, Mir LE, Rhouma KB, Abdelmelek H and Sakly M (2015) Effects of nanoparticle zinc oxide on emotional behavior and trace elements homeostasis in rat brain. *Toxicology and industrial health* 31: 1202-1209.

Andón FT and Fadeel B (2012) Programmed cell death: molecular mechanisms and implications for safety assessment of nanomaterials. *Accounts of chemical research* 46: 733-742.

Ansar S, Abudawood M, Hamed SS and Aleem MM (2016) Exposure to Zinc Oxide Nanoparticles Induces Neurotoxicity and Proinflammatory Response: Amelioration by Hesperidin. *Biological trace element research*: 1-7.

Ansari SA and Husain Q (2012) Potential applications of enzymes immobilized on/in nano materials: A review. *Biotechnology advances* 30: 512-523.

Aschner M, Sonnewald U and Tan KH (2002) Astrocyte modulation of neurotoxic injury. *Brain pathology* 12: 475-481.

Auffan M, Rose J, Bottero J-Y, Lowry GV, Jolivet J-P and Wiesner MR (2009) Towards a definition of inorganic nanoparticles from an environmental, health and safety perspective. *Nature nanotechnology* 4: 634-641.

Aydin Sevinç B and Hanley L (2010) Antibacterial activity of dental composites containing zinc oxide nanoparticles. *Journal of Biomedical Materials Research Part B: Applied Biomaterials* 94: 22-31.

Baek M, Chung H-E, Yu J, Lee J-A, Kim T-H, Oh J-M, Lee W-J, Paek S-M, Lee JK and Jeong J (2012) Pharmacokinetics, tissue distribution, and excretion of zinc oxide nanoparticles. *Int J Nanomedicine* 7: 3081-3097.

Baek M, Kim M, Cho H, Lee J, Yu J, Chung H and Choi S (2011). Factors influencing the cytotoxicity of zinc oxide nanoparticles: particle size and surface charge. Journal of Physics: Conference Series, IOP Publishing.

Bai W, Zhang Z, Tian W, He X, Ma Y, Zhao Y and Chai Z (2010) Toxicity of zinc oxide nanoparticles to zebrafish embryo: a physicochemical study of toxicity mechanism. *Journal of Nanoparticle Research* 12: 1645-1654.

Bao G, Mitragotri S and Tong S (2013) Multifunctional nanoparticles for drug delivery and molecular imaging. *Annual review of biomedical engineering* 15: 253-282.

Barreto GE, Gonzalez J, Capani F and Morales L (2011). Role of astrocytes in neurodegenerative diseases. Neurodegenerative Diseases-Processes, Prevention, Protection and Monitoring, InTech.

Blackburn D, Sargsyan S, Monk PN and Shaw PJ (2009) Astrocyte function and role in motor neuron disease: a future therapeutic target? *Glia* 57: 1251-1264.

Blinova I, Ivask A, Heinlaan M, Mortimer M and Kahru A (2010) Ecotoxicity of nanoparticles of CuO and ZnO in natural water. *Environmental Pollution* 158: 41-47.

Block ML and Hong J-S (2005) Microglia and inflammation-mediated neurodegeneration: multiple triggers with a common mechanism. *Progress in neurobiology* 76: 77-98.

Boldogh IR and Pon LA (2006) Interactions of mitochondria with the actin cytoskeleton. *Biochimica et Biophysica Acta (BBA)-Molecular Cell Research* 1763: 450-462.

Bondarenko O, Juganson K, Ivask A, Kasemets K, Mortimer M and Kahru A (2013) Toxicity of Ag, CuO and ZnO nanoparticles to selected environmentally relevant test organisms and mammalian cells in vitro: a critical review. *Archives of toxicology* 87: 1181-1200.

Borenfreund E and Puerner JA (1985) Toxicity determined in vitro by morphological alterations and neutral red absorption. *Toxicology letters* 24: 119-124.

Boya P and Kroemer G (2008) Lysosomal membrane permeabilization in cell death. *Oncogene* 27: 6434-6451.

Brayner R, Dahoumane SA, Yéprémian C, Djediat C, Meyer M, Couté A and Fiévet F (2010) ZnO nanoparticles: synthesis, characterization, and ecotoxicological studies. *Langmuir* 26: 6522-6528.

Brown GC and Neher JJ (2010) Inflammatory neurodegeneration and mechanisms of microglial killing of neurons. *Molecular neurobiology* 41: 242-247.

Buerki-Thurnherr T, Xiao L, Diener L, Arslan O, Hirsch C, Maeder-Althaus X, Grieder K, Wampfler B, Mathur S and Wick P (2013) In vitro mechanistic study towards a better understanding of ZnO nanoparticle toxicity. *Nanotoxicology* 7: 402-416.

Buzea C, Pacheco II and Robbie K (2007) Nanomaterials and nanoparticles: sources and toxicity. *Biointerphases* 2: MR17-MR71.

Chang Y-N, Zhang M, Xia L, Zhang J and Xing G (2012) The toxic effects and mechanisms of CuO and ZnO nanoparticles. *Materials* 5: 2850-2871.

Chen B-A, Jin N, Wang J, Ding J, Gao C, Cheng J, Xia G, Gao F, Zhou Y and Chen Y (2010) The effect of magnetic nanoparticles of Fe3O4 on immune function in normal ICR mice. *International journal of nanomedicine* 5: 593.

Chen Y and Swanson RA (2003) Astrocytes and brain injury. *Journal of Cerebral Blood Flow & Metabolism* 23: 137-149.

Cho N-H, Cheong T-C, Min JH, Wu JH, Lee SJ, Kim D, Yang J-S, Kim S, Kim YK and Seong S-Y (2011) A multifunctional core-shell nanoparticle for dendritic cell-based cancer immunotherapy. *Nature nanotechnology* 6: 675-682.

Cho W-S, Duffin R, Howie SE, Scotton CJ, Wallace WA, MacNee W, Bradley M, Megson IL and Donaldson K (2011) Progressive severe lung injury by zinc oxide nanoparticles; the role of Zn 2+ dissolution inside lysosomes. *Particle and fibre toxicology* 8: 1.

Cho W-S, Kang B-C, Lee JK, Jeong J, Che J-H and Seok SH (2013) Comparative absorption, distribution, and excretion of titanium dioxide and zinc oxide nanoparticles after repeated oral administration. *Particle and fibre toxicology* 10: 1.

Choi J, Kim H, Kim P, Jo E, Kim H-M, Lee M-Y, Jin SM and Park K (2015) Toxicity of zinc oxide nanoparticles in rats treated by two different routes: single intravenous injection and single oral administration. *Journal of Toxicology and Environmental Health, Part A* 78: 226-243.

Choi J and Wang NS (2011). Nanoparticles in biomedical applications and their safety concerns, INTECH Open Access Publisher.

Choudhury SR, Ordaz J, Lo C-L, Damayanti NP, Zhou F and Irudayaraj J (2017) From the Cover: Zinc oxide Nanoparticles-Induced Reactive Oxygen Species Promotes Multimodal Cyto-and Epigenetic Toxicity. *Toxicological Sciences* 156: 261-274.

Colombo E, Di Dario M, Capitolo E, Chaabane L, Newcombe J, Martino G and Farina C (2014) Fingolimod may support neuroprotection via blockade of astrocyte nitric oxide. *Annals of neurology* 76: 325-337.

Colton CA and Gilbert DL (1987) Production of superoxide anions by a CNS macrophage, the microglia. *FEBS letters* 223: 284-288.

Cooper RJ and Spitzer N (2015) Silver nanoparticles at sublethal concentrations disrupt cytoskeleton and neurite dynamics in cultured adult neural stem cells. *Neurotoxicology* 48: 231-238.

Corona JC and Duchen MR (2015) Impaired mitochondrial homeostasis and neurodegeneration: towards new therapeutic targets? *Journal of bioenergetics and biomembranes* 47: 89-99.

Degen A and Kosec M (2000) Effect of pH and impurities on the surface charge of zinc oxide in aqueous solution. *Journal of the European Ceramic Society* 20: 667-673.

Deng X, Luan Q, Chen W, Wang Y, Wu M, Zhang H and Jiao Z (2009) Nanosized zinc oxide particles induce neural stem cell apoptosis. *Nanotechnology* 20: 115101.

Deng ZJ, Mortimer G, Schiller T, Musumeci A, Martin D and Minchin RF (2009) Differential plasma protein binding to metal oxide nanoparticles. *Nanotechnology* 20: 455101.

Deponte M (2013) Glutathione catalysis and the reaction mechanisms of glutathione-dependent enzymes. *Biochimica et Biophysica Acta (BBA)-General Subjects* 1830: 3217-3266.

Devi R, Yadav S and Pundir C (2012) Amperometric determination of xanthine in fish meat by zinc oxide nanoparticle/chitosan/multiwalled carbon nanotube/polyaniline composite film bound xanthine oxidase. *Analyst* 137: 754-759.

Dröse S (2013) Differential effects of complex II on mitochondrial ROS production and their relation to cardioprotective pre-and postconditioning. *Biochimica et Biophysica Acta (BBA)-Bioenergetics* 1827: 578-587.

Dudev T and Lim C (2008) Metal binding affinity and selectivity in metalloproteins: insights from computational studies. *Annu. Rev. Biophys.* 37: 97-116.

Duvall MN (2012) "FDA regulation of nanotechnology." Washington, DC, USA: Beveridge & Diamond, PG.

Fang L, Huang K, Zhang B, Liu B, Liu Y and Zhang Q (2014) Nanosheet-based 3D hierarchical ZnO structure decorated with Au nanoparticles for enhanced electrochemical detection of dopamine. *RSC Advances* 4: 48986-48993.

Fernández-García M and Rodriguez JA (2011) Metal oxide nanoparticles. *Encyclopedia of Inorganic and Bioinorganic Chemistry*.

Fink SL and Cookson BT (2005) Apoptosis, pyroptosis, and necrosis: mechanistic description of dead and dying eukaryotic cells. *Infection and immunity* 73: 1907-1916.

Foo LC, Allen NJ, Bushong EA, Ventura PB, Chung W-S, Zhou L, Cahoy JD, Daneman R, Zong H and Ellisman MH (2011) Development of a method for the purification and culture of rodent astrocytes. *Neuron* 71: 799-811.

Fröhlich E (2012) The role of surface charge in cellular uptake and cytotoxicity of medical nanoparticles. *Int J Nanomedicine* 7: 5577-5591.

Garedew A, Henderson SO and Moncada S (2010) Activated macrophages utilize glycolytic ATP to maintain mitochondrial membrane potential and prevent apoptotic cell death. *Cell Death & Differentiation* 17: 1540-1550.

Gaumet M, Vargas A, Gurny R and Delie F (2008) Nanoparticles for drug delivery: the need for precision in reporting particle size parameters. *European journal of pharmaceutics and biopharmaceutics* 69: 1-9.

Geiser M and Kreyling WG (2010) Deposition and biokinetics of inhaled nanoparticles. *Particle and fibre toxicology* 7: 1.

Grimm A, Biliouris EE, Lang UE, Götz J, Mensah-Nyagan AG and Eckert A (2016) Sex hormone-related neurosteroids differentially rescue bioenergetic deficits induced by amyloid-β or hyperphosphorylated tau protein. *Cellular and molecular life sciences* 73: 201.

H. Müller K, Kulkarni J, Motskin M, Goode A, Winship P, Skepper JN, Ryan MP and Porter AE (2010) pH-dependent toxicity of high aspect ratio ZnO nanowires in macrophages due to intracellular dissolution. *ACS nano* 4: 6767-6779.

Hanley C, Layne J, Punnoose A, Reddy K, Coombs I, Coombs A, Feris K and Wingett D (2008) Preferential killing of cancer cells and activated human T cells using ZnO nanoparticles. *Nanotechnology* 19: 295103.

Hayes AW and Kruger CL (2014). Hayes' principles and methods of toxicology, CRC Press.

He W, Jia H, Cai J, Han X, Zheng Z, Wamer WG and Yin J-J (2016) Production of reactive oxygen species and electrons from photoexcited ZnO and ZnS nanoparticles: a comparative study for unraveling their distinct photocatalytic activities.

Heinicke U, Kupka J, Fichter I and Fulda S (2016) Critical role of mitochondria-mediated apoptosis for JNJ-26481585-induced antitumor activity in rhabdomyosarcoma. *Oncogene* 35: 3729-3741.

Hernández-Sierra JF, Ruiz F, Pena DCC, Martínez-Gutiérrez F, Martínez AE, Guillén AdJP, Tapia-Pérez H and Castañón GM (2008) The antimicrobial sensitivity of Streptococcus mutans to nanoparticles of silver, zinc oxide, and gold. *Nanomedicine: Nanotechnology, Biology and Medicine* 4: 237-240.

Hsiao I-L and Huang Y-J (2011) Effects of various physicochemical characteristics on the toxicities of ZnO and TiO 2 nanoparticles toward human lung epithelial cells. *Science of the Total Environment* 409: 1219-1228.

Hua J, Vijver MG, Richardson MK, Ahmad F and Peijnenburg WJ (2014) Particle-specific toxic effects of differently shaped zinc oxide nanoparticles to zebrafish embryos (Danio rerio). *Environmental Toxicology and Chemistry* 33: 2859-2868.

Huang C-C, Aronstam RS, Chen D-R and Huang Y-W (2010) Oxidative stress, calcium homeostasis, and altered gene expression in human lung epithelial cells exposed to ZnO nanoparticles. *Toxicology in vitro* 24: 45-55.

Huber KL and Hardy JA (2012) Mechanism of zinc-mediated inhibition of caspase-9. *Protein Science* 21: 1056-1065.

Huerta-García E, Pérez-Arizti JA, Márquez-Ramírez SG, Delgado-Buenrostro NL, Chirino YI, Iglesias GG and López-Marure R (2014) Titanium dioxide nanoparticles induce strong oxidative stress and mitochondrial damage in glial cells. *Free Radical Biology and Medicine* 73: 84-94.

Hwa K-Y and Subramani B (2014) Synthesis of zinc oxide nanoparticles on graphene–carbon nanotube hybrid for glucose biosensor applications. *Biosensors and Bioelectronics* 62: 127-133.

Ivask A, Titma T, Visnapuu M, Vija H, Kakinen A, Sihtmae M, Pokhrel S, Madler L, Heinlaan M and Kisand V (2015) Toxicity of 11 metal oxide nanoparticles to three mammalian cell types in vitro. *Current topics in medicinal chemistry* 15: 1914-1929.

Jaattela M, Cande C and Kroemer G (2004) Lysosomes and mitochondria in the commitment to apoptosis: a potential role for cathepsin D and AIF. *Cell death and differentiation* 11: 135-136.

Jedlovszky-Hajdú Al, Bombelli FB, Monopoli MP, Tombácz E and Dawson KA (2012) Surface coatings shape the protein corona of SPIONs with relevance to their application in vivo. *Langmuir* 28: 14983-14991.

Jessen KR and Mirsky R (2005) The origin and development of glial cells in peripheral nerves. *Nature Reviews Neuroscience* 6: 671-682.

Jiang J, Oberdörster G, Elder A, Gelein R, Mercer P and Biswas P (2008) Does nanoparticle activity depend upon size and crystal phase? *Nanotoxicology* 2: 33-42.

Kao Y-Y, Cheng T-J, Yang D-M, Wang C-T, Chiung Y-M and Liu P-S (2012) Demonstration of an olfactory bulb–brain translocation pathway for ZnO nanoparticles in rodent cells in vitro and in vivo. *Journal of Molecular Neuroscience* 48: 464-471.

Kauppinen TM, Higashi Y, Suh SW, Escartin C, Nagasawa K and Swanson RA (2008) Zinc triggers microglial activation. *Journal of Neuroscience* 28: 5827-5835.

Kesmati M and Torabi M (2014) Interaction between Analgesic Effect of Nano and Conventional size of Zinc Oxide and Opioidergic System Activity in Animal Model of Acute Pain. *Basic and clinical neuroscience* 5: 80-87.

Kessler R (2011) Engineered nanoparticles in consumer products: understanding a new ingredient. *Environ Health Perspect* 119: A120-A125.

Khare P, Sonane M, Pandey R, Ali S, Gupta KC and Satish A (2011) Adverse effects of TiO2 and ZnO nanoparticles in soil nematode, Caenorhabditis elegans. *Journal of biomedical nanotechnology* 7: 116-117.

Kigerl KA, de Rivero Vaccari JP, Dietrich WD, Popovich PG and Keane RW (2014) Pattern recognition receptors and central nervous system repair. *Experimental neurology* 258: 5-16.

Kim C-S, Nguyen H-D, Ignacio RM, Kim J-H, Cho H-C, Maeng EH, Kim Y-R, Kim M-K, Park B-K and Kim S-K (2014) Immunotoxicity of zinc oxide nanoparticles with different size and electrostatic charge. *International journal of nanomedicine* 9: 195.

Kim I-S, Baek M and Choi S-J (2010) Comparative cytotoxicity of Al2O3, CeO2, TiO2 and ZnO nanoparticles to human lung cells. *Journal of nanoscience and nanotechnology* 10: 3453-3458.

Kim Y-R, Park J-I, Lee EJ, Park SH, Seong N-w, Kim J-H, Kim G-Y, Meang E-H, Hong J-S and Kim S-H (2014) Toxicity of 100 nm zinc oxide nanoparticles: a report of 90-day repeated oral administration in Sprague Dawley rats. *International journal of nanomedicine* 9: 109.

Kołodziejczak-Radzimska A and Jesionowski T (2014) Zinc oxide—from synthesis to application: a review. *Materials* 7: 2833-2881.

Kozlovskaya L, Abou-Kaoud M and Stepensky D (2014) Quantitative analysis of drug delivery to the brain via nasal route. *Journal of controlled release* 189: 133-140.

Kroemer G, Galluzzi L, Vandenabeele P, Abrams J, Alnemri E, Baehrecke E, Blagosklonny M, El-Deiry W, Golstein P and Green D (2009) Classification of cell death: recommendations of the Nomenclature Committee on Cell Death 2009. *Cell Death & Differentiation* 16: 3-11.

Kumar R, Al-Dossary O, Kumar G and Umar A (2015) Zinc oxide nanostructures for NO2 gas–sensor applications: a review. *Nano-Micro Letters* 7: 97-120.

Kumar SG and Rao KK (2015) Zinc oxide based photocatalysis: tailoring surface-bulk structure and related interfacial charge carrier dynamics for better environmental applications. *RSC Advances* 5: 3306-3351.

Kumar SS, Venkateswarlu P, Rao VR and Rao GN (2013) Synthesis, characterization and optical properties of zinc oxide nanoparticles. *International Nano Letters* 3: 30.

Lakhani SA, Masud A, Kuida K, Porter GA, Booth CJ, Mehal WZ, Inayat I and Flavell RA (2006) Caspases 3 and 7: key mediators of mitochondrial events of apoptosis. *science* 311: 847-851.

Li P, Wei Y, Liu H and Wang X-k (2005) Growth of well-defined ZnO microparticles with additives from aqueous solution. *Journal of Solid State Chemistry* 178: 855-860.

Li X-b, Zheng H, Zhang Z-r, Li M, Huang Z-y, Schluesener HJ, Li Y-y and Xu S-q (2009) Glia activation induced by peripheral administration of aluminum oxide

nanoparticles in rat brains. *Nanomedicine: Nanotechnology, Biology and Medicine* 5: 473-479.

Liu B and Hong J-S (2003) Role of microglia in inflammation-mediated neurodegenerative diseases: mechanisms and strategies for therapeutic intervention. *Journal of Pharmacology and Experimental Therapeutics* 304: 1-7.

Liu M, Gu X, Zhang K, Ding Y, Wei X, Zhang X and Zhao Y (2013) Gold nanoparticles trigger apoptosis and necrosis in lung cancer cells with low intracellular glutathione. *Journal of Nanoparticle Research* 15: 1745.

Lockman PR, Koziara JM, Mumper RJ and Allen DD (2008) Nanoparticle surface charges alter blood–brain barrier integrity and permeability. *Journal of drug targeting*.

Long TC, Saleh N, Tilton RD, Lowry GV and Veronesi B (2006) Titanium dioxide (P25) produces reactive oxygen species in immortalized brain microglia (BV2): implications for nanoparticle neurotoxicity. *Environmental Science & Technology* 40: 4346-4352.

Lowry OH, Rosebrough NJ, Farr AL and Randall RJ (1951) Protein measurement with the Folin phenol reagent. *Journal of Biological Chemistry* 193: 265-275.

Ma H, Williams PL and Diamond SA (2013) Ecotoxicity of manufactured ZnO nanoparticles–a review. *Environmental Pollution* 172: 76-85.

Manke A, Wang L and Rojanasakul Y (2013) Mechanisms of nanoparticle-induced oxidative stress and toxicity. *BioMed research international* 2013.

Manzo S, Rocco A, Carotenuto R, Picione FDL, Miglietta ML, Rametta G and Di Francia G (2011) Investigation of ZnO nanoparticles' ecotoxicological effects towards different soil organisms. *Environmental Science and Pollution Research* 18: 756-763.

Marklund S and Marklund G (1974) Involvement of the superoxide anion radical in the autoxidation of pyrogallol and a convenient assay for superoxide dismutase. *The FEBS Journal* 47: 469-474.

Márquez-Ramírez SG, Delgado-Buenrostro NL, Chirino YI, Iglesias GG and López-Marure R (2012) Titanium dioxide nanoparticles inhibit proliferation and induce morphological changes and apoptosis in glial cells. *Toxicology* 302: 146-156.

Matarrese P, Cauda R and Malorni W (2003) Activation-associated mitochondrial hyperpolarization hijacks T cells toward an apoptosis-sensitized phenotype. *Cell Death & Differentiation* 10.

McCord MC and Aizenman E (2014) The role of intracellular zinc release in aging, oxidative stress, and Alzheimer's disease. *Frontiers in aging neuroscience* 6.

Mendonça MCP, Soares ES, de Jesus MB, Ceragioli HJ, Irazusta SP, Batista ÂG, Vinolo MAR, Júnior MRM and Cruz-Höfling MA (2016) Reduced graphene oxide: nanotoxicological profile in rats. *Journal of nanobiotechnology* 14: 53.

Miclăuş T, Beer C, Chevallier J, Scavenius C, Bochenkov VE, Enghild JJ and Sutherland DS (2016) Dynamic protein coronas revealed as a modulator of silver nanoparticle sulphidation in vitro. *Nature communications* 7.

Mize CE and Langdon RG (1962) Hepatic glutathione reductase I. Purification and general kinetic properties. *Journal of Biological Chemistry* 237: 1589-1595.

Moezzi A, Cortie M and McDonagh A (2011) Aqueous pathways for the formation of zinc oxide nanoparticles. *Dalton Transactions* 40: 4871-4878.

Monteiro-Riviere N, Wiench K, Landsiedel R, Schulte S, Inman A and Riviere J (2011) Safety evaluation of sunscreen formulations containing titanium dioxide and zinc oxide nanoparticles in UVB sunburned skin: an in vitro and in vivo study. *Toxicological Sciences*: kfr148.

Moos PJ, Chung K, Woessner D, Honeggar M, Cutler NS and Veranth JM (2010) ZnO particulate matter requires cell contact for toxicity in human colon cancer cells. *Chemical research in toxicology* 23: 733-739.

Moron MS, Depierre JW and Mannervik B (1979) Levels of glutathione, glutathione reductase and glutathione S-transferase activities in rat lung and liver. *Biochimica et Biophysica Acta (BBA)-General Subjects* 582: 67-78.

Mueller NC and Nowack B (2008) Exposure modeling of engineered nanoparticles in the environment. *Environmental Science & Technology* 42: 4447-4453.

Muhammad F, Guo M, Qi W, Sun F, Wang A, Guo Y and Zhu G (2011) pH-triggered controlled drug release from mesoporous silica nanoparticles via intracelluar dissolution of ZnO nanolids. *Journal of the American Chemical Society* 133: 8778-8781.

Nel A, Xia T, Mädler L and Li N (2006) Toxic potential of materials at the nanolevel. *science* 311: 622-627.

Nel AE, Mädler L, Velegol D, Xia T, Hoek EM, Somasundaran P, Klaessig F, Castranova V and Thompson M (2009) Understanding biophysicochemical interactions at the nano–bio interface. *Nature materials* 8: 543-557.

Nie L, Gao L, Feng P, Zhang J, Fu X, Liu Y, Yan X and Wang T (2006) Three-Dimensional Functionalized Tetrapod-like ZnO Nanostructures for Plasmid DNA Delivery. *Small* 2: 621-625.

Nohynek G, Dufour E and Roberts M (2008) Nanotechnology, cosmetics and the skin: is there a health risk? *Skin pharmacology and physiology* 21: 136-149.

O'Malley EK, Sieber B-A, Black IB and Dreyfus CF (1992) Mesencephalic type I astrocytes mediate the survival of substantia nigra dopaminergic neurons in culture. *Brain research* 582: 65-70.

Oberdörster G, Elder A and Rinderknecht A (2009) Nanoparticles and the brain: cause for concern? *Journal of nanoscience and nanotechnology* 9: 4996-5007.

Oberdörster G, Sharp Z, Atudorei V, Elder A, Gelein R, Kreyling W and Cox C (2004) Translocation of inhaled ultrafine particles to the brain. *Inhalation toxicology* 16: 437-445.

Ohkawa H, Ohishi N and Yagi K (1979) Assay for lipid peroxides in animal tissues by thiobarbituric acid reaction. *Analytical biochemistry* 95: 351-358.

Ong KJ, MacCormack TJ, Clark RJ, Ede JD, Ortega VA, Felix LC, Dang MK, Ma G, Fenniri H and Veinot JG (2014) Widespread nanoparticle-assay interference: implications for nanotoxicity testing. *PLoS One* 9: e90650.

Osmond-McLeod MJ, Oytam Y, Osmond RI, Sobhanmanesh F and McCall MJ (2014) Surface coatings protect against the in vitro toxicity of zinc oxide nanoparticles in human hepatic stellate cells. *Journal of Nanomedicine & Nanotechnology* 2014.

Ostrovsky S, Kazimirsky G, Gedanken A and Brodie C (2009) Selective cytotoxic effect of ZnO nanoparticles on glioma cells. *Nano Research* 2: 882-890.

Panyala NR, Peña-Méndez EM and Havel J (2009) Gold and nano-gold in medicine: overview, toxicology and perspectives. *J Appl Biomed* 7: 75-91.

Pellegrin S and Mellor H (2007) Actin stress fibres. *Journal of Cell Science* 120: 3491-3499.

Perl A, Gergely P, Nagy G, Koncz A and Banki K (2004) Mitochondrial hyperpolarization: a checkpoint of T-cell life, death and autoimmunity. *Trends in immunology* 25: 360-367.

Premanathan M, Karthikeyan K, Jeyasubramanian K and Manivannan G (2011) Selective toxicity of ZnO nanoparticles toward Gram-positive bacteria and cancer cells

by apoptosis through lipid peroxidation. *Nanomedicine: Nanotechnology, Biology and Medicine* 7: 184-192.

Punnoose A, Kongara MR and Wingett D (2012). Preferential killing of cancer cells and activated human T cells using ZnO nanoparticles, Google Patents.

Rainbolt TK, Atanassova N, Genereux JC and Wiseman RL (2013) Stress-regulated translational attenuation adapts mitochondrial protein import through Tim17A degradation. *Cell metabolism* 18: 908-919.

Rasmussen JW, Martinez E, Louka P and Wingett DG (2010) Zinc oxide nanoparticles for selective destruction of tumor cells and potential for drug delivery applications. *Expert opinion on drug delivery* 7: 1063-1077.

Rice SB, Chan C, Brown SC, Eschbach P, Han L, Ensor DS, Stefaniak AB, Bonevich J, Vladár AE and Walker ARH (2013) Particle size distributions by transmission electron microscopy: an interlaboratory comparison case study. *Metrologia* 50: 663.

Robert A, Liu Y, Nguyen M and Meunier B (2015) Regulation of copper and iron homeostasis by metal chelators: A possible chemotherapy for Alzheimer's disease. *Accounts of chemical research* 48: 1332-1339.

Roos WP, Thomas AD and Kaina B (2016) DNA damage and the balance between survival and death in cancer biology. *Nature Reviews Cancer* 16: 20-33.

Rotruck J, Pope A, Ganther H, Swanson A, Hafeman DG and Hoekstra W (1973) Selenium: biochemical role as a component of glutathione peroxidase. *science* 179: 588-590.

Roy R, Parashar V, Chauhan L, Shanker R, Das M, Tripathi A and Dwivedi PD (2014) Mechanism of uptake of ZnO nanoparticles and inflammatory responses in macrophages require PI3K mediated MAPKs signaling. *Toxicology in vitro* 28: 457-467.

Sanches EA, Carolino AdS, Santos ALd, Fernandes EG, Trichês DM and Mascarenhas YP (2015) The use of le bail method to analyze the semicrystalline pattern of a nanocomposite based on polyaniline emeraldine-salt form and α-Al2O3. *Advances in Materials Science and Engineering* 2015.

Sasidharan A, Chandran P, Menon D, Raman S, Nair S and Koyakutty M (2011) Rapid dissolution of ZnO nanocrystals in acidic cancer microenvironment leading to preferential apoptosis. *Nanoscale* 3: 3657-3669.

Schlegelmilch T, Henke K and Peri F (2011) Microglia in the developing brain: from immunity to behaviour. *Current opinion in neurobiology* 21: 5-10.

Seil JT and Webster TJ (2008) Decreased astroglial cell adhesion and proliferation on zinc oxide nanoparticle polyurethane composites. *Int J Nanomedicine* 3: 523-531.

Setyawati MI, Tay CY and Leong DT (2015) Mechanistic investigation of the biological effects of SiO2, TiO2, and ZnO nanoparticles on intestinal cells. *Small* 11: 3458-3468.

Sharma V, Anderson D and Dhawan A (2012) Zinc oxide nanoparticles induce oxidative DNA damage and ROS-triggered mitochondria mediated apoptosis in human liver cells (HepG2). *Apoptosis* 17: 852-870.

Sharma V, Singh P, Pandey AK and Dhawan A (2012) Induction of oxidative stress, DNA damage and apoptosis in mouse liver after sub-acute oral exposure to zinc oxide nanoparticles. *Mutation Research/Genetic Toxicology and Environmental Mutagenesis* 745: 84-91.

Shrivastava R, Raza S, Yadav A, Kushwaha P and Flora SJ (2014) Effects of sub-acute exposure to TiO2, ZnO and Al2O3 nanoparticles on oxidative stress and histological changes in mouse liver and brain. *Drug and chemical toxicology* 37: 336-347.

Sirelkhatim A, Mahmud S, Seeni A, Kaus NHM, Ann LC, Bakhori SKM, Hasan H and Mohamad D (2015) Review on zinc oxide nanoparticles: antibacterial activity and toxicity mechanism. *Nano-Micro Letters* 7: 219-242.

Smijs TG and Pavel S (2011) Titanium dioxide and zinc oxide nanoparticles in sunscreens: focus on their safety and effectiveness. *Nanotechnology, science and applications* 4: 95.

Smulders S, Kaiser J-P, Zuin S, Van Landuyt KL, Golanski L, Vanoirbeek J, Wick P and Hoet PH (2012) Contamination of nanoparticles by endotoxin: evaluation of different test methods. *Particle and fibre toxicology* 9: 41.

Soenen SJ, Rivera-Gil P, Montenegro J-M, Parak WJ, De Smedt SC and Braeckmans K (2011) Cellular toxicity of inorganic nanoparticles: common aspects and guidelines for improved nanotoxicity evaluation. *Nano Today* 6: 446-465.

Sofroniew MV (2009) Molecular dissection of reactive astrogliosis and glial scar formation. *Trends in neurosciences* 32: 638-647.

Song W, Zhang J, Guo J, Zhang J, Ding F, Li L and Sun Z (2010) Role of the dissolved zinc ion and reactive oxygen species in cytotoxicity of ZnO nanoparticles. *Toxicology letters* 199: 389-397.

Sruthi S, Millot N and Mohanan P (2017) Zinc oxide nanoparticles mediated cytotoxicity, mitochondrial membrane potential and level of antioxidants in presence of melatonin. *International Journal of Biological Macromolecules* 103: 808-818.

Sruthi S and Mohanan P (2016) Engineered zinc oxide nanoparticles; biological interactions at the organ level. *Current medicinal chemistry*.

Sruthi S and Mohanan P (2015) Investigation on cellular interactions of astrocytes with zinc oxide nanoparticles using rat C6 cell lines. *Colloids and Surfaces B: Biointerfaces* 133: 1-11.

Streit WJ and Xue Q-S (2009) Life and death of microglia. *Journal of neuroimmune pharmacology* 4: 371-379.

Sudhagar S, Sathya S, Pandian K and Lakshmi BS (2011) Targeting and sensing cancer cells with ZnO nanoprobes in vitro. *Biotechnology letters* 33: 1891-1896.

Suzuki H, Toyooka T and Ibuki Y (2007) Simple and easy method to evaluate uptake potential of nanoparticles in mammalian cells using a flow cytometric light scatter analysis. *Environmental Science & Technology* 41: 3018-3024.

Takeda K, Suzuki K-i, Ishihara A, Kubo-Irie M, Fujimoto R, Tabata M, Oshio S, Nihei Y, Ihara T and Sugamata M (2009) Nanoparticles transferred from pregnant mice to their offspring can damage the genital and cranial nerve systems. *Journal of Health Science* 55: 95-102.

Taratula O, Galoppini E, Wang D, Chu D, Zhang Z, Chen H, Saraf G and Lu Y (2006) Binding studies of molecular linkers to ZnO and MgZnO nanotip films. *The Journal of Physical Chemistry B* 110: 6506-6515.

Tian L, Lin B, Wu L, Li K, Liu H, Yan J, Liu X and Xi Z (2015) Neurotoxicity induced by zinc oxide nanoparticles: age-related differences and interaction. *Scientific reports* 5.

Toduka Y, Toyooka T and Ibuki Y (2012) Flow cytometric evaluation of nanoparticles using side-scattered light and reactive oxygen species-mediated fluorescence–correlation with genotoxicity. *Environmental Science & Technology* 46: 7629-7636.

Torabi M, Kesmati M, Harooni HE and Varzi HN (2013) Effects of nano and conventional Zinc Oxide on anxiety-like behavior in male rats. *Indian journal of pharmacology* 45: 508.

Tsan M and White JE (1992) Kinetics of pulmonary superoxide dismutase in interleukin-1-induced oxygen-tolerant rats. *American Journal of Physiology-Lung Cellular and Molecular Physiology* 263: L342-L347.

Valdiglesias V, Costa C, Kiliç G, Costa S, Pásaro E, Laffon B and Teixeira JP (2013) Neuronal cytotoxicity and genotoxicity induced by zinc oxide nanoparticles. *Environment International* 55: 92-100.

Vance ME, Kuiken T, Vejerano EP, McGinnis SP, Hochella Jr MF, Rejeski D and Hull MS (2015) Nanotechnology in the real world: Redeveloping the nanomaterial consumer products inventory. *Beilstein journal of nanotechnology* 6: 1769-1780.

Vandebriel RJ and De Jong WH (2012) A review of mammalian toxicity of ZnO nanoparticles. *Nanotechnology, science and applications* 5: 61.

Velázquez-Delgado EM and Hardy JA (2012) Zinc-mediated allosteric inhibition of caspase-6. *Journal of Biological Chemistry* 287: 36000-36011.

Wang B, Feng W-Y, Wang T-C, Jia G, Wang M, Shi J-W, Zhang F, Zhao Y-L and Chai Z-F (2006) Acute toxicity of nano-and micro-scale zinc powder in healthy adult mice. *Toxicology letters* 161: 115-123.

Wang C and Youle RJ (2009) The role of mitochondria in apoptosis. *Annual review of genetics* 43: 95-118.

Wang G, Tan X, Zhou Q, Liu Y, Wang M and Yang L (2014) Synthesis of highly dispersed zinc oxide nanoparticles on carboxylic graphene for development a sensitive acetylcholinesterase biosensor. *Sensors and Actuators B: Chemical* 190: 730-736.

Wang H, Wingett D, Engelhard MH, Feris K, Reddy K, Turner P, Layne J, Hanley C, Bell J and Tenne D (2009) Fluorescent dye encapsulated ZnO particles with cell-specific toxicity for potential use in biomedical applications. *Journal of Materials Science: Materials in Medicine* 20: 11-22.

Wang J, Deng X, Zhang F, Chen D and Ding W (2014) ZnO nanoparticle-induced oxidative stress triggers apoptosis by activating JNK signaling pathway in cultured primary astrocytes. *Nanoscale research letters* 9: 1-12.

Wang ZL (2004) Nanostructures of zinc oxide. *Materials today* 7: 26-33.

Wang ZL (2004) Zinc oxide nanostructures: growth, properties and applications. *Journal of Physics: Condensed Matter* 16: R829.

Weinstein DE (2001) Isolation and purification of primary rodent astrocytes. *Current Protocols in Neuroscience*: 3.5. 1-3.5. 9.

Wiench K, Wohlleben W, Hisgen V, Radke K, Salinas E, Zok S and Landsiedel R (2009) Acute and chronic effects of nano-and non-nano-scale TiO 2 and ZnO particles on mobility and reproduction of the freshwater invertebrate Daphnia magna. *Chemosphere* 76: 1356-1365.

Wolfbeis OS (2015) An overview of nanoparticles commonly used in fluorescent bioimaging. *Chemical Society Reviews* 44: 4743-4768.

Wu Y, Fu S, Tok A, Zeng X, Lim C, Kwek L and Boey F (2008) A dual-colored bio-marker made of doped ZnO nanocrystals. *Nanotechnology* 19: 345605.

Xia T, Kovochich M, Liong M, Mädler L, Gilbert B, Shi H, Yeh JI, Zink JI and Nel AE (2008) Comparison of the mechanism of toxicity of zinc oxide and cerium oxide nanoparticles based on dissolution and oxidative stress properties. *ACS nano* 2: 2121-2134.

Xia T, Zhao Y, Sager T, George S, Pokhrel S, Li N, Schoenfeld D, Meng H, Lin S and Wang X (2011) Decreased dissolution of ZnO by iron doping yields nanoparticles with reduced toxicity in the rodent lung and zebrafish embryos. *ACS nano* 5: 1223-1235.

Xie Y, Wang Y, Zhang T, Ren G and Yang Z (2012) Effects of nanoparticle zinc oxide on spatial cognition and synaptic plasticity in mice with depressive-like behaviors. *Journal of biomedical science* 19: 1.

Xu C, Yang C, Gu B and Fang S (2013) Nanostructured ZnO for biosensing applications. *Chinese Science Bulletin* 58: 2563-2566.

Xu M, Li J, Iwai H, Mei Q, Fujita D, Su H, Chen H and Hanagata N (2012) Formation of nano-bio-complex as nanomaterials dispersed in a biological solution for understanding nanobiological interactions. *Scientific reports* 2: 406.

Yamabi S and Imai H (2002) Growth conditions for wurtzite zinc oxide films in aqueous solutions. *Journal of Materials Chemistry* 12: 3773-3778.

Yan G, Huang Y, Bu Q, Lv L, Deng P, Zhou J, Wang Y, Yang Y, Liu Q and Cen X (2012) Zinc oxide nanoparticles cause nephrotoxicity and kidney metabolism alterations in rats. *Journal of Environmental Science and Health, Part A* 47: 577-588.

Yanagisawa H, Miyakoshi Y, Kobayashi K, Sakae K, Kawasaki I, Suzuki Y and Tamura Ji (2009) Long-term intake of a high zinc diet causes iron deficiency anemia accompanied by reticulocytosis and extra-medullary erythropoiesis. *Toxicology letters* 191: 15-19.

Yang H, Liu C, Yang D, Zhang H and Xi Z (2009) Comparative study of cytotoxicity, oxidative stress and genotoxicity induced by four typical nanomaterials: the role of particle size, shape and composition. *Journal of applied Toxicology* 29: 69-78.

Yang X, Shao H, Liu W, Gu W, Shu X, Mo Y, Chen X, Zhang Q and Jiang M (2015) Endoplasmic reticulum stress and oxidative stress are involved in ZnO nanoparticle-induced hepatotoxicity. *Toxicology letters* 234: 40-49.

Yang Z, Liu Z, Allaker R, Reip P, Oxford J, Ahmad Z and Reng G (2013). A review of nanoparticle functionality and toxicity on the central nervous system. Nanotechnology, the Brain, and the Future, Springer**:** 313-332.

Yin H, Casey PS, McCall MJ and Fenech M (2010) Effects of surface chemistry on cytotoxicity, genotoxicity, and the generation of reactive oxygen species induced by ZnO nanoparticles. *Langmuir* 26: 15399-15408.

Yin Y, Lin Q, Sun H, Chen D, Wu Q, Chen X and Li S (2012) Cytotoxic effects of ZnO hierarchical architectures on RSC96 Schwann cells. *Nanoscale research letters* 7: 1.

Yuan Q, Hein S and Misra R (2010) New generation of chitosan-encapsulated ZnO quantum dots loaded with drug: synthesis, characterization and in vitro drug delivery response. *Acta biomaterialia* 6: 2732-2739.

Yuste VcJ, Bayascas JR, Llecha N, Sánchez-López I, Boix J and Comella JX (2001) The Absence of Oligonucleosomal DNA Fragmentation during Apoptosis of IMR-5 Neuroblastoma Cells DISAPPEARANCE OF THE CASPASE-ACTIVATED DNase. *Journal of Biological Chemistry* 276: 22323-22331.

Zaman M, Ahmad E, Qadeer A, Rabbani G and Khan RH (2014) Nanoparticles in relation to peptide and protein aggregation. *Int J Nanomedicine* 9: 899-912.

Zatta P, Drago D, Bolognin S and Sensi SL (2009) Alzheimer's disease, metal ions and metal homeostatic therapy. *Trends in Pharmacological Sciences* 30: 346-355.

Zhang L, Chen J, Wang Y, Yu L, Wang J, Peng H and Zhu J (2014) Improved enzyme immobilization for enhanced bioelectrocatalytic activity of choline sensor and acetylcholine sensor. *Sensors and Actuators B: Chemical* 193: 904-910.

Zhang P and Liu W (2010) ZnO QD@ PMAA-co-PDMAEMA nonviral vector for plasmid DNA delivery and bioimaging. *Biomaterials* 31: 3087-3094.

Zhang Y, Nguyen KC, Lefebvre DE, Shwed PS, Crosthwait J, Bondy GS and Tayabali AF (2014) Critical experimental parameters related to the cytotoxicity of zinc oxide nanoparticles. *Journal of Nanoparticle Research* 16: 1-13.

Zhao C-Y, Tan S-X, Xiao X-Y, Qiu X-S, Pan J-Q and Tang Z-X (2014) Effects of dietary zinc oxide nanoparticles on growth performance and antioxidative status in broilers. *Biological trace element research* 160: 361-367.

Zhao D, Song H, Hao L, Liu X, Zhang L and Lv Y (2013) Luminescent ZnO quantum dots for sensitive and selective detection of dopamine. *Talanta* 107: 133-139.

Zheng W and Monnot AD (2012) Regulation of brain iron and copper homeostasis by brain barrier systems: implication in neurodegenerative diseases. *Pharmacology & therapeutics* 133: 177-188.

Zhu M, Nie G, Meng H, Xia T, Nel A and Zhao Y (2012) Physicochemical properties determine nanomaterial cellular uptake, transport, and fate. *Accounts of chemical research* 46: 622-631.

ANNEXURE

LIST OF PUBLICATIONS

1. **Sruthi S,** Mohanan PV. (2015) Investigation on cellular interactions of astrocytes with Zinc oxide nanoparticles using rat C6 cell line. Colloids and Surfaces B: Biointerfaces, 133, 1-11.

2. **Sruthi S**, Mohanan PV. (2016) Engineered zinc oxide nanoparticles; biological interactions at the organ level. Current Medicinal Chemistry, 23(35), 4057-4068.

3. **Sruthi S**, Mohanan PV. (2017) Enhanced toxicity of Zinc oxide nanoparticles on glial cells in presence of pharmacological concentration of melatonin. International Journal of Biological Macromolecules, *International Journal of Biological Macromolecules***103**: 808-818.

4. Reshma VG, Syama S, **Sruthi S**, Reshma SC, Remya NS and Mohanan PV (2017) Engineered nanoparticles for Antimicrobial property, Current Medicinal Chemistry, DOI: 10.2174/1389200218666170925122201

5. **Sruthi S**, Millot N, Lizard G and Mohanan PV, Zinc oxide nanoparticles mediated necrosis in microglial cells (BV2), Neurotoxicology (under review)

6. **Sruthi S** and Mohanan PV, ZnO nanoparticles: Biomedical application, neurotoxicity and mechanism of toxicity- an overview, Toxicology letters (Under review)

7. **Sruthi S**, Millot N and Mohanan PV, Nano-specific toxicity of ZnO nanoparticle on primary astrocytes, Toxicology (Under review)

8. **Sruthi S**, Millot N, Manoj K, Chinju B and Mohanan PV, inductively coupled plasma atomic absorption spectroscopy for the elemental analysis in target organs of rats exposed to ZnO nanoparticles and associated toxicity, Toxicological science (Under review)

CONFERENCES

1. **S. Sruthi**, A. Loiseau, J. Boudon, G. Lizard, P.V. Mohanan, N. Millot. 2016. Comparative study on the cellular interaction of titanate nanotubes and zinc oxide nanoparticles with glial cells. European Material Research Society, 2-6 May 2016 (EMRS- spring meeting 2016), Lille, France- Poster

2. **Sruthi S**, Mohanan PV (2015) Effect of melatonin on zinc oxide nanoparticles induced neurotoxicity. 'Nanotechnology congress expo 2015, Frankfurt Germany, August 11-13. Poster

3. **Sruthi S**, Mohanan PV. 2014. Glioma cells interaction with Zinc Oxide nanoparticles: effect on oxidative stress, DNA damage and cell viability. International Conference on Advancements in Materials, Health and Safety towards Sustainable Energy and Environment, 7-8 August (MHS-2014), Chennai – Poster

APPENDICES

A.1. SDS-PAGE REAGENTS

Acrylamide and N,N'-methylene-bis-acrylamide: 29% (w/v) acrylamide and 1% (w/v) N,N'-methylene-bis-acrylamide was dissolved in warm de-ionized water. pH of the solution was ensured to be less than 7.0 and was stored in dark bottle at 4°C.

Sodium dodecyl sulphate (SDS): 10% (w/v) stock solution was prepared in de-ionized water and stored at RT.

Tris buffers: 1.5M tris (pH-8.8) buffer for resolving gel and 1.0M tris (pH-6.8) for stacking gel was used. pH was adjusted using HCl.

Ammonium persulfate: 10% (w/v) stock solution was freshly prepared in de-ionized water.

1x Tris-glycine electrophoresis buffer: 5x stock of electrophoresis buffer was prepared by dissolving 15.1g of Tris base and 94g of glycine in 900ml of de-ionized water. 50ml of 10% (w/v) stock solution of SDS was added and volume adjusted to 1000 ml of deionized water. 1x buffer was prepared by taking 200ml of 5x buffer and making it up to 1000ml using de-ionized water.

1x SDS gel-loading buffer: The composition of the buffer used was 50mM Tris-Cl (pH-6.8), 100mM dithiothreitol, 2% (w/v) SDS, 0.1% bromophenol blue and 10% (v/v) glycerol. It was stored at RT.

Gel preparation: The glass plates were cleaned thoroughly and assembled as per the manufacturer's instructions. Resolving gel was prepared as per the Table A.1 given

below. As soon as Tetramethylethylenediamine (TEMED) was added, polymerization began and the mix was gently swirled and poured into the gaps between the glass plates. This was layered with butanol to prevent oxygen from diffusing into the gel and inhibiting polymerization. After completion of polymerization (30 min), the overlay was poured off and the gel was washed thoroughly with de-ionized water. Next the stacking gel was prepared according to the Table A.1 below and poured. The comb was inserted gently into the stacking gel solution and the gel was allowed to polymerize. After this, the gel was washed thoroughly with de-ionized water and dried.

Components	**12% resolving gel**	**5% stacking gel**
De-ionised water	3.3	2.1
30% acrylamide mix	4.0	0.5
1.5M Tris (pH-8.8) for resolving gel or 0.1M Tris (pH- 6.8) for stacking gel	2.5	0.38
10% SDS	0.1	0.03
10% ammonium persulfate	0.1	0.03
TEMED	0.004	0.003

A.2. COOMASSIE BRILLIANT BLUE STAINING OF SDS-PAGE GEL

Methanol acetic acid solution: 500ml of methanol: 400ml of water:100ml of glacial acetic acid was used.

Coomassie brilliant blue stain: 0.25g of Coomassie Brilliant blue R-250 per 100ml of methanol acetic acid solution was prepared and filtered through Whatman No:1 filter paper to remove particulate matter. The gel was removed carefully from the glass plates

and immersed in 5 times gel volume Coomassie brilliant blue stain solution on a slowly rocking platform overnight. Gel was destained in methanol acetic acid solution with gentle shaking for 4h. The destaining solution was changed 3- 4 times